



<https://theses.gla.ac.uk/>

Theses Digitisation:

<https://www.gla.ac.uk/myglasgow/research/enlighten/theses/digitisation/>

This is a digitised version of the original print thesis.

Copyright and moral rights for this work are retained by the author

A copy can be downloaded for personal non-commercial research or study, without prior permission or charge

This work cannot be reproduced or quoted extensively from without first obtaining permission in writing from the author

The content must not be changed in any way or sold commercially in any format or medium without the formal permission of the author

When referring to this work, full bibliographic details including the author, title, awarding institution and date of the thesis must be given

Enlighten: Theses

<https://theses.gla.ac.uk/>
research-enlighten@glasgow.ac.uk

**THE ROLE OF SYNAPTOTAGMINS IN INSULIN-STIMULATED
GLUCOSE UPTAKE IN THE 3T3-L1 ADIPOCYTE**

© Steven Charles Maclean Miller

B.Sc. (Hons.), M.B.Ch.B., M.R.C.P. (U.K.)

**A Thesis Submitted for the Degree of Doctor of Philosophy to the
Faculty of Medicine of the University of Glasgow.**

September 2006

Division of Cardiovascular And Medical Sciences

Faculty of Medicine

and

Division of Biochemistry and Molecular Biology

Faculty of Biological and Life Sciences

University of Glasgow

ProQuest Number: 10391044

All rights reserved

INFORMATION TO ALL USERS

The quality of this reproduction is dependent upon the quality of the copy submitted.

In the unlikely event that the author did not send a complete manuscript and there are missing pages, these will be noted. Also, if material had to be removed, a note will indicate the deletion.



ProQuest 10391044

Published by ProQuest LLC (2017). Copyright of the Dissertation is held by the Author.

All rights reserved.

This work is protected against unauthorized copying under Title 17, United States Code
Microform Edition © ProQuest LLC.

ProQuest LLC.
789 East Eisenhower Parkway
P.O. Box 1346
Ann Arbor, MI 48106 – 1346

GLASGOW
UNIVERSITY
LIBRARY:

Declaration

I declare that this thesis has been compiled exclusively by myself. The work described herein has, unless otherwise stated, been carried out by myself. It has not, in whole or in part, been submitted for any other degree.

Steven Charles Maclean Miller

September 2006.

Acknowledgements

There are many people to whom I wish to show my sincere gratitude. Firstly I would like to thank my joint supervisors Professor John Connell and Professor Gwyn Gould. Professor Gould has provided daily laboratory supervision, essential technical advice, patience, friendship and occasional company on the lunchtime run. Without the invaluable career advice, mentorship and support of Professor Connell I would not have been able to embark upon a career in both Medicine and Science. Whenever asked, both Prof Connell and Gwyn have provided words of motivation, guidance and constructive criticism, and in spite of multiple commitments both have always been approachable and available at all times.

I am grateful to all the members of Lab 241 over the last 3 years without whose assistance, advice, camaraderie and friendship the time in the lab would have been far less enjoyable. I am thankful to Professor M Fukuda for supplying SYT cDNA plasmids, and I am particularly grateful to Professor M Czech and colleagues for hospitality and technical assistance with siRNA and electroporation. I would like to acknowledge the clinical colleagues who made my necessary regular returns to Clinical Medicine an enjoyable experience. I am appreciative of the financial support provided by the Medical Research Council (in the form of a Clinical Research Training Fellowship) and the Diabetes Research and Wellness Foundation.

Finally, I would not have been able to complete this work without the endless support of my family. To Catherine and Alasdair I would like to say thank you for understanding why Daddy wasn't around at conference time, and in the evenings and weekends during the time I was writing. To my wife Amanda I am indebted for your lifelong partnership, and for coping with the kids essentially alone during the write-up, an especially impressive accomplishment during the ninth month of pregnancy. And to baby Alice, a huge thank you for delaying your entrance into the world until after Daddy had completed his thesis!

Abstract

Within the adipocyte, skeletal myocyte and cardiac myocyte the sugar transporter GLUT4 exists in numerous distinct subcellular membrane compartments, and a complex series of trafficking steps are known to regulate its distribution. When insulin binds to its receptor at the cell surface, the ensuing cascade of protein-protein and protein-lipid interactions leads to the translocation of a GLUT4-containing vesicle (GSV) to the plasmalemma (PM), where it docks, binds and fuses in a SNARE-dependent manner. In this way GLUT4 is delivered to its intended site of action, and glucose can enter the cell. The precise steps which regulate intracellular GLUT4 trafficking and those which govern GSV-PM fusion are hitherto unknown. GSV-PM fusion is known to be disrupted in insulin resistant states such as Type-2 Diabetes, which is a growing global healthcare concern.

Such SNARE-mediated fusion events are best understood in neurons, where membrane fusion occurs in a calcium-dependent manner. The calcium-sensing species is an isoform of the 15-member Synaptotagmin (SYT) family, which binds the SNARE complex and the target and vesicle membranes. As a result, otherwise opposing thermodynamic forces between adjacent lipid bilayers are overcome and fusion can occur. In this thesis experiments designed to investigate the role of SYTs in insulin action in the 3T3-L1 adipocyte are described.

Using RTPCR, the expression SYT isoforms in 3T3-L1 cells was demonstrated. SYT7 (calcium-dependent) and SYT11 (calcium-independent) were shown to be the predominant isoforms, and SYT11 expression was seen to be upregulated as cells acquire insulin sensitivity during differentiation. Following their generation, novel affinity-purified SYT7- and SYT11- specific antisera were used to investigate the subcellular localisation of each SYT protein, and both were found to occupy intracellular membrane compartments in common with GLUT4. siRNA-mediated knockdown of SYT7 potentiates glucose uptake, and SYT11 knockdown leads to abrogated insulin-stimulated glucose uptake and reduced intracellular GLUT4. Finally, SYT7 can be seen to bind the Syntaxin4 / SNAP23 / VAMP2 SNARE complex *in vitro*.

Together these data point to an important role for SYT7 and SYT11 in the 3T3-L1 adipocyte, which may represent control of GSV-PM fusion, the regulation of intracellular GLUT4 trafficking or both.

CONTENTS

	Page
Declaration	ii
Acknowledgements	iii
Abstract	v
Contents	vii
List of Figures	xvi
List of Tables	xix
Abbreviations	xx

Chapter 1: Introduction

1.1 Diabetes Mellitus: a Brief History	1
1.2 Diabetes Mellitus	6
1.2.1 Type-1 Diabetes Mellitus	8
1.2.2 Type-2 Diabetes Mellitus	10
1.2.3 Obesity	14
1.2.4 Complications of Diabetes	15
1.2.5 Insulin Secretion	18
1.2.6 The Metabolic Syndrome	21
1.3 Cellular Actions of Insulin	23
1.3.1 Glucose Transporter Proteins (GLUTs)	24
1.3.2 GLUT4	25
1.3.2.1 GLUT4 knockout Mouse Models	26

1.3.3	Insulin Signalling	
1.3.3.1	Insulin Receptor	28
1.3.3.2	Insulin Receptor Substrate Family	30
1.3.3.3	PI3K and PI(3,4,5)P3	32
1.3.3.4	PDK / AKT / PKC	34
1.3.3.5	AS160	35
1.3.3.6	PIKfyve	37
1.3.3.7	The Alternative CAP / Cbl / TC10 Signalling Pathway	39
1.3.4	Subcellular Regulation of GLUT4 Trafficking	43
1.4	SNARE Hypothesis	47
1.4.1	The Neuronal SNARE Complex	49
1.4.2	SNARES Involved in GLUT4 Translocation	51
1.4.3	The Role of Calcium in Insulin-stimulated GLUT4 Translocation	51
1.5	Synaptotagmins	
1.5.1	Overview	55
1.5.2	Synaptotagmin Genetics	56
1.5.3	C2 Domains	66
1.5.4	SYT Interactions	
1.5.4.1	SYT Oligomerisation	68
1.5.4.2	SYT - SNARE Interactions	69
1.5.4.3	Other SYT – Protein interactions	72

1.5.4.4	Phosphorylation	72
1.6	Aims of this Thesis	74
 Chapter 2: Materials & Methods		
2.1	Materials	
2.1.1	General Reagents	75
2.1.2	Radioactive Reagents	78
2.1.3	Kits	79
2.1.4	Molecular Biology Reagents	79
2.1.5	Tissue Culture Reagents	80
2.1.6	Cell Biology Reagents	83
2.1.7	Molecular Biology Buffers	84
2.1.8	Cell Biology Buffers	84
2.1.9	Microbiology Media	86
2.2	Methods	
	Molecular Biology Methods	
2.2.1	Preparation of Murine Brain mRNA	87
2.2.2	Preparation of Murine Skeletal Muscle mRNA	87
2.2.3	Preparation of mRNA from 3T3-L1 Cells	88
2.2.4	Human Brain mRNA	89
2.2.5	Pooled Human Adipose Tissue mRNA	89
2.2.6	Reverse Transcription of RNA into cDNA	90

2.2.7	Polymerase Chain Reaction	90
2.2.8	Agarose Gel Electrophoresis	92
2.2.9	Taqman Semi-Quantitative Polymerase Chain Reaction	93
2.2.10	Restriction Endonuclease Digestion	96
2.2.11	Cloning Restriction Endonuclease Digestion Products into Plasmid Vectors	96
2.2.12	TA Cloning	97
 Tissue Culture Methods		
2.2.13	3T3-L1 Fibroblasts	98
2.2.14	Passage of 3T3-L1 Fibroblasts	98
2.2.15	Differentiation of 3T3-L1 Fibroblasts	99
2.2.16	HEK 293 Cells	100
2.2.17	Trypsinisation and Passage of HEK-293 Cells	101
2.2.18	Freezing and Storage of Cells	101
2.2.19	Resurrection of Cells Stored in Liquid Nitrogen	102
2.2.20	Transfection of Cultured Cells Using Lipid-Based Transfection Reagents	102
2.2.21	Transfection of 3T3-L1 Adipocytes by Electroporation	103
 Cell Biology Methods		
2.2.22	SDS-Polyacrylamide Gel Electrophoresis	105
2.2.23	Coomassie Staining of Protein Gels	106
2.2.24	Western Blotting	106

2.2.25 Staining Western Blots with Ponceau S	107
2.2.26 Immunodetection of Proteins	108
2.2.27 ECL Detection	108
2.2.28 Quantification of Signals	109
2.2.29 Preparation of Cell Lysates	109
2.2.30 The Insulin-Stimulated 2-Deoxyglucose Uptake Assay	110
2.2.31 Cell Surface Transferrin Receptor Estimation	111
2.2.32 Subcellular Fractionation of 3T3-L1 Adipocytes	112
<i>In vitro</i> Protein Binding Assays	
2.2.33 Pull Down Assays	113
2.2.34 Vesicle co-Floatation Assays	114

Microbiology Methods

2.2.35 Transformation of Competent E Coli by Heat Shock	117
2.2.36 Preparation of Agarose Plates	117
2.2.37 Selection and Overnight Culture of Transformed <i>E. coli</i>	118
2.2.38 Induction of Protein Expression	118
2.2.39 Purification of Epitope-Tagged Proteins	119

Chapter 3: Synaptotagmin Expression in Murine Brain, Murine Muscle, Human Brain, Pooled Human Adipose and the 3T3-L1 Cell

3.1 Introduction	121
------------------	-----

3.2 Methods

3.2.1 Synaptotagmin Gene-specific Nucleotide Sequences	123
3.2.2 Synaptotagmin Gene-specific Oligonucleotide PCR	
Primers	124
3.2.3 Synaptotagmin Gene-specific Taqman Realtime	
PCR Primers and Oligonucleotide Probes	125
3.2.4 Murine Control cDNA	125
3.2.5 Human Control cDNA	126
3.2.6 3T3-L1 Cell cDNA	126
3.2.7 Murine Muscle cDNA	126
3.2.8 Human Adipose Tissue cDNA	127

3.3 Results

3.3.1 Synaptotagmin Expression in Murine Brain	128
3.3.2 Cloning and Sequencing of Murine SYT PCR	
Products	132
3.3.3 GLUT4 Expression in 3T3-L1 Cells During	
Differentiation	136
3.3.4 Synaptotagmin Expression in 3T3-L1 cells During	
Differentiation	140
3.3.5 GLUT4 and SYT Expression in Murine Skeletal	
Muscle	150
3.3.6 Synaptotagmin Expression in Pooled Human Adipose	156

3.3.7	GLUT4 and SYT Expression in 3T3-L1 Cells as Determined by Taqman Semi-Quantitative Realtime PCR	158
3.4	Discussion	171
 Chapter 4: Cellular Localisation of SYT7 and SYT11 in the 3T3-L1 Adipocyte		
4.1	Introduction	176
4.2	Methods	
4.2.1	Identification of Potential Immunogenic SYT7 and SYT11 Sequences	177
4.2.2	Generation of SYT7 and SYT11 Antisera	178
4.2.3	Characterisation of SYT7 and SYT11 Antisera	179
4.3	Results	
4.3.1	Characterisation of SYT7 and SYT11 Antisera	180
4.3.2	Subcellular Localisation of SYT7 and SYT11 within the 3T3-L1 Adipocyte	185
4.4	Discussion	191

**Chapter 5 siRNA-Mediated Gene Depletion in the 3T3-L1
Adipocyte**

5.1	Introduction	196
5.2	Methods	
5.2.1	Design of siRNA	197
5.3	Results	
5.3.1	Efficiency of Transfection by Electroporation	199
5.3.2	Influence of siRNA Mediated Knockdown of PTEN and AKT2 on Insulin-Stimulated Deoxyglucose Uptake	205
5.3.2	Influence of siRNA Mediated SYT11 Knockdown	207
5.3.3	Influence of siRNA Mediated SYT7 Knockdown	220
5.4	Discussion	222

**Chapter 6 Interaction of SYT7 and SYT11 with VAMP-2, Syntaxin-4
and SNAP-23**

6.1	Introduction	228
------------	---------------------	-----

6.2	Methods	
6.2.1	Generation of Epitope-Tagged Soluble SYT7 and Soluble SYT11	230
6.2.2	The Vesicle co-Floatation Assay	231
6.3	Results	
6.3.1	Sol SYT7 and SYT11	232
6.3.2	Interaction of Sol SYT7 and Sol SYT11 with GSV SNARE Proteins	236
6.4	Discussion	241
Chapter 7	Conclusions	244
Appendix		252
References		276

List of Figures

Figure	Page
1.1 The Insulin Signalling Cascade	41
1.2 Schematic Representation of Intracellular GLUT4 Trafficking	46
1.3 Schematic Representation of the Neuronal SNARE Complex	48
1.4 Amino Acid Sequence Alignment of Murine SYT 1- 15	61
1.5 Cladogram Derived From Murine SYT Protein Sequences	64
1.6 Synaptotagmin Domain Structure	66
1.7 Schematic Representation of Synaptotagmin Interacting with the Neuronal SNARE Complex	71
3.1 Synaptotagmin Expression in Murine Brain	130
3.2 Subcloning of SYT PCR Products	134
3.3 GLUT4 Expression in 3T3-L1 Cells	138
3.4 Insulin-Stimulated 2-Deoxyglucose Uptake in 3T3-L1 Adipocytes	139
3.5 SYT1, 2, 4 and 6 Expression in 3T3-L1 Cells	143
3.6 SYT3, 5 and 7- 14 Expression in 3T3-L1 Cells	145
3.7 GLUT4 and SYT Expression in Murine Skeletal Muscle	152
3.8 SYT7 and SYT11 Expression in Murine Skeletal Muscle	155
3.9 SYT7 and SYT11 Expression in Human Adipose	157
3.10 Taqman Primer and Probe Standard Curve	161
3.11 SYT Expression in Murine Brain Tissue	162
3.12 GLUT4 Expression in 3T3-L1 Cells During Differentiation	164

3.13	Synaptotagmin Expression in Confluent 3T3-L1 Fibroblasts	165
3.14	Synaptotagmin Expression in 3T3-L1 Adipocytes	166
3.15	SYT7 Expression in 3T3-L1 Cells During Differentiation	168
3.16	SYT11 Expression in 3T3-L1 Cells During Differentiation	169
3.17	SYT11 Expression in 3T3-L1 Cells During Differentiation: Additional Timepoints	170
4.1	Affinity-Purified SYT7 Antisera	181
4.2	Affinity-Purified SYT11 Antisera	183
4.3	Subcellular Fractionation of 3T3-L1 Adipocytes	187
4.4	SYT7 and SYT11 Distribution in 3T3-L1 Adipocytes	188
4.5	3T3-L1 Cell PM and LDM Fractions	189
5.1	Efficiency of Transfection	201
5.2	2-Deoxyglucose Uptake in siRNA-Transfected 3T3-L1 Adipocytes: PTEN and AKT2	206
5.3	Light Microscopy Appearance of Transfected Cells	210
5.4	Influence of SYT11 Knockdown on Insulin-Stimulated 2-Deoxyglucose Uptake	213
5.5	SYT11 siRNA	214
5.6	IRAP, Syntaxin4, SNAP23 and GAPDH in SYT11 Knockdown 3T3-L1 Adipocytes	217
5.7	Cell Surface Transferrin Binding in SYT11 Knockdown 3T3-L1 Adipocytes	219

5.6	Influence of SYT7 Knockdown on Insulin-Stimulated 2-Deoxyglucose Uptake	221
6.1	Soluble SYT7 and SYT11 Protein	233
6.2	Antibody Recognition of Soluble SYT7 and SYT11	235
6.3	Interaction of SYT7 with Syntaxin4, SNAP23 and VAMP2	238
6.4	Interaction of SYT11 with Syntaxin4, SNAP23 and VAMP2	239
6.5	Distribution of v-SNARE and t-SNARE Vesicles in Nycodenz Gradients	240
A1	Schematic Representation of the Genomic Structure of the Murine SYT7 Gene	255

List of Tables

Table Number		Page
1.1	Classification of Diabetes Mellitus	7
1.2	Obesity Status Defined by BMI	14
1.3	The Macrovascular and Microvascular Complications of Diabetes	16
1.4	Classification of Regulated Exocytosis	49
1.5	Chromosomal Location and Gene Structure of Human and Murine SYT Genes	58
A1	Genbank Accession Numbers for Murine and Human Synaptotagmin Genes	252
A2	Murine RTPCR Primer Location and Expected Product Sizes	256
A3	Human RTPCR Primer Location and Expected Product Sizes	259
A4	Peptides Used to Generate SYT7 and SYT11Antisera	275

Abbreviations

ACE	Angiotensin Converting Enzyme
AGE	Advanced Glycation End products
AKT	Protein Kinase B
AS160	AKT Substrate of 160kDa
ATP	Adenosine Triphosphate
ATPIII	Adult Treatment Panel III
APS	Adaptor Protein containing PH- and SH2-domains
AP-1	Adaptor Protein-1
BLAST	Basic Local Alignment Search Tool
BMI	Body Mass Index
CaMKII	Calmodulin Kinase-II
CAP	c-Cbl Associated Protein
CaskII	Casein kinase-II
CD-MPR	Cation-dependent Mannose-6-phosphate Receptor
CHD	Coronary Heart Disease
CMV	Cytomegalovirus
CNS	Central Nervous System
DDP-IV	Dipeptidyl peptidase-IV
DEP-domain	Dishevelled-, Egl10- and PH-domain
DIDMOAD	Diabetes Insipidus, Diabetes Mellitus, Optic Atrophy and Deafness
DMEM	Dulbecco's Modern Eagle Medium
DNA	Deoxyribonucleic Acid

cDNA	Complementary DNA
EEA1	Early Endosomal Antigen-1
ER	Endoplasmic Reticulum
FCS	Fetal Calf Serum
GAPDH	Glyceraldehyde Phosphate Dehydrogenase
GDP	Guanosine Diphosphate
GTP	Guanosine Triphosphate
GSV	GLUT4 Storage Vesicle
HDM	High-Density Microsomes
HEK cells	Human Embryonic Kidney Cells
HLA	Human Leukocyte Antigen
HRP	Horseradish Peroxidase
IDF	International Diabetes Federation
IGFR	Insulin-like Growth Factor Receptor
IGF-2R	Insulin-like Growth Factor-2 Receptor
IR	Insulin Receptor
IRAP	Insulin-Regulated Aminopeptidase
IRS	Insulin Receptor Substrate
ISG	Immature Secretory Granules
K _{ATP}	ATP-sensitive Potassium Channels
LDCV	Large Dense Core Vesicles
LDM	Low-Density Microsomes
LIRKO	Liver Insulin Receptor Knockout
MIRKO	Muscle Insulin Receptor Knockout
MSG	Mature Secretory Granules

NCBI	US National Centre for Biotechnology Information
NCS	Newborn Calf Serum
PARP	Poly-ADP Ribose Polymerase
PDK1	3-Phosphoinositide-Dependent Protein Kinase-1
PH-domain	Pleckstrin Homology Domain
PI3K	Phosphatidyl Inositol-3 Kinase
PIKFyve	Phosphatidyl Inositol 3-phosphate 5-kinase
PI3P	Phosphatidyl Inositol-3 Phosphate
PI(3,4)P ₂	Phosphatidyl Inositol-3,4 bisphosphate
PI(4,5)P ₂	Phosphatidyl Inositol-4,5 bisphosphate
PI(3,4,5)P ₃	Phosphatidyl Inositol-3,4,5 trisphosphate
PKC	Protein Kinase-C
PM	Plasma Membrane
PPAR _γ	Peroxisome Proliferator-activated Receptor- γ
PTB-domain	Phosphotyrosine Binding Domain
PTEN	Phosphatase and Tensin-homolog Deleted on Chromosome Ten
MHC	Major Histocompatibility Complex
MODY	Maturity Onset Diabetes of the Young
MTOC	Microtubulin Organising Centre
mTOR	Mammalian Target of Rapamycin
PCR	Polymerase Chain Reaction
mRNA	Messenger Ribonucleic Acid
siRNA	Short Inhibitory Ribonucleic Acid
RT-PCR	Reverse Transcription Polymerase Chain Reaction

SDS-PAGE	SDS-Polyacrylamide Gel Electrophoresis
SGLT	Sodium-dependent Glucose Transporters
SH2-Domain	Src-Homology Domain
SHIP2	Type-II SH2 Domain-containing Inositol 5-Phosphatase
SNARE	Soluble N-Ethylmaleimide-Sensitive Factor Attachment Protein Receptor
t-SNARE	Target Membrane SNARE Protein
v-SNARE	Vesicle SNARE Protein
SYT	Synaptotagmin
T1DM	Type-1 Diabetes Mellitus
T2DM	Type-2 Diabetes Mellitus
TfR	Transferrin Receptor
TGN	<i>trans</i> -Golgi Network
UKPDS	UK Prospective Diabetes Study
UV	Ultraviolet
WHO	World Health Organisation
WNK1	With No Lysine Kinase-1

Chapter 1: Introduction

1.1. Diabetes Mellitus: a Brief History

Throughout history mankind has acknowledged the challenges presented by Diabetes Mellitus. A papyrus written by the ancient Egyptian physician Hesy-Ra was the first to document the disease c1500 BC, citing polyuria as a predominant symptom. Early in the 2nd century AD the Greek Arateus coined the term "diabetes" or siphon to describe "the melting down of flesh and limbs into urine". Not until the Middle Ages when the urine was tasted in an attempt to reach a diagnosis was "mellitus" used to describe the sweet or honey-like taste of urine from affected individuals. In the early 19th century the development of biochemical assays for sugars formally confirmed the presence of glycosuria, when it was first also observed that dietary restriction could be used to suppress the loss of sugar in urine. Around this time Lancereaux described diabete maigre (1) and diabete gras (obese), and is acknowledged as the first to attempt to classify the two commonly observed clinical diabetic syndromes on the basis of aetiology (2).

By the late 19th century work by Minkowski and von Mering became noteworthy for demonstrating that a dog could be rendered diabetic by surgically removing its pancreas (3). By this time the explosion in medical research meant that numerous clinicians and scientists worldwide were attempting to determine the precise nature of

the pancreatic factor responsible for controlling blood and urine sugar. Separate experiments by Zuelzer in Berlin in 1906, Scott in Chicago in 1912, Paulescu in Romania 1916 and Kleiner in New York in 1919 all resulted in the lowering of blood or urine sugar content by administering a crude pancreatic extract, but all shared significant side effects and misinterpretation of results.

In summer 1921 the young surgeon Frederick Banting (working in Toronto with Charles Best under the supervision of JJR Macleod) used pancreatic duct ligation to first isolate the Islets of Langerhans, and then successfully used a crude islet extract to treat a (surgically) diabetic dog. The extract first termed "Isletin" came to be known as Insulin. Soon afterwards in January 1922 Leonard Thomson became the first human diabetic subject to be successfully treated with injections of insulin. Rapid advances (initially led by Collip) in insulin production and its commercialization followed, and numerous patients were given this successful treatment for their hitherto invariably fatal disease. The 1923 Nobel Prize for Medicine and Physiology was awarded to Banting and Macleod (who in turn shared the prize with Best and Collip) for the discovery of Insulin.

The revolution in diabetic treatment that followed the discovery and widespread use of insulin, appropriately heralded as a major scientific and therapeutic breakthrough at the time, consequently was proven to be a double edged sword. Diabetes was transformed from a rapidly fatal

illness (due to uncontrolled ketoacidosis) to a chronic disease, the result of which individuals developed retinitis leading to blindness, proteinuria and azotaemia, and premature vascular death. It was to be many years before the connection between maintaining tight glycaemic control and the prevention of these complications of diabetes would be met with widespread acceptance (1;4)

Soon after its discovery Falta and Himsworth observed that thin individuals who required insulin for the prevention of ketoacidosis were sensitive to its glucose lowering effects, whereas obese patients were often insensitive or resistant to insulin. The use of techniques devised in the 1970s to precisely quantify the extent of insulin resistance also revealed the role of β -cell failure in the pathogenesis of what is now known as Type-2 Diabetes Mellitus. In contrast, the "insulinitis" observed by Opie in thin, insulin deficient individuals was not associated with β -cell loss or acknowledged to be of autoimmune in origin until this was proposed by Gepts in 1965 and Doniach and Gianfrance in 1979 respectively. Diabetes due to such autoimmune β -cell loss is now known as Type-1 Diabetes Mellitus.

Since the early days the understanding of clinical diabetes and its consequences has flourished. The development of effective analogue insulins, oral hypoglycaemic agents and modifications of cardiovascular risk have provided physicians with an efficient armoury with which to treat diabetes and prevent the complications that are the result of many years

of this now chronic disease. Detailed epidemiological studies have provided insight into factors which seemingly promote the pathogenesis of the disease, and also give an indication of the contribution made by heredity to both major types of diabetes. Advances in such major scientific disciplines as Genetics, Molecular Biology and Cell Biology have allowed scientists to gain tremendous insight into the molecular pathogenic mechanisms involved in diabetes and its complications. Ongoing fruitful collaborations between clinicians and scientists promise to deliver novel effective treatments destined to reduce both morbidity and mortality associated with the disease.

In recent years reporting of the alarming rise in the incidence of type-2 diabetes in developed countries has dominated the epidemiological literature. In fact the incidence of diabetes in developing countries is anticipated to increase by more than 150%. Current WHO predictions for escalating Diabetes incidence foresee a global doubling of diabetes prevalence in the 30 years from the year 2000, with an estimated 366 million affected individuals by the year 2030 (5). In spite of the detailed descriptions of many aspects of normal physiology and biochemistry the precise mechanisms underlying many fundamental cellular processes, not least the precise steps which regulate insulin action in adipose and skeletal muscle cells (which is known to be deranged in T2DM) remain to be elucidated. Without a clear understanding of what is normal, there can be little hope for the development of therapeutics which may facilitate an effective cure. Thus,

type-2 diabetes is set to become one of the most challenging global healthcare issues of our time.

1.2. Diabetes Mellitus

The most recent internationally agreed definition of Diabetes Mellitus is

“a metabolic disorder of multiple aetiology characterised by chronic hyperglycaemia with disturbances of carbohydrate, fat and protein metabolism resulting from defects in insulin secretion, insulin action or both” (5)

Strict diagnostic criteria based upon the presence of osmotic symptoms alongside elevated blood glucose values (either fasting or random), or elevated blood glucose following an oral glucose load in the absence of any significant intercurrent illness require to be met before the diagnosis can be made. The different types of diabetes are classified according to their aetiology. The most commonly encountered forms are Types 1 and 2 Diabetes and Gestational Diabetes. Other specific types exist but these are uncommon and rarely encountered in clinical practice (see TABLE 1.1 below).

Type-1 Diabetes	Autoimmune β -cell destruction Idiopathic
Type-2 Diabetes	Insulin Resistance Insulin Secretory Defect
Gestational Diabetes	Pregnancy
Genetic Defect of β-cell Function	Maturity Onset Diabetes of the Young (MODY) Mitochondrial Diabetes
Genetic Defect of Insulin Action	Type-A Insulin Resistance Leprechaunism Rabson-Medenhall Syndrome Lipoatrophic Diabetes
Diseases of the Exocrine Pancreas	Pancreatitis Trauma / Surgery Neoplasia Cystic Fibrosis / Haemachromatosis
Endocrinopathies	Cushing's Syndrome Acromegaly Pheochromocytoma Thyrotoxicosis
Drug or Chemical induced	Glucocorticoids Pentamidine Thiazides β -blockers
Infections	Congenital Rubella Congenital CMV
Uncommon immune Forms	Anti-Insulin Receptor Antibodies Stiff Man Syndrome
Other Genetic Syndromes Associated with Diabetes	Down's Syndrome Klinefelter's Syndrome Turner's Syndrome Lawrence-Moon-Biedl Syndrome Myotonic Dystrophy Prader-Willi Syndrome DIDMOAD

Table 1.1: Classification of Diabetes Mellitus (adapted from (5))

1.2.1. Type-1 Diabetes Mellitus

Type-1 Diabetes (T1DM) is characterised by autoimmune cell-mediated destruction of the β -cells in the Islets of Langerhans of the pancreas leading to insulin deficiency. The immune stimulus is a combination of both genetic factors and environmental stimuli. Family studies reveal that siblings of an affected individual have a 6% chance of becoming affected, and monozygotic twins have a 36% lifetime risk of developing T1DM. The genomic region with the strongest diabetes association lies within the HLA (Human Leukocyte Antigen) locus within the MHC (Major Histocompatibility Complex) located on the short arm of chromosome 6, however the existence of numerous other type-1 diabetes association loci throughout the genome within different study populations (alongside various environmental factors known to influence T1DM susceptibility) to point to a complex and multifactorial disease aetiology.

Exposure to environmental factors such as viruses (Coxsackie, Mumps, Cytomegalovirus, Epstein-Barr virus and rubella), toxins (nitrosamines, cows milk protein) and other early life events (foetal blood group incompatibility, environmental temperature and "stressful" experience) have been shown to be associated with increased T1DM occurrence (6). In 80% of affected individuals, circulating antibodies to β -cell antigens can be detected at the time of diagnosis, and these can be used as disease markers in siblings at risk.

Disease onset is predominantly in childhood or early adulthood (although individuals can be affected at any age). Affected individuals are no longer capable of producing insulin sufficient to maintain adequate glucose homeostasis and so usually present with symptoms of hyperglycaemia such as thirst, polyuria and blurred vision. Weight loss is common, and represents the general catabolic state induced by insulin deficiency.

Individuals with T1DM are at particular risk of diabetic ketoacidosis, a life-threatening metabolic dysregulation which occurs as a result of insulin deficiency and insulin counter-regulatory hormone excess (glucagon, catecholamines, cortisol and growth hormone) and elevation of proinflammatory cytokines (tumour necrosis factor α , interleukin-6, interleukin-1 β and interleukin-8), free fatty acids, and plasminogen activator inhibitor-1 (reviewed in (7)). Uncorrected hyperglycaemia and ketone body formation lead to a profound osmotic diuresis and metabolic acidosis. Untreated this is manifest clinically as circulatory collapse, Kussmaul respiration and eventual coma and death. In spite of advances in care diabetic ketoacidosis is associated with 5% mortality. Patients with T1DM therefore have an absolute requirement for lifelong treatment with exogenous insulin, usually delivered via multiple daily subcutaneous bolus injections.

1.2.2. Type-2 Diabetes Mellitus

Type-2 Diabetes (T2DM) accounts for 85% of all diabetes encountered in a Caucasian population, and is characterised by a combination of resistance to the actions of insulin accompanied by impaired secretion of insulin from the pancreatic β -cell. There is absence of insulin- or β -cell autoantibodies, or any other known cause of diabetes (as detailed in table 1 above). Many cellular mechanisms have been identified that may be responsible for both the cardinal features of insulin resistance and defective insulin secretion. In any given individual with T2DM it is likely that more than one such defect is present, reflecting the heterogeneous nature of the disease. Often T2DM is associated with abnormalities of blood pressure and lipid metabolism and this triad is termed the Metabolic Syndrome (8).

Susceptibility to T2DM has a stronger genetic contribution compared with T1DM, and is proposed to account for 40-80% disease susceptibility. Dizygotic twins have a 17-37% chance of developing the disease (9;10), whilst studies in monozygotic twins reveal 60-90% concordance (11-13). Candidate genes include those which transduce the insulin derived signal in target tissues, and genes concerned with insulin generation, secretion and β -cell survival. That no single genetic locus has been identified to be responsible for T2DM predisposition

reflects the likely contribution made by many of these mechanisms in any affected individual or pedigree.

Environmental factors are known to significantly contribute to T2DM susceptibility. There is a strong association between low birth weight and development of T2DM in later life, suggesting that foetal malnutrition plays an important role. Furthermore, the modernisation of society has been associated with reduced physical activity and increased calorie intake, which has led to an explosion of obesity. Both phenomena are evidence for the "Thrifty Gene" hypothesis, which suggests that under conditions of undernutrition (either in development or under environmental stress e.g. at times of famine) such thrifty genes operate to maximise energy economy, and capitalise at times of plenty to store for times of future need (14). This would provide a clear evolutionary survival benefit. However, under conditions of chronic net overnutrition the result of such a genotype would be excess adiposity, insulin resistance and the development of T2DM. The increase in T2DM prevalence observed to occur alongside industrialisation in developing countries, in addition to the dramatic prevalence amongst individuals from certain ethnic groups when a "Westernised" lifestyle is adopted provide further support for the Thrifty Gene hypothesis.

The majority of individuals diagnosed with T2DM are obese. Most are over 40 years of age with the peak incidence seen in the 7th decade, although the incidence in young adults and children is increasing. The

diagnosis is often coincidental with another unrelated presentation (1/3rd), or is made following presentation with a complication of diabetes. Ketoacidosis is seldom seen but can occur in individuals with T2DM.

The most important risk factor for the development of T2DM is obesity, as evidenced by the many epidemiological observations between diabetes prevalence and average population weight (15). A rise in obesity in any given population is followed closely by increasing T2DM prevalence. For any given individual the risk of diabetes is associated with body fat distribution (central or visceral obesity being more important than peripheral or subcutaneous) (16). Evidence is emerging that deposition of fat outwith adipose tissue, so-called ectopic fat (e.g. intramyocellular lipid, hepatic steatosis, pancreatic β -cells) can be linked to insulin resistance and diabetes (17). The rate of increase in weight (18) has also been shown to be an important contributor to diabetes risk (19). That only 50% of those individuals with BMI > 40kg/m² develop diabetes and observations that a significant number of patients with T2DM are not (and have never been) overweight, merely confirms the complex multifactorial aetiology of diabetes.

Insulin resistance is an early feature of T2DM, and in any individual with this form of diabetes probably exists for around a decade prior to the loss of normal tight metabolic control. At the same time, the development of insulin secretory defects in the pancreatic β -cell leads to an inability to compensate for resistance to insulin. Together, this

becomes apparent with the development over time of impaired glucose tolerance, fasting hyperglycaemia and ultimately the diagnostic criteria for T2DM are met (5).

The treatment of T2DM can be broadly divided into two categories; treatments aimed at achieving glycaemic control and treatments to reduce cardiovascular risk. The former begins with advice regarding weight reduction, diet and physical activity, to oral hypoglycaemic agents to enhance insulin secretion from the β -cell (Sulphonyl-ureas), improve insulin sensitivity and suppress gluconeogenesis (Metformin) when more simple measures fail. In advanced disease insulin is used to control hyperglycaemia, and the large doses required reflect the insulin resistance present. Control of dyslipidaemia with Statins and tight blood pressure control with agents which modulate the Renin-Angiotensin System (with or without traditional antihypertensives) has been shown not only to reduce cardiovascular risk but also to slow the progression of particular diabetic complications (20). Newer antidiabetic agents such as the PPAR γ -agonists have multiple effects which include improvement in insulin sensitivity, lipid profile and blood pressure, which makes these drugs a particularly attractive therapeutic candidate. Agents currently in development such as the incretin-mimetics and DDP-IV inhibitors improve pancreatic function, enhance insulin sensitivity and have shown beneficial weight loss, and are likely to become valuable clinical tools.

1.2.3. Obesity

The clinical condition of excess body weight as a consequence of excess adipose tissue accumulation is termed obesity. The internationally used measurement of obesity, the Body Mass Index (BMI) as defined by the weight in kilograms divided by height in metres squared was originally described in the early 19th century by the Belgian statistician Adolphe Quetelet (1796- 1874). The accepted classification of obesity status based on measurement of BMI is shown in TABLE 1.2 below.

Classification	BMI
Underweight	<18.5
Normal weight	18.5- 25
Overweight	≥25
Obese	>30

Table 1.2: Obesity Status Defined By BMI

Despite being independent of age or sex, caution must be exercised in interpretation of any given BMI. It does not take into account the contribution to body weight made by other body tissues (e.g. skeletal muscle), or the effects of differing body proportions. Furthermore, population studies have demonstrated body fat composition varies with

ethnicity within similar BMI ranges (18). Despite these drawbacks, the ease of calculation of the BMI has led to its universal acceptance.

Increasing weight is associated with increased morbidity due to osteoarthritis, gout, breathlessness and sleep apnoea, and subfertility. More importantly increasing weight is associated with increased mortality principally due to T2DM and Coronary Heart Disease (CHD), (and also cancer;(21). The global prevalence of obesity is rising at an alarming rate: the 2000 WHO Technical Report on Obesity (Reprinted 2004) (22) described in great detail the rise of obesity prevalence amongst children and adults in developed and developing countries alike. Many strategies exist in order to effect weight loss and to prevent excess weight gain, however none have demonstrated sustained benefit over time, or improved healthcare endpoints (reviewed in (23)).

1.2.4. Complications of Diabetes

Diabetes has long been known to cause specific complications which lead to significant morbidity. As early as the 10th century ad. in his Arabic medical encyclopaedia Avicenna described gangrene and impotence in diabetic patients. Englishman John Rollo was the first to describe symptoms of diabetic peripheral neuropathy, German von Jaeger documented the first detailed description of diabetic retinopathy, and Kimmelsteil and Wilson (of renal syndromic fame) whilst working in the USA made the connection between diabetes and glomerular disease.

In the years soon after the discovery and widespread use of insulin in the treatment of diabetes it soon became apparent that an excess of premature cardiovascular mortality was occurring in affected individuals. It was not until Lundbaek's paper of 1954 that "Diabetic Angiopathy" was accepted, in spite of ancient observations some 3000 years earlier (24). Diabetic complications are listed in Table 1.3 below.

Macrovascular	Microvascular
Ischaemic Heart Disease	Nephropathy
Cerebrovascular Disease	Retinopathy
Peripheral Vascular Disease	Neuropathy

Table 1.3: The Macrovascular and Microvascular Complications of Diabetes.

Excess cardiovascular mortality is still seen in all age groups with both T1DM and T2DM, and macrovascular disease remains the main cause of death in both T1DM and T2DM (25). The risk of macrovascular complication i.e. myocardial infarction, cerebrovascular disease or peripheral vascular disease is increased up to fivefold in an individual with T2DM (26). Arterial disease is commonly diffuse at presentation. Despite thrombolytic therapy and both percutaneous and surgical

revascularisation, the rates of re-stenosis are higher in diabetic patients versus non-diabetic controls (26).

Diabetes remains the commonest cause of end-stage renal failure worldwide, and is the underlying cause responsible for more than half of all kidney transplants and the initiation of renal dialysis. Furthermore, graft survival is reduced, and morbidity and mortality whilst on dialysis is increased amongst diabetic individuals compared with non-diabetic controls (27). Diabetic retinopathy is the leading cause of blindness in developed countries (28). Specific treatments with panretinal photocoagulation and surgical vitrectomy can prevent blindness, but there are currently no agents which specifically prevent retinopathy (29). Lifetime risk of neuropathy is around 50%, and the presence of neuropathy is associated with significant morbidity (and mortality due to autonomic neuropathy and sudden cardiac death)(30).

The clear relationship between glycaemic control and the incidence of diabetic complications is well established (4). The damaging cellular processes initiated by hyperglycaemia within the vascular endothelium and leading to the vascular complications described above are modulated by genetic susceptibility and factors such as hypertension and hyperlipidaemia. Clear benefit is gained in terms of reducing complication incidence and severity by both reducing blood pressure (1) and by lipid lowering treatment with a statin (31) in diabetic individuals. Treatment with an agent that modulates the Renin-Angiotensin system

(such as an ACE-inhibitor (32) or an Angiotensin II Receptor antagonist (33)) provides additional preservation of renal function independent of blood pressure reduction.

It is now recognised that increased polyol pathway flux, increased advanced glycation endproduct (AGE) formation, activation of protein kinase-C (PKC) isoforms and increased hexosamine pathway flux are all responsible for endothelial damage, and are the consequence of increased intracellular reactive oxygen species (ROS) production due to hyperglycaemia (34;35). Whilst there are no current therapeutic agents in widespread use designed to specifically address these defects, this area of fruitful research has identified multiple novel targets which may prove to be effective in preventing diabetic complications: Transketolase activators (36), PARP inhibitors (37) and catalytic antioxidants (38) demonstrate promising preliminary efficacy.

1.2.5. Insulin Secretion

Despite the presence of elevated circulating levels, the secretion of insulin is impaired in T2DM since the level of hyperinsulinaemia observed is far lower than would be seen in a non-diabetic individual with a similar degree of hyperglycaemia (39). Insulin is synthesised in the β -cell of the Islets of Langerhans. Initially translated as preproinsulin this precursor is post-translationally modified in a stepwise manner by cleavage to proinsulin, and insulin and C-peptide which are stored in intracellular

vesicles. In response to increasing blood glucose (thus increased glucose entry into the β -cell and its subsequent metabolism to generate ATP) these vesicles then translocate to the cell surface where they fuse with the plasma membrane (PM) releasing insulin into the extracellular space (40). Insulin release in response to glucose has a characteristic biphasic pattern. The first rapid phase is believed to be due to the rapid mobilisation and ATP-independent release of secretory vesicles from the so-called ready-releasable pool. The second, more sustained phase of insulin secretion is dependent upon ATP, required to mobilise these granules from the storage pool to the readily-releasable pool (41).

The release of insulin is largely determined by the activity of the glucose sensor glucokinase. This enzyme phosphorylates glucose immediately upon its entry into the β -cell, which in turn affects cellular energy balance (in terms of available ATP). ATP-sensitive potassium channels (K_{ATP}) subsequently close, which leads to the depolarisation of the cell. Depolarisation leads to opening of voltage-gated calcium channels, which increases intracellular calcium concentrations and initiates insulin vesicle translocation and exocytosis.

The stimulation of insulin secretion can be modulated by a variety of metabolic (amino-acids), hormonal (glucagon and the incretins) and neural stimuli in both a positive and negative manner. These factors mediate their effects via a range of intracellular secondary messengers

which either alter the β -cells resting potential, influence Ca^{2+} -channel sensitivity or modify vesicle mobilisation and fusion.

Maturity Onset Diabetes of the Young (MODY) is characterised by autosomally inherited non-insulin dependent diabetes at an early age (42). The particular gene defects observed are associated with β -cell dysfunction and defective insulin secretion. Mutations in glucokinase and the K_{ATP} channel subunit Kir6.2 have been elucidated in pedigrees with rare monogenic diabetes syndromes (e.g. MODY2). Other mutations affecting transcription factors (HNF1 α , HNF4 α , HNF1 β , IPF-1 and NeuroD1) which in turn influence the expression of genes implicated in the regulation of insulin secretion are now understood to be responsible for other MODY phenotypes (43).

The UKPDS study revealed that around 50% of the insulin-secreting capacity of the β -cell is lost at the time of diagnosis of T2DM, and that this continues to decline with time in spite of intense glycaemic management. Backwards extrapolation of the rate of decline suggests that, contemporaneous with the onset of insulin resistance, β -cell failure is an early event in the pathogenesis of T2DM and begins around ten years before diagnosis is made.

Insulin secretion is an exceedingly complex multi-step phenomenon, and it is not surprising that defects can be demonstrated at multiple levels of the secretory pathway in T2DM. Whilst some genetic

defects that produce a clear clinical phenotype are well characterised (MODY) it is likely that impaired insulin secretion is the manifestation of combinations of multiple inherited factors (as evidenced by the subtle abnormalities in β -cell function seen in relatives of individuals with T2DM). Other suggested mechanisms are glucotoxicity, amyloid deposition and ectopic lipid deposits, and it is likely more than one will contribute in any given individual (44).

1.2.6. The Metabolic Syndrome

The term Metabolic Syndrome X coined by Reaven in his 1988 Banting Lecture described individuals with impaired glucose tolerance (or diabetes) with one or more cardiovascular risk components (hypertension, hyperlipidaemia, microalbuminuria) who were at increased risk of cardiovascular disease compared with risk attributable to any individual component. With the addition of obesity to the definition, the Metabolic Syndrome became the widely favoured descriptive term (45). Since its conception the Metabolic Syndrome has been the matter of much discussion, with subtly differing diagnostic criteria used by disparate panels of experts (WHO (5); ATPIII: (46); IDF: (47); reviewed in (48)). Recently the clinical value in making the diagnosis has been questioned, with opponents supporting the idea that, if present cardiovascular risk factors should be addressed aggressively and independently (49). Proponents still value its use, with recent evidence to support elevated global cardiovascular risk in an individual "labelled" with

the Metabolic Syndrome greater than the risk attributable by each independent factor (50).

Given that cardiovascular risk factors are often present for many years prior to clinically evident loss of glycaemic control there may be some value in the use of the term in such individuals who are also overweight; strategies to reduce weight and increase physical activity, and thus improve insulin sensitivity may be adopted earlier by primary care physicians who manage the vast majority of such patients.

1.3. Cellular Actions of Insulin

Insulin is a pluripotent peptide hormone produced and released from the β - cells of the pancreatic islets of Langerhans. Insulin is essential for life: untreated diabetic ketoacidosis is fatal (51;52); insulin gene knockout mice exhibit growth retardation and die within 48 hours of birth from ketoacidosis (53). The most prominent, best studied and arguably most important actions of insulin are the stimulation of glucose uptake into skeletal muscle, the stimulation of glucose uptake into adipose cells (and the suppression of lipolysis), and suppression of hepatic gluconeogenesis. By virtue of these actions, insulin exerts control over carbohydrate metabolism and whole body glucose homeostasis.

Insulin is also known to modulate protein and lipid metabolism, suppress inflammation, maintain a healthy vascular endothelium and influence cell growth, differentiation and survival (further detailed discussion of which is outwith the scope of this thesis).

In order to stimulate post-prandial glucose uptake in a sensitive (54) cell insulin must stimulate the translocation of the facilitative sugar transporter GLUT4 (see section 1.6.7) from an intracellular location to the plasma membrane. Only once insulin binds its receptor can it exert influence over this, or any other of its varied metabolic effects within any individual cell.

1.3.1. Glucose Transporter Proteins (GLUTs)

In order to be utilised as a cellular energy substrate circulating glucose must first cross the lipid bilayer of the target cell. To facilitate this glucose requires a specific transport protein, since its intrinsic hydrophilicity prohibits traversing the hydrophobic PM. There are two such families of glucose transporters; the Na⁺-dependent glucose transporters (55) and the facilitative glucose transporters (GLUTs). The SGLT family harness the electrochemical energy generated by transmembrane sodium exchange to move glucose against its concentration gradient into the cell, and are responsible for glucose entry into enterocytes (SGLT 1-2) or proximal renal tubular epithelial cells (SGLT-3). The GLUTs allow glucose to enter the cell by moving down its concentration gradient (reviewed in (55)).

There are 13 known GLUTs, each with different substrate specificity, tissue distribution and kinetic properties. They share the same basic structure of twelve transmembrane domains, possess sugar transporter signatures required for the transporter function and can be divided into three classes based upon sequence similarity. Most tissues express a combination of GLUT molecules at the cell surface to ensure a continued energy substrate supply at physiological blood glucose concentrations (55;56).

1.3.2. GLUT4

The specialised insulin-responsive facilitative sugar transporter GLUT4 (57) is expressed in those tissues demonstrated to exhibit insulin-mediated glucose accumulation i.e. skeletal muscle, adipose and cardiac muscle. Subsequent study confirmed the low level expression of GLUT4 in specific brain regions (58;59) where it may function in a glucose-sensing capacity alongside other GLUTs, and regulate memory (60). In response to insulin stimulation of the surface-bound Insulin Receptor (IR), a cascade of protein-protein and protein-lipid interactions (described in detail below) result in the movement of GLUT4-containing vesicles (GSVs) from their intracellular location to the plasmalemma where the vesicles tether, dock and then fuse. In this way GLUT4 is delivered to its intended site of action, and glucose can enter the cell by passing down its concentration gradient.

GLUT4 translocation and subsequent glucose uptake also occurs following other stimuli such as muscle contraction, hypoxia and hypertonicity of the extracellular fluid (61-64). Whilst certain steps are shared between these mechanisms each should be considered distinct. The major focus of this study shall be on insulin-stimulated GLUT4 translocation.

1.3.2.1. GLUT4 knockout Mouse Models

The study of mice genetically engineered with relative, tissue-specific or global knockout of GLUT4 protein has provided confirmation of the key metabolic role played by this glucose transporter. Mice with global GLUT4 knockout show impaired insulin-stimulated glucose uptake, slightly impaired insulin sensitivity and only mild hyperinsulinaemia (65). There is no upregulation in any other glucose transporter in skeletal muscle or adipose, but GLUT2 expression is enhanced in the liver, which thus may provide enhanced glucose disposal. In contrast, mice heterozygous for GLUT4 knockout are severely insulin resistant, hyperglycaemic and hyperinsulinaemic (66) (which may be due to the developmental stage at which relative GLUT4 deficiency is established).

Muscle-specific GLUT4 knockout mice show substantially reduced global insulin-stimulated glucose uptake (67). Uptake is reduced in adipose tissue, insulin-mediated suppression of hepatic gluconeogenesis is impaired, and these mice develop hyperglycaemia and a diabetic phenotype. Interestingly, when diabetes is prevented with the use of an agent which reduces intestinal glucose uptake and renal tubular glucose reabsorption, adipose and hepatic responses normalise, indicating that glucotoxicity is responsible for impaired action of insulin in these tissues.

Adipose-specific GLUT4 knockout mice have normal growth and development (68). From around 13 weeks they develop hyperinsulinaemia, and glucose intolerance soon follows. Only a proportion develop frank diabetes (10%). As expected they have markedly reduced insulin-stimulated glucose uptake in adipose tissue, but also in muscle (in vivo, despite normal GLUT4 expression: ex-vivo muscle insulin sensitivity is normal) and liver. Circulating Free Fatty Acids (FFAs), TNF α , leptin, resistin and adiponectin are all within normal limits.

Thus, absent adipocyte GLUT4 promotes global insulin resistance; does increased adipocyte GLUT4 promote insulin sensitivity? This theory was tested when GLUT4 was overexpressed in the adipose tissue of GLUT4 muscle knockout mice (69). In this model the adipose-specific overexpression of GLUT4 rescued the diabetic phenotype previously described. Indeed, insulin sensitivity (as determined by hyperinsulinaemic euglycaemic clamp study) was improved when compared with wild-type levels. Given that GLUT4 expression and insulin sensitivity is increased with physical exercise (70), and reduced in the adipocytes of individuals with T2DM, (and their non-diabetic but insulin resistant first degree relatives) these studies support the idea that increasing GLUT4 delivery to the adipocyte plasma membrane in insulin resistant individuals may improve whole body insulin sensitivity (and therefore reverse insulin resistance), and thus represents a realistic therapeutic goal.

1.3.3. Insulin Signalling

1.3.3.1. Insulin Receptor

The insulin receptor (IR) is a plasma membrane-bound heterotetrameric glycoprotein composed of two α - and two β - subunits (linked by disulphide bonds) which are the product of a single gene (71). The IR is expressed in most mammalian cells studied, albeit at levels which vary by orders of magnitude (72), and is thought to exist as a homodimer at the plasma membrane of the classical insulin-sensitive tissues: skeletal muscle, adipose and liver. The IR shares homology with the Insulin-like Growth Factor Receptors (IGF-1 R and IGF-2 R) and the orphan receptor IR-R (Insulin receptor related protein), between which heterodimerisation is thought to occur. Together they form the IR / IGFR family of receptor tyrosine kinases, which bind insulin and the insulin-like peptides with differing affinities (reviewed in Nakae, 2001). Like the IR, signalling via the IGF receptors also has influence upon growth and metabolism. In spite of such overlap the IR remains the only unique element of insulin signalling upstream to its glucose uptake effects.

Individuals with mutation (including functional knockout) of the insulin receptor gene exhibit a phenotype which varies from mild insulin resistance to leprochaunism (73). In contrast, transgenic mice engineered to be heterozygous for deletions of the IR die in the early neonatal period

with hyperglycaemia and ketoacidosis (74;75). This demonstrates different regulation of fetal growth and development, and control of neonatal glucose metabolism between mice and man which is almost certainly the consequence of species differences in the function of IR / IGFR family signalling.

The key signalling role played by the IR is further confirmed by animal metabolic studies in which tissue-specific knockout of the IR has been achieved. Mice lacking the IR in liver (LIRKO) fail to suppress hepatic gluconeogenesis in response to insulin infusion, and subsequently become hyperglycaemic and hyperinsulinaemic with a phenotype resembling T2DM (76). Mice which lack IR expression in adipose tissue show decreased fat mass, normoglycaemia, normal circulating insulin concentrations, and have only slightly impaired insulin sensitivity (77). Despite the fact that most insulin-stimulated glucose disposal is achieved by skeletal muscle, mice genetically engineered to have skeletal muscle-specific IR knockout (MIRKO) show only mild hyperglycaemia and hyperinsulinaemia. Insulin-induced glucose uptake into skeletal muscle is reduced, however glucose uptake in adipose tissue is greatly increased in MIRKO mice. These mice become obese (with a visceral distribution) and exhibit dyslipidaemia reminiscent of T2DM (78). This apparent compensation of impaired skeletal muscle insulin action in adipose tissue reflects the complex interplay of insulin-mediated energy disposal and storage in different depots.

Upon insulin binding to the α - subunits a conformational change in the receptor activates kinase domains within the β - subunits. These activated kinase domains then auto-phosphorylate the receptor itself. This in turn results in activation of the ability of the receptor to bind and phosphorylate downstream effector proteins. Thus cascades of protein-protein interactions (principally further phosphorylation events) and protein-lipid interactions lead to the many downstream effects of insulin (reviewed in (79) and described below).

1.3.3.2. Insulin Receptor Substrate Family

The Insulin Receptor Substrate (IRS) molecules are central to the activation of insulin signalling. All 4 family members share the same basic structure of an amino terminal Pleckstrin Homology (PH) domain (80;81) followed by a Phospho-tyrosine Binding domain (PTB). The carboxy-terminal domain is composed of numerous serine and tyrosine residues.

IRS-1 (82) and IRS-2 (83) are recruited to the activated IR via the PTB domain and then rapidly phosphorylated (by the IR) on multiple sites within the carboxy-terminal domain (recently reviewed in (84)). This serves to provide binding sites which recruit further downstream effector molecules such as PI3K (see below), thus propagating the insulin-derived signal.

Transgenic mice engineered with global IRS-1 knockout are growth retarded and insulin resistant (85). IRS-1 knockout mice do not develop diabetes but can be shown to develop compensatory β -cell hyperplasia and hyperinsulinaemia. Further studies demonstrated that lack of IRS-1 was compensated by IRS-2 in the liver of these animals (86) but not in skeletal muscle or adipose tissue. This suggests a degree of functional redundancy between IRS-1 and IRS-2 in the liver, and implies a predominant role for IRS-1 in skeletal muscle and adipocytes. These findings are largely supported by studies of IRS-1 expression levels and phosphorylation status in obese humans and individuals with T2DM (reviewed in (87)).

IRS-2 knockout mice (88) are growth retarded and insulin resistant, developing diabetes in the first 10 weeks of life. There is failure of the compensatory β -cell hyperplasia and hyperinsulinaemia seen in IRS-1 knockout mice, alongside marked hepatic insulin resistance resulting in the diabetic phenotype which closely resembles T2DM. Together these data imply that the functions of IRS-2 predominate in the liver and β -cell.

IRS-3 (89) and IRS-4 (90) molecules are described in rodents. Whilst knockout studies reveal some influence on adipogenesis and glucose homeostasis (91), their precise role in conventional insulin signalling remains to be thoroughly determined and is not thought to be significant (92).

1.3.3.3. PI3K and PI(3,4,5)P₃

Class 1A Phosphoinositide 3-kinase (PI3K) is the first major effector molecule downstream of the IR in most insulin signalling pathways. This ubiquitous lipid kinase has been linked with anti-apoptotic, mitogenic and anabolic functions (93). The p85 regulatory subunit of this heterodimeric protein complex is recruited to the phosphotyrosine residues (generated by IR kinase activity) of the IRS molecules via its SH2 domains. This serves to both activate PI3K kinase activity (located in the p110 subunit) and bring the enzyme into close proximity with its catalytic target: phosphatidyl inositol 4,5- bisphosphate (PI(4,5)P₂).

The conversion of PI(4,5)P₂ to PI(3,4,5)P₃ is central to the downstream effects of PI3K. Inhibition of PI3K activity with the pharmacological agent Wortmannin prevents insulin-stimulated GLUT4 translocation (94-96), a result mirrored in studies where cells are transfected with dominant negative p85 subunit lacking the p110 binding motif (97) or the N-SH2 domain of p85 in isolation (98). Conversely, GLUT4 translocation is induced when cells are transfected with constitutively active p110 (99), and wortmannin's inhibitory effect on insulin stimulated glucose uptake is abolished in the presence of synthetic PI(3,4,5)P₃ esters (100). These reports affirm the key role played by PI(3,4,5)P₃, and it is this phospholipid species, when generated

at the plasma membrane which recruits the next step in the insulin signalling cascade.

Endogenous negative regulation of PI(3,4,5)P₃ exists in the form of type-II SH2-Domain containing inositol 5-phosphatase (SHIP2) and Phosphatase and Tensin Homolog Deleted on Chromosome 10 (PTEN). These phosphoinositide phosphatases convert PI(3,4,5)P₃ to PI(3,4)P₂ and PI(4,5) P₂ respectively owing to their 5' and 3' phosphatase activity (101).

Overexpression of wild-type PTEN in 3T3-L1 adipocytes reduces insulin-stimulated glucose uptake (102;103), whereas no effect is seen when the phosphatase-dead mutant form of PTEN is overexpressed (104). siRNA-mediated depletion of PTEN leads to enhanced basal and insulin-stimulated glucose uptake in 3T3-L1 cells (105). The same method used to deplete SHIP2 failed to influence insulin action in these cells (105), whereas the earlier study of transgenic SHIP2 knockout mice demonstrated improved insulin sensitivity, glucose tolerance and increased GLUT4 translocation in heterozygotes. Such data support the key role played by these enzymes in the modulating of polyphosphoinositide species at the plasma membrane.

1.3.3.4. PDK1 / AKT / PKC

The 3-Phosphoinositide-Dependent Protein Kinase-1 (PDK1) and Protein Kinase B (or AKT) are recruited to the plasma membrane by virtue of their Pleckstrin Homology (PH) domains (106) which bind specifically to PI(3,4,5)P₃. AKT requires phosphorylation at two specific residues for its activation: S473 and T308 (107). PDK1 was shown to be the upstream kinase for phosphorylation at residue T308 following its initial purification from rabbit skeletal muscle (108). The elusive S473 upstream kinase was eventually identified as the rictor-mTOR protein complex (109). Originally identified as the mammalian target of Rapamycin, mTOR is known to be central to a unique cellular signalling pathway that integrates nutrient, energy status and growth factor signals and so its intimate relationship with insulin signalling to glucose uptake is logical. Dysregulated mTOR pathway signalling is becoming increasingly apparent in human diseases such as diabetes and cancer (reviewed in (110)).

The role of activated AKT as a downstream effector of insulin was initially suggested by use of a dominant negative construct in L6 myotubes and 3T3-L1 adipocytes, where it was shown to induce glucose uptake without activation of PI3K (111-114). Subsequent studies of microinjection and growth factor response in 3T3-L1 cells and *ex-vivo* rat adipocytes (115), transgenic mice knockout models (116;117) and siRNA

mediated gene knockout in 3T3-L1 adipocytes (118) established that AKT2 (or PKB β) was the isoform which was most active in the insulin signalling cascade.

The third group of candidate effector molecules downstream of PI(3,4,5)P3 are the Atypical Protein Kinase C (119) isoforms (119). The role of aPKC isoforms appears to be tissue-specific: PKC ζ is the active isoform in muscle and PKC λ in adipose tissue and liver. Hepatic aPKC is a major determinant of hepatic lipid content and influences whole body insulin sensitivity (120). siRNA depletion of PKC in 3T3-L1 and L6 cells in culture abrogates insulin-stimulated glucose uptake (121). The roles of the aPKC isoforms in insulin action and insulin resistance are discussed in (119;122).

1.3.3.5. AS160

In spite of much research the precise molecules downstream of AKT2 leading to GSV translocation and glucose uptake remain elusive (107). One such target has been identified by immunoprecipitation (using an antibody specific for the phospho-motif generated by AKT within its putative substrates) and mass-spectrometry in 3T3-L1 cells (123). AKT Substrate of 160kDa (AS160) is a putative Rab GAP, and its phosphorylation at 5 distinct sites in response to insulin stimulation is required for maximal GLUT4 translocation (124) (only when the Rab GAP domain is intact). AS160 has also been implicated in both insulin-

stimulated and contraction-stimulated glucose uptake in skeletal muscle (125).

Rab proteins are the largest branch of the Ras superfamily of small GTP-binding proteins, and have been shown to play an important role in the regulation of vesicle traffic (126;127). They function as molecular switches, existing as GDP-bound inactive and GTP-bound active forms, and are believed to be key regulators of vesicle transport specificity (128). Furthermore, Rab proteins are known to integrate with many signalling pathways in diverse tissues, and individual isoforms are known to interact with effectors such as PI3K, AKT and PKC (129). Rab proteins have previously been implicated in GLUT4 translocation (127): rab4 (130); rab5 (131); rab11 (54), and more recently 3 Rab species (Rab 10, Rab 11 and Rab 14) were shown to be present on GLUT4 vesicles (132). In spite of this, none are known to interact with AS160, and the cognate AS160 Rab remains unknown.

Targeted disruption of AS160 using RNAi methods results in redistribution of GLUT4 from intracellular locations to the plasma membrane, and is associated with a corresponding increase in insulin-stimulated glucose uptake (40;132). The subsequent re-expression of AS160 restores GLUT4 translocation (and insulin-stimulated glucose uptake) to wild-type levels; this is not seen when a mutant with absent Rab-GAP activity is expressed (40). Furthermore, AS160 has been shown to associate with the Insulin Regulated Amino-Peptidase (IRAP)

when present on GSVs, and is released upon insulin stimulation (132). These data point to a role for AS160 (and its downstream effector(s)) in the basal intracellular restriction of GLUT4.

AS160 has recently been shown to interact with members of the 14-3-3 family of proteins in an insulin and AKT-dependent manner (133). 14-3-3 proteins are a highly conserved seven-member family (in mammals) which interact with phospho-residues in a variety of different proteins (>200 identified to date) in a multitude of cellular processes in all tissues studied (134). In spite of apparent specificity, the observed interaction of AS160 with all 7 of the 14-3-3 isoforms described, together with the promiscuity observed in subsequent downstream 14-3-3 interactions, implies that AS160 / 14-3-3 interaction is unlikely to reflect the major role for AS160 in insulin action. Whether AS160's interaction with 14-3-3 has influence over its GAP activity will not be determined until the elusive cognate AS160 Rab is identified.

1.3.3.6. PIKfyve

Another downstream target of AKT identified by an identical immunoprecipitation / mass-spectrometry technique is Phosphatidylinositol 3-phosphate 5-kinase (PIKfyve; (135). This mammalian homologue of the yeast Fab1p protein (shown to regulate late endosome to lysosome trafficking (136) was originally identified in adipose tissue and was shown to be present in skeletal muscle (137;138). PIKfyve is

composed of a PI3P-binding FYVE domain, a DEP (dishevelled, Egl-10 and Pleckstrin-Homology) domain of uncertain function alongside the PI3P 5-kinase domain.

PIKFyve was initially shown to exist predominantly in the cytosol, with a portion in the LDM fraction (discrete from GLUT4) and the PM. Some PM PIKFyve was found in detergent-resistant PM microdomains (lipid rafts; see 1.4.4 below). Subcellular distribution of PIKFyve was shown to be altered by insulin (139). Further elegant studies (135) demonstrated insulin and PI3K-dependent PIKFyve (S318) phosphorylation, revealed colocalisation of PIKFyve with a highly mobile subpopulation of GLUT4-containing vesicles which travelled from the PM region to the perinuclear region, and demonstrated increased GLUT4 delivery to the PM in cells transfected with S318A PIKFyve mutant. Together these data point to a role for PIKFyve in the regulation of GLUT4 subcellular distribution, which may be altered by insulin.

PIKFyve is one of two enzymes that have been proposed to be capable of generating PI(3,5)P₂ and PI(5)P. These lipid species (found at low level in mammalian cell membranes) are part of a 7-member family of phosphoinositides, which are believed to be key regulators of various signal transduction mechanisms (reviewed in (140;141)). The role of other phosphoinositide species in the regulation of insulin action is described in section 1.4.2.3 above. That PI(3,5)P₂ and PI(5)P are found in 3T3-L1

adipocytes at significant levels suggests that they too may also play a role in regulating insulin action.

1.3.3.7. The Alternative CAP / Cbl / TC10 Signalling Pathway

The activated insulin receptor recruits additional downstream effector proteins implicated in a second signalling pathway leading ultimately to glucose uptake. Originally identified as a PH domain-, and SH2 domain-containing gene using the yeast 2-hybrid screening technique in Burkitt's Lymphoma cells and implicated in signalling downstream of the B-lymphocyte antigen receptor (142), Adaptor Protein Containing a Pleckstrin homology and SH2-domain (APS) is an adaptor protein expressed in skeletal muscle, adipose and cardiac muscle which is recruited to the phosphorylated IR via SH2 domains (143;144). APS is itself tyrosine phosphorylated by the IR (143;144), which then allows recruitment of c-Cbl (Cbl), with which it forms a complex.

Cbl is a cellular homologue of a murine retroviral oncogene (145) which is implicated in a variety of cell signalling cascades (EGF, PDGF, integrins, cytokines etc.; reviewed in (146)). Cbl Associated Protein (CAP) is also recruited to the IR / APS / Cbl complex. By virtue of its binding to the lipid raft domain protein Flotillin (147), CAP recruits activated Cbl to cortical F-actin in PM lipid raft microdomains. This microdomain targeting is required for insulin-stimulated GLUT4 translocation (148).

Insulin is known to stimulate tyrosine phosphorylation of Cbl, which in turn allows Cbl to bind Crk (another cellular oncogene (149); (150). This interaction has been shown to be dependent upon APS (151). Recruitment of Crk also brings the guanine-nucleotide exchange factor C3G to the PM on account of their constitutive association (152). C3G catalyses exchange of GTP for GDP in a number of small G proteins, including TC10 of the Rho-family (153;154).

Rho-family GTPases are well known to regulate cellular actin dynamics (reviewed in (155)), and this property of TC10 is recognised in 3T3-L1 cells (156). Activation of TC10 within caveolae leads to recruitment of other molecules (discussed in (157)) which interact with the cytoskeleton, and the exocyst complex, both of which have been implicated in insulin-stimulated GLUT4 translocation. Reviewed by (158).

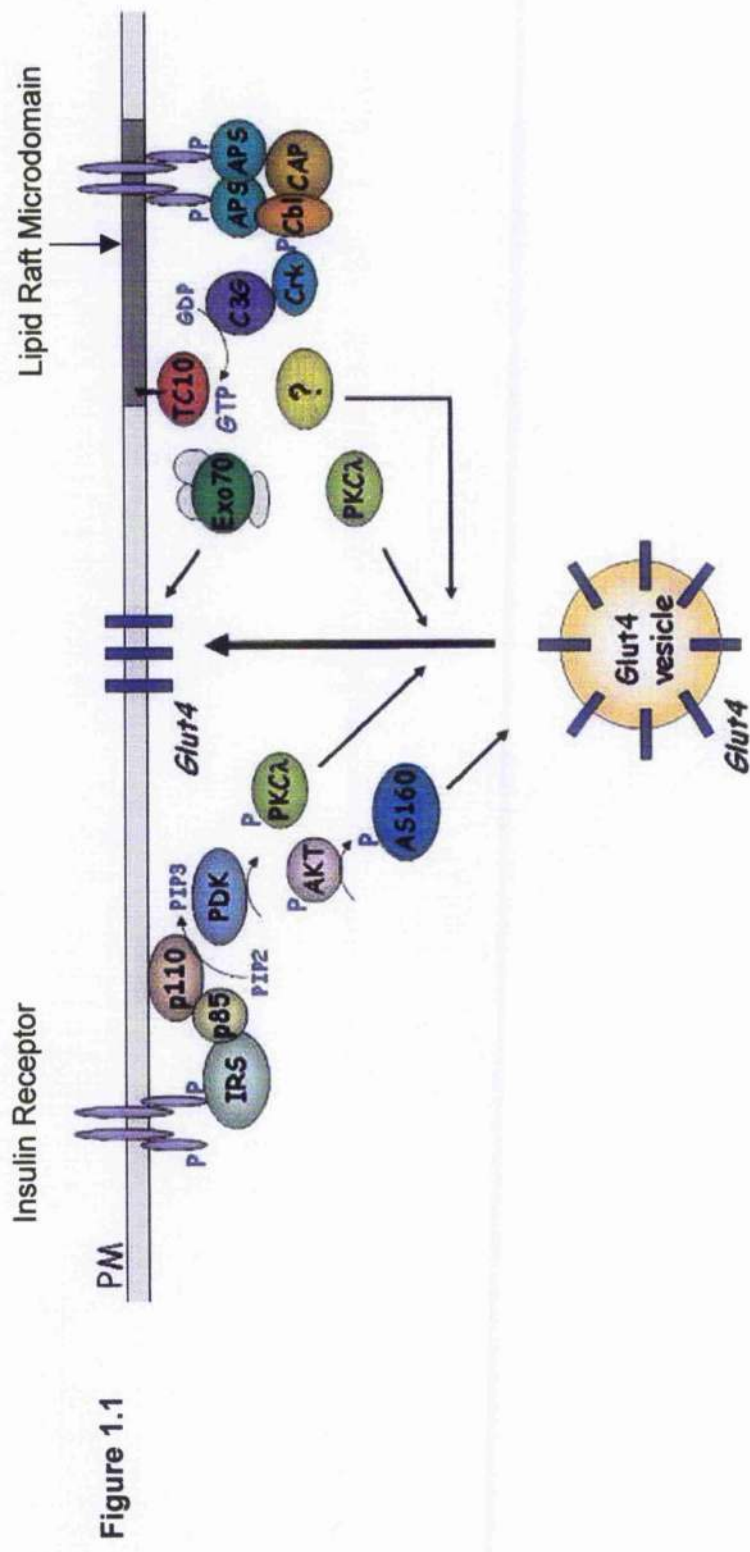


Figure 1.1

Figure 1.1: The Insulin Signalling Cascade (adapted from (158)).

IR= Insulin Receptor; PM= Plasma Membrane; PIP2= PI4,5,P2; PIP3= PI3,4,5,P3;

Exo70= exocyst complex; ?= unknown species

Evidence exists that challenges the alternative CAP / Cbl / TC10 pathway described above. APS deficient mice are more insulin sensitive than wild-type (159) and c-Cbl knockout mice have subsequently been shown to be more insulin sensitive than wild-type (160), the opposite phenotypes expected to that suggested by the alternative signalling pathway model. In direct opposition is the demonstration that siRNA-mediated depletion of Cbl, CAP and Crk had no effect on insulin-stimulated glucose uptake or labelled GLUT4 delivery to the PM in 3T3-L1 cells (161). The same authors observed that, at least in *ex-vivo* adipocytes, insulin-stimulated glucose uptake is identical in c-Cbl knockout and wild-type mice (compare with (160)). Furthermore, there are observed differences in the role of TC10 in the adipocyte and skeletal myocyte (162), and Cbl is not seen to be phosphorylated *in vivo* in response to insulin-stimulation (163).

Together, these data call into question the significance of the alternative pathway. Not until each step in this model is rigorously tested at the cellular, tissue or whole organism level will this issue be fully addressed.

A graphical model summarising the current pathways of insulin signalling to GLUT4 translocation is seen in Figure 1.1.

1.3.4. Subcellular Regulation of GLUT4 Trafficking

The finding that cell surface-labelled GLUT4 was rapidly internalised in unstimulated cells provides evidence that even in the basal state GLUT4 continually recycles between the PM and an intracellular location (164). By means of the complex signalling processes described above, insulin stimulation significantly increases exocytosis of GLUT4 vesicles (165;166) whilst also reducing the rate of internalisation of GLUT4 (167). The resulting net increase in cell surface GLUT4 (10 to 20-fold) is responsible for insulin stimulated glucose uptake.

Early experiments demonstrated glucose transporter activity cofractionated with markers of the Golgi apparatus (168). Subsequent more detailed subcellular analysis demonstrated the presence of GLUT4 in multiple membrane compartments within adipocytes and skeletal and cardiac myocytes (169) including sorting endosomes, recycling endosomes, the *trans* Golgi Network (TGN), and vesicles. The presence of GLUT4 within the endosomal compartments is reminiscent of other proteins (e.g.. the Transferrin Receptor (TfR)) which cycle between the PM and these intracellular locations in perpetuity. In skeletal muscle, cardiac muscle and adipose cells stimulation with insulin increases general endosomal to PM transport, resulting in delivery of many species including the TfR to the PM.

One important difference between these proteins and GLUT4 is that in the presence of insulin stimulation, the initial delivery of GLUT4 occurs at a much faster rate than that of the TfR (170). This, alongside observations that in unstimulated cells a significant quantity of intracellular GLUT4 is not located within the endosomal system (171), and that endosomal ablation failed to prevent insulin-stimulated GLUT4 translocation (172) suggests that GLUT4 is retained in a readily releasable pool outwith the endosomal system.

The TGN is known to play a role in the post-endosomal sorting and recycling of a subset of PM proteins (173). A significant fraction of GLUT4 is found in the TGN (20%), and an acidic motif at the carboxy-terminal has been shown to facilitate the transport of GLUT4 from the endosomes to the TGN (174). GLUT4 colocalises with Adaptor Protein 1 (175), a heterotetrameric coat protein which plays an important role in the genesis of vesicles which transport from the TGN, and the Cation-dependent Mannose-6-phosphate Receptor (CD-MPR). These molecules are known to traffic from the TGN back to the endosomal system, suggesting GLUT4 also recycles between these organelles (175).

The majority of intracellular GLUT4 is localised on vesicles (so-called GLUT4 Storage Vesicles or GSVs), which are responsible for the majority of the insulin-regulatable intracellular pool of GLUT4 (176). GLUT4 within these vesicles is discrete from the constitutively recycling AP-1 and CD-MPR described above (177;178). The GSVs contain

molecules such as IRAP, which is known to traffic with GLUT4, and the v-SNARE VAMP2, which participates in the delivery of GLUT4 to the PM (see 1.5.2 below).

Thus the current model of intracellular GLUT4 trafficking (as proposed by (179)) describes two continuous intracellular recycling pathways; the first between the PM and the endosomal system, and the second between the TGN and endosomes. Sorting occurring at the interface between the first and the second cycle would be the first step in the sequestration of GLUT4 into an insulin-responsive compartment. Once entered into the second cycle a further sorting step would be required to segregate the GLUT4 destined to become packaged into the specialised GSV pool, and GLUT4 not redirected in this way would be returned to the first cycle. Thus, PM GLUT4 in the basal state is largely derived from the first cycle. A schematic diagram of intracellular GLUT4 trafficking is seen in Figure 1.2 below.

Stimulation with insulin increases general endosomal trafficking, including the rates of both cycle 1 and cycle 2, but this would make only a minor contribution to the large upregulation of PM GLUT4 seen. Most apical GLUT4 in the insulin-stimulated state is due to GSV translocation to and subsequent SNARE-mediated fusion with the PM.

Figure 1.2

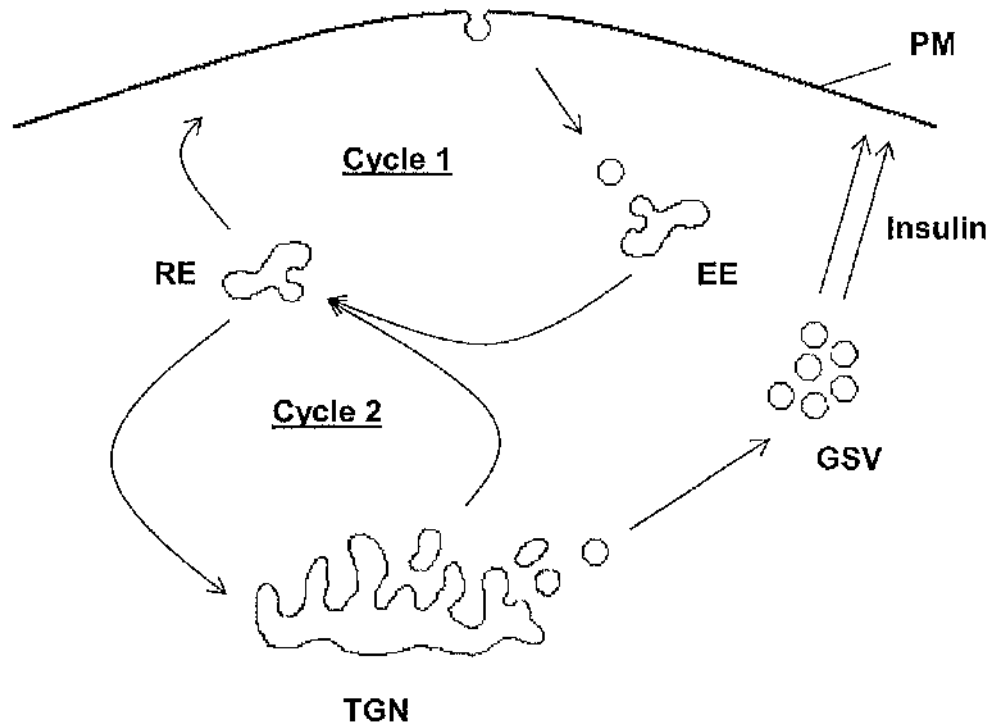


Figure 1.2 Schematic Representation of Intracellular GLUT4

Trafficking. In the basal cell GLUT4 continually cycles between the Plasma Membrane (PM), Early Endosome (EE) and Recycling Endosomal (RE) compartments (Cycle 1), and also between the RE and Trans-Golgi Network (TGN) (180). Sequestration from the TGN into the GLUT4 Storage Vesicle (GSV) compartment creates the insulin responsive GLUT4 pool, which is rapidly mobilised to the Plasma Membrane in response to insulin stimulation. Arrows indicate direction of trafficking.

1.4. The SNARE Hypothesis

Regulated Exocytosis, the tightly controlled process whereby membrane-limited cellular organelles fuse with the plasma membrane, governs a diverse array of cellular functions ((181;182) and Table 1.4 below). In all eukaryotic cells regulated exocytosis is controlled by SNARE (183) and SNARE-associated proteins (184). This well conserved group of membrane-tethered proteins possess conserved coiled-coil regions capable of specific interaction with cognate partners. Once located adjacent to the plasma membrane, the engagement of the v-SNAREs (185) and t-SNAREs (186) in a specific fashion to form a ternary complex (termed "docking") between the correct SNARE (and accessory) proteins allows the vesicle membrane and plasma membrane to come into close proximity, overcoming the energy barrier to membrane fusion (Figure 1.3). At this docking stage the involvement of further proteins (including Sec1-like and Munc18) contributes to the regulation of membrane fusion (reviewed in (187)).

Figure 1.3

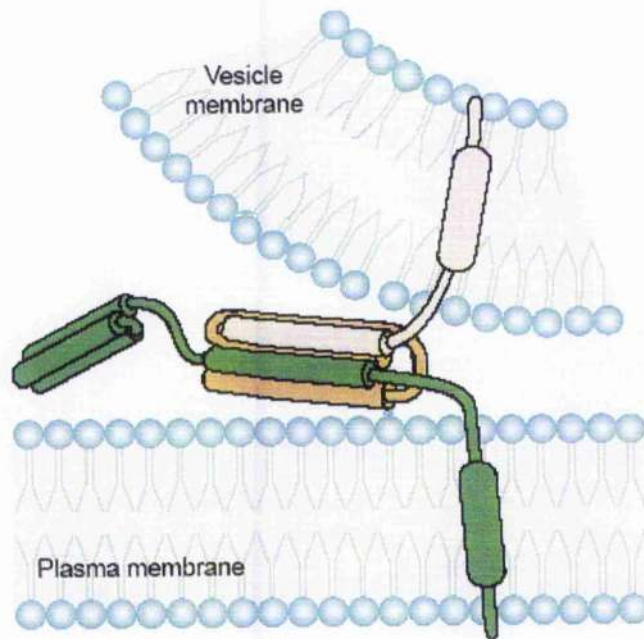


Figure 1.3 Schematic representation of the neuronal SNARE complex. VAMP (○), present on the vesicle membrane forms a 4-helix SNARE complex with Syntaxin (●) and SNAP (◐) located on the plasma membrane, bringing together the vesicle and plasma membranes, which ultimately fuse. Adapted from (188).

Classification of Regulated Exocytosis	
Secretory	Non-Secretory
Neurotransmission <hr/> Neurosecretory / Endocrine Cells <ul style="list-style-type: none"> • Adrenal • Pituitary 	Protein Translocation <ul style="list-style-type: none"> • Receptors • Channels • Pumps
Exocrine Glands <ul style="list-style-type: none"> • Pancreas • Breast <hr/> Macrophages / other immune cells	Membrane Donation <ul style="list-style-type: none"> • Cellularisation • Axon / dendron growth • Phagocytosis • Membrane repair

Table 1.4: Classification of Regulated Exocytosis

1.4.1. The Neuronal SNARE Complex

Neurotransmission depends upon SNARE-mediated fusion of synaptic vesicles with the presynaptic membrane, and is the best characterised example of SNARE-mediated regulated exocytosis. The neuronal SNARE complex is composed of the v-SNARE VAMP-2, and the t-SNARES Syntaxin-1A and SNAP-25 (184). That SNARE-complex formation occurs *in vitro*, followed by membrane fusion between vesicles

decorated with these SNARE proteins alone (189) suggests that no other species is absolutely required for cellular membrane fusion. The *in vitro* fusion occurs at a much slower rate than that observed *in vivo*, and many other proteins have been shown to interact with the SNARE proteins (190) thus influencing the speed of the reaction. Recently, post-translational modification of SNARE proteins, and especially phosphorylation (reviewed in (191) has been demonstrated to regulate SNARE complex formation and function. SNARE proteins and the SNARE protein complex are extensively reviewed in (192).

It has long been known that in neurons calcium is required to trigger exocytosis of synaptic vesicles (193) and that this calcium requirement reflects an important role for calcium ions in the formation of the ternary SNARE complex. It is envisaged that the SNAREs 'zipper-up' in a calcium-dependent manner, driving fusion (181). The calcium-sensing proteins involved at this step are known as synaptotagmins (SYTs) and function by binding the ternary complex and both the vesicular and presynaptic membranes (see 1.5 and Figure 1.6 below). Upon the arrival of calcium, a conformational change in the protein complex allows fusion of vesicle and target membranes and thus delivery of neurotransmitter to the cell surface.

1.4.2. SNARES Involved in GLUT4 Translocation

The identity of vesicles containing GLUT4 (194;195) moving to the plasmalemma of skeletal muscle and adipose cells in response to insulin stimulation (196) led to the analogy between this mechanism and that of neurotransmission being made. The resulting search for homologues of the neuronal SNAREs led to the identification of first VAMP-2 (197;198) and then Syntaxin-4 (195;199) in GLUT4-containing insulin responsive membrane compartments. The SNAP-25 homologue SNAP-23 was then described in rat adipocytes, was noted to bind Syntaxin-4 *in vivo* and to be capable of participating in an *in vitro* complex formation with Syntaxin-4 and VAMP-2 (200). The requirement for these species in insulin action was demonstrated by the reduction of insulin-stimulated GLUT4 translocation when their *in vivo* association is disrupted (201-203) or when the SNAREs are mutated to abrogate binding. Also, the study of ex-vivo human adipocytes taken from subjects with T2DM were shown to be docked but not fused with the plasma membrane (204), supporting the hypothesis that GSV-plasmalemma fusion is an essential step in both cellular and whole body insulin sensitivity.

1.4.3. The Role of Calcium in Insulin-stimulated GLUT4 Translocation

The role of calcium as the trigger for SNARE-mediated neuronal and neuroendocrine vesicle fusion is well established (see below and

(192). The role of calcium in insulin signal transduction or GSV-PM fusion in insulin sensitive tissues is less clear and has become the matter of much debate. The first studies of calcium in murine muscle cell line L6 myocytes (205), the murine adipocyte cell line 3T3-L1 (206), rat adipocytes (207), and rat cardiac myocytes (208) were universal in their conclusion that calcium played no apparent role. Around the same time results from independent experiments performed on rat adipocytes suggested that calcium played a permissive role in insulin action (209-211).

Upon further scrutiny, the techniques used in all of these systems to detect calcium concentration flux were rather crude; whilst sensitive to large changes in calcium concentration within the entire cell they would fail to detect small perturbations in local calcium concentrations such that would be expected to occur in a tightly-controlled physiological process. Along similar lines the ionophores and chelators used to influence intracellular calcium concentration would effect large whole-cell changes that would likely swamp normal physiology. Calcium is likely to exert its influence upon insulin action at one or more specific timepoints in the signal transduction pathway that are both temporarily and spatially limited within the cell. This is especially more likely in the case of skeletal muscle and cardiac muscle where intracellular calcium flux has a central regulatory influence over contractility and neuronal stimulation of contraction.

A more recent study in 3T3-L1 adipocytes provided strong evidence of a role for calcium in both insulin signal transduction and GSV-PM fusion (212). When a rapid calcium chelator was used insulin-stimulated AKT phosphorylation was reduced, and GLUT4 was present at the cytoplasmic but not the extracellular face of the PM (implying GSVs were docked but not fused). The implication is of a requirement for calcium at the final stages of GLUT4 translocation e.g. GSV-PM fusion.

Targeted knockout of Voltage-regulated Potassium Channel Kv1.3 has been shown to produce mice with lower body weight, resistance to diet-induced obesity and a significantly higher basal metabolic rate than their wild-type littermates (213). Intriguingly, pharmacological inhibition of the same channel improved peripheral insulin-sensitivity and apparently potentiated GLUT4 translocation in wild-type, obese and diabetic mice (214). The same group have recently reported a similar effect by toxin-mediated Kv1.3 inhibition in adipocytes and skeletal muscle (215). Inhibition of the Kv1.3 channel resulted in a wortmannin-insensitive increase in insulin-stimulated GLUT4 translocation. This increased GLUT4 translocation and glucose uptake was abolished by dantrolene, an agent which blocks the release of stored intracellular calcium. These data are in support of a requirement of calcium in insulin action downstream of PI3K.

Further evidence of a permissive role for calcium is provided by recently published work in which pharmacological modulation of non-

selective cation channels was used to influence insulin-stimulated glucose uptake in isolated murine muscle fibres and whole muscles from both normal and insulin resistant mice (216). The investigators report reduction in insulin-stimulated glucose uptake with reduced calcium influx, and increased insulin-stimulated glucose uptake with increased calcium. Interestingly there was no observed influence of either intervention over basal, hypoxia- or contraction-induced glucose uptake, and no observed changes in AKT phosphorylation. These data support a role for calcium downstream of AKT.

Thus three recent independent studies have produced robust data consistent with a requirement for calcium ions in insulin-stimulated glucose transport in sensitive cells. This requirement is downstream of PI3K or AKT, and may be at the level of GSV-PM fusion. The calcium can be derived from either intracellular stores or from inward flux from the extracellular space. Such a requirement for calcium suggests a calcium-sensing moiety is also required for insulin action: no such molecule has previously been confirmed to fulfil this role in any tissue studied.

1.5. Synaptotagmins

1.5.1. Overview

Synaptotagmin was initially identified as a 65kDa component of the neurotransmitter vesicle (217). Subsequent studies confirmed its ability to bind calcium (218) and its role in calcium-stimulated neurotransmitter vesicle fusion with the presynaptic axonal membrane. The highest level of expression of any SYT isoform is observed within the brain, and most of the published data describing SYTs is derived from studies of isoforms which participate in neural and neuroendocrine systems. Using high throughput expression profiling, transcripts of most SYT isoforms can also be detected in a variety of extraneuronal tissues (219) and particular family members have been assigned a key role in diverse biological processes (e.g., SYT1 and SYT2 in mast cells (220;221), SYT6 and SYT8 in the acrosome reaction (222), SYT7 in fibroblast membrane repair (223)). The precise role of most SYT isoforms outwith the neural and neuroendocrine systems remains largely unknown.

Each member of the SYT family of proteins shares the same basic structure (224): a single amino terminal transmembrane domain followed by tandem C2 domains (termed C2A and C2B) connected by a short linker region (Figure 1.6a and 1.6b). Constant Sequence 2 (C2) domains were originally described in Protein Kinase C, where they were shown to promote membrane localisation in response to binding of calcium ions

(225). This property was confirmed in SYTs during the initial work with SYT1, and was shown to be due to increased C2 affinity for phospholipids upon calcium binding (218). Subsequent studies have revealed variable SYT affinity for calcium, with some SYT isoforms unable to bind calcium at all (226;227).

1.5.2. Synaptotagmin Genetics

Genomic studies have revealed the presence of 16 highly conserved SYT genes in the higher eukaryotic genomes (228). SYT genes are located throughout the autosomes of both human and mouse genomes, and gene products are known to be translated from transcripts comprising 4- 11 exons (229). A similar (although not identical) intron position is observed within the coding sequence of family members (230;231), indicating a likely common ancestor. The transmembrane domain is always encoded by a single discrete exon, and splice variants resulting from transmembrane exon-skipping have been described for several isoforms (232;233). This suggests there may be an (as yet undefined) important physiological role for soluble versions of these normally membrane-bound proteins. Chromosomal location and gene structure for human and murine SYT1-15 is found in Table 1.5 below.

Splice variants resulting in altered molecular phenotype have been described for SYT1 (234;235), SYT7 (180;236) and SYT8 (237). Alternative transcripts are available in online databases for SYT2, SYT3

and SYT14 (229), although no corresponding functional data are published to date.

Synaptotagmins have been implicated in a variety of neurological and psychiatric diseases: SYT1 expression appears to be altered in certain brain regions in Alzheimer's disease (238) and Trisomy 13 (239), SYT4 knockout mouse has defects of memory and motor function (240), SYT4 and SYT11 are expressed in the substantia nigra and interact with proteins known to play a role in Parkinson's disease (241;242). Furthermore, SYT1 has been identified as key antigen in the paraneoplastic Lambert-Eaton Myaesthetic Syndrome (usually associated with small cell bronchial carcinoma) (243). Interestingly, the autoimmune myositis associated with the SYT7 knockout mouse is a similar phenotype (223). In spite of these disease associations no naturally occurring mutations or gene polymorphisms associated with human disease have been reported for any SYT family member.

Table 1.5

Isoform	Human		Murine	
	Chromosomal Location	Exons	Chromosomal Location	Exons
SYT1	12q21.2	11	10	11
SYT2	1q32.1	9	1	9
SYT3	19q13.33	11	7	10
SYT4	18q12.3	4	18	4
SYT5	19q13.42	9	7	8
SYT6	1p13.2	8	3	6
SYT7	16p12.3	8	19	13
SYT8	11p15.5	6	7	9
SYT9	11p15.4	7	7	6
SYT10	12p11.21	7	15	7
SYT11	1q22	4	3	4
SYT12	11q13.2	11	19	8
SYT13	11p11.2	6	2	6
SYT14	1q32.2	8	1	6
SYT15	11q2.2	7	14	8

Table 1.5 Chromosomal location and gene structure of human and murine SYT genes.

The transcriptional regulation of the SYT genes is in general poorly described in the literature. PDX-1, a transcription factor essential for pancreatic development and normal function (244) has been demonstrated to play a role in SYT1 expression in insulin-secreting cell lines (245). The promoter of SYT11 is known to possess a polymorphic 33bp repeat motif (246), increased copy number of which has been shown to result in increased expression of a downstream reporter gene. Cytosine residues on the coding strand of same gene promoter are known to be methylated (247). The same authors have demonstrated transcription factor binding to the promoter is reduced when residues are methylated, and reporter gene expression is subsequently reduced. The finding that the degree of SYT11 promoter methylation varies between tissues suggests this epigenetic phenomenon may play a role in regulation of SYT gene expression.

Comparison of the murine SYT protein sequences shows similarity between isoforms that can be attributed similar structure and function (78% alignment for SYT1 and SYT2, 61% alignment for SYT6 and SYT10). An alignment of 13% between the protein sequences of SYT9 and SYT14 is the lowest observed between any family members (Alignment of the murine SYT protein sequences is shown in Figure 1.4 below). The most highly conserved residues correspond to those amino acids with a key structural role e.g.. maintenance of the hydrophobic core of the C2 domains (248) whereas residues mapped to the surface of each

C2 domain are conserved only between related isoforms. Thus evolution of the SYT family has allowed conservation of domain structure (and by implication, function) whilst permitting the interaction of discrete family members with alternative effector molecules.

A cladogram of murine SYT protein sequences is shown in Figure 1.5 below.

Figure 1.4

```

Mus_byt1 -----ATE 3
Mus_syt2 -----MRNIFKRNQEPNVAPATTTATMPLAPVAPADNSTE 35
Mus_syt5 -----MFPE 4
Mus_syt8 -----MKMGHALN 8
Mus_syt6 -----MSGVWGAGGP-----RCQAAAVIATLSTCRA 25
Mus_syt10 -----MSFRKEDGVSS-----LCQKALHITTELCPA 26
Mus_syt9          AGRRRRAFSRARELPGAVRGC GGAMPGARDALCHQALQLLALCAR 44
Mus_syt3          -----MSGDYEDD-----LCRRALILVSDLCAR 23
Mus_syt7 -----
Mus_syt4          -----MAPITTSRVFDEIPT 16
Mus_syt11         -----MABITNTRPSPFVSPV 16
Mus_syt13         -----MVLSPVPVIALGATLGT 16
Mus_syt15         -----MAEQLAFLIGGIIGG 12
Mus_syt12         -----MAVDVTEYHLSVTKSPPGWEVG 25
Mus_syt14 MAIEGGERTCGVHELICIRKVSPEAVGFLSAVGVFIVLMLLFLFYINKKFCFENVGGFPD 60

Mus_syt1 PASPGEGKDDAF-SKLKQKFMNELHKIPL--PPWALIAIAIVAVLVVTCFCVCKKCL 59
Mus_syt2 STGPGESQEDMF-AKLKEKFFNEINKIPL--PPWALIAMAVVAGLLLTCFCCKKCC 91
Mus_syt5 PPTLQSP-----APKTPPDSRIRQGA---PAWVLATIVLGSGLLVFSSCFLYRKR- 54
Mus_syt8 PFSTAPLDATAGFSLIPDLITRIPSCAPGLGPRWLFIAIILAAGVLLVSCLLCVCCYC 68
Mus_syt6 RPFPLGLDVETCRSFELOQ-PEQSPSAADSGT'SVSLLAVVVIVCGVALVAVFLFVWKLK 84
Mus_syt10 G----QVWEDKCSG-IFPA-DRSGQGGGDTDISVSLAVVVSFCGLALLVSLFVWKLK 80
Mus_syt9 G----ALRHDSQDFTYHLRDRARPRLRDPDISVSLTLVVTACGLALFGVSLFVWKLK 100
Mus_syt3 VR--DADTNDRCQEFNELR-IRGYPRGPDADISVSLSVI'VTFPGIVLLGVSLFVWKLK 80
Mus_syt7 -----MYRDPBAASPGAPTRDVLVSAITTVSL-----VTIVL'CGLC 38
Mus_syt4 VVGIFSAFGLVFTVS--LFAWICQRRSAKSNKTPPYK'FVHVLVKGVDIYENLSSQKKEG 74
Mus_syt11 AAGLIGASV'LVVCSVTVFVWTCCHQQA'EKHKHTPPYKFIHMLKGLSIY'PETLSNKKKI 76
Mus_syt13 ATSILALCGV'TCLCRHMH'PKKGLLPRDREEDPEKAR'GVLQAAQ'QNIKKTE'PVQPRPL 76
Mus_syt15 LLLLCVSCCLWRRFCATYTYEELPETS'DPATISYPSR'KEDR'LYQYSGT'PPGR'LPSPV'PFV 75
Mus_syt12 VYAGALALLG'IAAVSLWKLWTSGS'FSPSPFP'PNYD'RYLQ'QKYGEAYVEAKLKR'VPPWN 82
Mus_syt14 LSGYNTRTNSQDKM'YNSYMDRDEPGSSSESEDEALGKYHEALSR'THNSRW'PLVDSR'QKS 120

Mus_syt1 FKKKNKKK-----GKE 70
Mus_syt2 CKKKKNKK-----EKG 102
Mus_syt5 CRRRMKKK-----SQA 65
Mus_syt8 HRRHRKQ-----PKD 79
Mus_syt6 WMPWRKK-----ASS-----PSSAN 100
Mus_syt10 WPCWKSCL-----VAPNLSVI-----PQSI 101
Mus_syt9 WVPWRERG-----LPSG-----SKDNN 117
Mus_syt3 WVPWRDKGSAVGGG'PLRKDLA'PGVGLAGLVGGG'CHL'GASLGGH'PLLGG'PHNHGHTA'HH 140
Mus_syt7 HWCQRKLG-----KRYK 50
Mus_syt4 GDDKSEVK-----GKTA 86
Mus_syt11 KVRDKDG-----PRRE 88
Mus_syt13 LKPPDIYG-----PRPA 88
Mus_syt15 VPPSHQGR-----DWWFL 88
Mus_syt12 DQRTTTRG-----PPSR 94
Mus_syt14 YAWETRQKYSP-----LSADY 136

Mus_syt1 KGGKNAINMKDVKDLG----- 86
Mus_syt2 KGMKNAMNMKDMK----- 115
Mus_syt5 QAQVHLQEVKELG----- 78
Mus_syt8 KETVGLGSARNST----- 92
Mus_syt6 PAPETLQSPSSRGNMA-----DKLKDPGALGFLEAAVKISHTSPDIPAEVQMSV-- 149
Mus_syt10 SAPTEVFETEEKKEVE-----ENEK--PAPKAIEPAIKISHTSPDIPAEVQ'FAL-- 148
Mus_syt9 QEPLNYTDFETNEQEN-----SEDELDPPTPCPSSMKISHTSPDIP'LTQ'PGG-- 166
Mus_syt2 PPFALLEPGLGGSE'PEPSYLD'WDSYFEAAVASVVAAGVK'PSQTSPEL'PSEGG'IGSGL 200
Mus_syt7 NSLETVGT'PDSGRGR-----EKKAIKL'PAG----- 76
Mus_syt4 LFNLSLHL'DLEKRDIN-----GNF'PKANPKAGSSSD----- 117
Mus_syt11 SGRGNLLINAESGLLS-----HKKDPRG'PSPAS'CMD----- 119
Mus_syt13 VTAP'EVINYADY'TLET-----TEESAAPAS'PQAQSDSR----- 121
Mus_syt15 HGGDN'AVAPQD'PCFVP-----EHMACTSS----- 112
Mus_syt12 KGLSIEDTFESI'SELG----- 111
Mus_syt14 DGYSTEASMEDGN'CIQR-----MRRTPPLDELQPPYQDSDSGS'PHLSCT'PSEIGDA 187

```

```

Mus_syt1 -----
Mus_syt2 -----
Mus_syt5 -----
Mus_syt8 -----
Mus_syt6 -----KEHIMRHTKIQRTTTPASSTRHTSPKRHLRQMHVSSVDY-----GNELPP 196
Mus_syt10  . . . . .KEHLIKHARVQRQTTEPTSSSRHNSFRRLRQMHVSSVDFSV-----GTEPIL 197
Mus_syt9   -----QKNCAMAVRVQRQVTEPTSPARHNSIR----RQLNLSNEDF-----NIQQL 208
Mus_syt2   LLLPSPGGGLPSAQSHQVTSLAPTRYPALRPLTQQTLLTQADPSTERRPPALPLPLP 260
Mus_syt7   -----GKAVNTAPVPGQTPHDESRRRT-----R 99
Mus_syt4   -----I 118
Mus_syt11  -----Q 120
Mus_syt13  -----L 122
Mus_syt15  -----
Mus_syt12  -----PLELM 116
Mus_syt14  KCEISHCSNSPRCSFNKCFSEGSTGHEAESYIIN-----KGYE 224

```

```

Mus_syt1   -KTKKDQALKDDDAETGLTDGR---FKKEPKKEERLQKLSLDYDFQANQLLVGI IQA 141
Mus_syt2   -----GQDDDDAETGLTEGEG---EGEESKEPENLQKLSLDYDFQANQLTVGVLQA 166
Mus_syt5   -----RSYIDKVQPEIRLDRSFSM-FGQQVSEKHLQGRQLQYSLDYDFQQLLVGILQA 132
Mus_syt8   -----THLVQPDVDCLEPCS-----GGEQQNGRLLLSLEDFGSSQHIRVGLRQA 137
Mus_syt6   AAAEQPTSIGRIKPELYKQKSVDG--DDAKSBAKSCCKINFLRYDYESTLIVRILKA 254
Mus_syt10  QRGETRTSIGRIKPELYKQKSVDS--EGNRKDDVKTCGKINFLALQYDYENLLVVKI IKA 255
Mus_syt9   QRQEQLTGIGRIKPELYKQKSLDN--DDGRRSNSKACGKLNFLKYDCDLBQLIVKI IKA 266
Mus_syt3   GGEEKAKLIGQIKPELYQGTGPGRRGGSSBAGAPCGRI SFALRYLYGSDHLVVRILQA 320
Mus_syt7   TRSSVSDLVNSLTSEMLMLSPGSEEDAEHGGCSRENLRGRIQFSVGYNFQESTLTVKVMKA 159
Mus_syt4   ENVTPEKLPETETKEANSPELKS-STSLTSEBKQKGLTFLSLEYNFEKAFVVMKEA 177
Mus_syt11  LPKRDYGBELRSPMTSLTPGESKPTSPSSPEEDVMLGSLTFSVDYNTPKKALVVTIQEA 180
Mus_syt13  KRQVTEELSIREFQNGVVEDVCVNETWNPKEAASWQAPKLFHFLDYDQKKAELFVPSLEA 182
Mus_syt15  AKPGDACEMGSINPELYKSPEDTS---ETGFPDGLGRLWFSVEYQCESERLLVGLIKA 168
Mus_syt12  GRRLDLAPYGLTKKSQSADSLNSISSVNTLFGQDFTLGQVEVSMYDGCASHTLHVAVLQ 176
Mus_syt14  DDVPSDSTAVLSPEDMSAQSSQLPKFPDPPEPEAKYGTLDVTFDYSERQKLLVTVTAV 284

```

```

Mus_syt1   AELPALD-MCGTSDPPYKVFLLPDK-KKKFETKVHRKTLNPNVFNQFTFK-VPYSELGGK 198
Mus_syt2   AELPALD-MCGTSDPPYKVFLLPDK-KKKYETKVHRKTLNPNVFNQFTFK-VPYSELGGK 223
Mus_syt5   QGLAALD-LGGSSDPYVSVYLLPDK-RRRHETKVHRKTLNPNVFNQFTFAFK-VPYVELGGR 189
Mus_syt8   GNLKA---EGTADPYAWVSVTQS-GRRHETKVHRKTLNPNVFNQFTFCFL-VPPAELPKA 191
Mus_syt6   FDLPAKD-FCGSDPPYKVIYLLPDR-KCKLQTRVHRKTLNPNVFNQFTFENPHFP-VPYEELADR 311
Mus_syt10  LDLPAKD-FTGTSDDPYKVIYLLPDR-KKKFQTRVHRKTLNPNVFNQFTFQFP-VYDQLSNR 312
Mus_syt9   VNLPAKD-FSGTSDPPYKVIYLLPDR-KTKHQTKVHRKTLNPNVFNQFTFVLEFP VHYNDLEAR 323
Mus_syt3   LDLPAKD-SNGFSDPPYKVIYLLPDR-KKKFQTKVHRKTLNPNVFNQFTFQFS-VPLAELAQ 377
Mus_syt7   QDLPAKD-FSGTSDPPYKVIYLLPDK-KHKLETKVHRKTLNPNVFNQFTFLEFEGFPYKVVQR 217
Mus_syt4   QGI PAMDRQSMISDPYIKMTILPEK-KHRVKTIVLRKTIIDPVFQETFTFYGTPYPHIQEL 236
Mus_syt11  HGLPVMDDQTCGSDPYIKMTILPDK-RHRVKTIVLRKTIIDPVFQETFTFYGTPYBQLQDL 239
Mus_syt13  VTSDEG---GDCYIQGSAVKTGSVEAQTALKKRQLHTTWEESGLALP-LGEEELPTA 227
Mus_syt15  QQLQVPS---ETCSILVKLHLLPDE-RRFLQSKTKHKICNPFQDENFIQ-VSSKSVTQR 233
Mus_syt12  KDLLERE-EATFESCFMRVSLPDE QIVGISRIQRNAYSIFPDEKFSVP-LDPTALEBK 233
Mus_syt14  TILPTYN-RIGGNSWQVHLVLLPDK-KQRAKTSTQRG-PCPVFTETFKFNHVESEMIGKY 341

```

```

Mus_syt1   TLVMAVYDFDRFSKHDIGEFKVP--MNTVD-----FGH-VTEE 234
Mus_syt2   TLVMAVYDFDRFSKHDIGEFKVP--MNTVD-----LGQ-PIBE 229
Mus_syt5   VLVMAVYDFDRFSRNDAGEVRVP--MSSVN-----LGR-FVQA 255
Mus_syt8   TIKVQLWDFKRFSEHEPLGELQDP--LGTVD-----LQH-VLES 227
Mus_syt6   XLHLSVDFDRFSRHDMEVILDNLFESD-----LSR-ETS I 349
Mus_syt10  KLHFSIYDFDRFSRHDMEVILDNLFESD-----LSR-EATV 350
Mus_syt9   KLHFSVYDFDRFSRHDMEVILDNLFESD-----FPR-ECIL 361
Mus_syt3   KLHFSVYDFDRFSRHDMEVILDNLFESD-----QPP-DRPL 415
Mus_syt7   VLXLQVLDYDFDRSRNDPIGEVSI P--LNKVD-----LTQ-MQTF 253
Mus_syt4   SLHFTVLSDFDRSRDDVIGVVIIP--LSGIE-----LSDGKMLM 273
Mus_syt11  VLHFLVLSDFDRSRDDVIGVVMVP--LAGVD-----PSTGKVQL 276
Mus_syt13  TLTLTLRTRCDRFSRHSVIGELRLG--LDGAS-----VFL-GAAQ 273
Mus_syt15  LKFSVYIIVNKKRKHQLLQVLEP LKNETL-----AGDHHRI I 261
Mus_syt12  SLRFSVFGIDEDERNVSTGVVLEK--LSVLD-----LPLQZFSG 270
Mus_syt14  AVRFRLYGVHRMKKFKIYVGEKIFYLTKLNLQKMSLPLVILEBSYVNSPGCDSQVLSLEASC 401

```

```

Mus_syt1 WRDLQSAEKEEQEKLGDICFSLRYVPTAGKLTVVILEAKNLKMKMDVGGLS--DPYVKIHL 292
Mus_syt2 WRDLQGGGKEEPEKLGDICTSLRYVPTAGKLTVCILEAKNLKMKMDVGGLS--DPYVKIHL 317
Mus_syt5 WRDLQVAPKEEQEKLGDICFSLRYVPTAGKLTVVILEAKNLKMKMDVGGLS--DPYVKVHL 283
Mus_syt8 WYQLGPPGTTPEPEQMGELCFSLRYVPSGGSLTVVILEARGLN----PGLA--EAYVKIQL 281
Mus_syt6 WKDLQYA-TSESVDLGELMFSLCYLPTAGRLTTLVIKCRNLKAMDITGYS--DPYVKVSL 406
Mus_syt10 WKDIHCA-TTESIDLGEIMFSLCYLPTAGRMTLTVIKCRNLKAMDITGSS--DPYVKVSL 407
Mus_syt9 WRDIEYV-TNDNVDLGBELMFSLCYLPTAGRLTITIKARNLKAMDITGAS--DPYVKVSL 418
Mus_syt3 WRDILEG-GSEKADLGBELNFSLCYLPPTAGRLTITIKASNLKAMDITGFS--DPYVKASL 472
Mus_syt7 WRDLKPC-SDGSGSRGELLLSLCYNPSANSIIVNIKARNLKAMDITGCTS--DPYVKVSL 310
Mus_syt4 TRELIKRNAKKSSGRGELLVSLCYQSTNTLTVVVLKARHLPKSDVSCLS--DPYVKVSL 331
Mus_syt11 TRDIKRNKIQKCLSRGELQVLSYQFVAQRMTVVVVKARHLPKMDITGLSC-NPYVKVAV 335
Mus_syt13 WQELKTTAKRPSAGAGFVIJISTSYIPAAANRLVVLTKAKNLHNSQSKELLGKDVSVKVTL 333
Mus_syt15 WRDLEAKNLEPPSEFGDIQFCLSYNDYLSRLTVVVLRAKGLQLQDQSRVSV--VFVKVSL 319
Mus_syt12 WLVLQDQ-NKAADAVGEILLLSLYLPTAERLTVVVKAKNLWTNPKSTA--DPYVKVYI 327
Mus_syt14 GDSTSSCQSLQHGVSPEILIGLLYNATTGRLSAEVIKGSHEKNLAANRPP--NTYVKLTL 459
      : : * : : : ** :

Mus_syt1 MQ-NGKRIKKKTTIKKNTLNPYNEFSFVEVPEEQIQKVQVVTVLDYDKIGKKAICK 351
Mus_syt2 MQ-NGKRLKKKTTVKKKTLNPFYNEFSFVEIPPEEQIQKVQVVTVLDYDKLGNKRAIGK 376
Mus_syt5 LQ-GGKKVRKKKTTIKKNTLNPYNEAFSFEVPECDQKQVQVELTVLDYDKLGNKRAIGR 342
Mus_syt8 ML-NQRKWKKKTSSKKGTTPYFNEAFVFLVPSQLQSVLVLAVWARGLQLRTEPVGK 340
Mus_syt6 LC-DGRRLLKKKTTIKKNTLNPVYNEALFDIPPENMDQVGLLISVMYDRVGHINEIGV 465
Mus_syt10 MC-EGRRLLKKKTTIKKNTLNPVYNEALFDIPPENVDQVSLCIAVMYDRVGHINEVIGV 466
Mus_syt9 MC-DGRRLLKKKTTSTKNTLNPVYNEALVFDVPPESIDQIHLSTIAVMYDRVGHINEVIGV 477
Mus_syt3 IS-EGRRLLKKKRTSISKKNTLNPYNEALVFDVAPRSVENVGLSIAVVEYDCIGHNEVIGV 531
Mus_syt7 MY-KDKRVEKKKTTVKKRNLNPIFNESEAFDIPTEKURETTIITVMEKDKLSRNDVIGK 369
Mus_syt4 YE-AKKRISKKKTTHVKCTPNAVFNELFVFDIPCESELEESVEFVLESEKRSRNEVIGR 390
Mus_syt11 YY-GRKRISKKKTTHVKCTLNPVYNEAFIYDIPDLDLSDISIEFLVIDFDRTTKNEVVGK 394
Mus_syt13 KI-QAKLKKKQTKRAKHKTNPVWNEVEMFELPDDLLRASSVELEVLGQGEESPCSELGH 392
Mus_syt15 MN-HNKFVKCKRTSAVLGVSVPVYNETFSFKVDTNELDTASLSLVLQTEGKNSKSPGK 378
Mus_syt12 LQ-DCKRMSKKTAVKRDENPVFNEAMIFSVFATVLDQLGLRVTVAESSDGRGDVVGH 386
Mus_syt14 I NSMGQEMSKKCTSTRGQPNVYKETFVVFQVALFQLSDVTLISLVYNNRRSMKRMKMG 519
      : * : : * : : : : * :

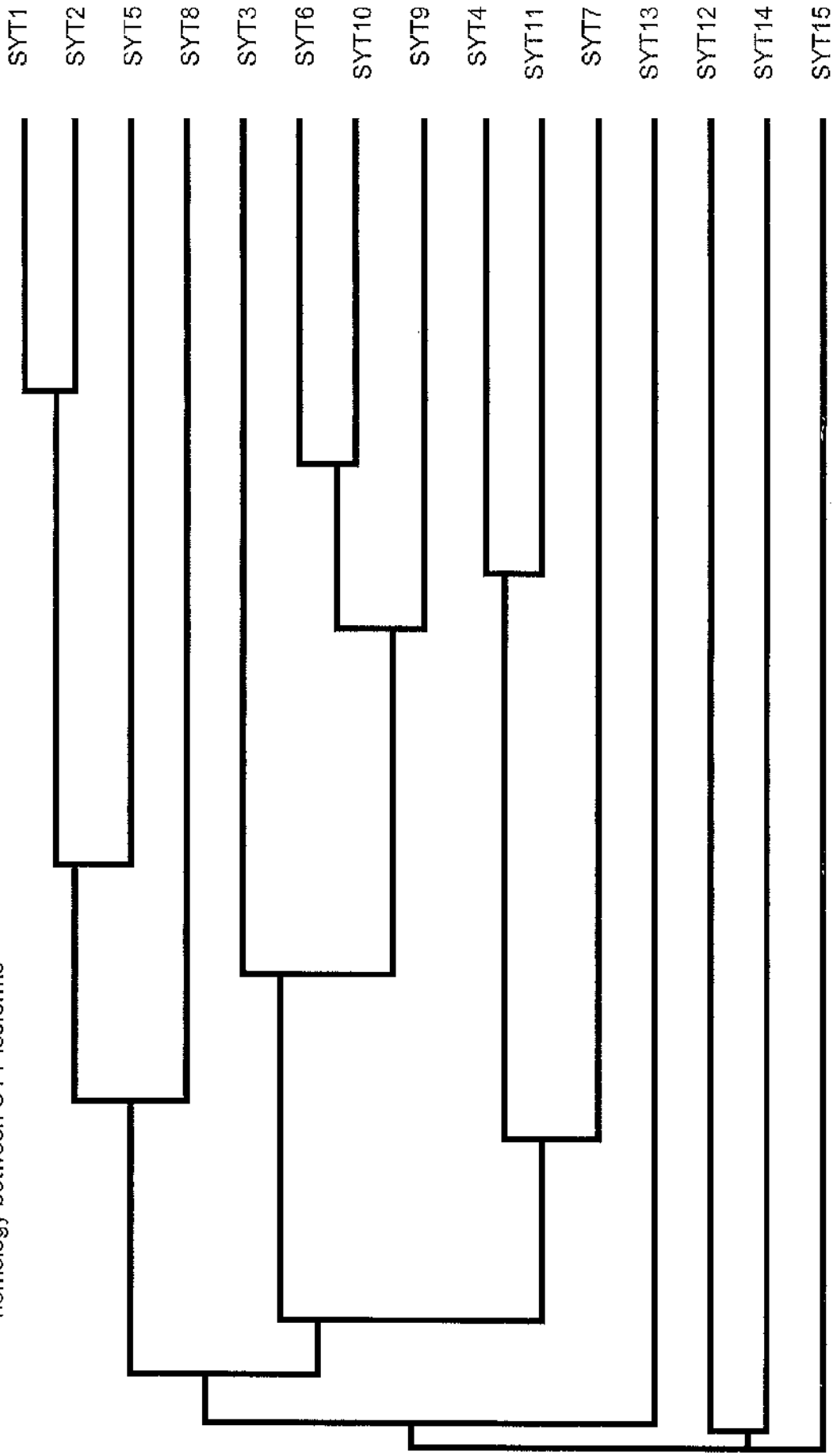
Mus_syt1 VFVGYNSTG--AELRIWSDMLANPRRPIAQWHILQVEEVDAMLAVKK----- 397
Mus_syt2 IFVGSNATG--TELPHWSDMLANPRRPIAQWHSLSKPEEVDALLGKKN----- 422
Mus_syt5 VAVGAAVGG--AGLRHWADMLANPRRPIAQWHSLSRPPDRARPIAP----- 386
Mus_syt8 VLLGSRASG--QPLQHWADMLAHARRPIAQWHSLSRPREVDRLALQFRLPLLRPS-- 395
Mus_syt6 CRVGINAEG--LGRDHWNEMLAYPRKPIAHWHSLSVEVK---KSFKEG---TPRL--- 511
Mus_syt10 CRTGLDAEG--LGRDHWNEMLAYHRKPIATHWHSLSLPLGFRATSPFDSQCSCSPRPESTP 523
Mus_syt9 CQVQNEAER--LGRDHWSEMLSYPRKPIAHWHSLSMEKR----- 513
Mus_syt3 CRVGPBAADP-HGREHWAEMLANPRKPEVHWHQLVRFKT-ISSFTKCKKCLSEKENSE 587
Mus_syt7 IYLSWKSQP--GEVVKIWKDMLARPRQVPAQWHQLKA----- 403
Mus_syt4 LVLGATAEG--SGGGHWKKEICDFPRRQIAKWHMLCDG----- 425
Mus_syt11 LILGAHSVTT-SGALHWKREVCSSPRKPIAKWHSLSBY----- 430
Mus_syt13 CSLGLHAGS--SERSHWBEMLKMPRRQIAMWHSLSL----- 426
Mus_syt15 VVVGPMYTRGKBLEHWGEMLRKPKELVKRWHALCRPEP----- 418
Mus_syt12 VIIGPGVGG--MGTTHWNQMLATLRRPVSMWHPVRRN----- 421
Mus_syt14 ISLGLNSSGE-EELRIWTAMKESKGGQVCRWHALLE----- 554
      * : : * :

```

Figure 1.4 Amino acid sequence alignment of murine SYT1-15.

Mus_syt1, Mus_syt2 indicate murine SYT 1, murine SYT2 etc.. * indicates an identical residue, : indicates a conserved substitution and . indicates a semi-conserved substitution. Sequence alignment performed using Clustalw software (249).

Figure 1.5 Cladogram derived from murine SYT protein sequences. Calculated using Clustalw software (249) indicating relative homology between SYT isoforms



1.5.3. C2 Domains

The structure of the C2A domain of SYT1 (the first C2 domain structure to be determined) is composed of a rigid 8-stranded structure of two 4-stranded β -sandwiches with protruding flexible loops which contain coordinating residues required for the binding of calcium (250). Upon binding calcium in the presence of phospholipid membranes, the tips of these coordinating residues are inserted into the lipid bilayer (251;252) (Figure 1.6c), which serves to further increase the avidity of calcium binding by providing negatively charged phospholipid headgroups to assist in the coordination of calcium ions (218).

Differences exist in the properties of distinct C2 domains. SYT1 C2A binds 3 calcium ions whereas C2B binds only 2 (253;254). Isolated SYT1 C2A interacts with calcium and phospholipid (phosphatidyl-serine and phosphatidyl-choline) bilayers as described above, but isolated C2B domains of SYT1 bind only weakly to phospholipids in the presence of calcium during *in vitro* assays (253). Soluble constructs containing mutant C2A domains (in which the calcium ligands are mutated) alongside wild-type C2B domains exhibited increased lipid binding compared to C2B domains alone (255) (256). These data indicate that cooperativity exists between the tandem C2 domains of SYT1, such that the affinity of C2B for phospholipid in the presence of calcium is increased by the presence of C2A.

Figure 1.6a

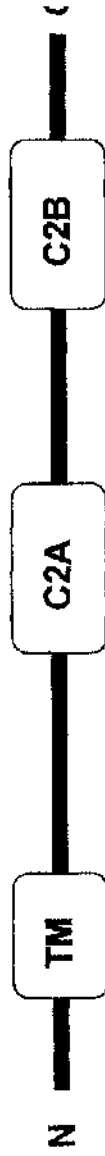


Figure 1.6b

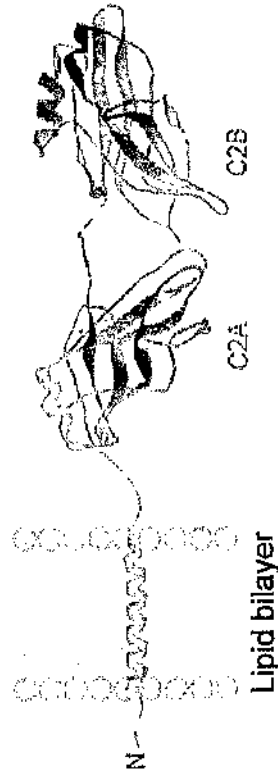


Figure 1.6c

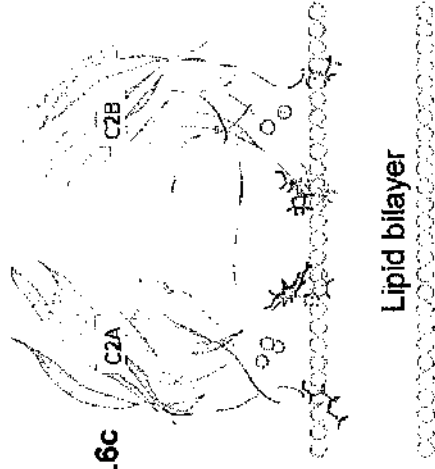


Figure 1.6: Figure 1.6a depicts a schematic representation of the structure shared by all members of the SYT family:

(N= amino-terminus; TM= Transmembrane Domain; C2A= C2A Domain; C2B= C2B Domain)

Figure 1.6b depicts a ribbon diagram demonstrating SYT domain organisation in relation to the lipid bilayer.

Figure 1.6c depicts calcium chelating residues (in yellow, green and blue) of C2 domains inserted into the lipid bilayer in response to calcium (257) (1.6a and 1.6b adapted from (188)).

Like the insulin signalling pathways described above, neurotransmission and neuroendocrine secretion depend upon the regulation of polyphosphoinositide species (258;259). SYT C2B domains have been shown to bind in inositol polyphosphates in a calcium independent manner via a 30 amino acid motif, whereas C2A binding to the same species is dependent on calcium (260). Subsequent studies confirmed that C2B bound polyphosphoinositide membranes (with variable specificity depending upon the presence of calcium) with only minimal contribution of C2A (261). Further work has shown that the presence of particular phosphoinositide species in a target membrane may act as physiological modulators of SYT calcium affinity (262). These data suggest a mechanism by which SYT species can integrate signalling cascades with depolarisation-induced changes in intracellular calcium concentrations to promote vesicle fusion.

In spite of variable calcium and phosphoinositide binding, overall C2 domain structure is highly conserved between different isoforms which possess differing biochemical properties, and across phyla (228), suggesting that loss of metal ion binding ability does not necessarily reflect loss of function.

1.5.4. SYT Interactions

1.5.4.1. SYT Oligomerisation

SYT can form oligomeric complexes (both homo- and hetero-oligomers) either dependent or independently of calcium. The calcium-dependent oligomerisation is mediated by residues in the C2B domain (263-265), whereas calcium independent self-binding depends upon residues present at the amino terminus, the region between the transmembrane domain and C2A, and the spacer region between C2 domains (266-268).

The function of SYT oligomerisation is unclear. The recruitment of additional SYT molecules to an assembled SNARE complex via calcium-dependent oligomerisation may drive fusion ; C2B mutations that abolish this property have been shown to impair SYT / SNARE complex formation *in vitro* and neurotransmission *in vivo* (269;270). It has been proposed that hetero-oligomerisation of SYTs *in vivo* resulting in the production of long multimeric complexes may function to bring together protein complexes present on opposing intracellular membranes, thus contributing to the specificity of membrane fusion events (271). Whilst it has been demonstrated that SYT isoform ratio can influence calcium dependency and formation of certain specialised neuroendocrine exocytosis intermediates (SYT1 and SYT4 and the fusion pore (272);

SYT1 and SYT4 and the choice between "kiss and run" and full fusion (273), this hypothesis is yet to be fully tested experimentally.

1.5.4.2. SYT - SNARE Interactions

The t-SNARE Syntaxin was initially identified in a coimmunoprecipitation experiment using an antibody against SYT1 (274) and as the target of an antibody raised against partially purified neuronal proteins (275). Subsequent study has confirmed the essential role for members of this protein family in functional (neuronal and extraneuronal) SNARE complexes (192). SYT binds with syntaxins in a calcium-dependent manner involving residues distinct from those which mediate phospholipid binding (276) within the C2A domain (277). The linker between the C2 domains also participates (278), reflecting further cooperativity between C2 domain function.

SYT also interacts with the other neuronal t-SNARE SNAP25 in a calcium-dependent manner. Indeed, calcium promotes SYT interaction with assembled Syntaxin / SNAP25 heterodimers, and a complex composed of both t-SNARES and Synaptobrevin (VAMP) (278). Elegant studies in which vesicle fusion is reconstituted *in vitro* have confirmed that SYT and the SNARE complex comprising t-SNARES Syntaxin and SNAP25 and v-SNARE VAMP represent the minimal protein requirement for calcium-dependent membrane fusion (185). Subsequent analysis of the SYT-SNARE complex interaction using Fluorescence Resonance

Energy Transfer techniques suggested that interaction between the C2B and linker domains of SYT and the membrane-proximal area of the SNARE complex facilitate their interaction (279). A schematic representation of the interaction between SYT and the SNARE complex is found in Figure 1.7.

SYT isoforms have been noted to interact with additional synaptic proteins. In support of their role in calcium-dependent neurotransmitter release SYTs interact with molecules that are known to influence voltage-gated calcium signalling such as neurexins and calmodulin (280). SYTs also interact directly with N-type (281) and P and Q-type calcium channels (282), an observation that seems logical if SYTs are to rapidly detect changes in intracellular calcium concentration.

The role of SYTs in endocytosis is established. Isoforms have been shown to directly interact with components of the endocytosis machinery including clathrin, stonin and stoned A and B (283-285). The detailed role of SYT in endocytosis is reviewed in (286).

Figure 1.7

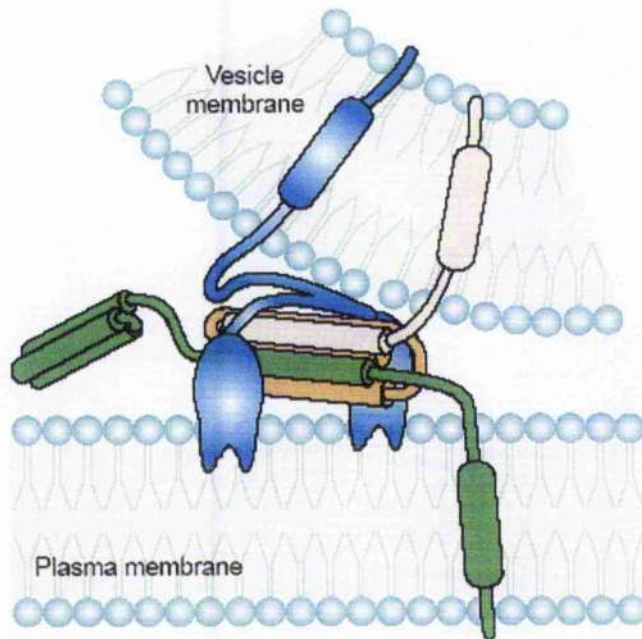


Figure 1.7 Schematic representation of SYT (●) interacting with the neuronal SNARE complex. Interaction between the C2 domains and linker domain of SYT facilitates the formation of the SNARE complex composed of VAMP (○), Syntaxin (●) and SNAP (○). Insertion of the tandem C2 domains of SYT into the plasma membrane subsequently drives PM-vesicle fusion. Adapted from (188).

1.5.4.3. Other SYT – Protein interactions

SYT function has also been linked directly to the cytoskeleton, with the observation that both C2 domains interact with tubulin in a calcium-dependent manner (287). Studies of SYT9 knockdown in a rat leukaemia cell line reveal reduced endocytic compartment to PM recycling. This observation, along with others which describe coimmunoprecipitation of tubulin with SYT9, and SYT9 colocalisation with the microtubulin organising centre (MTOC) imply a role for particular SYT isoforms in the regulation of intracellular vesicle transport via microtubules (288).

Using the yeast 2-hybrid screen followed by coimmunoprecipitation methods it was shown that SYT11 binds to and is ubiquitinated by the ubiquitin ligase Parkin (242). By virtue of this post-translational modification Parkin targets misfolded proteins to the proteasome for degradation, therefore ubiquitination may represent an additional mode of SYT regulation.

1.5.4.4. Phosphorylation

Examination of the amino acid sequences of all SYT isoforms reveals multiple potential phosphorylation motifs for a variety of distinct protein kinases, thus suggesting that SYT function could be at least in part regulated by phosphorylation. That SYTs are phosphoproteins *in vivo*

was first evidenced by immunoprecipitation of phosphorylated SYT from intact synaptic vesicles (289). SYT1 was shown to be phosphorylated on a conserved residue (T132) by casein kinase II (CaskII) (290), a protein family implicated in multiple diverse cellular roles. SYT1 was subsequently shown to be phosphorylated by PKC, CaskII and Calmodulin Kinase II (291) *in vitro* but not *in vivo* (PKC and CaMKII targeted T112; CaskII targeted T125 and T128). Due to the detection of endogenous SYT phosphorylated at T112 the authors suggested SYT phosphorylation by PKC and CaMKII could contribute to the regulation of vesicle fusion (292).

Further evidence in support of this theory is provided by observations that SYT2 coimmunoprecipitates With No Lysine Protein Kinase 1 (293). Phosphorylation of SYT2 by WNK1 alters the calcium-dependent actions of the C2 domains (293). Furthermore, PKC-mediated regulation of SYT6 C2B domain phosphorylation has been implicated in controlling the acrosome reaction (294). PKC has also been shown to regulate targeting of SYT9 to the endocytic recycling compartment (see 1.6.2.3 above). Thus it is likely further mechanisms of SYT regulation by the action of protein kinases shall be elucidated.

1.6. Aims of this Thesis

The studies described in this thesis aim to determine whether a particular SYT isoform(s) contributes to the regulation of insulin-stimulated glucose transport in the 3T3-L1 adipocyte.

Firstly the expression of the SYT genes shall be determined in 3T3-L1 adipocytes by Reverse Transcription PCR and compared with murine skeletal muscle and pooled human adipose cDNA. The relative expression of candidate genes shall be determined by Taqman Semi-Quantitative Reverse Transcription PCR and compared at various stages throughout differentiation. These experiments shall identify the predominant isoform expressed in the adipocyte and will guide further investigation.

The expression of the candidate SYT protein in 3T3-L1 adipocytes shall be confirmed, its subcellular location determined and subcellular trafficking in response to insulin demonstrated. siRNA shall be used to achieve targeted deletion of the candidate protein in 3T3-L1 adipocytes, and studies made of the resulting phenotype. The *in vitro* binding of the identified candidate with known members of the GSV SNARE complex shall be investigated.

In this way the contribution made by a SYT isoform to insulin-stimulated glucose uptake in the 3T3-L1 adipocyte shall be determined.

Chapter 2: Materials & Methods

2.1 Materials

High quality reagents were obtained from the following suppliers for use in analysis:

2.1.1 General Reagents

Amersham International Plc, Aylesbury, Buckinghamshire, UK

Horseradish peroxidase (HRP)-conjugated donkey anti-rabbit IgG antibody

Horseradish peroxidase (HRP)-conjugated sheep anti-mouse IgG antibody

ECL Western Blotting detection reagents

Anachem Ltd, Luton, Bedfordshire, UK

30% Acrylamide / bisacrylamide

BioRad Laboratories Ltd, Hemel-Hempstead, Hertfordshire, UK

N,N,N',N'-tetramethylethylenediamine (TEMED)

Boehringer Mannheim, Germany

Protease Inhibitor cocktail tablets, complete™

Protease Inhibitor cocktail tablets, complete™, Mini

Fisher Ltd, Loughborough, Leicestershire, UK

Ammonium Persulphate (APS)

Ammonium Sulphate

Calcium Chloride (CaCl₂)

Diaminoethanetetra-acetic acid, disodium salt (EDTA)

Disodium hydrogen orthophosphate (Na₂HPO₄)

Ethanol

Glucose

Glycerol

Glycine

N-2-hydroxyethylpiperazine-N-2'-2ethanesulphonic acid (HEPES)

Hydrochloric acid (HCl)

Isopropanol

Magnesium sulphate (MgSO₄)

Methanol

Potassium Chloride (KCl)

Potassium dihydrogen orthophosphate (KH₂PO₄)

Sodium dodecyl sulphate (266)

Sodium chloride (NaCl)

Sodium dihydrogen orthophosphate dehydrate (NaH₂PO₄)

Sodium hydrogen carbonate (NaHCO₃)

Sucrose

Trichloroacetic acid

Glaxo Smith Kline

Rosiglitazone

Kodak Ltd, Hemel-Hempstead, Hertfordshire, UK

X-Omat S Photographic film

Merck Ltd (BDH), Lutterworth, Leicestershire, UK

Magnesium Chloride (MgCl₂)

Tween 20

New England Biolabs (UK) Ltd, Hitchin, Hertfordshire, UK

Pre-stained protein marker, broad range (6-175kDa)

Novo Nordisk, Denmark

Insulin (Porcine)

Morrison's Grocers

Marvel powdered milk

Schleicher & Schuell, Dassel, Germany

Nitrocellulose membrane

Whatman International Ltd, Maidstone, UK

Whatman No.1 filter paper

Whatman No.3 filter paper

Whatman 3mm filter paper

2.1.2 Radioactive Reagents

Amersham International Plc, Aylesbury, Buckinghamshire, UK

2-deoxy-d-(³H)-glucose

¹²⁵I-Transferrin

2.1.3 Kits

Qiagen

Maxiprep™ DNA purification kit

Miniprep™ DNA purification kit

Qiaspin™ DNA purification kit

RNEasy™ RNA purification kit

2.1.4 Molecular Biology Reagents

Eurogentec, Brussels, Belgium

Taqman oligonucleotide primers

Taqman oligonucleotide probes

Taqman realtime PCR buffer

Taqman Hot Gold Star enzyme

Invitrogen

pAD-CMV-V5-DEST plasmid

pENTR 1A plasmid

pENTR D-topo plasmid

BL-21 *E. coli*

"Top 10" *E. coli*

"Mach-1" *E. coli*

Molecular Bio-Products

Certified DNase- and RNase-free sterilised PCR tubes

Promega

Restriction endonucleases

Restriction endonuclease buffers

Bovine serum albumin

Thermus Aquaticus (Taq) DNA Polymerase

Mg-Free Taq DNA Polymerase buffer

T4 DNA Ligase

T4 DNA ligase buffer

2.1.5 Tissue Culture Reagents

American Type Culture Collection, Rockville, USA

3T3-L1 fibroblasts

HeLa cells

HEK 293 cells

BioRad

Gene-Pulser II Electroporator

0.2cm Electrode Gap cuvettes

0.4cm Electrode Gap cuvettes

Dharmacon, USA

Dharmafect transfection reagent

Lamin A/C siGLO™ control siRNA

SMARTPOOL™ siRNA

Custom siRNA synthesis

Invitrogen

Lipofectamine 2000

Gibco, Paisley, Renfrewshire, UK

Foetal bovine serum (FCS)

Newborn calf serum (NCS)

Dulbecco's Modified Eagle's Medium (without sodium pyruvate, with
4500mg/l glucose) (DMEM)

Dulbecco's Phosphate Buffered Saline (D-PBS)

10000U/ml Penicillin, 10000U/ml Streptomycin

Trypsin/EDTA solution

Costar (Corning)

10cm cell culture plates

75cm² cell culture flasks

Falcon

10cm cell culture plates

20cm cell culture plates

6 well cell culture plates

12 well cell culture plates

24 well cell culture plates

15ml centrifuge tubes

50ml centrifuge tubes

Bibby Sterlin Ltd, Stone, Staffordshire, UK

Sterile pipettes

2.1.6 Cell Biology Reagents

Avanti Polar Lipids, Alabaster, AL, USA

1-palmitoyl 2-oleoyl phosphatidylcholine (POPC)

1,2-dioleoyl phosphatidylserine (231)

N-(7-nitro-2,1,3-benzoxadiazole-4-yl)-1,2-dipalmitoyl
phosphatidylethanolamine (NBD-DPPE)

N-(lissamine rhodamine B sulphonyl) 1,2-dipalmitoyl
phosphatidylethanolamine (Rhodamine-DPPE)

Sigma-Aldrich, UK

Accudenz^R

Lysozyme

Monoclonal ANTI-FLAG[®] M1 Antibody from mouse

Monoclonal ANTI-FLAG[®] M2 Antibody from mouse

Monoclonal ANTI-FLAG[®] M5 Antibody from mouse

2.1.7 Molecular Biology Buffers

TAE Buffer

2M Tris base, 50mM EDTA in 800ml dH₂O, pH to 8.0 with Glacial Acetic Acid, make up to 1l with dH₂O. Dilute 1:50 with dH₂O immediately prior to use.

2.1.8 Cell Biology Buffers

A200 Buffer

25mM HEPES, 200mM KCl, 10% w/v glycerol, 10mM DTT

Binding Buffer

150mM NaCl, 50mM Tris pH7.4, 0.5 w/v Tween-20

Coomassie Brilliant Blue

0.25g Coomassie Brilliant Blue (R250), 90ml 50% Methanol in H₂O, 10ml Glacial Acetic Acid

SDS-PAGE Electrophoresis Buffer

15.1g TRIS, 94g Glycine in 900ml dH₂O, 50ml 10% SDS

HES Buffer

20mM HEPES, 250mM Sucrose, 1mM EDTA, pH 7.4

KRP Buffer

1.28M NaCl, 47mM KCl, 50mM NaH₂PO₄, 12.5mM MgSO₄, 12.5mM
CaCl₂, Dilute 1:10, bring to 37°C, pH 7.4

Phosphate Buffered Saline (PBS)

136mM NaCl, 10mM NaH₂PO₄, 2.5mM KCl, 1.8mM KH₂PO₄, pH 7.2

Phosphate Buffered Saline / T (PBS-T)

136mM NaCl, 10mM NaH₂PO₄, 2.5mM KCl, 1.8mM KH₂PO₄, 0.02%
Tween-20, pH 7.2

Protein Transfer Buffer

48mM Tris, 39mM Glycine, 1.3mM SDS, 20% Methanol

Dilute 125ml in 875ml dH₂O and 300ml Methanol

2.1.9 Microbiology Media

2YT

16g Tryptone, 10g Yeast Extract, 5g NaCl, make up to 1 litre with dH₂O,
autoclave and store at 4°C until use

Terrific Broth

12g Tryptone, 24g Yeast Extract, 4ml Glycerol, 2.31g KH₂PO₄, 12.54g
K₂HPO₄, make up to 1 litre with dH₂O, autoclave and store at 4°C until
use

2.2 Methods

Molecular Biology Methods

2.2.1 Preparation of Murine Brain mRNA

A wild-type adult *Mus-musculus* laboratory mouse was euthanised by means of decapitation, the brain immediately dissected and removed and placed on ice in a sterile polypropylene tube. Once weighed, the brain was divided in the midline and each cerebral hemisphere processed separately. Following the instruction of the RNEasy (Qiagen) kit protocol, brain tissue was minced with a clean scalpel blade and disrupted by hand-homogenisation in the presence of lysis buffer (supplied with the kit). Cell membranes were disrupted by passing 5 times through a sterile 18G diameter needle attached to a sterile 5ml syringe. Total RNA was isolated by applying cell lysates to RNEasy (Qiagen) columns with strict cleanliness in order to minimise risk of nuclease contamination. All processing steps were carried out on ice and in a refrigerated centrifuge to prevent degradation of nucleic acids.

Once isolated, total brain RNA was quantified spectrophotometrically and immediately stored at -80°C .

2.2.2 Preparation of Murine Skeletal Muscle mRNA

Once euthanised, whole *Mus-musculus* hind leg musculature was immediately dissected and placed in a sterile polypropylene tube on ice. Further dissection on ice was carried out to remove any remaining neuronal or connective tissues. Murine skeletal muscle RNA was then isolated as for mouse brain RNA using RNEasy (Qiagen) columns, quantified spectrophotometrically and immediately stored at -80°C .

2.2.3 Preparation of RNA from 3T3-L1 cells

3T3-L1 cells were cultured and differentiated as described in plastic 10cm diameter tissue culture dishes. At the indicated timepoints (e.g. confluent fibroblasts, 2 days following differentiation, 4 days following differentiation etc.) dishes of cells were removed from the incubators and placed on ice. Culture media was removed by aspiration and cell lysis buffer (including RNase inhibitors) applied. Processing continued as for mouse brain RNA following the steps highlighted in the RNEasy (Qiagen) protocol. Once isolated, 3T3-L1 cell RNA was quantified spectrophotometrically and immediately stored at -80°C .

2.2.4 Human Brain mRNA

Human brain total RNA was a generous gift from Dr Scott Mackenzie of the Blood Pressure Laboratory, Division of Cardiovascular and Medical Sciences, University of Glasgow, Western Infirmary, Glasgow.

2.2.5 Pooled Human Adipose Tissue mRNA

Pooled Human Adipose Tissue RNA (Firstchoice Total RNA, catalogue # 7956, Ambion, Austin, TX, USA) was a generous gift from Dr Scott Mackenzie of the Blood Pressure Laboratory, Division of Cardiovascular and Medical Sciences, University of Glasgow, Western Infirmary, Glasgow.

2.2.6 Reverse Transcription of RNA into cDNA

Whole cell RNA samples were prepared as described. Synthesis of first-strand complementary DNA was carried out by incubating RNA samples with AMV Reverse Transcriptase (Promega) in the presence of an oligo d(T) (15) primer (Promega). Samples were kept on ice at all times to minimise degradation (unless otherwise stated).

In accordance with the manufacturer's instructions 0.5µg oligo d(T) primer per µg RNA was added to RNA in a sterile nuclease-free plastic tube. Nuclease-free water was added to a total volume of 10 µl per reaction. Samples were then heated to 70°C for 5 minutes in a PCR machine, placed on ice for 5 minutes and spun briefly in a centrifuge to ensure all contents collected at the bottom of the tube.

5µl 5X AMV RT Buffer (Promega), 10mM dNTP (10mM each dATP, dTTP, dCTP and dGTP) mix, 10 units AMV Reverse transcriptase (Promega) and nuclease-free water were then added to give a final reaction volume of 25µl (final concentration 50mM Tris HCl, 40mM KCl, 8.75mM MgCl₂, 10mM DTT). Reverse transcription of cDNA was performed at 42°C for 1 hour in a PCR machine, after which samples were immediately removed and kept on ice. DNA concentration was then determined spectrophotometrically and samples immediately stored at –20°C prior to analysis.

2.2.7 Polymerase Chain Reaction

In order to detect expression of each target gene, amplification of a specific section of the cDNA sequence was performed by Polymerase Chain Reaction (PCR). Gene specific oligonucleotide primers (Appendix 1) were synthesised by TAGN, Newcastle. All PCR reagents were kept on ice during preparation.

Into a sterile nuclease-free polypropylene tube were placed in order:

10x Mg-free Taq DNA Polymerase Reaction Buffer	5 μ l
25mM MgCl ₂	3 μ l
10mM dNTP mix	1 μ l
Forward Primer	2.5 μ l
Reverse Primer	2.5 μ l
Template cDNA	1 μ l
dH ₂ O	34 μ l
Taq DNA Polymerase	1 μ l

TOTAL VOLUME	50 μ l

Tubes were then spun briefly in a benchtop centrifuge to ensure all contents were at the bottom of the tube, then placed in a pre-set PCR machine.

The precise cycling conditions for each primer set depended upon the melting temperature (T_m) of the primers.

95°C	2 minutes	

95°C	15 seconds	
55°C	30 seconds	X 30
72°C	15 seconds	

72°C	5 minutes
4°C	<i>ad infinitum</i>

PCR products were analysed by agarose gel electrophoresis and images recorded by digital photography. To ensure amplification of the expected gene-specific target sequence PCR products were sub-cloned into pCR 2.1 plasmids and sequenced directly.

2.2.8 Agarose Gel Electrophoresis

PCR products, restriction enzyme digests and plasmid purifications were analysed by agarose gel electrophoresis. Percentage of agarose depended upon the expected size of DNA fragment (1% (w/v) for fragments >250bp, 2% (w/v) for fragments <250 bp).

Analytical-grade agarose was weighed on a digital balance and placed in a sterilised Pyrex conical flask. An appropriate volume of TAE buffer was added and the flask placed in a microwave oven and heated on "High" until all of the agarose was in suspension. With care, the flask was removed and cooled on the benchtop until hand hot with occasional agitation. Ethidium Bromide was added to the agarose suspension, which was then poured into the gel mould. A comb with an appropriate number and size of wells was placed in the still liquid agarose suspension, and the gel was left to solidify.

Once solidified the agarose gel was placed into a gel tank filled with TAE buffer, ensuring the agarose was covered, and the comb removed. Samples in DNA loading buffer were carefully pipetted into individual wells in the agarose alongside a DNA marker of an appropriate size and electrophoresed at 65 – 100V until individual DNA bands were resolved. DNA bands were visualised under UV light and recorded by digital photography. Images were stored as individual photographs and scanned into PC documents for presentation.

2.2.9 Taqman Semi-Quantitative Polymerase Chain Reaction

Taqman Realtime PCR was performed according to the manufacturer's instruction (Applied Biosystems, Foster City, California, USA). Primers and fluorogenic oligonucleotide probes were designed using the sequence of the RT-PCR products as template (Appendix 2). PCR reactions were performed in the ABI-prism 7700 Sequence detector, which contains a Gene-AMP PCR system 9600 (295). A total reaction volume of 25µl was used comprising 10mM Tris-HCl buffer pH 8.3, 1µl cDNA sample, 50mM KCl, 10mM EDTA, 200µM dATP, dCTP, dGTP and dUTP, 5mM MgCl₂, 300nM each primer, 200nM probe and 0.625 U Hot Gold Star Polymerase Enzyme (all Eurogentec, Seraing, Belgium). Each PCR amplification was performed in triplicate under the following conditions:

50°C

2 minutes

90°C	10 minutes	

95°C	15 seconds	
60°C	60 seconds	X 40 / 45
72°C	30 seconds	

4°C	<i>ad infinitum</i>	

Data analysis was performed using the Applied Biosystems Sequence Detection Software and results downloaded in Microsoft Excel format. GLUT4 expression was used as a positive control and samples were normalised against β -Actin mRNA.

Taqman realtime RT-PCR allows quantification of the initial amount of target template in comparison with a control (housekeeping) gene. In addition to gene-specific PCR primers a dual-labelled gene-specific oligonucleotide probe was designed to bind within each target amplicon (for both target and control genes), and synthesised with 5' FAM reporter and 3' TAMRA quencher dyes. Unbound, the transfer of FRET energy from reporter to quencher dye results in no probe fluorescence. As the reaction proceeds the 5'-3' exonuclease activity of the advancing polymerase enzyme digests labelled probe bound to template, and the FAM reporter fluorescence may be detected.

The strength of the observed signal is directly proportional to the amount of PCR product. By detecting fluorescence at the end of each amplification cycle it is possible to determine the cycle number at which a significant increase in the observed fluorescence is noted (Threshold Cycle or C_T). The C_T value is determined when the earliest exponential increase in reporter fluorescence above baseline (ΔR_n) is detected (linear phase of a logarithmic plot of Cycle number vs. observed fluorescence). The higher the initial amount of template, the lower the C_T value.

By comparing the C_T value obtained with a target gene with that obtained using the control gene it is possible to calculate the amount of initial template relative to the control template (247). The amount of target template is given by:

$$2^{-\Delta\Delta C_T}$$

where $\Delta\Delta C_T = C_T(\text{target}) - C_T(\text{control})$

For this calculation to be valid it is essential that the efficiencies of amplification of both target and control are identical. Efficiency can be determined by performing multiple amplifications using serial dilution of the same template and examining the gradient of the slope of log [template] vs. C_T . The gradient should be as close as possible to 0 (<0.1) (User Bulletin #2: ABI PRISM 7700 Sequence Detection System (295)).

2.2.10 Restriction Endonuclease Digestion

DNA to be digested was placed in a sterile microcentrifuge tube containing 1 unit of the appropriate restriction endonuclease in the appropriate manufacturer's buffer (with which it was supplied) with or without Bovine Serum Albumin. Digests were carried out at 37 °C for 3 hours on a PCR machine. In the case of double restriction digests an appropriate buffer (that permits >50% activity of both enzyme) was chosen as recommended by the manufacturer. If no such buffer was available digests were carried out individually. Following digestion, fragments were resolved by 1% Agarose gel (containing ethidium bromide) electrophoresis and visualised under UV light. If required for downstream cloning applications fragments were cut out of the gel using a sterile scalpel blade and purified using the Qiagen Qiaspin DNA purification kit.

2.2.11 Cloning Restriction Endonuclease Digestion Products into Plasmid Vectors

Both the plasmid vector and the insert were digested with compatible restriction endonucleases to ensure efficient cloning and gel purified using the Qiagen Qiaspin kit. For each cloning reaction two separate mixtures containing a 1:1 and 3:1 v/v insert to vector ratio were prepared.

To a sterile microcentrifuge tube were added 1 μ l 10x T4 ligase buffer, 1 μ l T4 ligase, 1 μ l digested vector, 1 μ l (or 3 μ l) digested insert and the volume was made up to 10 μ l with dH₂O (vector and insert both approximately 1 μ g/ μ l). Ligations were performed at 16°C in a PCR machine overnight. The following morning the entire ligation reaction was transformed into competent *E. coli*.

2.2.12 TA Cloning

TA cloning utilises the innate ability of *vaccinia* topoisomerase to bind to double stranded DNA at specific sites and cleave the phosphodiester backbone, resulting in its covalent 3' phosphotyrosyl attachment to the cleaved DNA, which is left with an overhanging deoxythymidine residue. TA vectors are supplied with topoisomerase covalently attached. PCR products produced by *Taq* polymerase possess a 3' deoxyadenosine residue which targets the deoxythymidine of the vector ensuring correct orientation of the insert. The phosphotyrosyl bond between the DNA and topoisomerase is cleaved, the enzyme is released and the phosphodiester bond between the deoxythymidine of the vector and the 3' residue of the insert completes the cloning reaction.

TA cloning reactions were performed as suggested by the manufacturer. 1 μ l of fresh PCR product (around 1 μ g) was added to a sterile microcentrifuge tube containing 1 μ l of TOPO vector and 4 μ l dH₂O. The reaction was incubated on the benchtop at room temperature for 5

minutes, then placed on ice. The entire reaction was then transformed into *E. coli* as described above.

Tissue Culture Methods

2.2.13 3T3-L1 Fibroblasts

3T3-L1 fibroblasts were cultured at 37°C in incubators generating a humidified atmosphere of 10% CO₂ in 75cm² flasks containing DMEM, 10% (v/v) Newborn calf serum and 1% (v/v) Penicillin and Streptomycin, replaced every 48h. At 80% confluency cells were passaged into culture plates and dishes of variable size alongside a further 75cm² carry-on flask. Cell culture proceeded until 4 days post-confluency when the fibroblasts were differentiated.

2.2.14 Passage of 3T3-L1 Fibroblasts

Cell culture media was aspirated from a 75cm² flask of 3T3-L1 fibroblasts and 1ml of trypsin / EDTA solution was added to remove residual media from the cells. Once removed by aspiration this was replaced by 3ml trypsin / EDTA solution and the flask incubated at 37°C in a humidified atmosphere of 10% CO₂ for 5 minutes. Gentle agitation and trituration allowed the cells to lift from the surface of the flask. This cell suspension was then added to an appropriate volume of DMEM containing 10% (v/v) Newborn calf serum and 1% (v/v) Penicillin and

Streptomycin and re-seeded onto cell culture plates and a further carry-on flask (with gentle agitation to ensure an even distribution of cells in all wells filled).

2.2.15 Differentiation of 3T3-L1 Fibroblasts

3T3-L1 fibroblasts were induced to differentiate into adipocytes by the addition of differentiation media containing DMEM, Foetal Calf Serum 10% (v/v), Penicillin and Streptomycin 1% (v/v), Porcine Insulin 1 μ g/ml, Dexamethasone 0.25 μ M and isobutyl-methylxanthine (IBMX) 0.5mM.

Dexamethasone was stored as a 2.5mM stock solution. A sterile 500x (55mg/ml) stock solution of IBMX was prepared by dissolving 0.055g in 1ml 1M KOH and passing the resulting solution through a 0.22-micron filter. 1 mg/ml Insulin was prepared in 0.01M HCl and also filter-sterilised by passing through a 0.22-micron filter.

Differentiation Media was prepared by the addition of 0.1ml 2.5mM Dexamethasone stock solution to 1.9ml DMEM. 0.2ml of the resulting 0.125M Dexamethasone solution was added to 5ml DMEM containing 0.1ml 1mg/ml Stock Insulin and 0.2ml Stock IBMX, and the resulting mixture was passed through a 0.22-micron filter into DMEM containing Foetal Calf Serum 10% (v/v), Penicillin and Streptomycin 1% (v/v) to a total volume of 100ml.

3T3-L1 fibroblasts were grown in tissue culture plates until 4 days post-confluency. Growth media was removed by aspiration and replaced with differentiation media. 48 hours later this was replaced with DMEM, Foetal Calf Serum 10% (v/v), Penicillin and Streptomycin 1% (v/v) and Insulin at 1 μ g/ml.

Once differentiated, 3T3-L1 adipocytes were cultured in a humidified atmosphere of 10% CO₂. 48 hours following insulin feeding and at 48 hour intervals thereafter media was replaced with DMEM, Foetal Calf Serum 10% (v/v), Penicillin and Streptomycin 1% (v/v).

2.2.16 HEK 293 Cells

HEK-293 Cells were cultured at 37°C in incubators generating a humidified atmosphere of 5% CO₂ in 75cm² flasks containing DMEM, 10% (v/v) Foetal calf serum, 5% L-Glutamine and 1% (v/v) Penicillin and Streptomycin, replaced every 48h. At confluency cells were passaged into culture plates and dishes of variable size alongside a further 75cm² carry-on flask. Cells were continually cultured regardless of passage.

2.2.17 Trypsinisation and Passage of HEK-293 Cells

Cell culture media was aspirated from a 75cm² flask of HEK-293 Cells and 1ml of trypsin / EDTA solution was added to remove residual media from the cells. Once removed by aspiration this was replaced by 3ml trypsin / EDTA solution and the flask incubated at 37°C in a humidified atmosphere of 5% CO₂ for 5 minutes. Gentle agitation allowed the cells to lift from the surface of the flask. This cell suspension was then added to an appropriate volume of DMEM containing 10% (v/v) Foetal calf serum, 5% (v/v) L-Glutamine and 1% (v/v) Penicillin and Streptomycin and re-seeded onto cell culture plates and a further carry-on flask (with gentle agitation to ensure an even distribution of cells in all wells filled).

2.2.18 Freezing and Storage of Cells

Cells were cultured until 80% confluent in a 75cm² tissue culture flask. After removing the media, cells were washed with 1ml trypsin/EDTA solution. This was replaced by 3ml trypsin/EDTA solution and the cells were then incubated for 5 min at 37°C in an atmosphere of 10% CO₂. Gentle shaking allowed cells to lose adherence to the surface of the flask and a further 3ml of DMEM with appropriate additives* were added to the resulting suspension, triturating to ensure no cells remained adherent. The suspension was then transferred into a sterile tube and centrifuged at

2000g for 4 minutes. After removing the supernatant the resulting cell pellet was resuspended in 1ml DMEM with appropriate additives* and 10% (v/v) DMSO. This suspension was then transferred into a 1.8ml cryovial and stored at -80°C overnight before being stored in liquid nitrogen.

- * -10% (v/v) Newborn calf serum in the case of 3T3-L1 fibroblasts
- 10% (v/v) Foetal calf serum and 5% L-Glutamine in the case of HEK293 cells.

2.2.19 Resurrection of Cells Stored in Liquid Nitrogen

A cryovial of cells stored in liquid nitrogen were removed and thawed at 37°C in a water bath. The thawed cell suspension was then transferred into a 75cm² flask containing DMEM, Foetal Calf Serum 10% (v/v), Penicillin and Streptomycin 1% (v/v) previously equilibrated at 37°C in a humidified atmosphere of 10% CO₂. The media was replaced after 24 hours and cells were cultured as previously described.

2.2.20 Transfection of Cultured Cells Using Lipid-Based Transfection Reagents

Cells were transfected using lipid-based transfection reagents (Lipofectamine 2000™ and Dharmafect™) as per the manufacturers instructions (Invitrogen and Dharmacon respectively).

Briefly, cells were grown in culture as described. On the day prior to transfection cells were incubated in appropriate media in the absence of antibiotics. Lipofectamine or Dharmafect lipid-nucleic acid complexes were prepared at room temperature in an appropriate volume as instructed and added to cells. Media was changed after 24 hours and cells were used 48 hours following transfection.

2.2.21 Transfection of 3T3-L1 Adipocytes by Electroporation

3T3-L1 cells grown in 150mm² cell culture dishes were differentiated as described above and transfected at day 5 post-differentiation. One dish per siRNA target was used. Cells were washed twice with 10ml Dulbecco's PBS (D-PBS) at room temperature then incubated at 37⁰C with 2ml of Trypsin-EDTA and 3ml of Collagenase (1 mg/ml in D-PBS). After a 10 minute incubation the dish was shaken gently until cells lifted off the surface of the dish. 10ml complete medium (DMEM, 10% FCS, 1% Penicillin / Streptomycin) was added to each dish, and cells were then transferred into a sterile centrifuge tube (with gentle trituration to ensure all cells were removed). Tubes containing cells in suspension were washed three times by spinning at 1200rpm for 5 mins in Beckman GP centrifuge at room temperature. At the end of each spin the pellet was gently resuspended in D-PBS. Following the final spin the pellet was resuspended in 0.65ml D-PBS per siRNA target and transferred to a sterile electroporation cuvette ready for electroporation.

siRNA was resuspended in RNase-free siRNA buffer (Dharmacon) to a concentration of 0.1mM and was kept on ice at all times. Immediately prior to electroporation the desired amount of siRNA was added to the cell suspension in each cuvette (20 nmoles per target) and mixed by gentle agitation. Cells were then electroporated in a Gene Pulser II (BioRad) Electroporator (voltage at 0.18 kV and Capacitance at 950 μ F) for 1-2 seconds.

1ml complete medium was then quickly added to each cuvette, and floating debris carefully removed. Cells were gently transferred into a centrifuge tube containing complete medium, and then reseeded in clean sterile tissue culture dishes (e.g. 1ml/well in 12-well plates for glucose uptake assays, 8ml per 10cm dish for preparing cell lysates).

Cell Biology Methods

2.2.22 SDS-Polyacrylamide Gel Electrophoresis

SDS / Polyacrylamide Gel Electrophoresis was performed using Bio-Rad mini-PROTEAN II apparatus. All reagents were of electrophoresis grade. Polyacrylamide concentrations varied in accordance with molecular weight of the target protein.

Separating gel was prepared using 30% acrylamide / bisacrylamide, 1.5M Tris-HCl (pH 8.8) (to a final concentration of 375mM), 10% (w/v) SDS (to a final concentration of 0.1%), polymerised with 10% (w/v) ammonium persulfate (to a final concentration of 0.1%) and TEMED (to a final concentration of 0.019%). Reagents were mixed in a sterile polypropylene tube, carefully added to the assembled Bio-Rad mini-PROTEAN II gel apparatus ensuring the absence of air bubbles, and covered with 0.5- 1ml isopropanol and left to set. The stacking gel was then prepared using 30% acrylamide / bisacrylamide, 1M Tris-HCl (pH 6.8) (to a final concentration of 125mM), 10% (w/v) SDS (to a final concentration of 0.1%), polymerised with 10% (w/v) ammonium persulfate (to a final concentration of 0.1%) and TEMED (to a final concentration of 0.05%).

Protein samples were prepared in 1X SDS-PAGE sample buffer (93mM Tris-HCl pH 6.8, 20mM dithiothreitol (added immediately prior to use), 1mM sodium EDTA, 10% (w/v) glycerol, 2% (w/v) SDS, 0.002% (w/v) bromophenol blue) and loaded into wells in the stacking gel. Broad range pre-stained molecular weight markers (Mw 6- 175kDa, New England Biolabs) were routinely used. Gels were electrophoresed in electrode buffer (25mM Tris, 190mM glycine and 0.1% (w/v) SDS) at a constant voltage (typically 80V to ensure optimal definition of protein bands).

2.2.23 Coomassie Staining of Protein Gels

During SDS/PAGE a 0.25% coomassie blue stain was prepared using 10ml glacial acetic acid, 90ml methanol: H₂O (1:1 v/v) and 0.25g Brilliant Blue R, filtered through a Whatman number 1 filter paper. The gel was submerged in the stain for 2hours and destained in an acetic acid, methanol:H₂O solution (prepared as above). Destaining was carried out between 3- 12 hours. Results were recorded by digital scanning and images stored as JPEG files.

2.2.24 Western Blotting

Once separated by SDS/PAGE as described proteins were transferred onto a nitrocellulose membrane either using a Bio-Rad mini or Bio-Rad trans-blot electrophoretic cell.

A multi-layered "sandwich" was assembled by placing in order two sheets of Whatman 3mm filter paper, nitrocellulose membrane (pore size 0.45mm), polyacrylamide gel and two further sheets of filter paper between two sponge pads. The filter paper and nitrocellulose membrane were cut to size and briefly equilibrated in transfer buffer (25mM NaH_2PO_4 , pH 6.5) prior to use. Care was taken to carefully eliminate any air bubbles found between layers of the sandwich. Transfer was carried out in the Bio-Rad mini apparatus at a constant current of 250mA for 3h or 40mA overnight in transfer buffer.

In the case of the BioRad trans-blot cell a "sandwich" of filter paper, nitrocellulose and polyacrylamide gel was prepared as above between the electrodes of the cell. Transfer was carried out at 180mA for 45 minutes or 50mA overnight.

2.2.25 Staining Western Blots with Ponceau S

Western blots were prepared as described. Before incubation with milk (see below) nitrocellulose membranes were incubated for 10 minutes in a 0.2% solution of Ponceau S in order to visualise the resolved proteins. This facilitated the subdivision of membranes to allow immunolabelling of proteins with different molecular weights from within the same sample with distinct antisera. The membrane was then washed repeatedly with PBS to remove all traces of the stain.

2.2.26 Immunodetection of Proteins

Once transferred onto nitrocellulose membrane, non-specific binding sites were blocked by incubation for at least 1 hour in 5% (w/v) skimmed milk in PBS-T buffer (20mM Tris, 150mM NaCl, 0.02% Tween-20, pH 7.4)

With care the membrane was then transferred into an appropriate receptacle with primary antibody (at variable dilution as indicated in each figure) in 0.5% skimmed milk and PBS-T, and incubated at room temperature for at least 2h with constant agitation. Then, following three washes in PBS-T buffer the membrane was incubated in a similar manner with an appropriate HRP-linked secondary antibody at 1:1000 dilution at room temperature for an hour. The membrane was then washed three times in PBS-T and once in PBS.

2.2.27 ECL Detection

An equal volume of "Detection Reagent 1" (Amersham) was mixed with "detection reagent 2" (Amersham) and used to incubate the washed membrane for 60 seconds at room temperature with constant agitation. After minimal drying the membrane was then carefully transferred onto transparent plastic sheet. The membrane was then used to expose

Kodak photographic film in a light-tight cassette, and the film developed in an X-OMAT processor.

2.2.28 Quantification of Signals

To determine signal strength developed film was digitally scanned onto a computer to generate a JPEG image file. Then, using Image-J software, band intensity was measured within an area of equal size around each signal. A background signal value was subtracted from each obtained value. Data were stored and analysed using Microsoft Excel Software.

2.2.29 Preparation of Cell Lysates

Cells were grown in culture as described. 500 μ l HPFE with 1% Thesit were added and the dish incubated at 4°C for 10 minutes, after which cells were scraped with a rubber policeman. The resulting solution was transferred to a clean, dry microcentrifuge tube and passed 10 times through a 20G needle attached to a 2ml syringe. This homogenate was spun in a benchtop microcentrifuge at 6000 RPM for 10 minutes at 4 °C. 4X SDS PAGE buffer were added to the resulting supernatant, and the lysates stored at -80°C prior to use.

2.2.30 The Insulin-Stimulated 2-Deoxyglucose Uptake Assay

3T3-L1 fibroblasts seeded and grown in 12-well tissue culture plates were differentiated as described (cells grown in 20 wells of 2 12-well plates were used for each experimental condition assayed). On the day before performing the assay adipocyte media was replaced with serum-free DMEM and cells cultured overnight. The following day tissue culture plates were transferred to heated plates at 37 °C, and the cells washed three times with KRP (pH 7.4 at 37 °C) to ensure all traces of media were removed. 500 µl KRP were added to each well.

To 4 wells of each experimental condition were added 50 µl KRP containing porcine insulin to give each quadruplet a final concentration of 0nM, 1nM, 10nM and 100nM respectively. Cytochalasin-B was added to 4 wells per condition to a final concentration of 20 µM (296). The cells incubated for 20 minutes with occasional gentle agitation.

After 20 minutes 50 µl 2-deoxyglucose solution containing ³H-2-deoxyglucose and cold 2-deoxyglucose were added to each well such that the final content per well was 0.25 µCi and 50µM cold 2-deoxyglucose. After a further 2 minutes the reaction was terminated by immersing the entire plate in ice-cold PBS. The plates were allowed to air-dry for at least 2 hours, after which 500 µl 1% Triton were added to each well. After a further 2 hours the resulting solution was transferred to

a clean scintillation tube containing 500 μ l scintillation fluid. These tubes were placed in an automated scintillation counter and read by liquid scintillation spectrophotometry.

2.2.31 Cell Surface Transferrin Receptor Estimation

3T3-L1 cells grown in 6-well tissue culture plates were differentiated and transfected with siRNA by electroporation as described above. Transferrin Receptor binding studies were performed approximately 36 hours following electroporation. For 2 hours prior to performing the assay cells were incubated in serum-free media. Cells were washed three times in ice-cold KRP containing 1mg/ml BSA (KRP/BSA). To three wells were added 1ml KRP/BSA containing 3nM 125 I-conjugated Transferrin, and to the parallel 3 wells on the same plate 1ml KRP/BSA containing 3nM 125 I-conjugated Transferrin and 10 μ M cold (i.e. not radioisotope-labelled) Transferrin. Cells were incubated on ice for 2 hours after which the media was discarded. Cells were again washed three times in ice-cold KRP/BSA to remove all traces of unbound transferrin.

The cells were then solubilised with 1ml 1% Triton for 1 hour and this solution was added to a clean scintillation vial containing 1ml scintillation fluid. These tubes were then placed in a γ -counter for assay.

2.2.32 Subcellular Fractionation of 3T3-L1 Adipocytes

Subcellular fractionation of 3T3-L1 adipocytes was performed as described (59;297). Briefly, 3T3-L1 cells were seeded in 10cm dishes, cultured, and differentiated as described in section 2.2.13- 2.2.15. On day 9 post-differentiation adipocyte culture media was replaced with serum-free media and the cells cultured overnight. For 30 minutes prior to commencement of the fractionation protocol cells were incubated with serum free media either alone, or with 100nM insulin.

The cell culture dishes were removed from the incubator and placed on ice. Cells were washed 3 times with 5ml ice cold HES buffer (with protease inhibitors). 2ml HES were added, cells were scraped using a cell scraper and homogenised with 10 up and down strokes of an appropriately sized Teflon homogeniser. The resulting cell homogenate was then transferred to chilled Oakridge centrifuge tubes and spun at 19 000 x g for 20 minutes at 4°C in a Beckman J2-21 centrifuge.

The resulting pellet was resuspended in 1ml ice-cold HES and carefully layered onto 0.8ml 1.12M sucrose in HES (sucrose cushion) and spun at 100 000 x g for 60 minutes at 4 °C in a TLS 55 swing-out rotor in a Beckman Optima TL benchtop ultracentrifuge. The resulting brown-coloured band (found at the interface between the sucrose cushion and the HES above) containing the plasma membrane fraction (PM) was

carefully removed using a 20g needle and 2ml syringe and resuspended in a 5-fold excess of HEPES/EDTA, and centrifuged for a further 60minutes at 4 °C in a fixed angle rotor in a Beckman Optima TL benchtop ultracentrifuge. The resulting pellet was resuspended in SDS PAGE buffer and stored at -80 °C prior to use.

The supernatant from the initial spin was transferred to clean Oakridge centrifuge tubes and centrifuged at 40 000 x g for 20 minutes in a Beckman J2-21 centrifuge at 4 °C. The resulting pellet containing High Density Microsomes (HDM) was resuspended in SDS PAGE buffer and stored at -80 °C prior to use. The supernatant was centrifuged at 180 000 x g for 60 minutes at 4°C in a TLA 100.4 fixed angle rotor in a Beckman Optima TL benchtop ultracentrifuge. The resulting pellet containing the Low Density Microsomes (LDM), SDS PAGE buffer was added to this and the supernatant containing the soluble proteins (SOL), and both were stored at -80°C prior to use.

***In vitro* Protein Binding Assays**

2.2.33 Pull Down Assays

GST Pull Down assays were performed using GST-tagged Syntaxin4, SNAP23 and VAMP2 immobilised on Glutathione Sepharose beads, and soluble SYT7 and SYT11 as “bait” either in binding buffer containing either 1mM calcium or 2mM EGTA. In each 150µl reaction

were 5 μ g of each tagged SNARE protein, and soluble SYT7 or SYT11 at a 0.5:1, 1:1 or 2.5:1 molar ratio.

Glutathione sepharose beads were washed in 3 x 1ml PBS (collecting the beads by centrifugation at 2500 rpm in a Beckman-Coulter Allegra X-12R centrifuge each time) before incubation with 5 μ g GST-tagged SNARE protein in binding buffer for 4 hours at 4 $^{\circ}$ C with constant rotation. Beads were washed again in 3 x PBS as before. Binding buffer with calcium or EGTA was then added, as was soluble SYT7 or SYT11 at the SNARE:SYT ratio indicated above. SYT / SNARE binding was permitted for 4 hours at 4 $^{\circ}$ C with constant rotation, after which time the beads were again washed in PBS (SDS-PAGE was added to the first supernatant i.e. binding buffer with either calcium or EGTA plus soluble SYT, which was later assayed by SDS-PAGE/Western blotting for unbound protein).

The beads were then resuspended in SDS-PAGE buffer and resolved by SDS-PAGE and analysed by analysed by Coomassie staining, or transferred to nitrocellulose for immunodetection.

2.2.34 Vesicle co-Floatation Assays

Vesicle co-floatation assays were performed as described in the online supporting material to (185). Purified epitope-tagged SNAP23, Syntaxin 4 and VAMP2 fusion proteins were prepared following

expression in *E. coli* or SF9-cells. v- and t-SNARE vesicles were prepared by rapid dilution and dialysis and subsequent purification by floatation in an Accudenz step gradient (as described in (189) and were a generous gift from Ms Fiona Brandie. v-SNARE vesicles comprised 82% 1-palmitoyl 2-oleoyl phosphatidylcholine (POPC), 15% 1,2-dioleoyl phosphatidylserine (231), 1.5% N-(7-nitro-2,1,3-benzoxadiazole-4-yl)-1,2-dipalmitoyl phosphatidylethanolamine (NBP-DPPE), 1.5% N-(lissamine rhodamine B sulphonyl) 1,2-dipalmitoyl phosphatidylethanolamine (Rhodamine-DPPE). t-SNARE (SNAP23/Syntaxin4 complex) vesicles comprised 85% POPC, 15% DOPS. Protein-free vesicles comprised 85% POPC and 15% DOPS.

40 μ l t-SNARE, v-SNARE or protein-free vesicles were incubated with 10 μ M Soluble SYT7 or SYT11 (lacking the TM-domain) in A200 buffer to a final volume of 70 μ l +/- 0.2mM EGTA or +/- 1.0mM CaCl₂ for 1 hour at 4°C with constant rotation. 70 μ l 80% Accudenz +/- 0.2mM EGTA or +/- 1.0mM CaCl₂ in A200 buffer were added in a sterile ultracentrifuge tube and the solutions mixed gently. This was overlaid with 1ml 30% Accudenz +/- 0.2mM EGTA or +/- 1.0mM CaCl₂ in A200 buffer followed by 1ml 5% Accudenz +/- 0.2mM EGTA or +/- 1.0mM CaCl₂ in A200 buffer. The resulting gradient was then spun at 46, 000 rpm in a Beckman Optima TL benchtop ultra centrifuge for 4 hours at 4°C. In the case of VAMP2 containing v-SNARE vesicles a visible coloured band was seen at the interface between the 30% and 5% Accudenz. The base of the centrifuge tube was carefully pierced using a sterile 20g needle. Fractions

were collected in a drop-wise manner, 4X SDS PAGE buffer was added and samples stored at -80°C prior to analysis by SDS-PAGE and Western Blotting.

Microbiology Methods

2.2.35 Transformation of Competent *E. coli* by Heat Shock

Chemically competent *E. coli* cells (purchased from Invitrogen) were thawed on ice for 10 minutes. 1µg plasmid DNA (or the indicated volume of cloning reaction) were added, mixed gently and incubated on ice for 30 minutes. The mixture was heat-shocked for 45 seconds by holding in a water bath at 42°C, then immediately placed on ice. 250µl SOC media at room temperature were added, and the tightly sealed tube (secured with tape horizontally on a 200rpm shaking platform within an incubator) was incubated at 37°C for 1 hour.

50µl and 150µl from the transformation reaction was spread on a separate prewarmed selective agar plate, and both were incubated at 37°C overnight. The following morning discrete colonies were selected as described below.

2.2.36 Preparation of Agarose Plates

2YT media was prepared as described in 2.1.9 above. Immediately prior to autoclaving 20g microagar was added. Following autoclaving the Agarose / media solution was allowed to cool until hand hot. Using aseptic technique the desired antibiotic (for selection purposes) was

added (Ampicillin to a concentration of 100 µg/ml; Kanamycin to a concentration of 50 µg/ml) and the solution poured into sterile 10cm microbiology plates and allowed to cool and solidify. Plates were stored at 4°C until use.

2.2.37 Selection and Overnight Culture of Transformed *E. coli*

Transformed *E. coli* were spread on an appropriate antibiotic-containing agarose plate and cultured overnight at 37°C as outlined above. The following day the resulting discrete clonal colonies were picked using a sterile micropipette tip and transferred into a sterile universal container containing 2YT media and the same antibiotic. This was again incubated overnight at 37°C. The following day plasmid DNA from the resulting bacterial suspension was purified using the Qiagen Miniprep Kit and analysed immediately or stored at -20°C.

2.2.38 Induction of Protein Expression

1ml of an overnight culture of *E. coli* transformed with a prokaryotic expression plasmid transformed with DNA encoding the gene of interest was used to inoculate 50ml 2YT media (with appropriate antibiotics) and grown overnight at 37°C. The following day the resulting cells were pelleted by centrifugation at 2500rpm for 10 minutes in a Beckman-Coulter Allegra X-12R centrifuge and resuspended in 1 litre of Terrific Broth (with appropriate antibiotics). This was grown at 37°C until the OD

reached the value previously determined to provide optimal protein expression (typically OD= 0.6- 0.8). IPTG was then added to a final concentration of 0.5nM and the culture continued overnight.

2.2.39 Purification of Epitope-Tagged Proteins

Protein expression was induced as described above. Following overnight culture cells were pelleted by centrifugation at 4000 rpm for 20 minutes in a Beckman-Coulter Allegra X-12R centrifuge at 4°C. From this point forward all steps were carried out on ice unless otherwise stated. The resulting cell pellet was resuspended in 50ml PBS containing protein inhibitor tablets. 1mg/ml Lysozyme was added and the suspension was incubated for 30 minutes at 4°C. Cells were broken by sonication for 3 x 20seconds with 20 second pauses. The broken cells were pelleted by centrifugation at 20 000rpm for 30 minutes in a Beckman centrifuge and a JA-20 rotor.

Meantime, 2ml Sepharose Beads labelled with the appropriate affinity tag were washed in 3 x 10ml PBS and 1% v/v Triton, collecting the beads by centrifugation at 2500 rpm in a Beckman-Coulter Allegra X-12R centrifuge each time. The cleared supernatant (containing the expressed protein) was incubated with the beads for 2 hours at 4°C with constant rotation after which the beads were again washed in 3 x 10ml PBS and 1% v/v Triton, collecting the beads by centrifugation at 2500 rpm in a Beckman-Coulter Allegra X-12R centrifuge each time.

Expressed protein was eluted from the beads by repeated (X 4) incubation with reduced glutathione (GST beads), reduced pH (Protein G Beads) or imidazole (nickel beads) for 5 minutes. The resulting protein fractions were then resolved by SDS-PAGE and analysed by Coomassie staining, or transferred to nitrocellulose for immunodetection.

Chapter 3: Synaptotagmin Expression in Murine Brain, Murine Muscle, Human Brain, Pooled Human Adipose and the 3T3-L1 Cells

3.1 Introduction

The role of the SNARE complex formed between VAMP2, Syntaxin-4 and SNAP-23 in the fusion of the GSV with the adipocyte and skeletal and cardiac myocyte plasma membrane is well established. As discussed in the introduction (1.3.8) there are conflicting data regarding the requirement for calcium in insulin-stimulated GLUT4 translocation, with convincing evidence emerging to suggest a role in the latter stages of GSV-Plasma membrane fusion in the 3T3-L1 adipocyte. To date the putative calcium sensor required to mediate such a requirement remains unknown.

In regulated exocytosis events in other tissues (e.g. neurotransmission, endocrine hormone secretion) the requirement for a member of the SYT family in governing the final fusion event between vesicle and plasmalemma is now universally accepted. Given that GSV-plasmalemma fusion represents a specialised form of regulated exocytosis, and the similarities described between all such events it remains possible that by facilitating GSV-PM fusion a particular SYT isoform may play an important role in mediating insulin stimulated

glucose uptake. To date there has been no published methodical investigation of SYT expression in peripheral insulin sensitive cells.

Reverse transcription PCR is an established method of determining the presence of a particular gene transcript in any given cell or tissue (i.e. whether or not the gene is expressed) and has previously been described for 3T3-L1 adipocytes (298). Taqman Realtime semi-quantitative PCR is a validated means of determining the level of expression of any given gene of interest (relative to the expression level a known constitutive or "housekeeping" gene (299)).

The 3T3-L1 murine fibroblast cell line is a standard tool in the study of insulin stimulated glucose uptake. 3T3-L1 cells grown in culture can be induced to undergo differentiation (by the addition of insulin, dexamethasone and IBMX) into mature insulin-sensitive adipocytes. The resulting phenotype produced whilst not indistinguishable, is remarkably similar to that of ex-vivo rodent or human adipose cells: 3T3-L1 adipocytes express GLUT4, which is upregulated to the PM in response to insulin, facilitating insulin-stimulated glucose uptake (300;301).

In this chapter the murine synaptotagmin genes expressed in skeletal muscle and 3T3-L1 cells, and the human synaptotagmin genes expressed adipose tissue shall be determined by Reverse Transcription PCR and compared. Using Taqman Semi-quantitative Realtime PCR the relative expression (to β -actin) of the expressed synaptotagmin

complement of 3T3-L1 cells shall be established during differentiation from fibroblast to adipocyte. In this way the comparative importance of any particular isoform expressed can be inferred, with the expectation that upregulation in expression of any candidate gene will coincide with acquisition of insulin sensitivity.

3.2 Methods

3.2.1 Synaptotagmin Gene-specific Nucleotide Sequences

The US National Centre for Biotechnology Information (NCBI) Genbank Database was interrogated using the search term "Synaptotagmin". All resulting murine and human sequences corresponding to part- or full-length synaptotagmin cDNA or mRNA were selected. Using Gene-Jockey software running on an Apple Power Macintosh 6500 PC species-specific sequences for each individual synaptotagmin isoform were compared, and the open reading frame identified. Genbank accession numbers for each published SYT sequence used are listed in TABLE A1 the Appendix. The human SYT9 sequence was not published at the time these sequences were identified (human SYT9 sequence subsequently published 2004).

3.2.2 Synaptotagmin Gene-specific Oligonucleotide PCR

Primers

18-mer oligonucleotide PCR primers were designed to amplify a 200 to 300bp fragment of each synaptotagmin isoform from the full open reading frame sequence identified in 3.2.1. Where possible, primers were designed to have T_m of around 55°C, identical GC content and to have two purine residues at the 3' end to assist in DNA polymerisation initiation. Primer sequences were compared with the published mouse or human transcriptome sequence using the NCBI Basic Local Alignment Search Tool (302) to ensure species and sequence specificity for each isoform. Where splice variants were known (e.g. SYT7) PCR primers were designed to amplify a PCR product with each variant that would be easily identified by virtue of product size. PCR primer sequences are listed in the Appendix.

It should be noted that although these primers were not originally designed to be intron-spanning further analysis has revealed that all primer pairs are indeed intron-spanning except those for SYT4, SYT9, SYT10, SYT12 and SYT14. The location (corresponding exon) of each primer is given in table A2 in the Appendix.

3.2.3 Synaptotagmin Gene-specific Oligonucleotide Taqman Realtime PCR Primers and Oligonucleotide Probes

21-mer oligonucleotide PCR primers and 18-mer oligonucleotide probes were designed to amplify a fragment of around 120 bp for each candidate synaptotagmin isoform from the full open reading frame sequence identified in 3.2.1. Primers were designed to have T_m of 55°C and designed to yield products that span intron-exon boundaries. Primer and probe sequences were compared with the published mouse transcriptome sequence using the NCBI Basic Local Alignment Search Tool (72) (302) to ensure specificity for each isoform. Where splice variants were known (e.g. SYT7) PCR primers were designed to amplify a PCR product from template sequence common to all variants. PCR primer and oligonucleotide probe sequences are listed in the Appendix.

3.2.4 Murine Control cDNA

Most synaptotagmin isoforms are known to be expressed in brain. RNA was isolated from the brain of a euthanised wild-type *Mus musculus* lab mouse using the Qiagen RNEasy™ Kit following the manufacturers instructions. cDNA was reverse transcribed as described in Chapter 2 (2.2.1.5). PCR reactions (2.2.1.6) were optimised using brain cDNA template, which was then used as a positive control for subsequent test reactions. PCR products were TA-cloned and subsequently sequenced to ensure specificity of amplification.

3.2.5 Human Control cDNA

Human brain cDNA was a generous gift from Dr Scott MacKenzie. Human Testis cDNA Library was a generous gift from Dr Andrew Fielding. PCR reactions (2.2.1.6) were optimised using either Brain or Testis cDNA template, which was then used as positive control for subsequent test reactions.

3.2.6 3T3-L1 Cell cDNA

3T3-L1 cells were grown in 10cm culture dishes and differentiated as described in Chapter 2 (2.2.2.1-3). RNA was isolated at confluent fibroblast stage and at 2 day intervals to day 14 post-differentiation using the Qiagen RNEasy Kit. cDNA was reverse transcribed as described in Chapter 2 (2.2.1.5) and used as template for test PCR reactions.

3.2.7 Murine Muscle cDNA

Insulin-stimulated glucose uptake in skeletal muscle is also known to depend upon fusion of GSVs with the plasmalemma. In parallel with the adipocyte, the skeletal muscle SNARE complex involved is composed

of the v-SNARE VAMP-2 and t-SNARES Syntaxin-4 and SNAP-23, and thus may employ the same synaptotagmin isoform.

Lower limb skeletal muscle was dissected from a euthanised wild-type *Mus Musculus* lab mouse and placed immediately on ice. RNA was then isolated using the Qiagen RNEasy kit. RNA was reverse transcribed to cDNA as described in chapter 2 (2.2.1.5) and used for test PCR reactions.

3.2.8 Human Adipose Tissue cDNA

Pooled Human Adipose Tissue RNA (Ambion Inc., Austin, TX, USA.) was a generous gift from Dr Scott MacKenzie. RNA was reverse transcribed into cDNA as described in Chapter 2 (2.2.1.5 and used for test PCR reactions).

3.3 Results

3.3.1 Synaptotagmin Expression in Murine Brain

Figure 3.1a shows products obtained when gene-specific murine SYT primers were used in a PCR reaction using murine brain cDNA as template. The primer annealing temperature and polymerase buffer magnesium concentration was optimised for each individual PCR reaction and identical conditions used for all subsequent reactions with that primer pair. Polymerase used (Taq polymerase) was non-proof reading.

In figure 3.1 PCR products obtained using primers specific for SYT 1-14 are of the expected nucleotide length (PCR primer location and expected product length is found in TABLE A2 in the Appendix). No product is seen for SYT15.

More than one PCR product can be seen for SYT7. It is expected that these products represent the alternatively spiced variants described in the Appendix (A1.2.2 and Figure A1). Additional unexpected bands can be seen for SYT8 and SYT10. In order to investigate their origin, these unidentified PCR products were resolved further in an additional gel (Figure 3.1b), then cloned and sequenced as described for the SYT PCR products in 3.3.1.2 below.

At the time of designing RTPCR primers used in these experiments consideration was not given to the location of intron-exon boundaries. As a result, although most primer pairs are indeed intron-spanning some are not (SYT4, SYT9, SYT10, SYT12 and SYT14). For those isoforms with intron-spanning PCR primers these data suggest that the transcripts of these isoforms are expressed in murine brain tissue. For those isoforms without intron-spanning primers it is not possible from these data to comment on expression in murine brain.

No product was obtained using SYT15 primers with murine brain cDNA. This may be due to lack of expression in brain, or due to a problem with the PCR primer pair (e.g. incorrect design, sequence error during synthesis, secondary structure). Published expression data suggest that SYT15 is not expressed in brain (303) and so these data are in support of this observation. However, a positive control would require to be shown for these primers to allow this conclusion to be drawn.

Important control PCR reactions using DNase treatment and non-reverse transcribed RNA as template were not performed. Further discussion of controls both employed and not is found in the discussion of this chapter (Section 3.4).

Figure 3.1 SYT Expression in Murine Brain

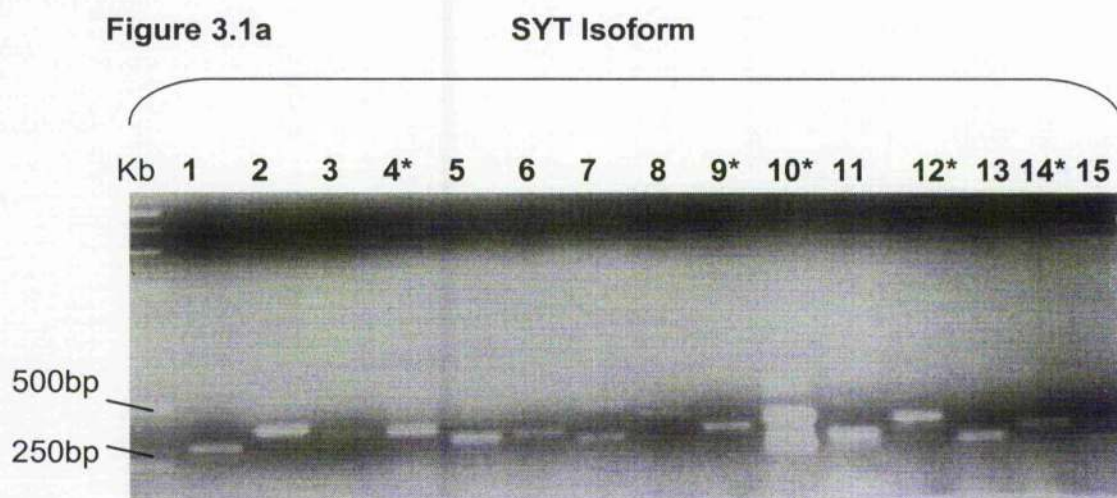


Figure 3.1a Photograph of PCR products obtained from RTPCR reactions with gene-specific SYT primers and murine brain cDNA template, resolved by agarose gel electrophoresis, stained with ethidium bromide and visualised under UV light. PCR products are compared with DNA size markers in the extreme left lane. PCR product bands can be seen of the expected nucleotide length (164). * indicates where primers were not intron-spanning.

Figure 3.1b

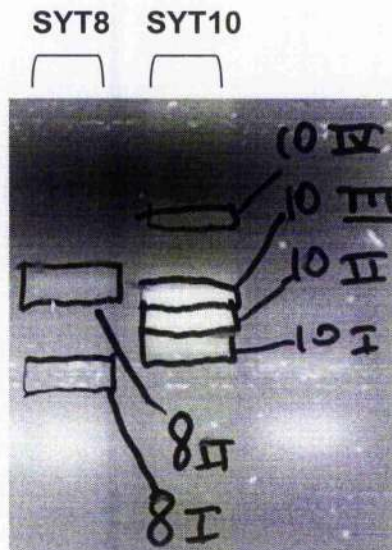


Figure 3.1b Photograph of PCR products obtained from RTPCR reactions with gene-specific SYT primers for SYT8 and SYT10, and murine brain cDNA template, resolved by agarose gel electrophoresis, stained with ethidium bromide and visualised under UV light. PCR products are compared with DNA size markers in the extreme left lane (as shown in Figure 3.1a above: not labelled in this figure). PCR product bands have been identified and labelled. Each product was cloned and sequenced as described in 3.3.1.2 below.

3.3.2 Cloning and Sequencing of Murine SYT RT PCR

Products

Fresh RTPCR products described in 3.3.1.1 above were carefully excised from the agarose gel with a clean scalpel blade, purified with the Qiaspin™ gel purification kit as instructed by the manufacturers and TA-cloned into the pCR-2.1 plasmid, again following the instructions of the manufacturer. The resulting plasmids were transformed into competent *E. coli* and grown overnight on selective Agar plates.

Two or three recombinant colonies for each PCR product were selected for further overnight growth and plasmid purification. Restriction enzyme digestion was performed to confirm the presence of an appropriately sized insert (cloned PCR product). One plasmid for each product was sequenced.

Figures 3.2a and 3.2b show successfully cloned PCR products of the expected size for SYT2 and SYT4- 9 (similar digestion products of the appropriate size were obtained for plasmids into which other isoforms were successfully cloned).

It can be seen that two SYT5 clones did not contain DNA insert (lanes 5.1 and 5.2 of Figure 3.2a). The strong band of approximately 3Kb most likely represents supercoiled (i.e. non-linearised) plasmid vector DNA, indicating that in this case the cloning was not successful. There is one clone of SYT8

(lane 8.1 in Figure 3.2b) for which there has been an unsuccessful plasmid purification. This may be either a failure of the plasmid purification procedure or even a spontaneous mutation in an un-transformed *E. coli* resulting in antibiotic resistance and thus growth on selective agar plates.

DNA sequences obtained confirm the sequence identity of each expected SYT RTPCR product (including those not shown) and are listed in the appendix. The SYT8 and SYT10 products (Figure 3.1b) yielded the expected 229 bp SYT8 sequence (8I) and the expected 269bp SYT10 sequence (10I). Sequencing of the remaining bands identified in Figure 3.1b (8II, 10II, 10III and 10IV) produced sequence that was identical to that of a variety of different prokaryotic and eukaryotic plasmid vectors and not recognised genomic or transcript sequence.

Figure 3.2 Sub-cloning of PCR Products

Figure 3.2a

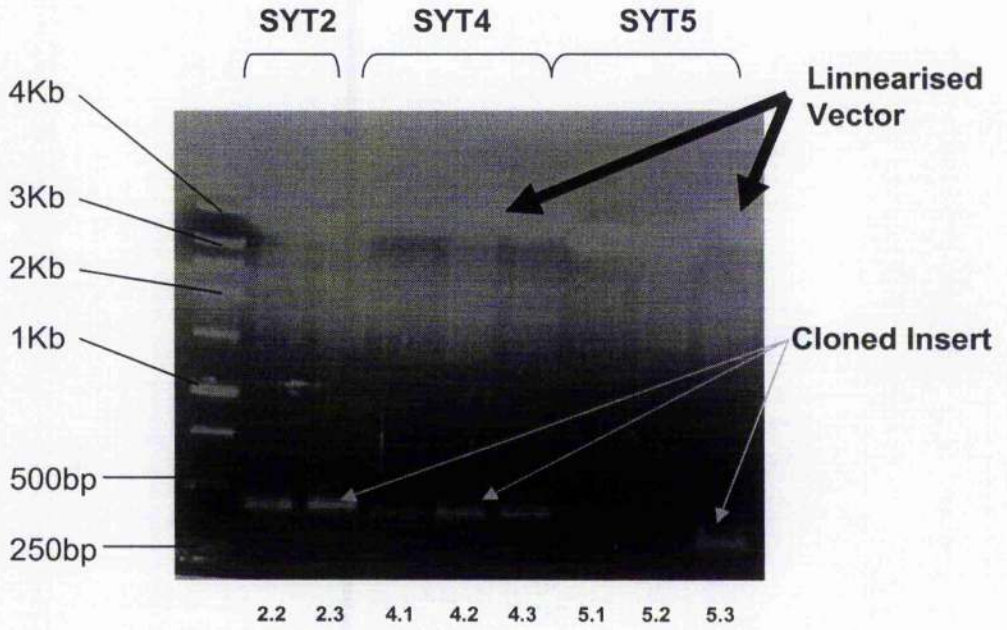


Figure 3.2b

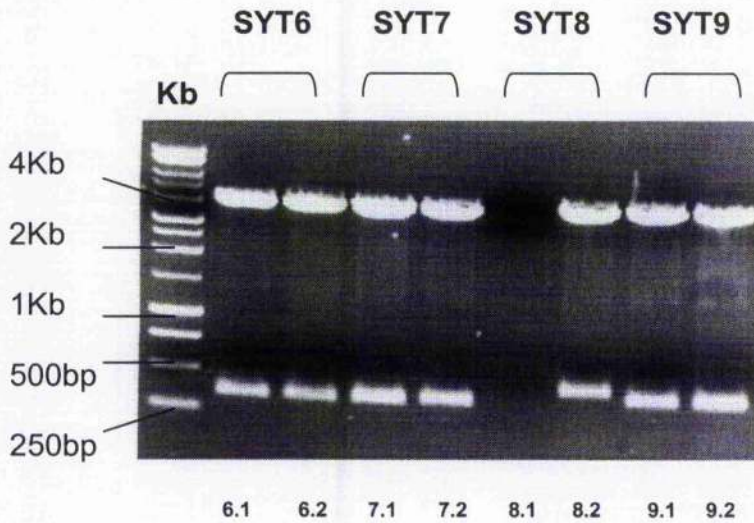


Figure 3.2

Figure 3.2a and b Photographs of resolved products obtained from restriction enzyme (EcoR1) digestion of pCR 2.1 plasmid DNA (into which the SYT RTPCR products have been cloned) compared to DNA size markers as indicated. Figure 3.2a digested plasmid DNA from two clones of SYT2 product (lanes 2.1 and 2.2) and three clones each of SYT4 and SYT5 product (lanes 4.1- 4.3 and 5.1- 5.3 respectively) are shown. Arrows indicate linearised plasmid DNA of the expected size (3.9Kb) and cloned PCR product of the expected size.

3.3.3 GLUT4 Expression in 3T3-L1 Cells During Differentiation

Figure 3.3 shows products obtained when gene-specific murine GLUT4 primers were used in a PCR reaction using cDNA from murine brain, confluent 3T3-L1 fibroblasts, and 3T3-L1 adipocytes at the indicated time from differentiation as template (all cells used were derived from the same passage) . The primer annealing temperature and polymerase buffer magnesium concentration was optimised using adipocyte cDNA prior to this experiment, and identical conditions were used for all subsequent reactions with this primer pair. As can be seen in figure 3.3 the PCR product obtained using intron-spanning primers specific for GLUT4 is of the expected nucleotide length (164).

These data suggest low level expression of GLUT4 in brain tissue. GLUT4 expression is not detected in confluent fibroblasts or immature day 2 adipocytes. As cells progress through the differentiation process and acquire insulin-sensitivity, high level GLUT 4 expression is detected from day 6, and this is maintained at all subsequent timepoints assessed. Insulin sensitivity of the cells used was confirmed (at day 12) by measurement of insulin-stimulated 2-deoxyglucose uptake (shown in Figure 3.4).

These data are in keeping with previously determined GLUT4 expression data in brain and throughout the 3T3-L1 differentiation

process. GLUT4 expression is seen to coincide with expected acquisition of insulin sensitivity. Alongside insulin-stimulated 2-deoxyglucose uptake data they confirm the cells used are typical of 3T3-L1 adipocytes at each timepoint, and as such the cDNAs prepared are representative and valid templates for use in subsequent experiments to determine SYT expression.

An appropriate additional control would be the PCR amplification of the cDNA of a housekeeping gene (304) in tandem with that of GLUT4. The observation of a uniform product from each timepoint would serve to confirm equivalence of template cDNA concentration and thus allow the relative expression at each timepoint to be inferred. This control experiment was not performed.

There are no additional PCR products observed, and this implies there is no contamination of samples with genomic DNA. However, it should be noted that DNase treatment of isolated RNA was not carried out, and RNA alone (i.e. prior to the reverse transcription step: non-RT) was not used as a negative control. From these data therefore it is not possible to completely exclude the possibility of genomic DNA contamination.

Figure 3.3: GLUT4 Expression in 3T3-L1 Cells

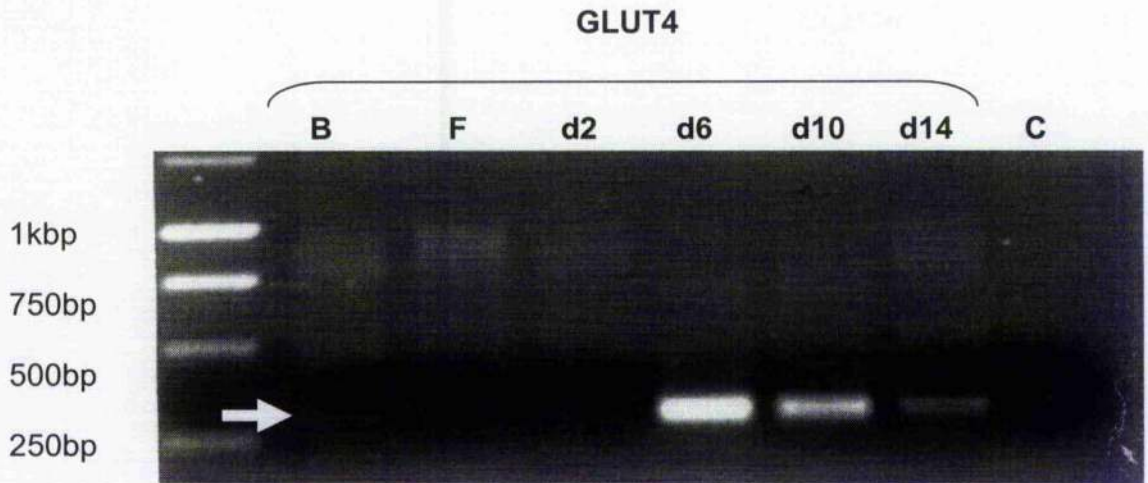


Figure 3.3 Photograph of PCR products obtained from RTPCR reactions with gene-specific GLUT4 primers and murine brain cDNA (B), 3T3-L1 confluent fibroblast cDNA (F), 3T3-L1 adipocyte cDNA at progressive stages throughout differentiation (d2= day 2, d6= day 6 etc.) templates, and no template (C), resolved by agarose gel electrophoresis, stained with ethidium bromide and visualised under UV light. PCR products are compared with DNA size markers in the extreme left lane. Single PCR product bands can be seen of the expected nucleotide length. The arrow indicates a faint band).

Figure 3.4 Insulin-Stimulated 2-Deoxyglucose Uptake in 3T3-L1 Adipocytes

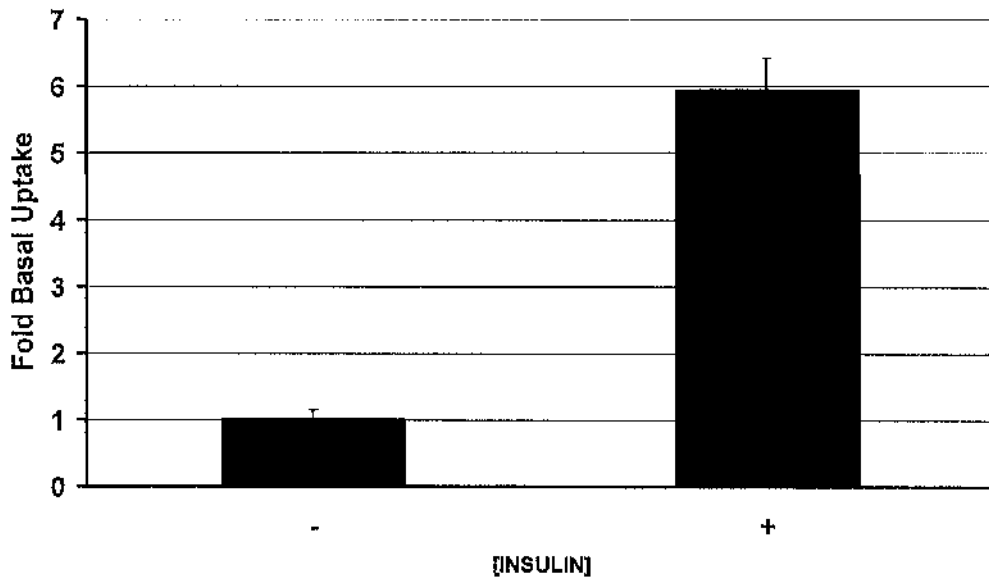


Figure 3.4 3T3-L1 adipocytes were assayed for insulin-stimulated deoxyglucose uptake using 100nM insulin where indicated. Data is presented relative to the rate of uptake in basal (unstimulated) cells. (N= 3 at each point; error bars indicate 1 standard deviation from mean values). Data are representative of a typical experiment.

3.3.4 Synaptotagmin Expression in 3T3-L1 cells During Differentiation

Figures 3.5 and 3.6 show products obtained when gene-specific murine SYT primers were used in a PCR reaction using 3T3-L1 cell cDNAs as template. Product of the expected size was obtained when murine brain cDNA was used as a positive control in each case.

As can be seen in the figures, although the positive control reaction yielded the expected product, no PCR product was obtained for SYTs 1, 2, 4, and 6 when 3T3-L1 cDNA was screened. These results suggest that these isoforms are not expressed in 3T3-L1 cells.

As before no product was obtained using SYT15 primers, suggesting this isoform is not expressed in 3T3-L1 cells. However, as with murine brain cDNA it would be important to obtain a positive control template for this primer pair prior to this conclusion being drawn.

PCR products of the appropriate size can be seen to be amplified from 3T3-L1 cell cDNA for SYT 3, 5 and 7 – 14. In the absence of parallel amplification of a housekeeping gene it is not possible to draw any conclusion regarding their relative expression at any given timepoint from these data.

On examining Figure 3.6a it is clear that an additional PCR product of between 750bp and 1Kb is present following amplifications using SYT5. This additional product is seen when both murine brain and 3T3-L1 cell cDNA templates are used. The SYT5 primers are intron spanning and there were no steps taken to exclude genomic DNA contamination. One possibility is that this band represents amplification of the intron(s) between the adjacent exons in which the SYT5 primers are located. This hypothesis was not tested by sequencing of the additional product.

Closer study of the SYT5 transcript and genomic sequence reveals that the forward primer is located in exon 6 and the reverse primer in exon 8. The expected product size is 289bp. If genomic contamination was present the resulting amplification of the 3' end of exon 6 (56bp), intron 6/7 (613bp), exon 7 (134), intron 7/8 (781) and the 5' end of exon 8 (99bp) would result in a PCR product of 1733bp, which is much larger than the extra band observed. The additional product may therefore represent non-specific off target amplification, however without sequencing of this product further hypothesis on its identity is futile.

Similar to the products observed for SYT5, an extra product is also seen for SYT14 when 3T3-L1 cDNA template is used. The SYT14 primers are not intron spanning, and so would not be expected to produce products of different lengths if genomic DNA contamination was present. Thus, the additional product may represent either non-specific off-target amplification or a hitherto undescribed splice variant. Further

attempts to characterise the additional SYT14 product were not carried out.

When the SYT7 primers are used in a PRC reaction with murine brain cDNA template three bands of a size corresponding to the expected splice variants (SYT7 α , SYT7 β and SYT7 γ) can be seen, with SYT7 β being the most prominent. When 3T3-L1 cDNA is used a band of the expected size of the SYT7 α product is seen at all timepoints. The SYT7 β and SYT7 γ products are not seen. These data suggest that SYT7 α is expressed in 3T3-L1 cells.

There are three products of 250- 500bp seen for SYT10. When brain cDNA template is used the predominant product is the smallest (~250bp). The predominant product is the larger of the three (~350bp) when 3T3-L1 fibroblast and day 2 cDNA is used for PCR amplification. By day 10 there are only two bands visible (the larger and the smaller) and by day 14 only the smaller band can be seen. The expected product size for SYT10 is 269bp, therefore the smaller band most probably denotes the expected product. The SYT10 primers are not intron spanning therefore (as for SYT14) the additional bands are unlikely to reflect genomic DNA contamination. The results could be explained by non-specific off-target amplification or by a possible novel splice variant. The chance of contamination with non-murine (e.g., human) DNA remains a possibility that was not investigated. No attempt to further characterise these bands was made.

Figure 3.5: SYT 1, 2, 4, & 6 Expression in 3T3-L1 Cells

Figure 3.5a

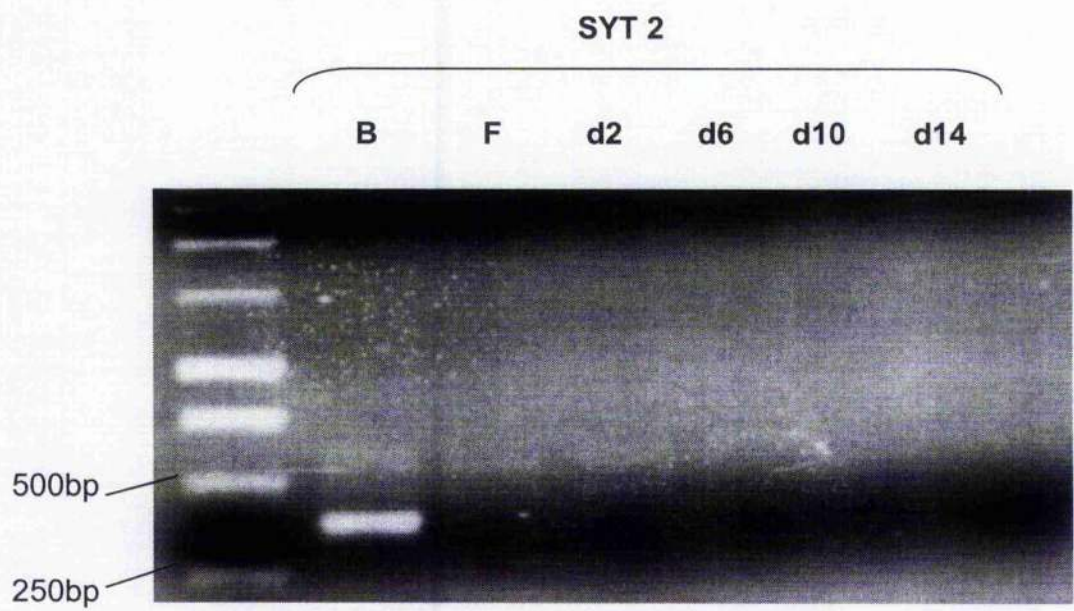
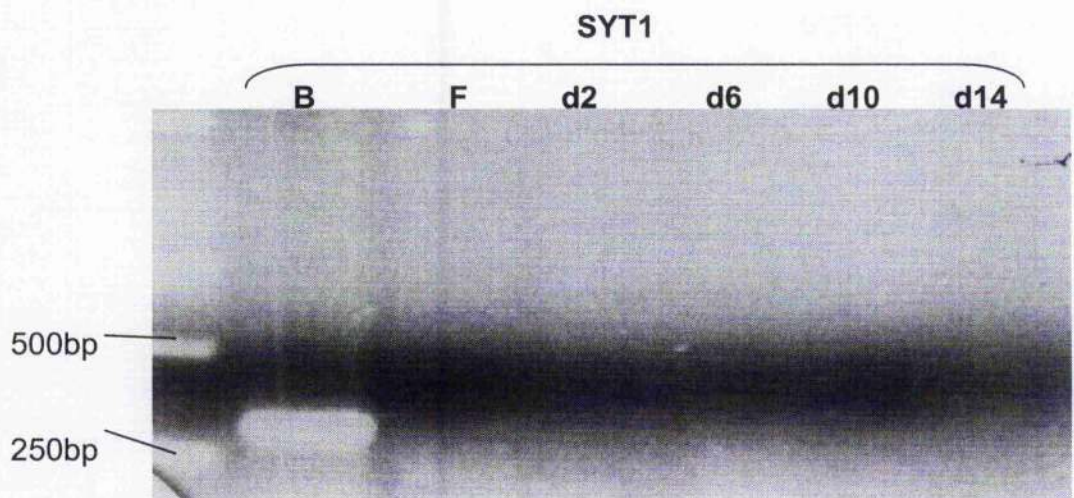


Figure 3.5b

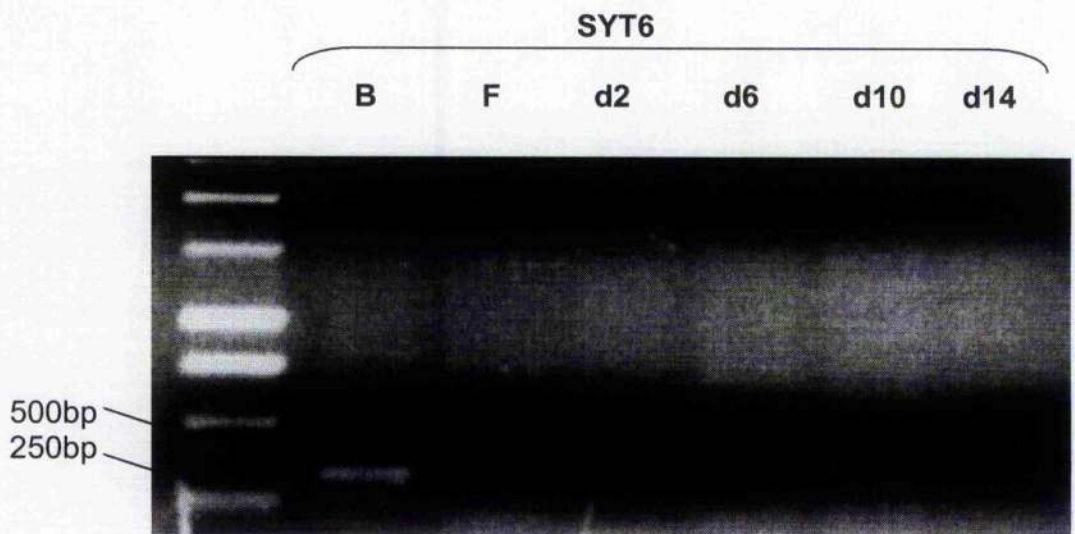
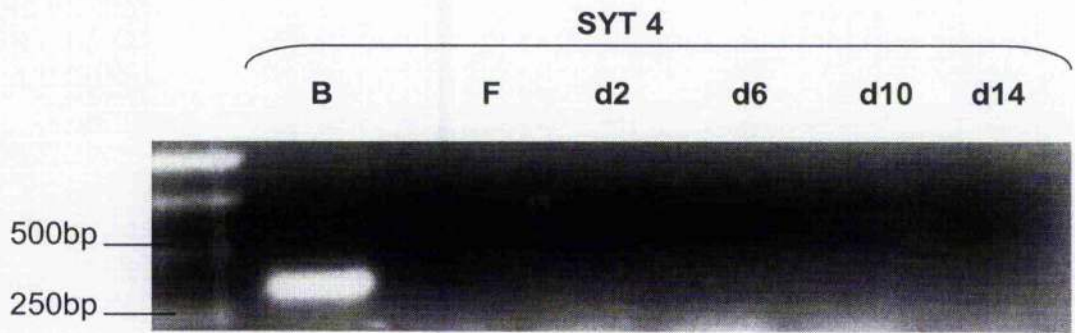


Figure 3.6: SYT 3, 5 & 7- 14 Expression in 3T3-L1 Cells

Figure 3.6a

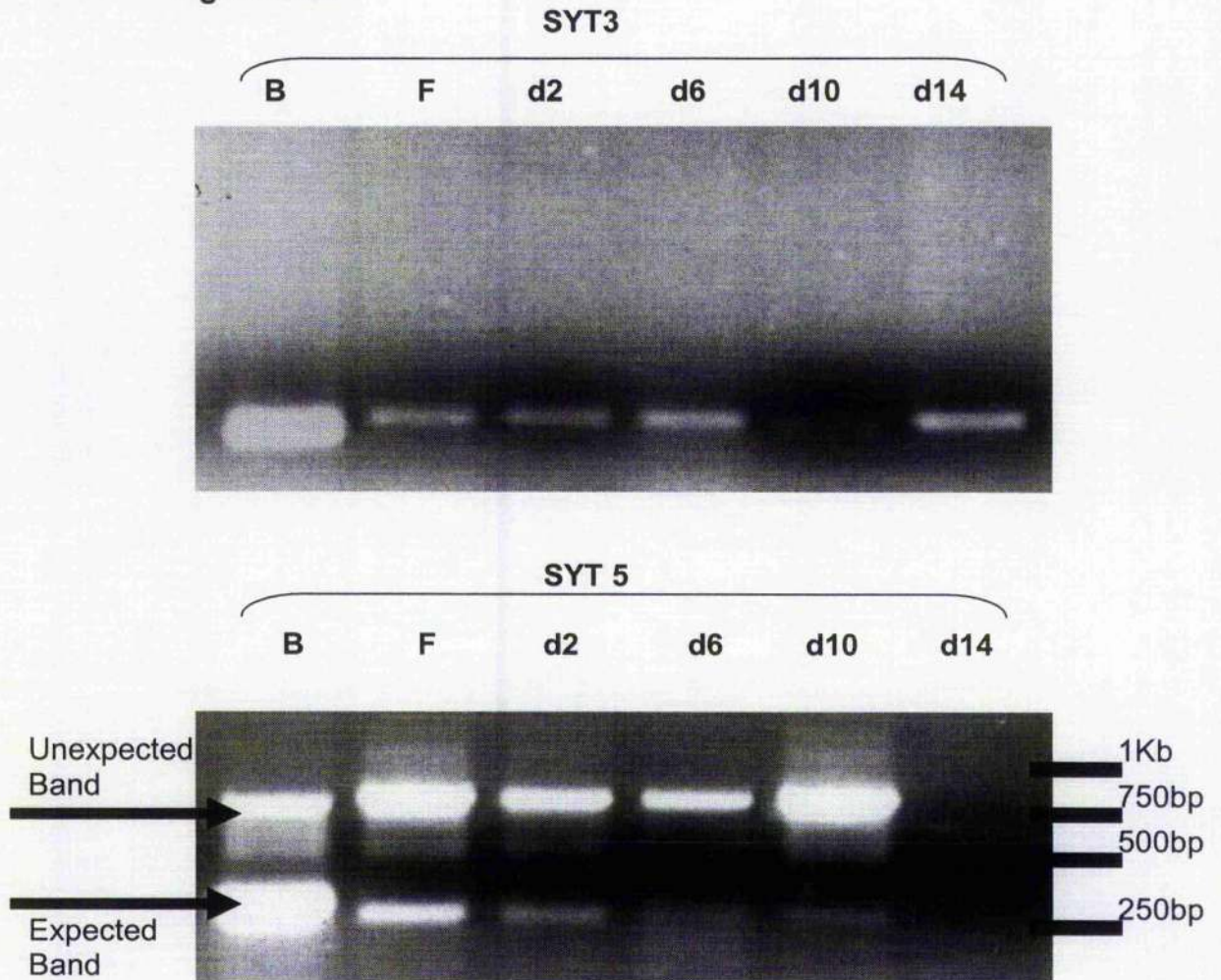


Figure 3.6b

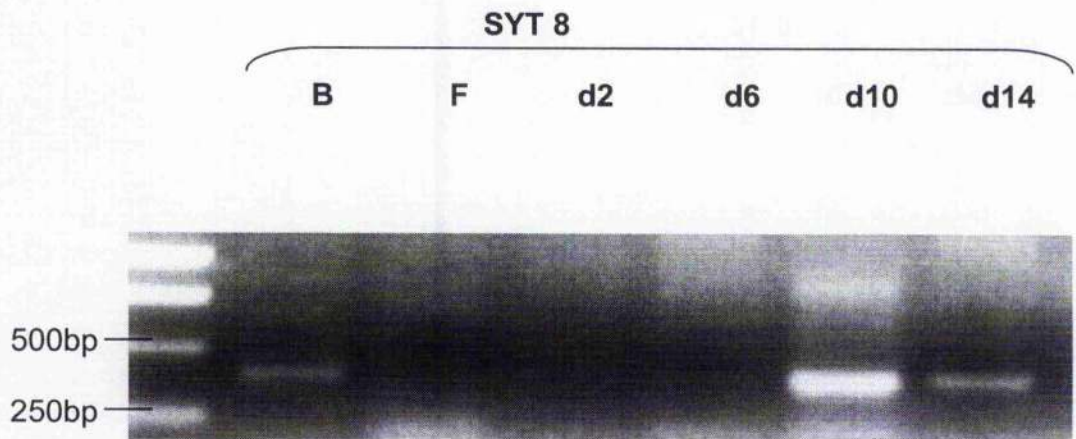
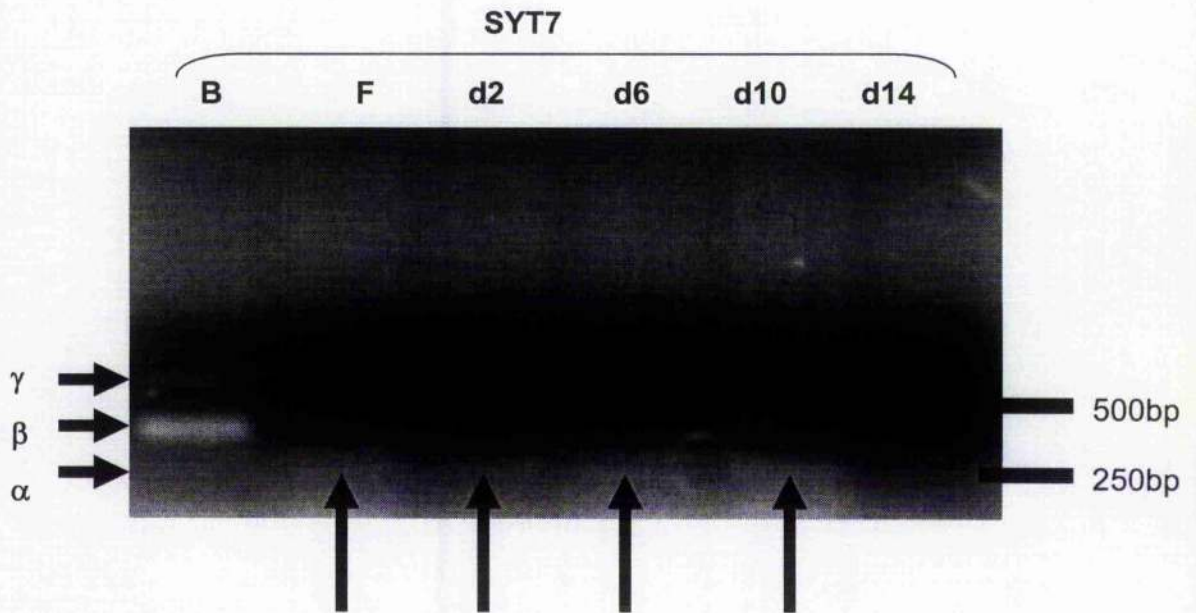


Figure 3.6c

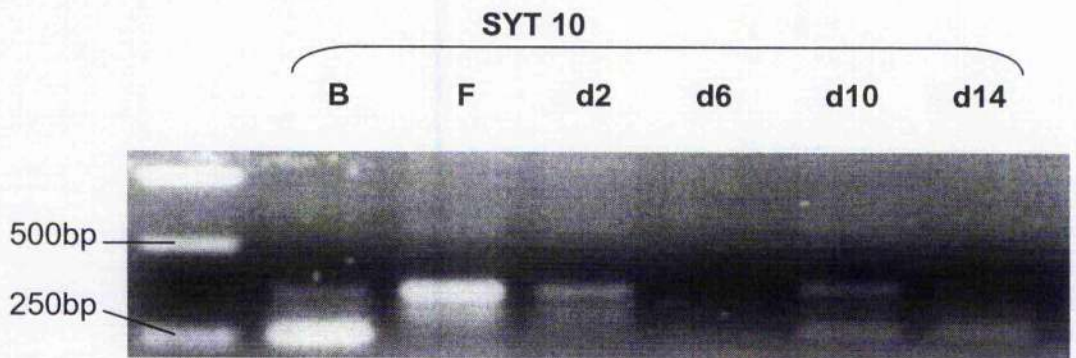
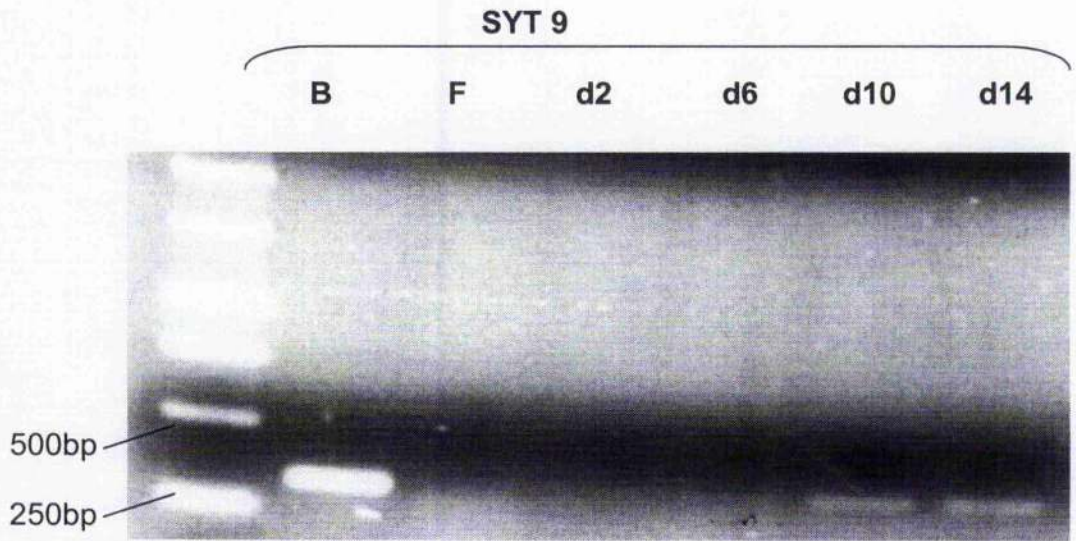


Figure 3.6d

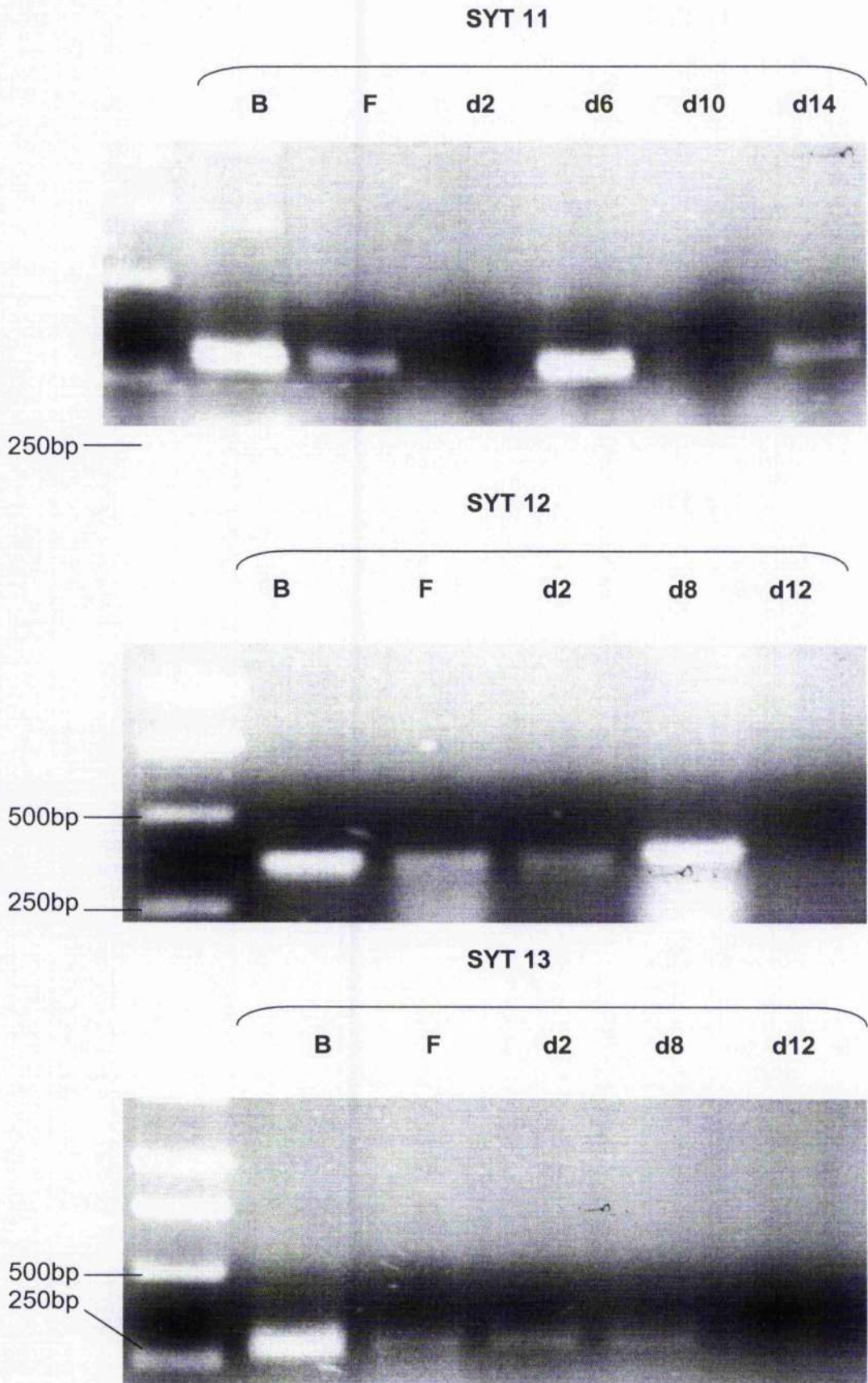
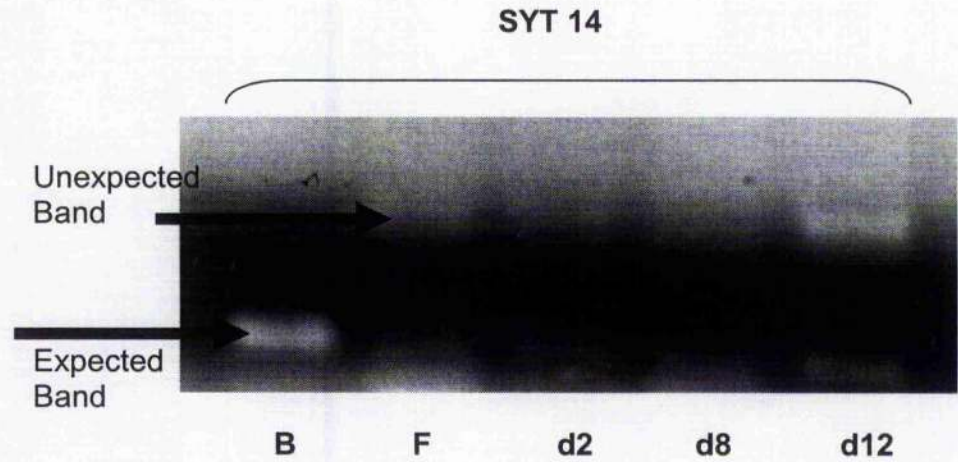


Figure 3.6e



Figures 3.6a- d

Photographs of PCR products obtained from RTPCR reactions using gene-specific SYT primers and cDNA template from murine brain (B), confluent 3T3-L1 fibroblast (F), 3T3-L1 adipocyte at progressive stages throughout differentiation (d2= day 2, d6= day 6 etc.) as indicated. PCR products were resolved by agarose gel electrophoresis, stained with ethidium bromide and visualised under UV light, and can be compared with the indicated DNA size markers. Arrows indicate faint bands. Data are representative of 2 identical experiments for each isoform using cDNA prepared from discrete cell populations of different passage.

3.3.5 GLUT4 and SYT Expression in Murine Skeletal Muscle

Figure 3.7a shows products obtained when gene-specific murine GLUT4 primers were used in a PCR reaction using cDNA from 3T3-L1 adipocytes (at day 10 post-differentiation) and murine skeletal muscle as template. As can be seen in the first panel of the figure, the PCR product obtained from murine skeletal muscle using intron-spanning primers specific for GLUT4 is of the expected nucleotide length and confirms the quality of this template for subsequent test reactions.

Figures 3.7b, 3.7c and 3.8 show products obtained from PCR reactions using gene-specific murine SYT primers and murine skeletal muscle template alongside murine brain cDNA positive control. These data indicate that SYT1, 2, 4, 5, 6, 8, 9, 13 and 14 are not expressed in murine skeletal muscle, and suggest that SYT3, 7, 10, 11 and 12 are expressed in murine skeletal muscle.

In Figure 3.7c the gel photograph does not clearly show a band in the positive control (Brain template) lane for SYT10 which was clearly visible at the time of performing these experiments.

The SYT15 PCR product band seen in Figure 3.7c is of the correct approximate expected size. This band was not further characterised by sequencing. In the absence of a positive control or further attempts to

identify this product it is not possible from these data to comment upon the expression of SYT15.

Given that a DNA-se treatment of RNA samples and non-RT controls were not performed for these experiments caution must be exercised in their interpretation, especially with those PCR products that do not span intron/exon boundaries (SYT10 and SYT12). In spite of this, the absence of PCR product with SYT4, SYT9 and SYT14 primers suggests that there is no genomic DNA contamination in samples derived from murine muscle tissue.

Figure 3.7: GLUT4 and Synaptotagmin Expression in Murine Skeletal Muscle

Figure 3.7a

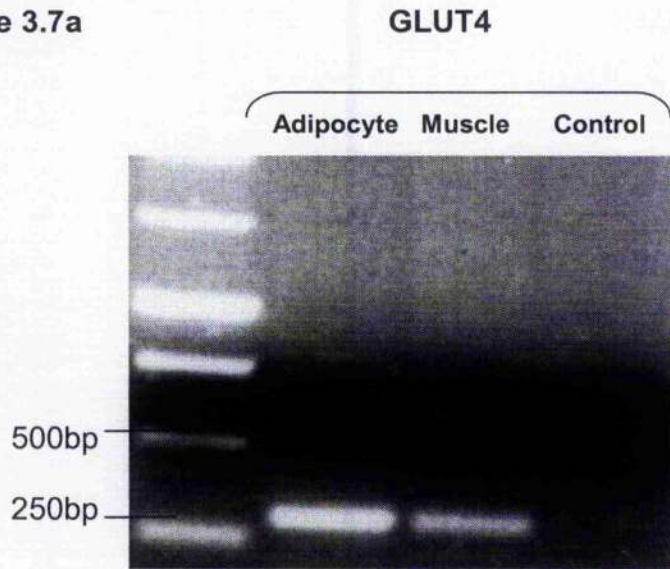


Figure 3.7b

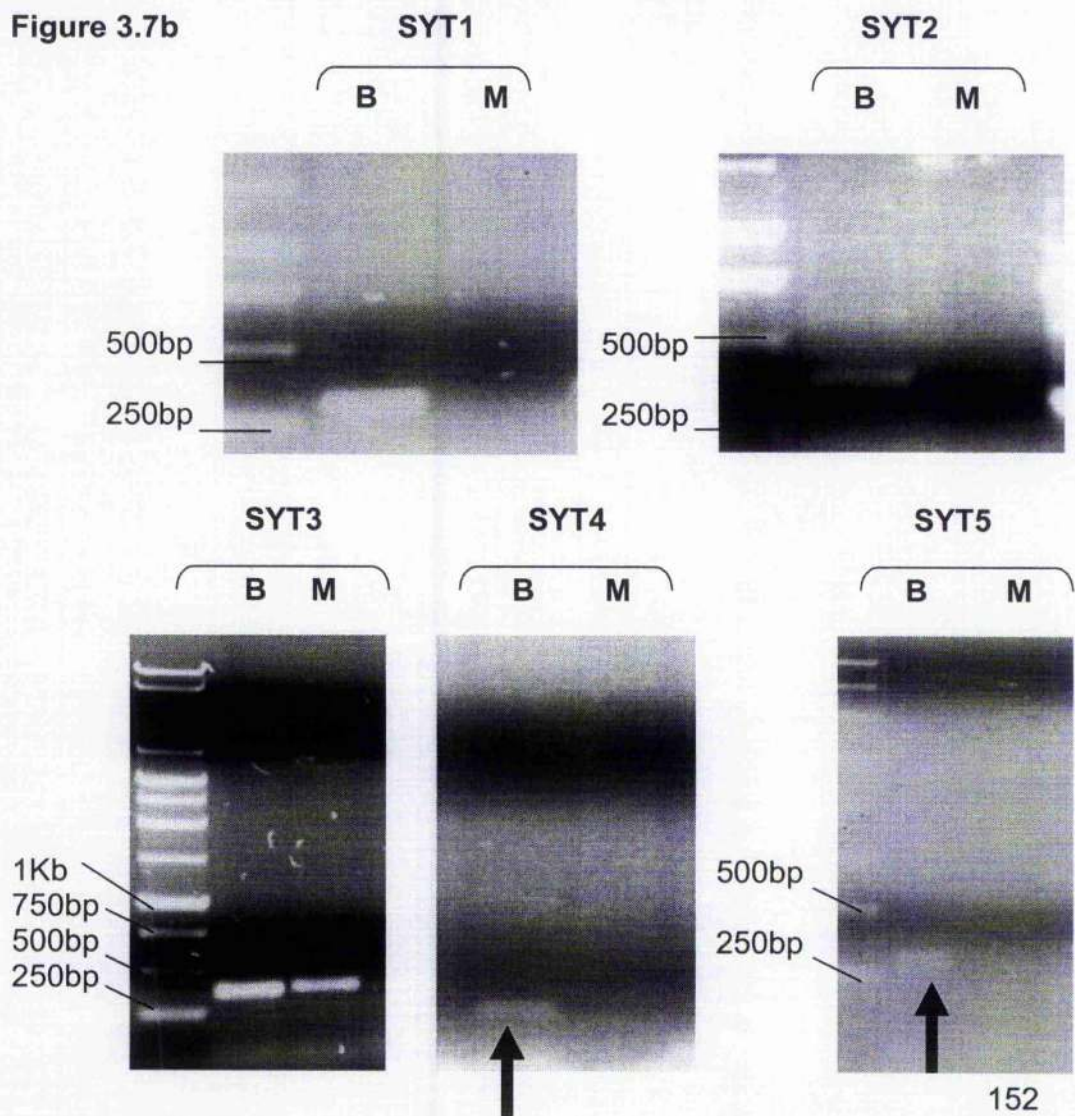


Figure 3.7c

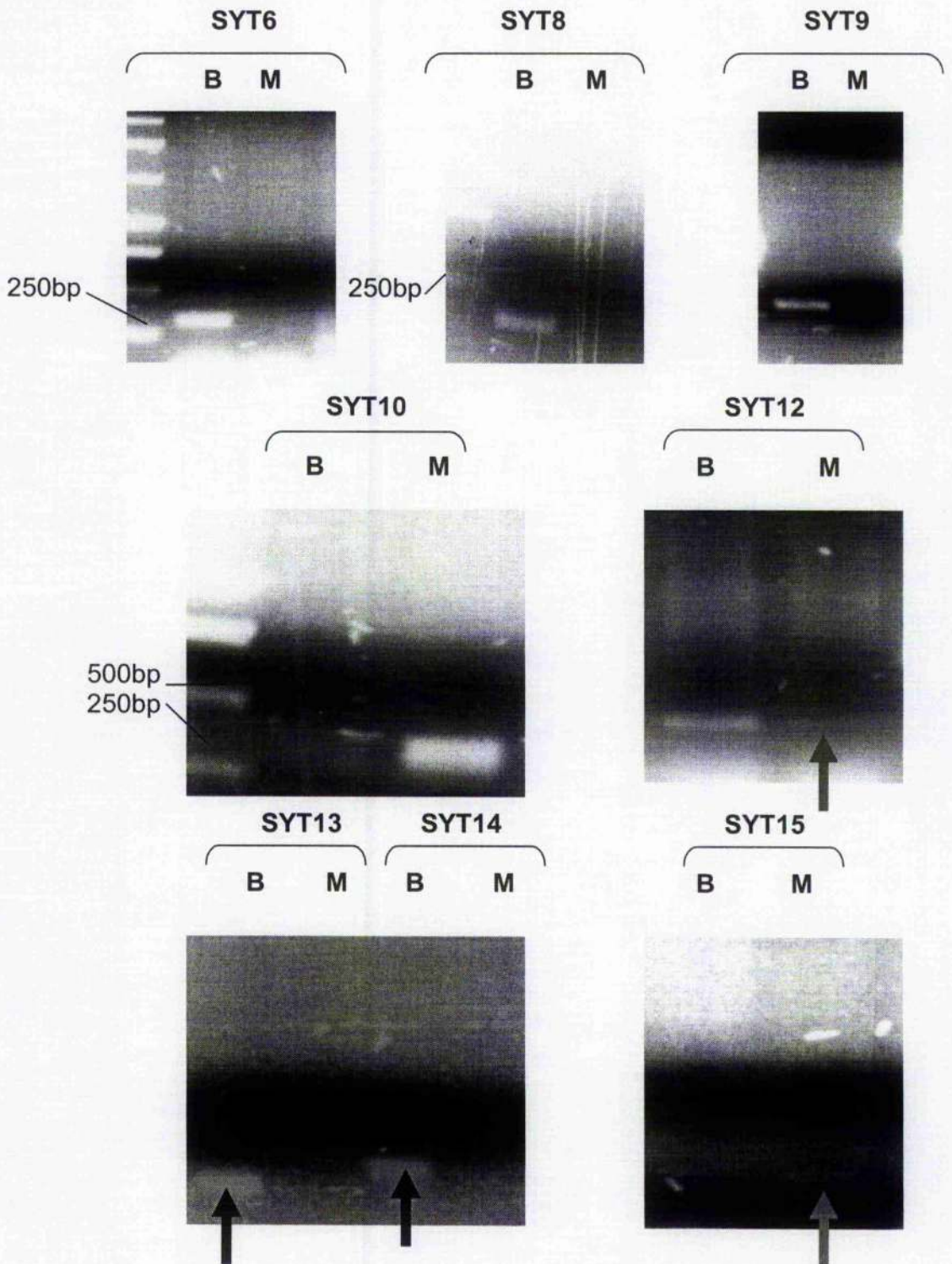


Figure 3.7a, 3.7b and 3.7c

Photographs of PCR products obtained from RTPCR reactions using gene-specific SYT primers and cDNA template from murine brain (B), murine skeletal muscle (M) and no template (C) as indicated. PCR products were resolved by agarose gel electrophoresis, stained with ethidium bromide and visualised under UV light, and can be compared with the indicated DNA size markers. Arrows indicate faint bands. Data are representative of 2 identical experiments for each isoform using cDNA prepared from muscles of the opposite leg of the same mouse.

Figure 3.8: SYT7 and SYT11 Expression in Murine Skeletal Muscle

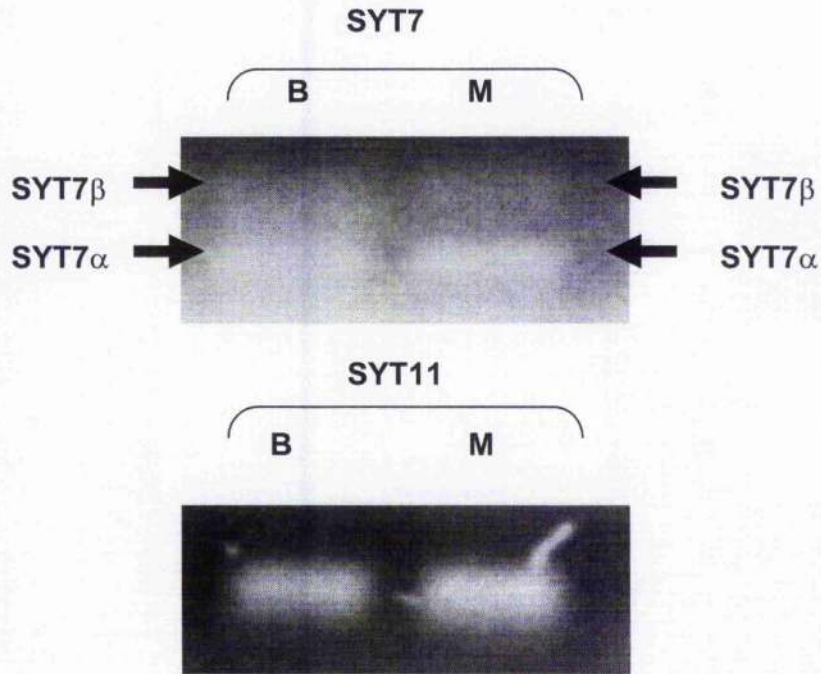


Figure 3.8 Photographs of PCR products obtained from RTPCR reactions using gene-specific SYT primers and cDNA template from murine brain (B) and murine skeletal muscle (M) as indicated. PCR products were resolved by agarose gel electrophoresis, stained with ethidium bromide and visualised under UV light, and can be compared with the indicated DNA size markers. Arrows indicate faint bands. Data are representative of 2 identical experiments for each isoform using cDNA prepared from muscles of the opposite leg of the same mouse.

3.3.6 Synaptotagmin Expression in Pooled Human Adipose

Figure 3.9 shows products obtained when gene-specific intron-spanning human SYT7 and SYT11 primers were used in a PCR reaction using cDNA from human testis and pooled human adipose tissue as template. Cycling conditions and polymerase buffer magnesium content were optimised for each primer pair using testis cDNA as template; PCR products were of the expected nucleotide length.

These data are suggestive that SYT7 and SYT11 are expressed in human adipose tissue, since a PCR product of the size expected can be seen. There are however additional products visible for both isoforms, which raises the possibility of genomic (or other) DNA contamination or off target amplification. These options were not addressed further experimentally. Furthermore, DNase treatment and non-RT controls were not performed, limiting the conclusions that may be drawn from these data.

The human adipose tissue cDNA was screened for the presence of transcripts of the other SYT isoforms. The results of these experiments are in accordance with results observed when 3T3-L1 adipocyte cDNA was used.

Figure 3.9: SYT7 and SYT11 Expression in Human Adipose Tissue

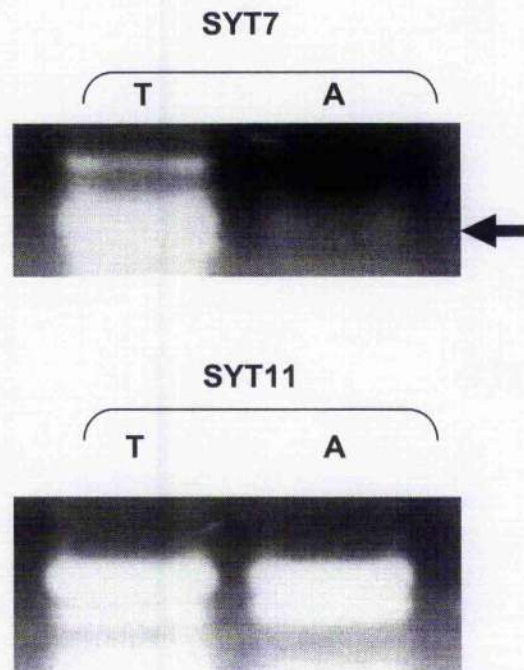


Figure 3.9 Photographs of PCR products obtained from RTPCR reactions using gene-specific SYT7 and SYT11 primers and cDNA template from human testis (T) and pooled human adipose tissue (A) as indicated. PCR products were resolved by agarose gel electrophoresis, stained with ethidium bromide and visualised under UV light. Arrow indicates a faint band. Data are from 1 experiment.

3.3.7 GLUT4 and SYT Expression in 3T3-L1 Cells as

Determined by Taqman Semi-Quantitative Realtime PCR

Prior to assessing relative SYT expression in 3T3-L1 cell cDNA a standard curve of ΔC_T vs. template concentration was prepared for all Taqman Realtime PCR primer and probe sets and can be seen in Figure 3.10. Murine Brain cDNA template was used. This demonstrates equal efficiency of amplification at all template concentrations for all primer and probe sets examined.

Figure 3.11 shows the relative expression (to β -actin) of the SYT isoforms examined in brain. The data for SYT11 expression are omitted from figure 3.11a but included in figure 3.11b (note different scale). Threshold cycle (C_T ; the point at which product amplification becomes log-linear) is indicated for each isoform, and all C_T values (except for SYT7) are seen to be ≤ 35 , indicating expression of the transcript in murine brain.

Figure 3.12 shows expression of murine GLUT4 relative to the expression of β -actin in cDNA prepared from 3T3-L1 fibroblasts and mature day 8 adipocytes. No expression of GLUT4 can be detected in fibroblast cDNA, and a high level of relative expression is observed in

adipocyte cDNA. It is expected that this is due to upregulation of GLUT4 expression during the differentiation process. These data confirm that the cDNA templates used are representative of 3T3-L1 adipocytes and are thus valid for use in experiments to assess SYT expression.

Figure 3.13 shows expression of the indicated murine SYT isoforms relative to the expression of β -actin in cDNA prepared from 3T3-L1 fibroblasts. SYT11 is the predominant isoform and is expressed at approximately 1.6 times the level of SYT7. As indicated by C_T values, the remaining isoforms are not expressed at a significant level.

Figures 3.14a and 3.14b show the relative expression of the indicated SYT isoforms in insulin-sensitive 3T3-L1 adipocytes. The data for SYT11 expression are omitted from figure 3.12a but included in figure 3.12b (note different scale). These data suggest that SYT11 expression is upregulated as 3T3-L1 cells differentiate and acquire insulin-sensitivity. SYT11 is the predominant 3T3-L1 adipocyte isoform. The relative expression of SYT7 and SYT11 are further determined in figures 3.15 and 3.16, where it can be seen that SYT7 expression is maintained, and SYT11 expression appears to increase ~18-fold during differentiation.

Expression of SYT11 during differentiation is further characterised in figure 3.17 where it can be seen that relative SYT11 expression increases

steadily during differentiation and is maximal at day 8. Thereafter the expression level falls, but remains significantly elevated at day 10 and day 12 above that of the fibroblast.

Figure 3.10: Taqman Primer and Probe Standard Curve

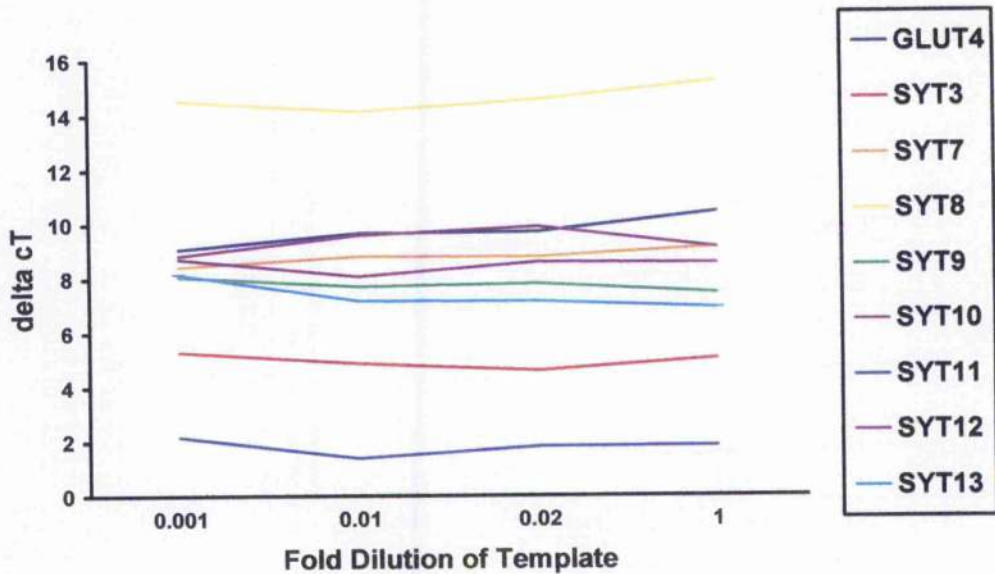


Figure 3.10 Standard curve of ΔcT at serial template DNA dilutions for all Taqman Realtime PCR primer and probe sets (a detailed description of the derivation of values is given in section 2.2.9). The parallel line for each set demonstrates equivalent PCR efficiency at the range of template concentrations indicated. That the lines are (near) horizontal indicates each reaction is within the linear dynamic range (i.e. the range of template concentrations which allow accurate determination relative to the control (GAPDH) gene). Data are from a single experiment using murine brain cDNA of $0.33\mu\text{g}/\mu\text{l}$ (determined spectrophotometrically).

Figure 3.11: SYT Expression in Murine Brain Tissue

Figure 3.11a

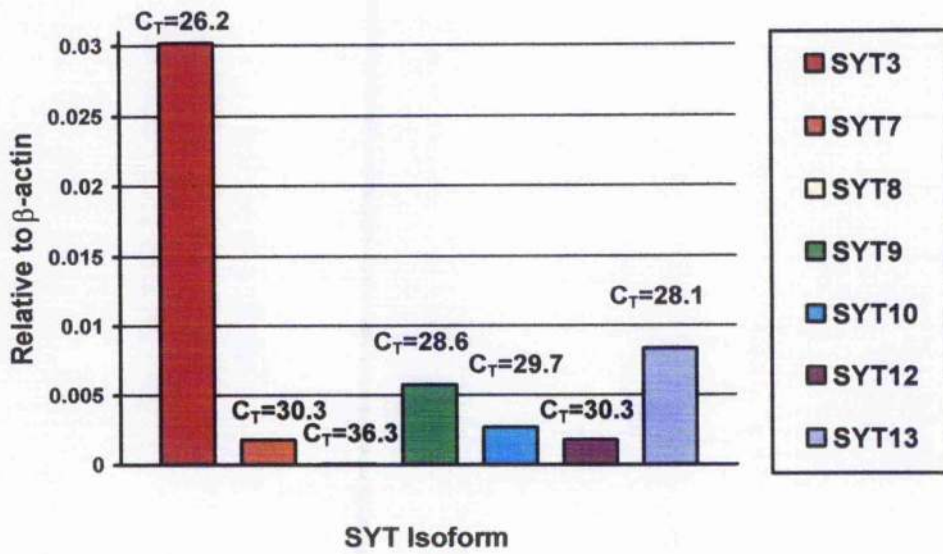


Figure 3.11b

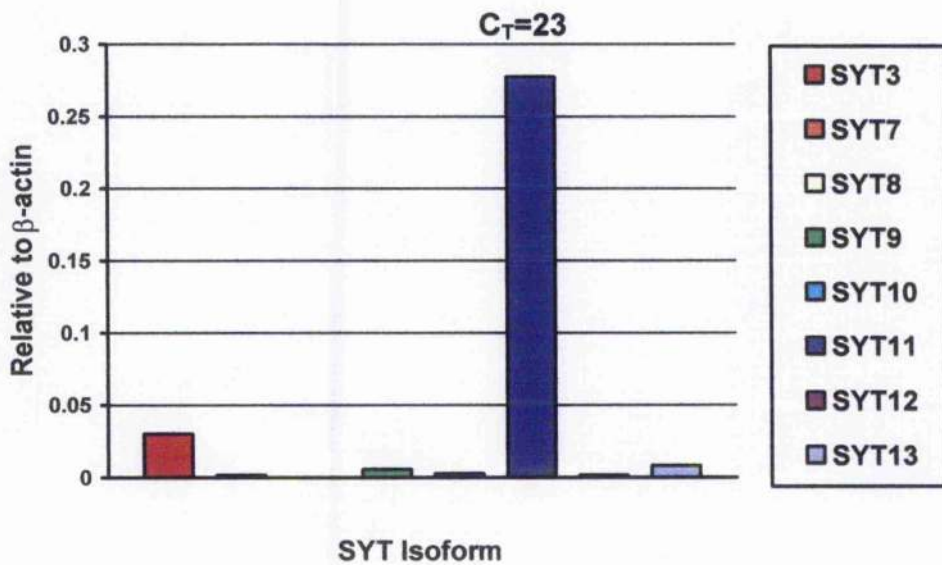


Figure 3.11 Relative (to β -actin) expression of murine SYT3 and SYT7-SYT13 as determined by Taqman semi-quantitative PCR using Murine Brain tissue cDNA template. The upper panel shows all except SYT11. The same data are presented in the lower panel including SYT11. Note different scale (Y-axis). (Data presented are from a single experiment). Values indicate the amount of each transcript relative to β -actin transcript in the sample analysed (a detailed description of the derivation of values is given in section 2.2.9). Threshold cycle (C_T) is shown for each isoform.

Figure 3.12: GLUT4 Expression in 3T3-L1 Cells During

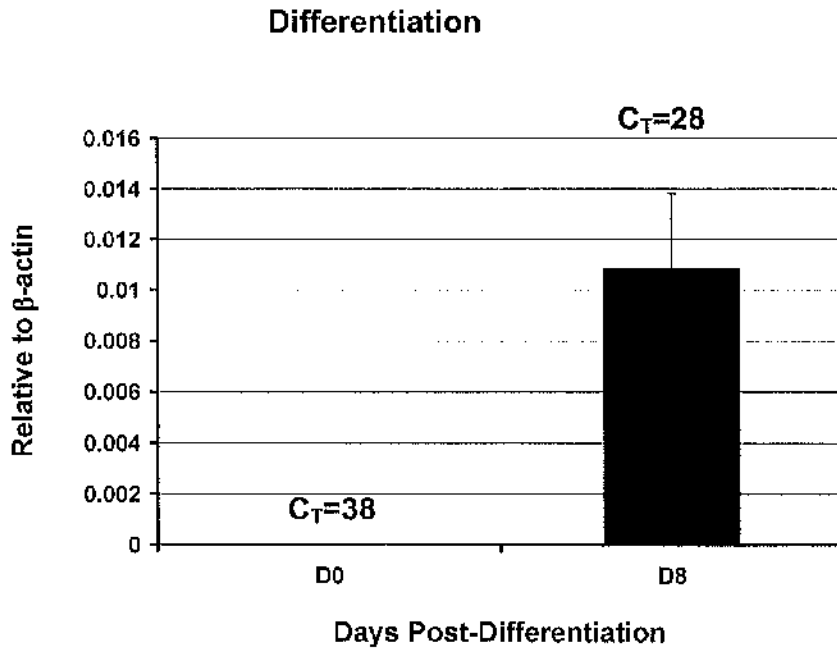


Figure 3.12 Relative (to β -actin) expression of murine GLUT4 as determined by Taqman semi-quantitative PCR using 3T3-L1 cDNA template generated at confluent fibroblast (D0) and day 8 (D8) post-differentiation. (Data presented are the mean of 8 identical experiments; error bars show 1 standard deviation). Values indicate the relative amount of GLUT4 transcript compared to β -actin transcript at each given timepoint. Threshold cycle (C_T) is shown.

Figure 3.13: SYT Expression in Confluent 3T3-L1 Fibroblasts

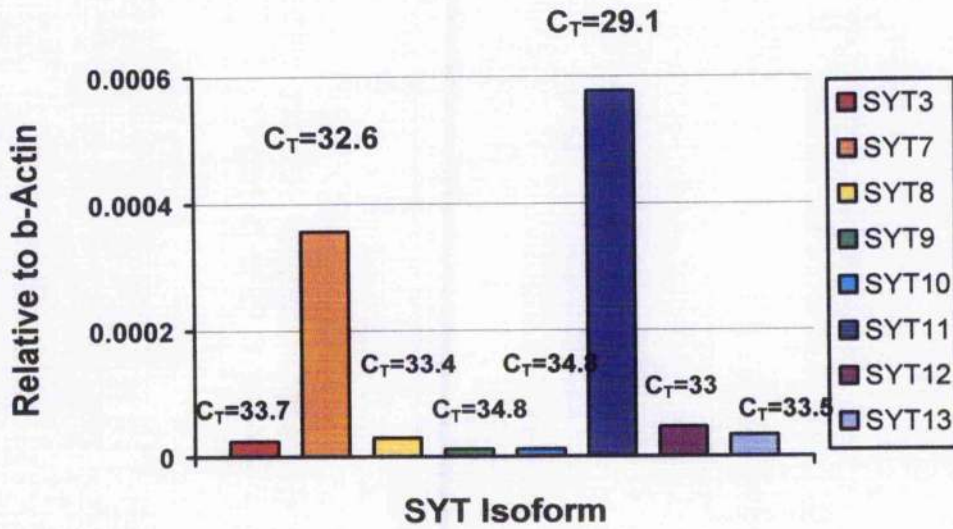


Figure 3.13 Relative (to β -actin) expression of murine SYT3 and SYT7-SYT13 as determined by Taqman semi-quantitative PCR using confluent fibroblast 3T3-L1 cDNA template. (Data presented are representative of multiple experiments using cDNA derived from discrete cell populations). Threshold cycle (C_T) for each isoform is shown.

Figure 3.14: SYT Expression in 3T3-L1 Adipocytes

Figure 3.14a

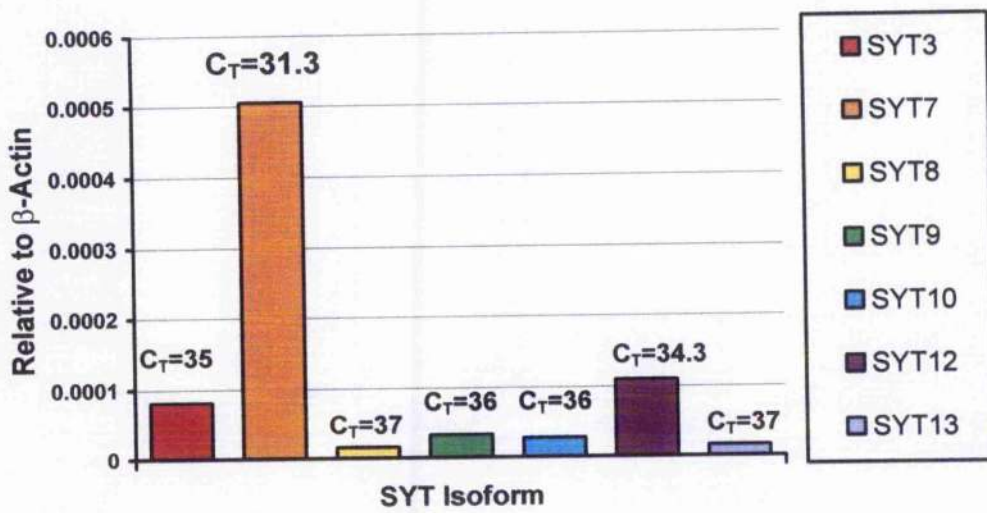


Figure 3.14b

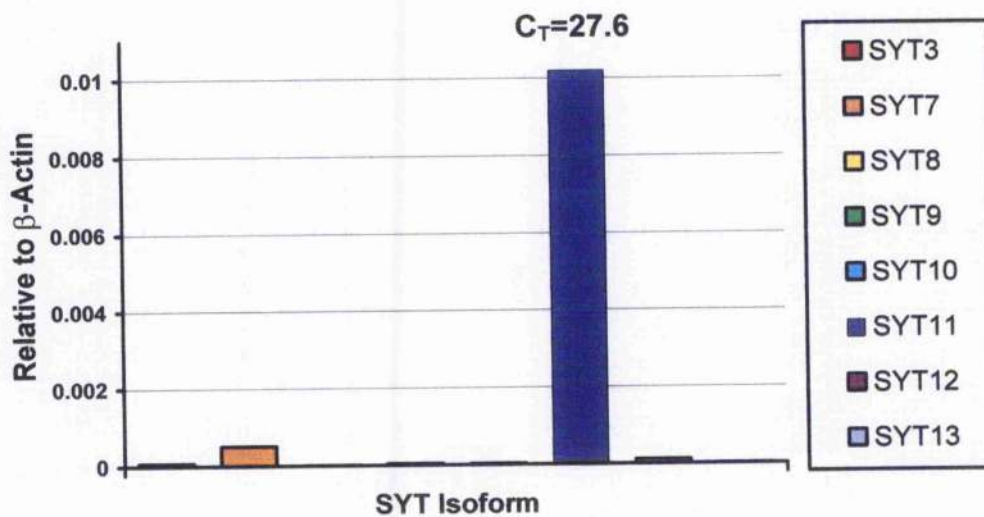


Figure 3.14 Relative (to β -actin) expression of murine SYT3 and SYT7-SYT13 as determined by Taqman semi-quantitative PCR using 3T3-L1 cDNA template at day 8 (D8) post-differentiation. The upper panel shows all except SYT11. The same data are presented in the lower panel including SYT11. Note different scale (Y-axis). (Data presented are from a single representative of multiple experiments using cDNA derived from discrete cell populations). Threshold cycle (C_T) for each isoform is shown.

Figure 3.15: SYT7 Expression in 3T3-L1 Cells During Differentiation

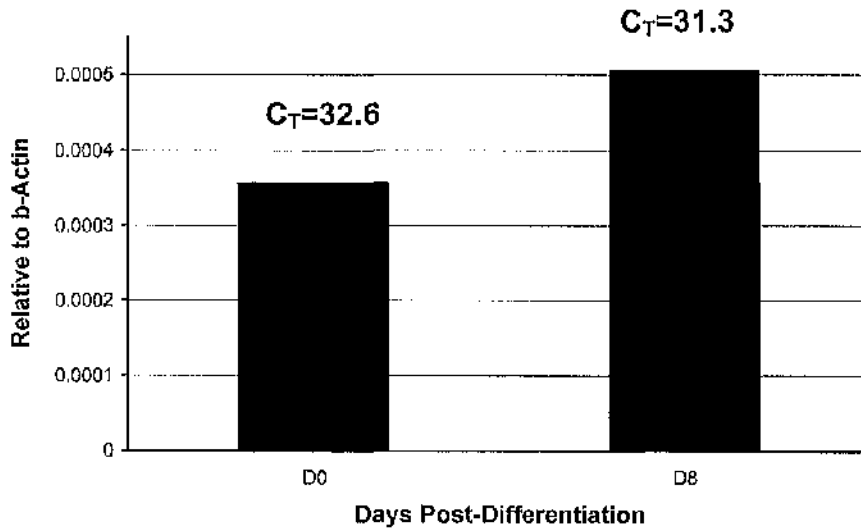


Figure 3.15 Relative (to β -actin) expression of murine SYT7 as determined by Taqman semi-quantitative PCR using 3T3-L1 cDNA template at confluent fibroblast (D0) and day 8 (D8) post-differentiation. (Data presented are typical of 3 identical experiments using cDNA derived from discrete cell populations). Threshold cycle (C_T) at each timepoint is shown.

Figure 3.16: SYT11 Expression in 3T3-L1 Cells During Differentiation

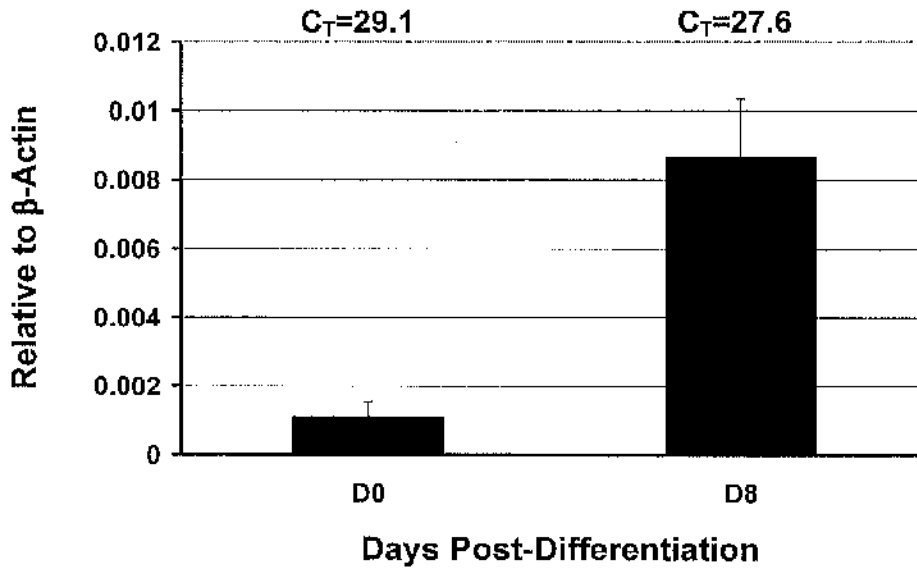


Figure 3.16 Relative (to β -actin) expression of murine SYT11 as determined by Taqman semi-quantitative PCR using 3T3-L1 cDNA template at confluent fibroblast (D0) and day 8 (D8) post-differentiation. (Data presented are the sum of 3 identical experiments using cDNA derived from discrete cell populations; error bars show 1 standard deviation). Threshold cycle (C_T) at each timepoint is shown.

**Figure 3.17: SYT11 Expression in 3T3-L1 Cells During
Differentiation: Additional Timepoints**

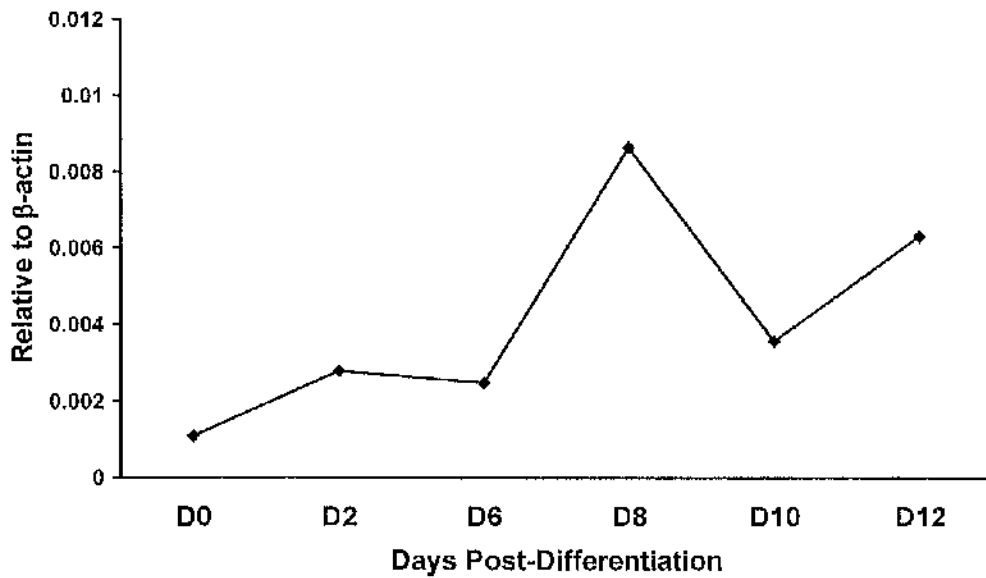


Figure 3.17 Relative (to β -actin) expression of murine SYT11 as determined by Taqman semi-quantitative PCR using 3T3-L1 cDNA template derived from confluent fibroblast (D0) and cells at the days indicated post-differentiation (Data presented are the sum of 3 identical experiments using cDNA derived from discrete cell populations).

3.4 Discussion

The initial experimental approach employed in the experiments described in this chapter limit the conclusions that can be drawn from the data described. In particular, the lack of appropriate controls does not allow the precise origin of PCR templates to be accurately determined. The RTPCR primers used were not initially designed to be intron-spanning. However, the finding that primers for murine GLUT4, human SYTs and most of the murine SYTs are indeed intron spanning (table A2) allows more certain interpretation of the data generated using them. Thus, the presence of an appropriately sized PCR product obtained using intron spanning SYT3, 5, 7, 8, 11 and 13 primers, which is identified as the target amplicon when sequenced suggests that these isoforms are expressed at the mRNA level in the 3T3-L1 adipocyte.

For those isoforms for which primers are not intron spanning (SYTs 4, 9, 10, 12 and 14) it is not possible from these data to determine the origin of the template DNA. Genomic DNA contamination at the RNA isolation stage could result in the products obtained in these experiments, and this would be indistinguishable from the intended product amplified solely from cDNA. This could have been investigated by using both RNA prior to reverse transcription as template, and by treating RNA with DNase enzyme as control experiments in which no product would be expected. These experiments were not performed. The absence of multiple additional PCR product bands in RTPCR reactions is reassuring, and suggests no genomic contamination, nevertheless appropriate

controls would be required to confirm these observations. Thus, from these data it is possible to conclude only that the PCR reactions using isoform-specific primer pairs for SYTs 4, 9, 10, 12 and 14 produce PCR products of the expected size, and no conclusion regarding possible expression.

The finding that SYTs 1-14 are expressed in murine brain tissue and SYT15 is not confirms published SYT expression profiles. These experiments confirm that SYTs are indeed expressed in 3T3-L1 cells, and the Taqman data suggest that relative SYT11 expression can change during the differentiation process. The developmental upregulation of a particular transcript implies a functional role for that gene product in the particular developmental stage studied. This has previously been observed to be the case with SYT1 in PC12 cells, various subpopulations of neurons and the retinal neuroepithelium (305-307), SYT1-SYT4 in the developing CNS (308) and SYT2 in murine embryo-derived cells (309).

In the absence of parallel experiments to amplify a similar sized product from the transcript of a known housekeeping gene using intron-spanning primers it is not possible from the RTPCR data to comment upon the relative expression level of any isoform at any given timepoint.

It is to be expected that the complement of SYT isoforms expressed in muscle and adipocytes is not identical: they are distinct and specialised cells. However, their shared embryonic origin is mesodermal,

and so it is not surprising that there is considerable overlap in the genes expressed: SYT3, 5, 7, and 11 are expressed by both skeletal muscle and adipocytes. It is possible that the factors regulating skeletal muscle and adipocyte GSV fusion differ. Since calcium plays a key role in skeletal muscle and cardiac muscle contraction it is possible that an alternative (non-calcium-dependent) SYT isoform interacts with the assembled GSV-SNARE complex in these tissues, and the differences in SYT expression observed between skeletal muscle and adipocytes reflects this difference.

Many of the gel images shown in this chapter demonstrate poor resolution of DNA bands, which makes accurate assessment of size difficult. An alternative strategy would have been to employ Polyacrylamide Gel Electrophoresis, which would allow better discrimination of PCR products. Furthermore, product identification by virtue of a target-specific oligonucleotide probe and Southern blotting would have obviated the need for the subcloning and sequencing strategy employed in these studies.

The data generated using Taqman Realtime PCR demonstrate that the two isoforms expressed in 3T3-L1 cells are SYT7 and SYT11. Transcripts of the other isoforms for which RTPCR products were observed are not expressed at a significant level over baseline. These differences serve to illustrate the advantage in employing a realtime quantitative PCR (qPCR) method over conventional RTPCR.

Quantitative realtime PCR has a dynamic range of 10^7 whereas conventional RTPCR has a dynamic range of 1000 fold. This allows qPCR to detect and to discriminate within a much wider range of template concentrations. Conventional RTPCR requires a post-amplification processing step for product analysis (agarose gel electrophoresis), whereas the readout data from qPCR is gathered in tandem with the amplification step. This also introduces a further degree of error, given that it is not possible to accurately estimate the relative concentration of DNA samples loaded onto an agarose gel. Finally, conventional RTPCR measures the sum total amount of product produced by all amplification steps whereas qPCR measures product after each step. This allows the initial exponential phase of target amplicon production to be identified, and relative concentration of template can then be calculated (as described in section 2.2.9).

The differences observed between the RTPCR data and the qPCR data serve to confirm these differences between the two methods. The finding of SYT isoforms for which a (228) product was obtained (SYT 3, 8 and 13) by RTPCR but not found to be expressed at a significant level relative to β -actin by qPCR illustrates that these transcripts are present in very low (insignificant) copy number. It is possible that there is no translation of these transcripts.

Taken together these data demonstrate that 3T3-L1 cells express SYTs. There is evidence that expression is regulated by differentiation.. In the insulin-sensitive 3T3-L1 adipocyte SYT11 and SYT7 are the isoforms expressed. SYT11 and SYT7 transcripts are also detected in murine skeletal muscle and human adipose tissue. The observed 18-fold upregulation of SYT11 as 3T3-L1 cells differentiate and acquire insulin-sensitivity implies a key role for this SYT isoform in the adipocyte, which may represent interaction with the STX4 / SNAP23 / VAMP2 SNARE complex and regulation of GSV-PM fusion.

The expression of a particular gene as determined by RTPCR (semi-quantitative or not) merely confirms the transcription of the gene of interest. The majority of transcribed genes are translated into functional proteins but not all. Furthermore, the stability of an individual mRNA within any individual cell is governed by a number of disparate factors, some endogenous and others exogenous. There is an increasing number of regulatory RNA sequences being described in the literature. Considering these points caution must be exercised in the interpretation of these data: in order to confirm SYT expression the demonstration of protein is required.

Chapter 4: Cellular Localisation of SYT7 and SYT11 in the 3T3-L1

Adipocyte

4.1 Introduction

Within the adipocyte GLUT4 is found in multiple cellular locations. In the basal state, GLUT4 is known to rapidly recycle from the PM to the endosomal system (186), from where it can enter a slower trafficking cycle between the endosomal system, the TGN and the GSV pool (186). The stimulation with insulin leads to an increase in the rate of transport observed in both cycle 1 and 2 above. Moreover, the intracellular GSV store is rapidly mobilised in response to insulin, ultimately leading to GSVs docking with the PM. SNARE-mediated GSV-PM fusion then delivers GLUT4 to its intended site of action (179).

If either or both candidates SYT7 and SYT11 identified as the predominant isoforms in Chapter 3 do indeed play a role in insulin stimulated GLUT4 translocation in the 3T3-L1 adipocyte then a temporal and spatial relationship to GLUT4 and the SNARE proteins Syntaxin4 SNAP23 and VAMP2 must be demonstrated.

To date there have been few published studies which describe the subcellular localisation of either SYT7 or SYT11, and none in adipocytes or other insulin-sensitive cells (SYT7 has been described in the lysosome and PM of fibroblasts (310); SYT11 has been observed in the PM,

neuronal synaptic vesicle and within Lewy bodies of the Substantia Nigra (242)). At the time of investigation there was no commercially available SYT7 antiserum, and there remains no such product available for SYT11.

This chapter will describe the generation and characterisation of specific antisera raised against SYT7 and SYT11. These antisera shall then be used to confirm the expression of SYT11 protein, and determine the subcellular localisation of SYT7 and SYT11 protein within the fully differentiated 3T3-L1 adipocyte.

4.2 Methods

4.2.1 Identification of Potential Immunogenic SYT7 and SYT11 Sequences

The amino acid sequences of murine SYT7 and SYT11 proteins were obtained from published sequences found in the US National Centre for Biotechnology Information (NCBI) Genbank Database. More than one version of each sequence was available; comparison using Vector NTI™ software revealed there were no sequence variations.

Careful comparison of the murine SYT7 and SYT11 sequences in turn with both the amino acid sequence and the solved structure of SYT3 (311) facilitated identification of amino acid residues that could be predicted to be present on exposed areas on the 'outside' of the molecule. By comparing such potential peptide sequences with the

sequences of all the other murine synaptotagmin protein sequences, candidate peptides were obtained. The NCBI Basic Local Alignment Search Tool (72) (302) was used to analyse potential sequences by comparing with all other published murine protein sequences.

In this way, two peptide sequences for SYT7 and SYT11 were identified that were both present on exposed areas of the molecule, and were specific to each synaptotagmin isoform. Peptide sequences used to generate SYT7 and SYT11 antisera are listed in Table A1.4 in the Appendix.

4.2.2 Generation of SYT7 and SYT11 Antisera

The generation of specific antisera raised against the peptide sequences identified above was performed commercially by Eurogentec, Brussels. Briefly, each peptide was chemically synthesised and the amino acid sequence verified by mass spectrometry prior to injection of each peptide into an otherwise healthy wild-type rabbit. After three booster injections, serum was collected and stored at -80°C. Samples of affinity purified antibody were prepared by Eurogentec.

4.2.3 Characterisation of SYT7 and SYT11 Antisera

In order to determine the specificity of each antiserum generated affinity purified antisera were used to probe Western blots of murine brain lysates and lysates prepared from HEK293 cells transfected with two distinct expression plasmids (pEF-BOS, which uses the human EF-1 α promoter(312) and pAD-CMV V5 DEST, which uses an adapted CMV virus promoter (313)), both containing epitope tagged murine SYT7 or SYT11. The quantity of each antiserum used in future experiments was optimised based upon the strength of signal produced using these control protein preparations.

4.3 Results

4.3.1 Characterisation of SYT7 and SYT11 Antisera

Figure 4.1 shows the specific recognition of SYT7 in cell lysates prepared from HEK cells in which SYT7 and SYT11 have been expressed from two different plasmid promoters. 4.1a shows the immunoreactive bands obtained when the commercially available SySy antibody is used, and 4.1b shows immunoreactive bands obtained using the affinity purified SYT7 antisera. Both antisera recognise two major bands, the largest of which is of ~47.5kDa (predicted molecular weight of murine SYT7 is 45.5kDa). No immunoreactive bands are seen in the SYT11 lanes indicating that both antisera are specific for SYT7.

Figure 4.2 shows the specific recognition of SYT11 in the same cell lysates. 4.2a shows the immunoreactive bands obtained when the SYT11 antibody obtained from Prof S Pulst (242) is used, and 4.1b shows immunoreactive bands obtained using the affinity purified SYT11 antisera. Both antisera recognise two major bands, the smaller of which is of ~47.5kDa (predicted molecular weight of murine SYT11 is 48.4kDa). No immunoreactive bands are seen in the SYT7 lanes indicating that both antisera are specific for SYT11.

Figure 4.1 Affinity Purified SYT7 Antisera

Figure 4.1a Commercial α SYT7 Antibody (Synaptic Systems)

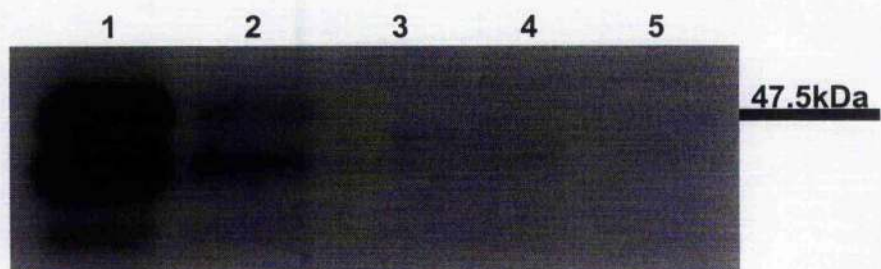


Figure 4.1b Affinity Purified α SYT7 Antisera

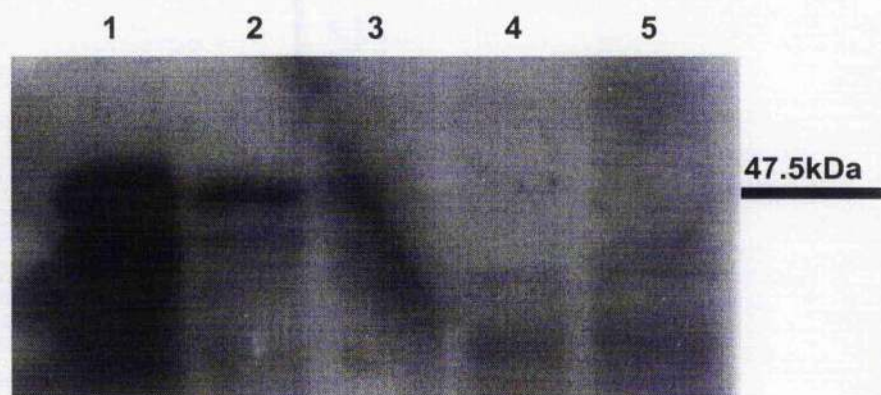


Figure 4.1a and 4.1b

Scanned images obtained from Western blots using commercially available Synaptic Systems (SySy) SYT7 antibody and pooled affinity-purified SYT7 antisera. Cell lysates prepared from HEK cells 48h following transfection with SYT7 (1 and 2), and SYT11 (3 and 4) expression plasmids, and non-transfected control (5) were resolved by SDS-PAGE (HEK cells were transfected with the following plasmids: (1) SYT7 pEF-BOS, (2) SYT7 pAD-CMV V5 DEST, (3) SYT11 pEF-BOS, (4) SYT11 pAD-CMV V5 DEST). In each case transfected cells from 2 wells of a 6-well tissue culture plate were used to prepare 500 μ l whole cell lysates; 20 μ l of each lysate in 4x SDS-PAGE buffer was loaded per lane. The marker corresponds to the molecular weight standard as indicated. SySy SYT7 antibody was used at 1:1000, and SYT7 antisera at 1:250 dilution. Data are from a single experiment.

Figure 4.2 Affinity Purified SYT11 Antisera

Figure 4.2a Pulst α SYT11 Antibody

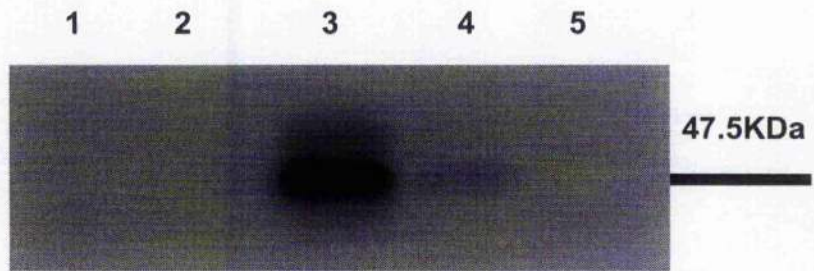


Figure 4.2b Affinity Purified α SYT11 Antisera

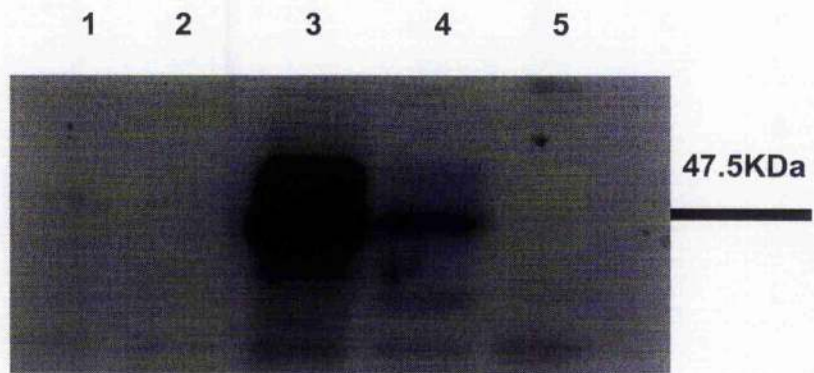


Figure 4.2a and 4.2b

Scanned immunoblot images obtained from Western blots using the previously characterised Pulst SYT11 antibody (242) and pooled affinity-purified SYT7 antisera. Cell lysates prepared from HEK cells 48h following transfection with SYT7 in pEF-BOS (1) and pAD-CMV (2), and with SYT11 in pEF-BOS (3) and pAD-CMV (4) expression plasmids, and non-transfected control (5) were resolved by SDS-PAGE. 20 μ l of each lysate in 4x SDS-PAGE buffer prepared as described in figure 4.1 was loaded per lane. The marker corresponds to the molecular weight standard as indicated. Pulst SYT11 antibody was used at 1:1000, and SYT11 antisera at 1:250 dilution. Data are from a single experiment.

4.3.2 Subcellular Localisation of SYT7 and SYT11 within the 3T3-L1 Adipocyte

Figure 4.3 shows the distribution of GLUT4 and the t-SNARE Syntaxin4 in subcellular membrane fractions prepared from fully differentiated mature 3T3-L1 adipocytes in the basal (unstimulated) state, and following 30minutes stimulation with insulin. In the basal state GLUT4 is found predominantly in the LDM fraction, which has previously been shown to comprise the endosomal system, the TGN and the GSV pool. Following stimulation with insulin there is a redistribution of GLUT4, with a reduction in the LDM fraction and a significant increase present at the plasma membrane. In these fractions there is a small GLUT4 signal in the HDM fraction which increases with insulin. No GLUT4 is detected in the soluble protein fraction.

The subcellular distribution of Syntaxin4 is different from that of GLUT4. Syntaxin4 is found in the PMs predominantly, with a smaller amount in the HDM, and LDM fractions. The distribution of Syntaxin4 does not change following stimulation with insulin.

These data are in accordance with previous descriptions of GLUT4 and SNARE protein distribution in 3T3-L1 adipocyte subcellular

membrane fractions. Thus, these fractions are of sufficient quality for the subsequent characterisation of SYT7 and SYT11 distribution.

Figure 4.4 demonstrates the distribution of SYT7 and SYT11 in subcellular fractions from 3T3-L1 adipocytes. Both SYT7 and SYT11 are found predominantly in the HDM fraction. Insulin has no effect on the distribution of either SYT7 or SYT11. At the exposure indicated neither isoform could be detected in other fractions, however with prolonged exposure immunoreactive bands were seen for both SYT7 and SYT11 in the other membrane fractions. Figure 4.5 examines the same PM and LDM fractions as in figure 4.4 above in more detail.

Figure 4.5a confirms the basal and insulin-stimulated distribution of GLUT4, and a translocation from the LDM to the PM in response to insulin can be clearly seen. IRAP, which has previously been shown to traffic alongside GLUT4 shows a similar distribution in both basal and insulin-stimulated cells.

Figure 4.5b shows the presence of SYT7 in the LDM and PM fractions in both basal and stimulated cells. SYT11 is detected in the LDM fraction, but not in the PM. This distribution is not altered by insulin.

Figure 4.3: Subcellular Fractionation of 3T3-L1 Cells

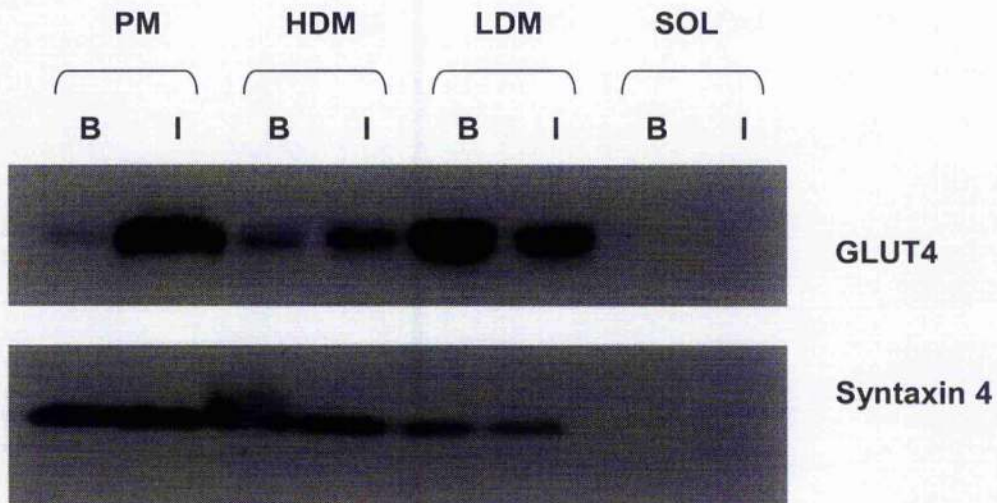


Figure 4.3

Subcellular fractions (plasma membrane (PM), high density microsomes (HDM), low density microsomes (LDM) and soluble proteins (SOL)) prepared from day 12 post-differentiation 3T3-L1 adipocytes under basal conditions (B) or following 30 minute stimulation with 100nM insulin (I) separated by SDS-PAGE and transferred to nitrocellulose. 4x 10cm cell culture dishes per condition ((B) or (I)) were subjected to fractionation; membrane fractions were resuspended in 150 μ l SDS-PAGE buffer and 15 μ l of each fraction loaded per well. Immunoblots using GLUT4 antibody (1:1000 dilution) or Syntaxin4 antibody (1:1000) are shown. Data are representative of 2 identical experiments using discrete populations of cells.

Figure 4.4 SYT7 and SYT11 Distribution in 3T3-L1 Adipocytes

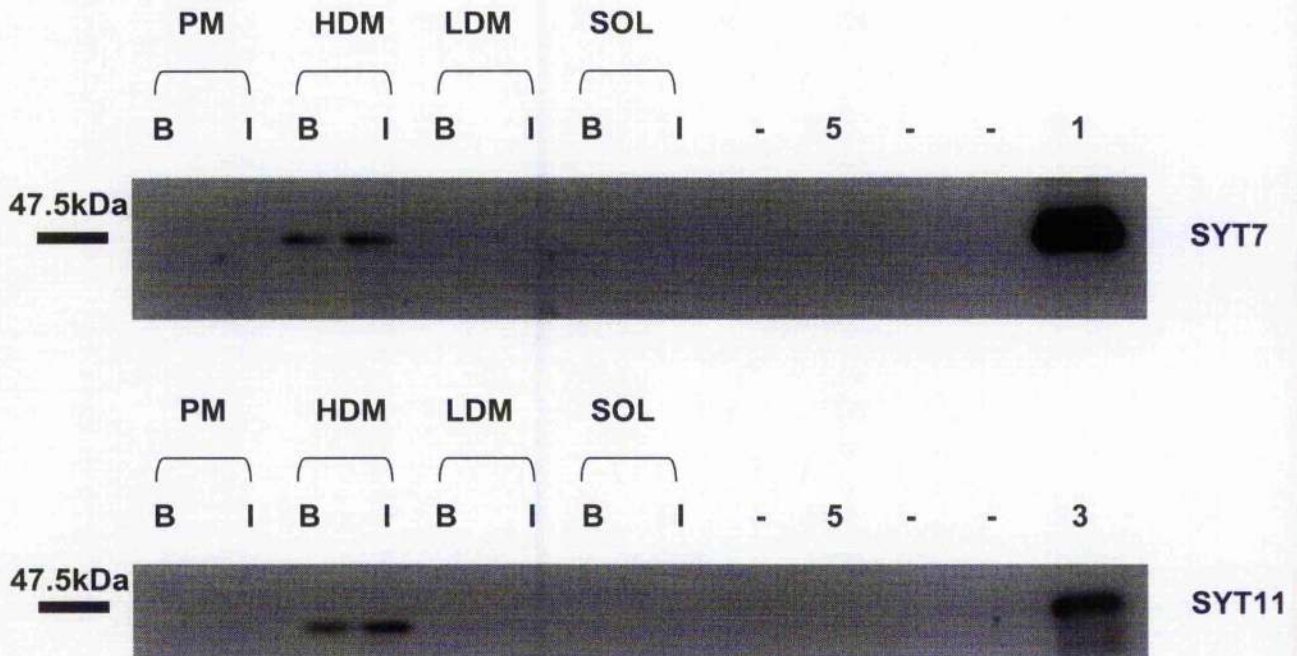


Figure 4.4

Subcellular fractions (plasma membrane (PM), high density microsomes (HDM), low density microsomes (LDM) and soluble proteins (SOL) prepared from day 12 post-differentiation 3T3-L1 adipocytes under basal conditions (B) or following 30 minute stimulation with 100nM insulin (I) separated by SDS-PAGE and transferred to nitrocellulose ((-) indicates empty well) alongside HEK cell lysates characterised in figures 4.1 and 4.2. 15 μ l of each fraction (prepared as described in figure 4.4) was loaded per well. Immunoblots using GLUT4 antibody (1:1000 dilution) or Syntaxin4 antibody (1:1000) are shown. Data are representative of 2 identical experiments using discrete populations of cells.

Figure 4.5 3T3-L1 Cell PM and LDM Fractions

Figure 4.5a

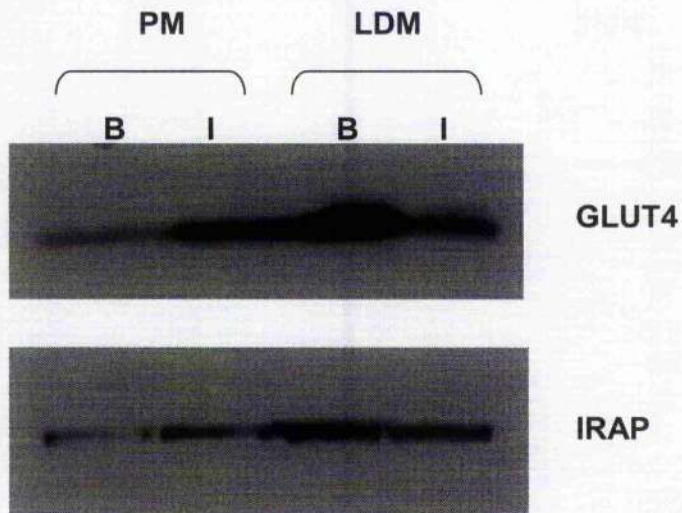


Figure 4.5b

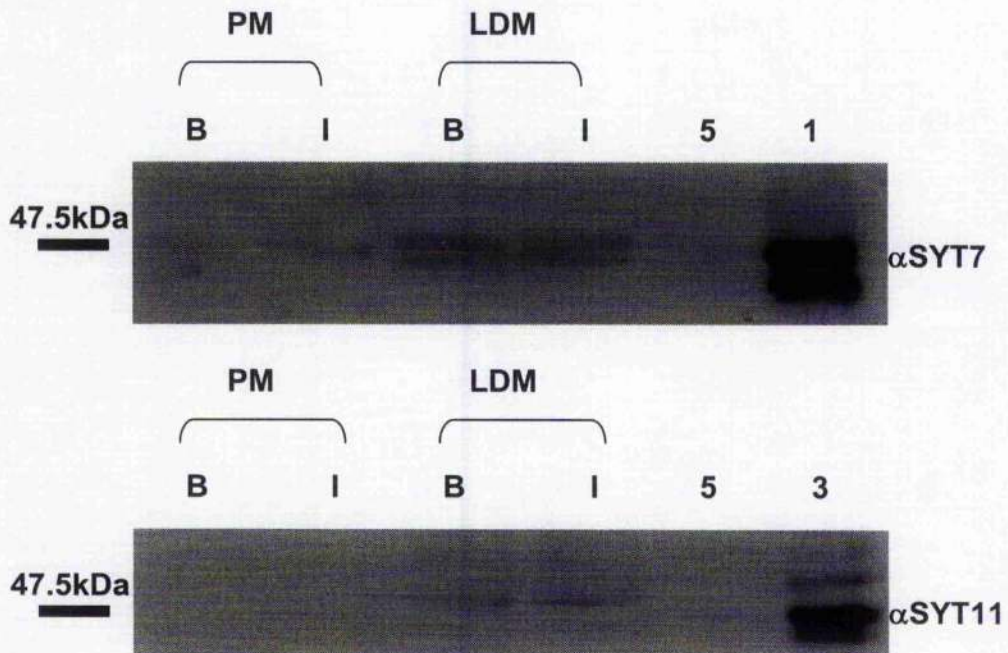


Figure 4.5

Plasma membrane (PM) and low density microsome (LDM) fractions prepared from day 12 post-differentiation 3T3-L1 adipocytes under basal conditions (B) or following 30 minute stimulation with 100nM insulin (I) separated by SDS-PAGE and transferred to nitrocellulose alongside HEK cell lysates characterised in figures 4.1 and 4.2. 25µl of the same fractions as described in Figure 4.5 above was loaded per well. Immunoblots using GLUT4 antibody (1:1000 dilution) or IRAP antibody (1:1000) are shown. Data are representative of 5 identical experiments using discrete populations of cells.

4.4 Discussion

The high degree of sequence homology that exists between isoforms of the SYT family (228), the similarities observed between the published C2 domain structures (250;311;314); Cheng et al. 2004), and evidence for redundancy between isoforms (315) together predict that the production of isoform-specific SYT antibodies is likely to be difficult. The observed lack of commercially available antibodies to many SYT isoforms is in support of these observations. In spite of this, the SYT7 and SYT11 antisera characterised in this chapter appear to be specific for their respective target proteins. However, in order to be certain of full specificity, determination of the binding of each antiserum to purified protein from each murine SYT isoform would be required.

The antisera characterised in section 4.3.1 were used in an attempt to demonstrate the subcellular localisation of SYT7 and SYT11 in 3T3-L1 adipocytes by immuno-fluorescent microscopy. Cellular staining produced was indistinct from that seen with secondary antibody alone, therefore not felt to be specific for either protein at the dilutions used, and probably due to non-specific binding as discussed above.

An equal molar concentration of each plasmid to express SYT7 and SYT11 was used to transfect identical cell populations. The difference in immunoreactivity between adjacent positive control wells for both antisera used (seen in figures 4.1 and 4.2) probably reflects a

combination of two factors: each plasmid possesses a distinct promoter which may drive different levels of expression in the same cells, and the plasmids are of significantly different size, and thus efficiency of transfection will be different for each plasmid (lower efficiency for the larger plasmid).

The subcellular distribution data presented in this chapter are largely descriptive, and show for the first time the localisation of both SYT7 and SYT11 within specific membrane compartments of the 3T3-L1 adipocyte. The absence of SYT7 or SYT11 in the soluble fractions demonstrates these are indeed membrane-bound proteins *in vitro*. Furthermore, from these data it is possible to conclude that SYT7 is predominantly localised within the HDM fraction, which has previously been shown to possess ER and lysosomal markers (316). A significantly smaller amount of SYT7 is present divided equally between the LDM fraction (which is known to contain markers for the TGN), and the PM. Insulin stimulation has no effect on the distribution of SYT7 in 3T3-L1 adipocytes.

SYT11 shows a similar subcellular distribution to SYT7: the majority of the intracellular SYT11 pool is located in the HDM fraction, with a small amount in the LDM fraction. Like SYT7, the subcellular distribution of SYT11 is independent of insulin effect.

The subcellular distribution of endogenous SYT11 has previously been described only in human substantia nigra neurons, where it was observed to be present in cell bodies and neurites (242). SYT11 was also seen to localise in the Lewy bodies in the substantia nigra of two individuals known to have Parkinson's Disease. Epitope-tagged SYT11 has been exogenously expressed in PC12 cells (242;317). On both occasions SYT11 was seen to localise with the Golgi and in immature vesicles. This distribution is very similar to the previously described subcellular distribution of the SYT family member with the greatest similarity to SYT11, SYT4 (318-321). The distribution of SYT11 described here is in agreement with these observations.

The subcellular distribution of SYT7 has previously been studied by a combined immunofluorescence microscopy / subcellular fractionation approach in the NRK fibroblast and L6 myoblasts (322). In these experiments SYT7 was seen to localise to the dense intracellular membranes of the mature lysosome and the PM. No SYT7 was detected in lower density Golgi fractions, and no colocalisation was seen with endosomal markers such as EEA1 or the TfR suggesting that SYT7 was not present within these compartments. The data presented here is generally in accord with that previously described. The small amount of SYT7 observed in the LDM fraction here may be a result of adipocyte differentiation, or may simply represent contamination of the LDM fraction with HDM proteins.

The observed distribution SYT7 and SYT11 is not at first glance in support of the hypothesis proposed in Chapter 1, where it was proposed that a particular SYT isoform may interact with the Syntaxin4 / SNAP23 / VAMP2 SNARE complex and drive GSV-PM fusion. However, the presence of a population of SYT7 at the PM remains consistent. From these data it is unlikely that SYT11 will prove to play such a role.

GLUT4 trafficking between the endosomal system and the TGN is known to be regulated by a number of factors including the t-SNARE proteins Syntaxin6 and Syntaxin16 (186;323;324). In addition, molecules such as the v-SNARE Vti1a (325) and the synaptogyrin homolog Cellugyrin (326) have been implicated. Members of the Golgi-localised γ -ear containing Arf-binding (GGA) family (327;328) and other species such as AP-1 (175) and COPI (304), so called Coat proteins which form complexes with clathrin (reviewed in (329)) have also been suggested as important molecules in the generation of specialised GLUT4-containing membrane compartments.

SYTs have previously been demonstrated to interact with SNAREs (as discussed in Chapter 1 section 1.5.6), and the C2B domain of SYT has been shown to bind the PM adaptin molecule AP-2, (which shares homology with its TGN homologue AP-1 and plays a key role in endocytosis) (330). Therefore in experiments designed to assess their function, either SYT7 or SYT11 may prove to play a role in a putative

GLUT4 sorting step at the endosome-TGN interface via interaction with molecules such as those listed above.

Chapter 5 siRNA-Mediated Gene Depletion in the 3T3-L1

Adipocyte

5.1 Introduction

The discovery of short inhibitory RNA as a further level of natural complexity surrounding regulation of eukaryotic gene expression (331) and its subsequent exploitation as a method of targeted gene depletion has gifted biologists with a means of *in vitro* genetic manipulation that is of immense power and yet provides exquisite specificity and control. This methodology has been previously described in the investigation of insulin action in 3T3-L1 cells (118;332).

This chapter shall describe the transfection of mature 3T3-L1 adipocytes with siRNA by electroporation. The use of siRNA oligonucleotides directed against key signal transduction molecules in the insulin signalling cascade shall confirm data obtained using similar methodology in other groups. These techniques shall then be used to investigate the phenotype consequent to siRNA-mediated knockdown of SYT7 and SYT11 in 3T3-L1 adipocytes with respect to insulin stimulated glucose uptake.

5.2 Methods

5.2.1 Design of siRNA

Lamin A/C siGLO™ control siRNA, Smartpool™ siRNA directed against PTEN, AKT and SYT7, and Non-targeting siRNA were obtained from Dharmacon, USA. Lamin A/C siGLO™ control siRNA used is an siRNA directed against a housekeeping gene covalently attached to a fluorescent reporter, thus allowing direct visualisation of transfected cells. Smartpool™ siRNA represents a group of 4 separate siRNA oligonucleotides directed against each specific target transcript. Non-targeting siRNA represents a 20-mer duplex siRNA oligonucleotide designed to have no activity against (thus no sequence homology with) any transcribed murine gene.

The siRNA directed against SYT11 was designed by Dr Prasenjit Mitra, Umass Medical School, Worcester, MA, USA. Briefly, the secondary tRNA structure was predicted using Vienna Secondary mRNA Structure Prediction software (333) . Target regions of 15-20 nucleotides were selected that were predicted to be present on the “exposed” surface of the mRNA. Each proposed siRNA sequence was then compared to the entire mouse transcriptome sequence using the NCBI Basic Local Alignment Search Tool (72) to ensure specificity for SYT11 (302); (the SYT11 siRNA nucleotide sequence is given in section A1.4 in the Appendix).

Scrambled SYT11 siRNA has identical base pair complement to the SYT11 siRNA sequence but the residues are in a randomised order. The sequence was compared with the mouse transcriptome using the NCBI Basic Local Alignment Search Tool (72) (302) to ensure there would be no unexpected activity against any other transcribed murine gene.

5.3 Results

5.3.1 Efficiency of Transfection by Electroporation

In order to assess the efficiency of transfection by electroporation a fluorescently labelled siRNA was transfected into 3T3-L1 adipocytes and the observed fluorescence compared to that present in cells simultaneously transfected with an unlabelled siRNA species. Concentration of siRNA transfected was similar to that used in subsequent experiments (4 nmoles/ 10^6 cells).

In Figure 5.1 a fluorescent signal can be seen in every cell transfected with siRNA. The strength of signal between cells is variable, with the reporter signal being stronger in some cells than in others. More fluorescence can be seen with cells transfected with 4.5nmoles/ 10^6 cells compared to 0.5nmoles/ 10^6 cells implying a dose-dependent effect. No fluorescence is seen with cells transfected with an unlabelled siRNA (4.5nmoles/ 10^6 cells), confirming the fluorescent signal observed is derived from the labelled siRNA used and not due to adipocyte autofluorescence.

Image data collected in transmission mode (46) confirms the typical adipocyte appearance of electroporated cells, with very few cells having a fibroblast appearance. This confirms the success of the adipocyte differentiation process, that the electroporation technique used

achieves transfection of these differentiated adipocytes, and that post-transfection survival of adipocytes is maintained.

These results suggest a 100% transfection efficiency when 3T3-L1 adipocytes are electroporated with siRNA.

Figure 5.1 Efficiency of Transfection

Figure 5.1a siGLO™ Lamin A/C siRNA 0.5nmoles/10⁶ cells

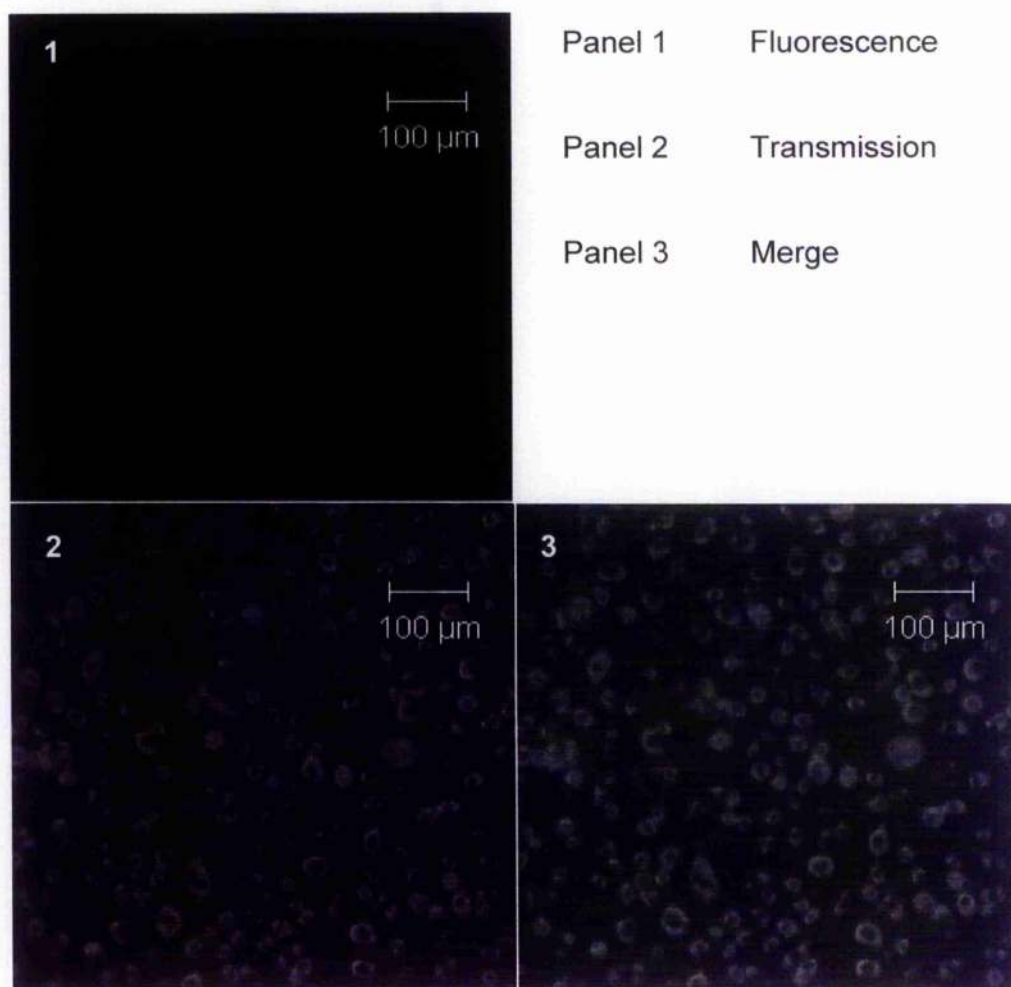


Figure 5.1 Efficiency of Transfection

Figure 5.1b siGLO™ Lamin A/C siRNA 4.5nmoles/10⁶ cells

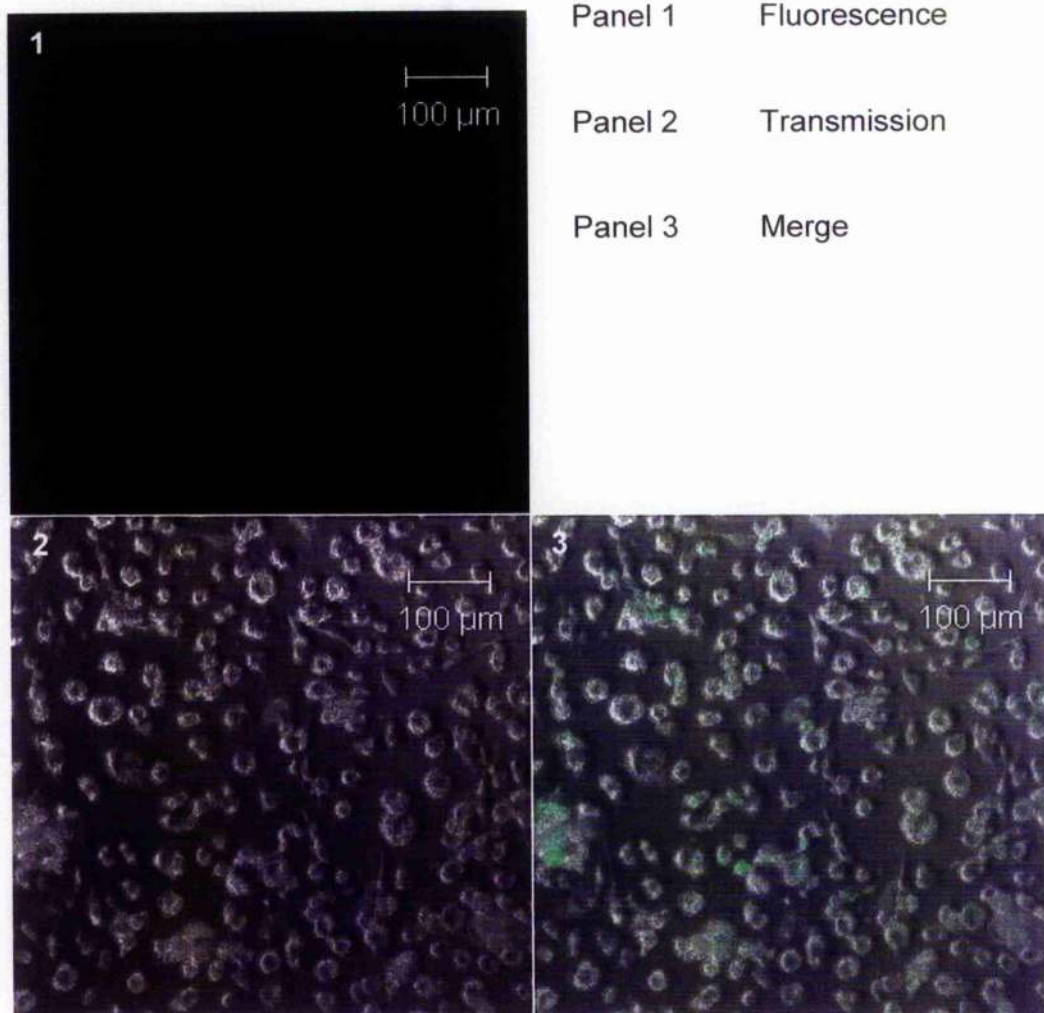


Figure 5.1 Efficiency of Transfection

Figure 5.1c Control cells

(Non Targeting siRNA 4.5nmoles/10⁶ cells)

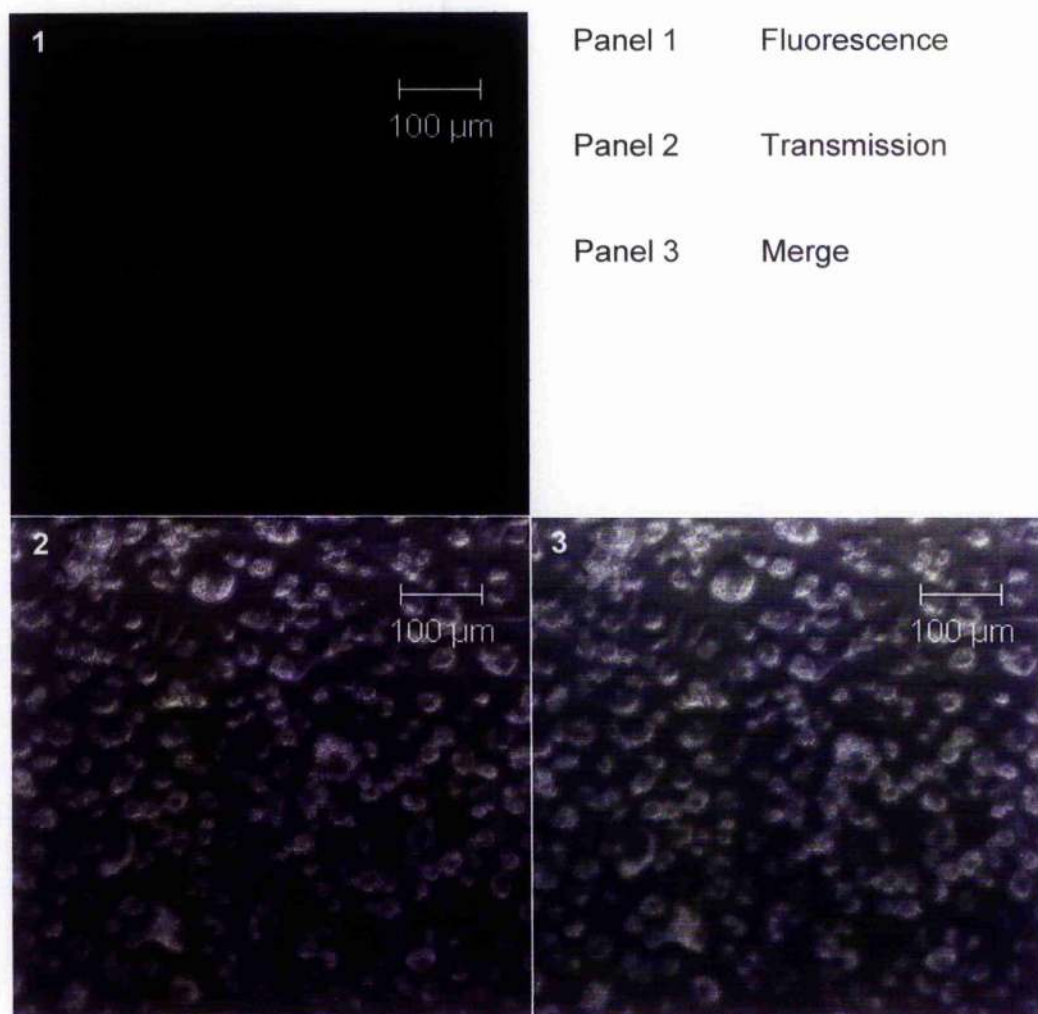


Figure 5.1a, 5.1b and 5.1c

Confocal microscopy images of 3T3-L1 adipocytes 48hours following transfection with the indicated concentration of fluorescently labelled siGLO™ Lamin A/C siRNA and unlabelled control siRNA (NT). Panel 1 shows image acquired using fluorescence microscopy. Panel 2 shows transmission image. Panel 3 merges Panels 1 and 2. 100µm size bar shown. Images acquired using a Carl Zeiss Pascal Confocal microscope, 488nm excitation energy, 510 1p detection filter and 63x objective lens. Data are from a single experiment.

5.3.2 Influence of siRNA Mediated Knockdown of PTEN and AKT2 on Insulin-Stimulated Deoxyglucose Uptake

Figure 5.2 shows insulin-stimulated 2-deoxyglucose uptake in 3T3-L1 adipocytes transfected with siRNA directed against PTEN, AKT2 and non-targeting control siRNA. In the basal state, and at all concentrations of insulin examined PTEN knockdown potentiated glucose uptake, and AKT2 knockdown reduced insulin-stimulated glucose uptake compared to cells transfected with a Non-Targeting control siRNA.

The extent of target knockdown was not assessed (either at the mRNA level e.g. by semi-quantitative PCR, or at the protein level e.g. by Western blotting). Nevertheless, these data show potentiation and abrogation of insulin action of the same magnitude to that previously reported when expression of PTEN and AKT are knocked down using the same siRNA sequences (105;118). Therefore, whilst efficient transfection cannot be confirmed, successful siRNA-mediated gene knockdown is implied.

Figure 5.2 2-Deoxyglucose Uptake in siRNA Transfected 3T3-L1 Adipocytes: PTEN and AKT

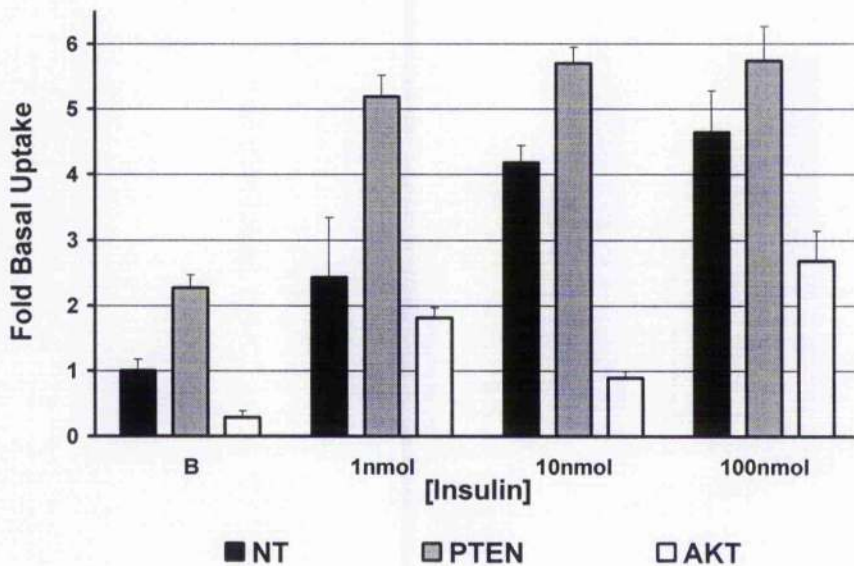


Figure 5.2 3T3-L1 adipocytes were electroporated with non-targeting (NT), PTEN or AKT siRNA SmartpoolsTM as described in section 123 and assayed for insulin-stimulated deoxyglucose uptake at the indicated concentrations of insulin as described. Data is presented relative to the basal rate in non-transfected cells. (N= 3 at each point; error bars indicate 1 standard deviation from mean values; p values indicating difference from non-transfected cells at that given insulin concentration determined using a two-sample Student's T-test assuming unequal variance; (*) indicates $p < 0.05$; (+) indicates $p < 0.005$; (†) indicates $p < 0.001$; (‡) indicates $p < 0.0001$; (334) indicates $p < 5 \times 10^{-5}$. Data are representative of two identical experiments with discrete populations of cells.

5.3.3 Influence of siRNA Mediated SYT11 Knockdown

siRNA-mediated knockdown of SYT11 in 3T3-L1 adipocytes has no apparent effect on cell size (Figure 5.3). Non Targeting, Scrambled and SYT11 knockdown cells are morphologically similar and have similar lipid content when examined by light microscopy. Intracellular lipid droplets are clearly visible within all cells. The number of electroporated cells per well were not formally counted however the light microscopic appearance indicates equal number of cells in each well. This suggests that surviving cell density is identical regardless of siRNA species used. The cells can be seen to be terminally differentiated there would not be expected to be further cell division. Together these data suggest post-transfection cell viability is identical for each siRNA studied.

Figure 5.4 reveals the effect of transfecting 3T3-L1 adipocytes with siRNA directed against SYT11 on insulin-stimulated glucose uptake. SYT11 knockdown has no effect on basal glucose uptake. In cells stimulated with insulin SYT11 knockdown results in reduced glucose uptake compared to cells transfected with a non-targeting (NT) control siRNA. The difference in glucose uptake between SYT11 and NT siRNA is significant at 10nM insulin ($P < 0.05$), and approaches significance at 1nM insulin ($p = 0.059$).

The immunoblots shown in figure 5.5 show a reduction in SYT11 protein detected in cells transfected with SYT11 siRNA. The reduction in

SYT11 protein compared to Non-targeting (NT) and Scrambled (SCR) siRNA was quantified and results are shown in figure 5.6. These data suggest a 30% knockdown compared to Non-targeting, and a 40% knockdown of SYT11 compared to Scrambled siRNA (Figure 5.6a and 5.6b respectively). These data suggest the SYT11 siRNA oligonucleotide has facilitated targeted disruption of the SYT11 transcript, and that there has been no such effect produced by NT or SCR siRNA. The size of the protein knockdown is disappointingly small. Furthermore, assessment of SYT11 transcript knockdown e.g. by Taqman RTPCR was not performed.

Figure 5.5 also shows that there has been no effect on TfR protein level with either NT, SCR or SYT11 siRNA. The third panel in figure 5.5 shows the effect of SYT11 knockdown on GLUT4 protein. There is no effect on GLUT4 protein with NT siRNA, and a reduction in GLUT4 protein in cells transfected with SYT11 siRNA. Surprisingly, there is reduced GLUT4 protein in cells transfected with SCR siRNA.

Data were not gathered to formally assess protein concentration in cell lysates from cells transfected with the siRNAs described. However, the data in figure 5.4 and 5.5 demonstrates there is no effect on the level of the Transferrin Receptor or GAPDH proteins relative to that of any other siRNA studied. Since both of these proteins can be considered as having a "housekeeping" role in 3T3-L1 cells these data serve to (at least in part) confirm that any observed effect is indeed due to the influence of gene knockdown over components of the insulin signalling mechanism as

opposed to influence over cell viability or survival. As can be seen in Figure 5.7 protein levels of species known to influence GSV-PM fusion such as Syntaxin4, and SNAP23 (and IRAP) remain unchanged in cells transfected with either NT, SCR or SYT11 siRNA.

Figure 5.8 shows there is no difference in fold-stimulation of insulin-stimulated cell surface transferrin labelling compared to basal cells when either SYT11 or NT siRNA are used. This confirms an intact endocytic trafficking system.

Figure 5.3 Light Microscopy Appearance of Transfected Cells

Figure 5.3a Non-Targeting siRNA

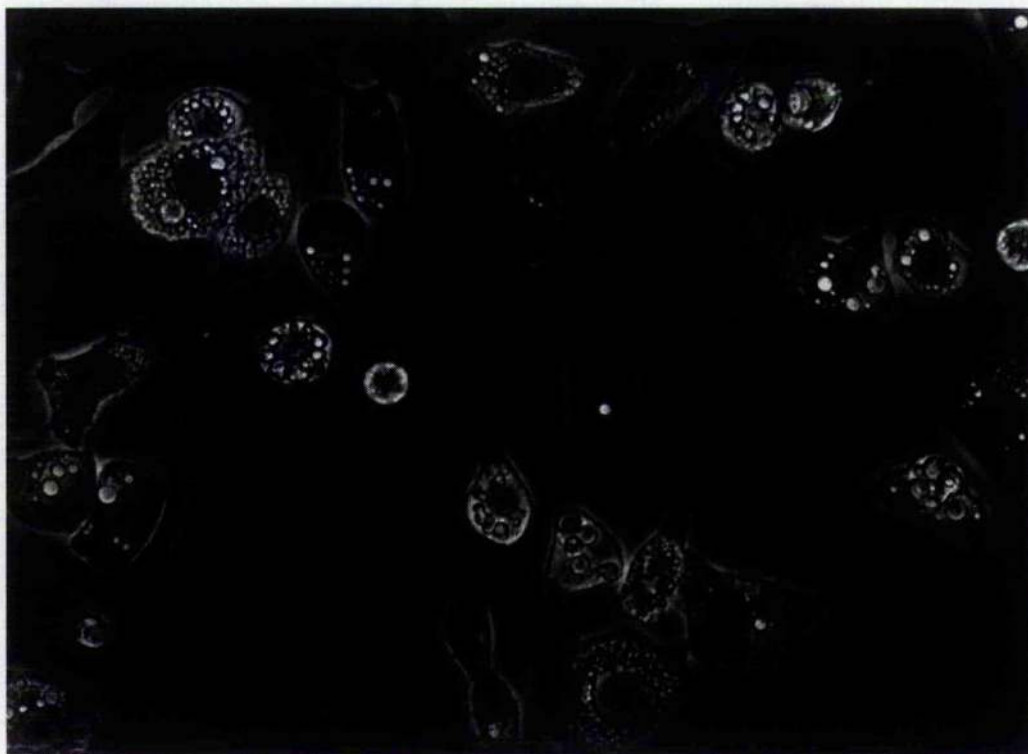


Figure 5.3 Light Microscopy Appearance of Transfected Cells

Figure 5.3b SYT11 Scrambled siRNA



Figure 5.3 Light Microscopy Appearance of Transfected Cells

Figure 5.3c SYT11 siRNA

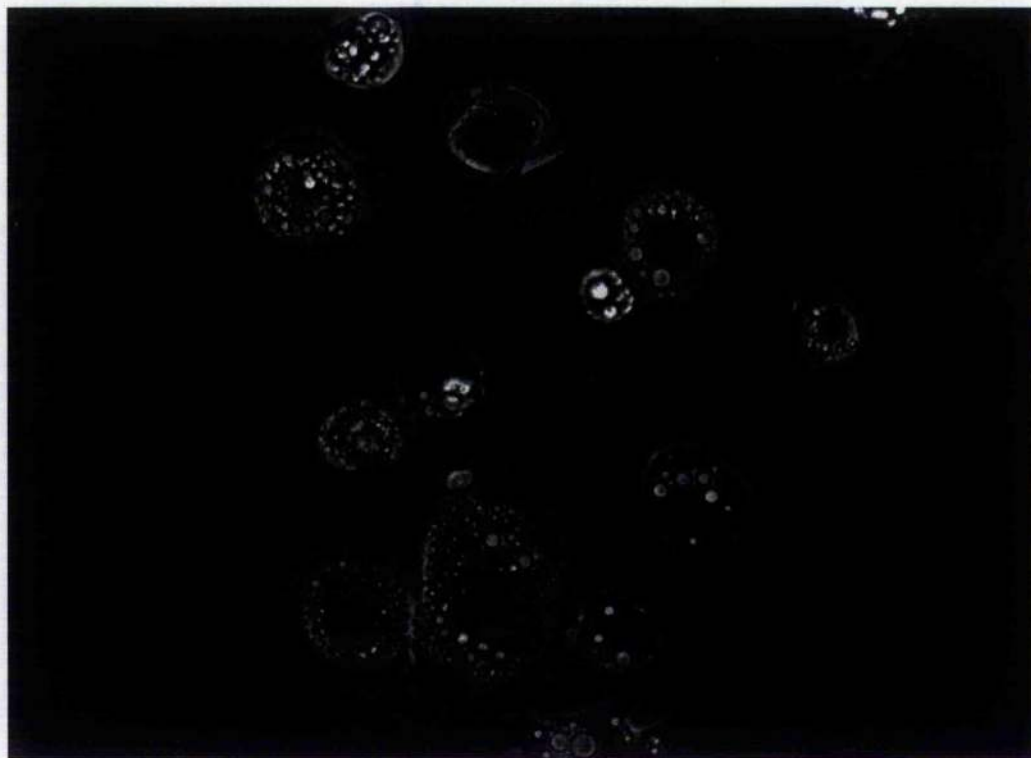


Figure 5.3 Light Microscopy of live 3T3-L1 cells 48 hours following transfection with the indicated siRNA by electroporation. Images acquired using a Carl Zeiss Axiovert 135 microscope and 135x objective lens. Data are from a single experiment.

Figure 5.4 Influence of SYT11 Knockdown on Insulin-Stimulated 2-deoxyglucose Uptake

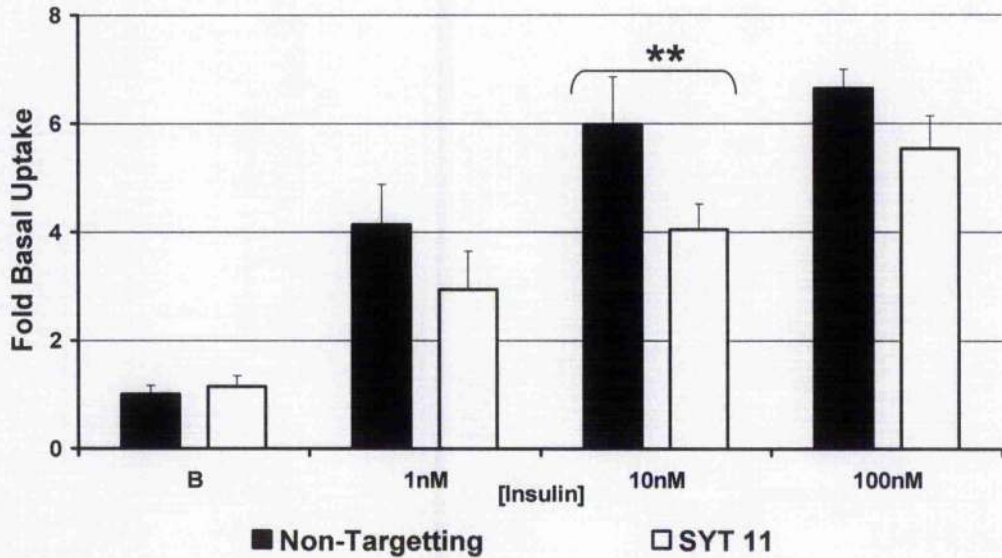


Figure 5.4 3T3-L1 adipocytes were electroporated with Non-Targetting or SYT11 siRNA and assayed for insulin-stimulated deoxyglucose uptake at the indicated concentrations of insulin as described. Data is presented relative to the basal rate in cells transfected with Non-Targetting siRNA. (N= 3 at each point; error bars indicate 1 standard deviation from mean values; (**)) indicates $p < 0.005$; Statistical differences were calculated by paired Student's t-test. Data are the mean of three identical experiments using discrete populations of cells.

Figure 5.5 SYT11 siRNA

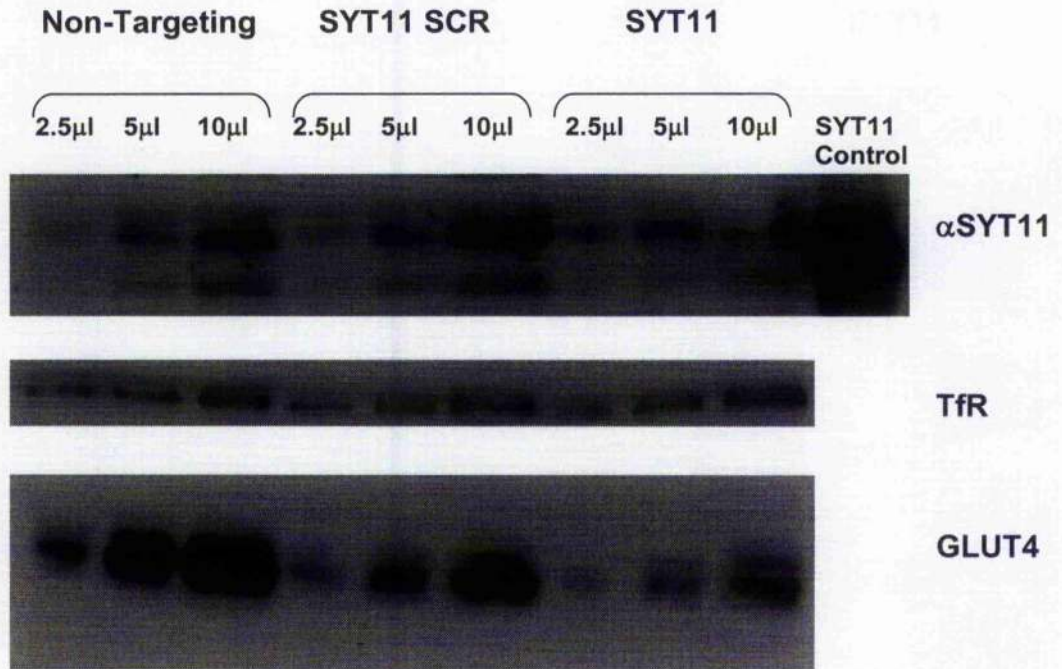


Figure 5.5

Scanned images obtained from Western blots using affinity-purified SYT11 antisera, transferrin receptor (238) and GLUT4 antibodies. Cell lysates prepared from 3T3-L1 adipocytes 72 hours following electroporation with Non-Targeting, SYT11 scrambled (SCR) and SYT11 siRNA, and the previously characterised SYT11-transfected HEK cell control (11) were resolved by SDS-PAGE. Cells from a 10cm tissue culture plate were used to prepare 500 μ l whole cell lysate; the volume indicated (in 4x SDS-PAGE buffer) in μ l was loaded per well. TfR and GLUT4 antibodies were used at 1:1000; SYT11 antibody was used at 1:250 dilution. Data are representative of three experiments using discrete populations of cells.

Figure 5.6 Quantification of SYT11 Knockdown

Figure 5.6a

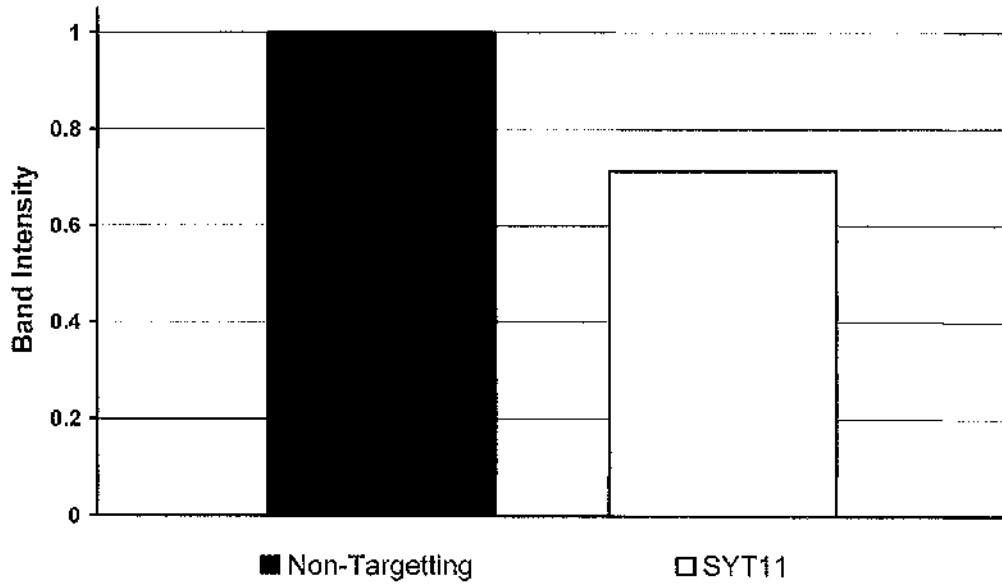


Figure 5.6b

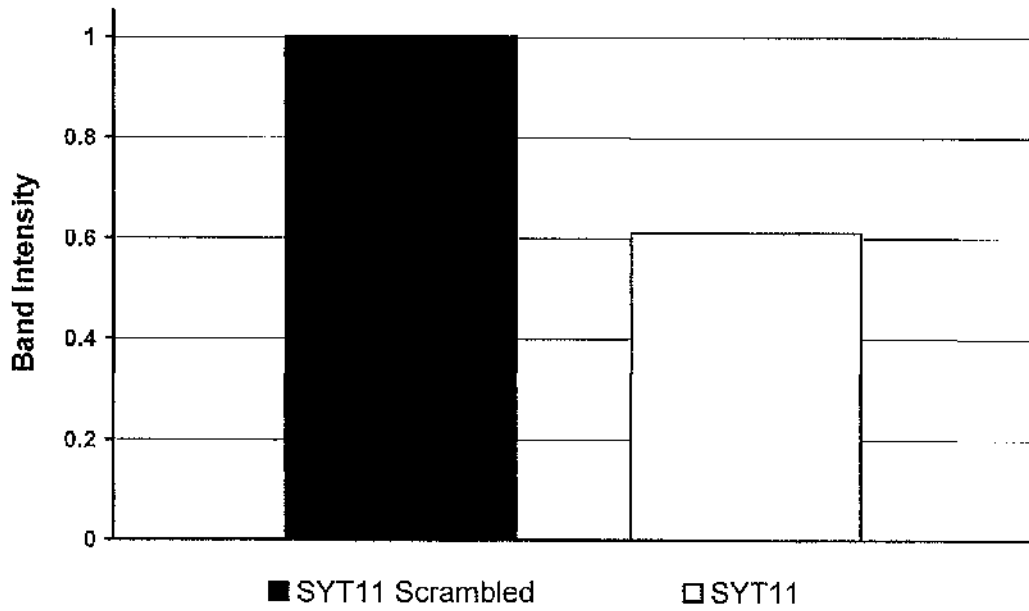


Figure 5.6a and 5.6b

Quantification of SYT11 knockdown. A Mercury scanner was used to generate a Photoshop digital image of the SYT11 immunoblot in 5.3 above, and the image analysed using Image J software to assess band intensity. Intensity of SYT11 immunoreactive band in SYT11 siRNA cells is compared to Non-targeting siRNA in 5.5a, and to Scrambled siRNA in 5.5b.

Figure 5.7 IRAP, Syntaxin4, SNAP23 and GAPDH in SYT11 siRNA-Transfected 3T3-L1 Adipocytes

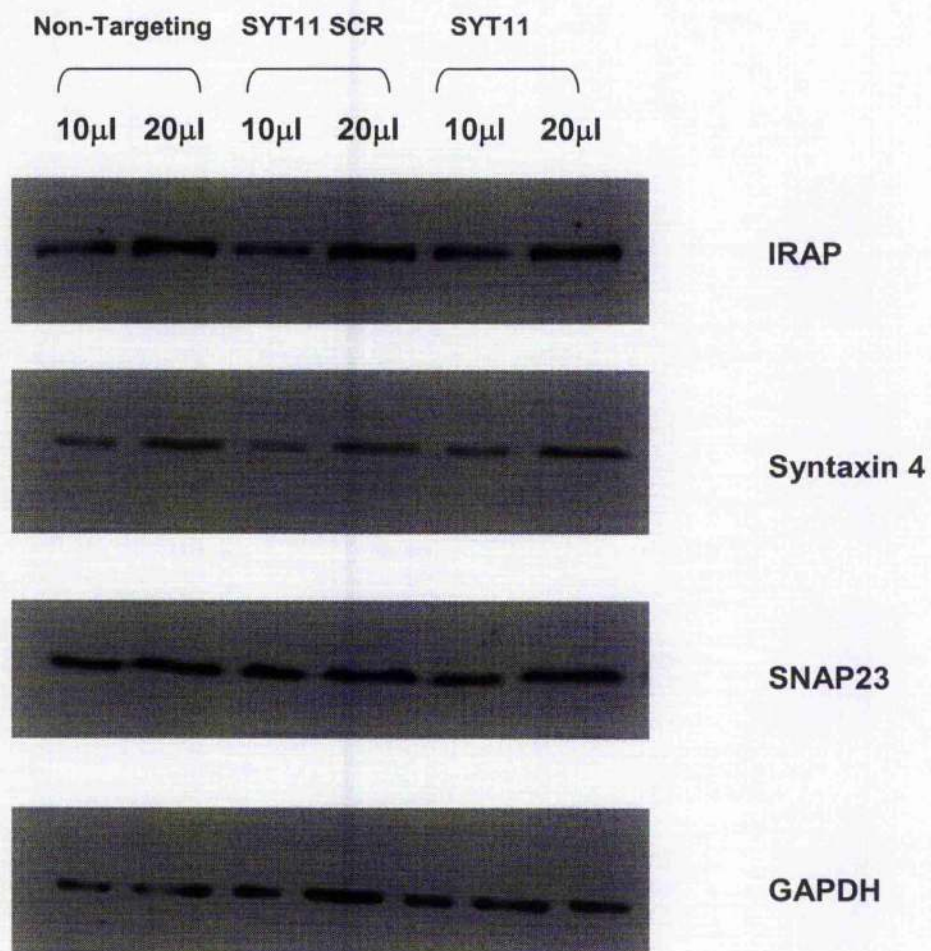


Figure 5.7

Scanned images obtained from Western blots using IRAP, Syntaxin4, SNAP23 and GAPDH antibodies. Cell lysates prepared from 3T3-L1 adipocytes 72 hours following electroporation with the indicated siRNA were resolved by SDS-PAGE. Cells from a 10cm tissue culture plate were used to prepare 500 μ l whole cell lysate; the volume indicated (in 4x SDS-PAGE buffer) in μ l was loaded per well. IRAP, Syntaxin4 and SNAP23 antibodies were used at 1:1000; GAPDH antibody was used at 1:2000 dilution. Data are representative of three experiments using discrete populations of cells.

Figure 5.8 Cell Surface Transferrin Binding in 3T3-L1 Adipocytes Transfected with SYT11 siRNA

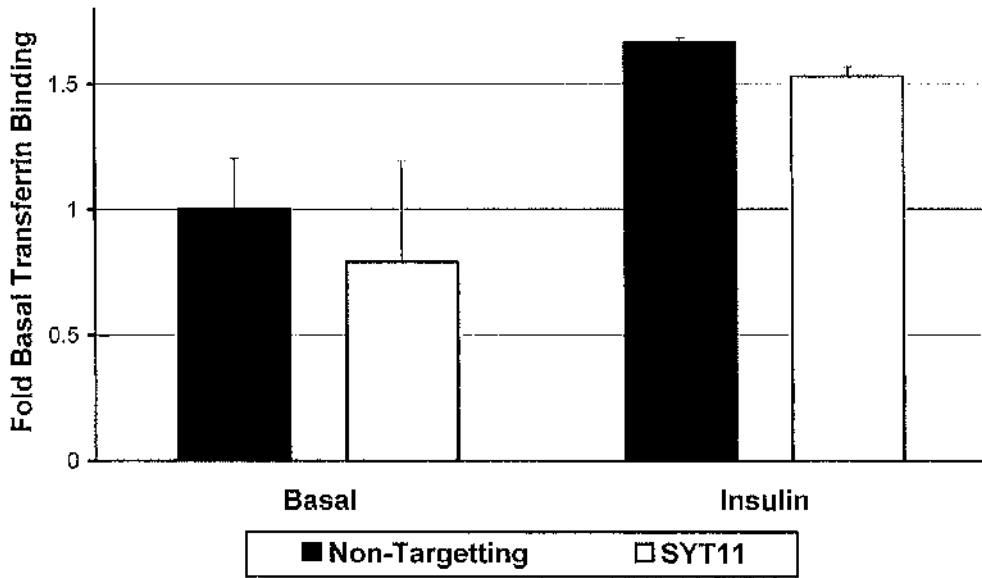


Figure 5.8

Fold basal cell surface radiolabelled transferrin binding in 3T3-L1 adipocytes transfected with Non-Targetting or SYT11 siRNA and stimulated with 1 μ M insulin. Data presented are from an individual experiment; error bars show 1 standard deviation from mean values; significance of variance was determined using a two-sample Student's T-test assuming unequal variance.

5.3.4 Influence of siRNA Mediated SYT7 Knockdown

Figure 5.9 reveals the effect of transfecting 3T3-L1 adipocytes with siRNA directed against SYT7 on insulin-stimulated glucose uptake. These data suggest that in the basal state, and at all insulin concentrations examined SYT7 knockdown results in a significant increase in glucose uptake compared to cells transfected with a non-targeting (NT) control siRNA. The difference observed between SYT7 and Non Targeting siRNA reaches statistical significance at 1nM insulin ($p < 0.05$) and at 100nM insulin ($p < 0.01$).

The extent of SYT7 knockdown at both the mRNA and protein level remains to be confirmed. Furthermore (and as for SYT11) the influence of SYT7 knockdown on GLUT4 (and other species known to be required for its effective delivery to the PM in response to insulin) requires to be assessed before any firm conclusion regarding the mechanism responsible for the effect seen in figure 5.9 can be drawn.

Figure 5.9 Influence of SYT7 Knockdown on Insulin-Stimulated 2-Deoxyglucose Uptake

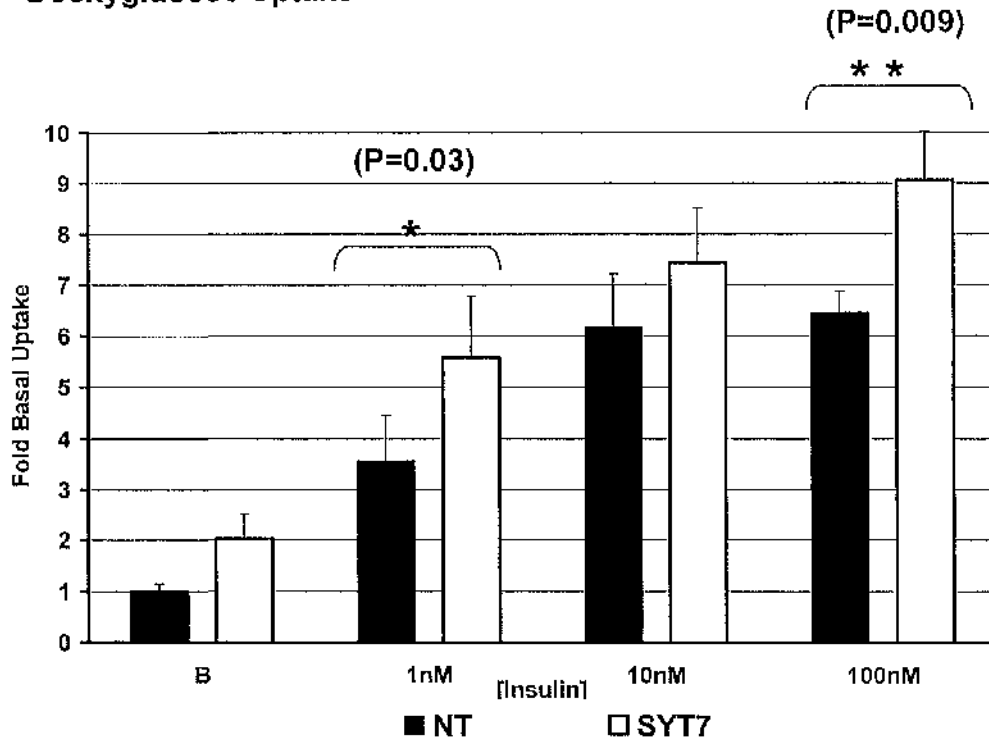


Figure 5.9

Fold basal 2-deoxy glucose uptake in 3T3-L1 cells transfected with Non-Targeting (NT) or SYT7 siRNA and stimulated with insulin at the concentration indicated. Data presented are the sum of 3 identical experiments using discrete cell populations; error bars show 1 standard deviation from mean values; (278) indicates $p \leq 0.05$, (**) indicates $p < 0.01$ calculated using paired Student's t-test.

5.4 Discussion

The efficiency of transfection of differentiated 3T3-L1 adipocytes with a fluorescently labelled siRNA by electroporation is shown here to be near 100%. For subsequent experiments the transfection efficiency was assumed to be identical regardless of siRNA sequence used.

PTEN acts as a negative regulator of insulin signalling by converting PM PI(3,4,5)P₃ to PI(3,5)P₂, thus reducing signalling via PI3K, and AKT plays a central role in the insulin signalling cascade downstream of PI3K (as discussed in Section 1.3.7 and 1.3.8 above). Czech and co-workers have optimised the technique of transfecting differentiated 3T3-L1 adipocytes by electroporation, and have used this powerful method to examine the role of these and other species in insulin-stimulated glucose uptake (Zhou et.al, 2004). In their experiments a 2-4 fold enhancement with PTEN, and 60% depletion with AKT2 knockdown was demonstrated in insulin-stimulated glucose uptake. These data have been reproduced in the current study by employing an identical technique and identical siRNA oligonucleotides.

As can be seen in Figure 5.1, in the basal state and at low concentrations of insulin \geq 2-fold increase in uptake is seen with PTEN siRNA when compared to a non-targeting control siRNA. This effect remains present, but is less pronounced at high (supra-physiological) insulin concentration. One can conjecture that the reduction of effect seen

with high insulin dose is due to saturation of the PM with PI(3,4,5)P₃ generated by PI3K, thus overcoming the effect of PTEN knockdown. In the same figure it is possible to see a reduction in insulin-stimulated glucose uptake in the basal state and with insulin-stimulation when AKT2 is targeted with siRNA when compared to control. The central signalling role played by this enzyme is supported by the observation that, in its absence not even stimulation with supra-physiological insulin doses can restore normal cellular glucose uptake.

These experiments were performed twice, and identical results were obtained on both occasions. However, neither assays of PTEN or AKT (157) nor RTPCR of their transcripts were performed. Thus whilst it is not possible to conclude that knockdown of PTEN and AKT were responsible for the effect, the data are in support of this.

The preceding results chapters in this thesis have identified the SYT11 and SYT7 transcripts as the predominant isoforms in the 3T3-L1 adipocyte. SYT11 mRNA is upregulated as cells differentiate and acquire insulin sensitivity. Upon subcellular fractionation, SYT7 and SYT11 proteins are present mostly in the high density microsome fraction. Both are also present at lower abundance in the low density microsomes, and SYT7 is present at low level in the plasma membrane. The distribution of neither SYT isoform is altered by insulin stimulation.

The immunoblot of lysates from SYT11 knockdown cells (seen in figure 5.3) shows only a small apparent reduction in SYT11 protein. When quantified directly from the immunoblot this amounts to around 30% knockdown of SYT11. This is disappointingly small. Possible reasons for this are manifold, and include reduced transfection efficiency with this oligonucleotide, poor target recognition resulting in reduced RISC activation, and a long half life of SYT11 protein.

The immunoblots examining the extent of SYT11 protein knockdown were performed using a whole cell lysate. Given that the SYT11 molecule has a transmembrane domain and is believed to be a membrane protein *in vivo* the preparation of whole cell membranes and subsequent immunoblotting may reveal a more profound protein knockdown.

On closer inspection of the scanned immunoblot image it is possible to observe that the signal from the adjacent SYT11 control protein lane is so strong as to increase the signal in the SYT11 siRNA lanes. The result is an overestimation of SYT11 protein signal in these lanes, and a corresponding underestimation of siRNA effect. The fact that a significant effect on glucose uptake is seen with such a small reduction in protein supports a major role for SYT11 within the adipocyte.

SYT11 siRNA-treated 3T3-L1 adipocytes exhibit abrogated insulin-stimulated glucose uptake regardless of insulin concentration used. Basal

uptake is unchanged. The reduction in insulin-stimulated glucose uptake is marked with 1nM and is significant with 10nM insulin. The effect is less marked when 100nM insulin is used to stimulate the cells. This suggests that the effect of SYT11 knockdown can be rescued by maximal stimulation with insulin in a similar way to PTEN knockdown as discussed above.

GLUT4 protein levels are reduced in SYT11 knockdown cells. These data support the suggestion that SYT11 in the adipocyte is at least in part concerned with the regulation of GLUT4. SYT11 may be required for the sequestration of GLUT4 from the endosomal recycling pathway into the slower TGN / endosomal / GSV pathway, and the subsequent production of GSVs. In the absence of SYT11 GLUT4 may be prevented from entering this pool, leading to less GLUT4 destined to become the GSV compartment and so fewer GSVs are produced within the cell. Such mistargetting of GLUT4 may lead its eventual degradation, accounting for the reduced levels seen in SYT11 knockdown cells.

A reduction of GLUT4 in the specialised insulin-regulatable compartment would reduce the GSV pool available for translocation in response to insulin, requiring more insulin for any given effect. The GLUT4 content of the endosomal system would be unchanged, therefore basal glucose uptake (to which GSV-derived GLUT4 makes only a small contribution), would be preserved. IRAP is however unaffected by SYT11 knockdown, and so the selection step for GLUT4 that leads to its

sequestration and ultimate degradation within this model would require to be specific for GLUT4, and occur prior to the formation of the GSV. Thus, in keeping with data from Chapter 3 and Chapter 4 concerning the timing of SYT11 expression during differentiation, the role of SYT11 may be in the generation of the GSV compartment in differentiating adipocytes.

It is unlikely that within the adipocyte SYT11 is regulated acutely by insulin. Experimental evidence supporting this idea is provided by figure 5.5. No reduction in cell surface TfR labelling (which in turn reflects general endosomal recycling) is observed in SYT11 knockdown cells. No reduction in TfR protein level is observed (Figure 5.3). These data are in support of a specialised role for SYT11 in post-endosomal or TGN sorting of GLUT4 since endosomal recycling is unaffected by its removal.

The SCR siRNA was not expected to target any adipocyte transcripts, and thus act as a negative control. In all experiments using both NT and SCR siRNA there was a small reduction in insulin-stimulated glucose uptake seen with SCR compared with NT. This difference was not statistically significant (data not shown). The GLUT4 immunoblots in figure 5.3 suggest that GLUT4 is reduced in SCR siRNA transfected cells. These data suggest that SCR siRNA does indeed have an effect on GLUT4 and thus it is not a valid control siRNA. Since the SCR oligonucleotide sequence was designed to have no homology to any murine transcript the nucleotide sequence of this siRNA may be incorrect.

Analysis by mass-spectrometry could be employed to further investigate these observations.

siRNA-mediated knockdown of SYT7 produces a 3T3-L1 adipocyte with both enhanced basal and insulin-stimulated glucose uptake. These data are from experiments performed at the very end of the time available for laboratory work, and so there are no data concerning the level of SYT7, GLUT4, TfR or SNARE proteins or the effect of SYT7 knockdown on cell surface TfR labelling. It is therefore not possible to confidently suggest a mechanism for this effect. However, the glucose uptake data alone suggest that SYT7 may have a negative effect on GSV-PM fusion, and that in its absence GSVs are more likely to fuse with the PM. Both the glucose uptake data and the subcellular localisation of SYT7 demonstrated in Chapter 4 suggest that SYT7 is also unlikely to be acutely regulated by insulin. SYT7 data presented here are incomplete, and future experimental investigation of GLUT4 and TfR (and its cell surface labelling) are required in SYT7 knockdown cells to clarify SYT7s role.

Chapter 6 Interaction of SYT7 and SYT11 with VAMP-2, Syntaxin-4 and SNAP-23

6.1 Introduction

The preceding results chapters in this thesis have identified the SYT11 and SYT7 transcripts as the predominant isoforms in the 3T3-L1 adipocyte. The mRNA of both is upregulated as cells differentiate and acquire insulin sensitivity SYT11 much more than SYT7. Upon subcellular fractionation, SYT7 and SYT11 proteins are present mostly in the high density microsome fraction. Both are also present at lower abundance in the low density microsomes, and SYT7 is present at low level in the plasma membrane. The distribution of neither SYT isoform is altered by insulin stimulation.

siRNA-mediated knockdown of SYT11 produces a 3T3-L1 adipocyte with abrogated insulin-stimulated glucose uptake, reduced GLUT4 protein, and normal cell surface TfR labelling. These data are in support of the hypothesis that the function of SYT11 in the adipocyte is concerned with the retention of GLUT4 outwith the endosomal system. SYT11 may also participate in the generation of the specialised GSV pool. The absence of SYT11 at the PM suggests this function is not in promoting GSV-PM fusion. Together these observations suggest that SYT11 would not be expected to participate in the Syntaxin4 / SNAP23 / VAMP2 SNARE complex.

The presence of SYT7 at the PM supports a fusogenic role for this isoform. However the increased basal, and potentiated insulin stimulated glucose uptake seen with SYT7 knockdown is the opposite of what would be expected if this was its role. The phenotype seen with siRNA-mediated SYT7 knockdown is in support of PM SYT7 restricting GSV-PM fusion, which it may do by regulating the Syntaxin4 / SNAP23 / VAMP2 SNARE complex.

In other experimental systems the *in vitro* interaction of other SYT isoforms with their SNARE partners has been clearly demonstrated by various experimental approaches including co-immunoprecipitation, pull-down assay and vesicle fusion assay. The data presented in this thesis so far suggests the interaction of the two candidate SYTs with the v- and t-SNARE proteins involved in GSV-PM fusion remains worthy of further investigation.

This chapter shall explore possible *in vitro* interaction between SYT7 and SYT11 and the SNARE proteins known to be required for insulin-stimulated translocation of GSVs in the skeletal muscle cell and adipocyte by examining the binding of a sol SYT7 (sol SYT7) or SYT11 (sol SYT11) molecule (devoid of the TM domain) with previously characterised epitope-tagged versions of both v- and t-SNAREs by two distinct methods: the "pull-down" assay and "vesicle floatation" assay.

6.2 Methods

6.2.1 Generation of Epitope-Tagged Sol SYT7 and Sol SYT11

cDNA encoding N-terminal FLAG-tagged full length murine SYT7 or SYT11 cloned into the pEF-BOS plasmid (a generous gift from M Fukuda, Fukuda Initiative Research Unit, The Riken Institute of Physical and Chemical Research, Wako, Saitama, Japan) was used as template for a PCR-based strategy to generate epitope-tagged SYT7 and SYT11 lacking the transmembrane (TM) domain.

Oligonucleotide PCR primers (designed to contain appropriate restriction enzyme sites at the extreme 5' and 3' ends of the amplified products) were used to amplify SYT7 and SYT11 cDNA corresponding to residues from the amino terminal to the TM domain, and from the TM domain to the translation stop signal. These PCR products were subjected to restriction endonuclease digestion followed by gel purification, and the resulting DNA fragments ligated into the pET-21 plasmid, itself previously digested with the same restriction endonucleases in order that the sol SYT cDNA fragment was in-frame with the C-terminal 6X HIS epitope tag. The resulting plasmid was transformed into *E. coli*, and induced protein was purified as described.

6.2.2 The Vesicle co-Floatation Assay

Binding of sol SYT7 or sol SYT11 protein with GSV SNARE proteins was also assessed using the Vesicle co-Floatation Assay as described in 2.2.3.12.2 and (185). Sol SYT7 or sol SYT11 protein was incubated in the presence of EGTA or Calcium ions with vesicle vesicles (prepared as described by(189) decorated with recombinant v-SNAREs (VAMP2) or t-SNAREs (Syntaxin 4 and SNAP 23). The vesicle-protein complexes were then resolved by centrifugation in a gradient of Accudenz and the resulting fractions analysed by SDS-PAGE and immunoblotting.

6.3 Results

6.3.1 Soluble SYT7 and SYT11

Figure 6.1a and 6.1b show sol SYT7 and sol SYT11 proteins (233) expressed and purified from *E coli*, resolved by SDS-Page and visualised after Coomassie staining. Both proteins are seen as the major band of a molecular weight slightly below that previously observed (due to the absent TM domain).

The same proteins are seen in the immunoblots in figure 6.2. Both sol SYT7 and SYT11 are fusion proteins tagged with N-terminal FLAG and c-terminal HIS(6) tags. As can be seen in the figure both are recognised by the α FLAG and the α HIS antibodies. Additionally, sol SYT7 and sol SYT11 are recognised by the SYT7 and SYT11 antisera respectively.

Figure 6.1: Sol SYT7 and SYT11 Protein

Figure 6.1a: Sol SYT7

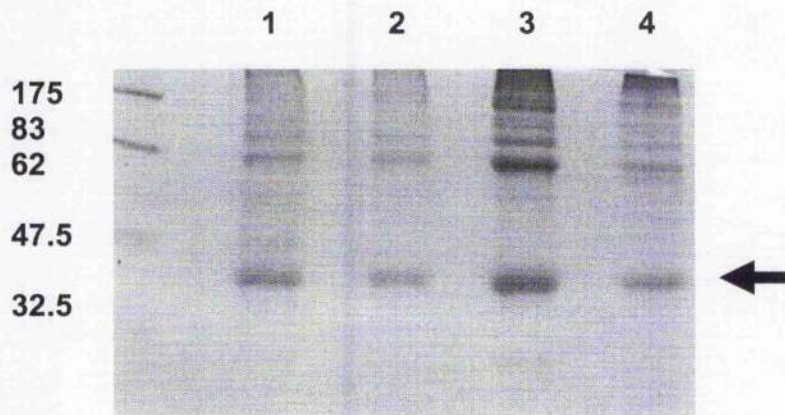


Figure 6.1b: Sol SYT11

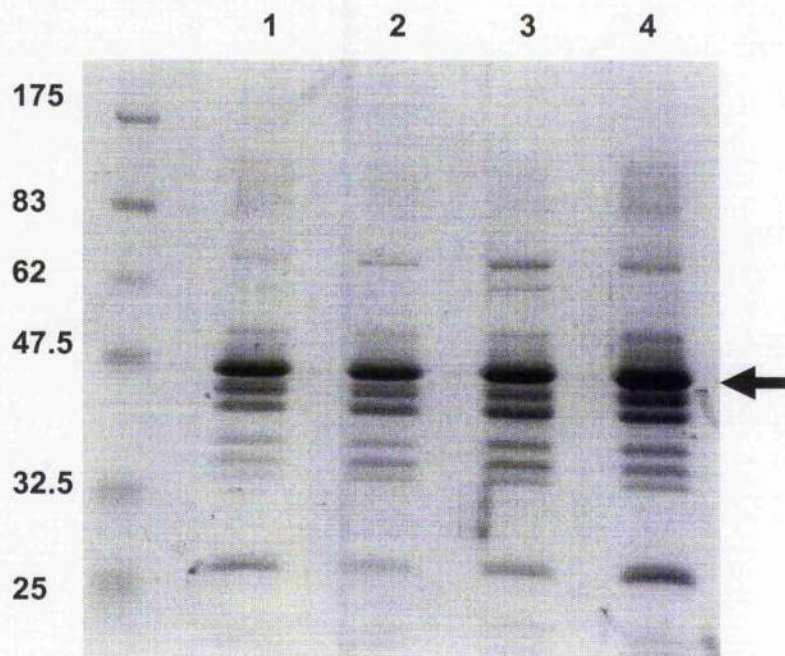


Figure 6.1a and 6.1b

Photographs of purified Sol SYT7 and SYT11 protein resolved by SDS-PAGE and visualised by Coomassie staining. The markers indicated correspond to the equivalent molecular weight (89). Lanes 1 to 4 in figure 6.1a contain 10 μ g, 6.4 μ g, 22 μ g and 6.8 μ g sol SYT7 protein respectively. Lanes 1 to 4 in figure 6.2 contain 7.4 μ g, 7.8 μ g, 9.3 μ g and 11.6 μ g sol SYT11 respectively. Arrows indicate the expected protein. Data are from a single experiment.

Figure 6.2: Antibody Recognition of Sol SYT7 and SYT11

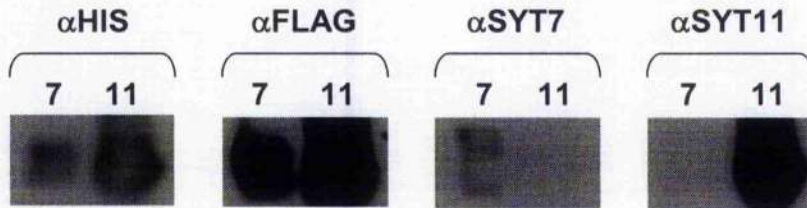


Figure 6.2

Scanned images obtained from Western blots using commercially available α HIS, α FLAG and affinity-purified SYT7 and SYT11 antisera. 50ng sol SYT7 (7) or sol SYT11 (11) was resolved by SDS-PAGE, transferred to nitrocellulose and probed with the antibody indicated. The markers correspond to the molecular weight standards as indicated. α HIS and α FLAG antibodies were used at 1:2000, SYT7 and SYT11 antisera at 1:250 dilution. Data are from a single experiment.

6.3.2 Interaction of Sol SYT7 and Sol SYT11 with GSV SNARE Proteins

Sol SYT7 and Sol SYT11 binding to Syntaxin4, SNAP23 and VAMP2 were initially assessed by GST-pulldown. In spite of repeated attempts using different binding conditions no consistent results could be produced (data not shown). Therefore binding was assessed by the vesicle co-floatation assay.

Figures 6.4 and 6.5, which show interaction of sol SYT7 and sol SYT11 with v- and t-SNARE vesicles should be viewed alongside Figure 6.6, which shows the SNARE-protein labelled vesicles alone.

The upper two panels of figure 6.4 show interaction of sol SYT7 with t-SNARE vesicles in the presence of either calcium or EGTA. Sol SYT7 can be seen to bind t-SNARE vesicles under both binding conditions, but binding is greatly enhanced in the presence of calcium. A similar binding pattern can be seen with v-SNARE vesicles in the middle two panels. Sol SYT7 can be seen to bind v-SNAREs with EGTA, and binding is enhanced in the presence of calcium. The lower two panels of figure 6.4 show that sol SYT7 also binds only weakly to protein-free vesicles in the presence of calcium, and that in the presence of EGTA no binding is observed.

Figure 6.5 show binding experiments performed with sol SYT11 and v- and t-SNARE vesicles in the presence of calcium and EGTA. As can be seen in the figure no binding is observed under any experimental conditions, and soluble SYT11 is collected from the bottom of the gradient.

Figure 6.6 shows the position of Syntaxin4 and VAMP2 in the same density-gradient centrifugation fractions. Both proteins can be seen to be present in most fractions however both are increased in fractions from 2/3rd through the gradient i.e. the interface of 5% and 30% Nycodenz (see Chapter 2 section 2.2.35). These fractions also correspond to binding of sol SYT7.

Together these data indicate that sol SYT7 binds both Syntaxin4 / SNAP23 t-SNARE complex and VAMP2 when present on vesicles, and that binding is enhanced by calcium. Sol SYT11 does not bind to either SNARE protein.

Figure 6.3 Interaction of SYT7 with Syntaxin4, SNAP23 and VAMP2

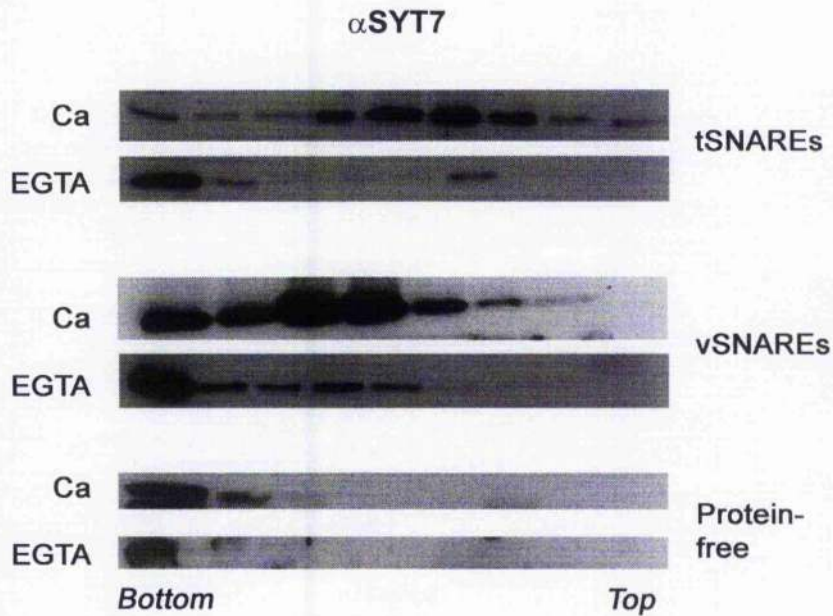


Figure 6.3

Scanned immunoblots using SYT7 antisera at 1:250 dilution. Each lane represents an equal fraction obtained from density gradients in which SYT7 incubated with the indicated v- or t-SNARE vesicles (in the presence of calcium or EGTA) have been resolved. Density-gradient fractions were resolved by SDS-PAGE (bottom-most fraction on the left, top fraction on the right) and transferred to nitrocellulose. Results are from an individual experiment.

Figure 6.4 Interaction of SYT11 with Syntaxin4, SNAP23 and VAMP2

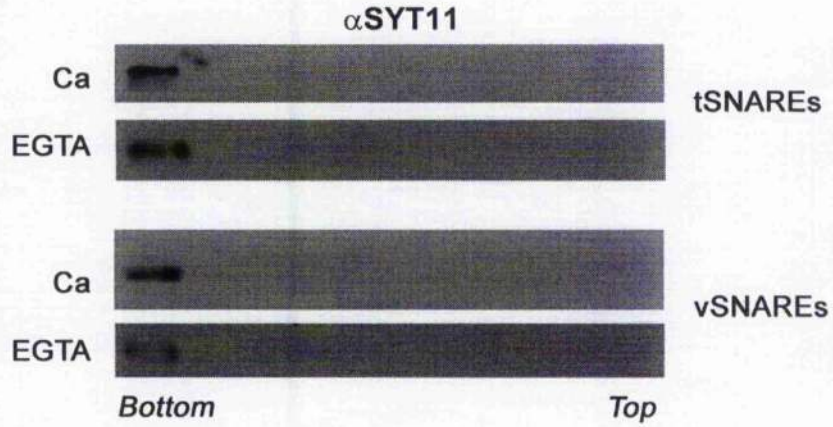


Figure 6.4

Scanned immunoblots using SYT11 antisera at 1:250 dilution. Each lane represents an equal fraction obtained from density gradients in which SYT7 incubated with the indicated v- or t-SNARE vesicles (in the presence of calcium or EGTA) have been resolved. Density-gradient fractions were resolved by SDS-PAGE (bottom-most fraction on the left, top fraction on the right) and transferred to nitrocellulose. Results are from an individual experiment.

Figure 6.5 Distribution of Syntaxin4 and VAMP2 vesicles in Nycodenz Gradients

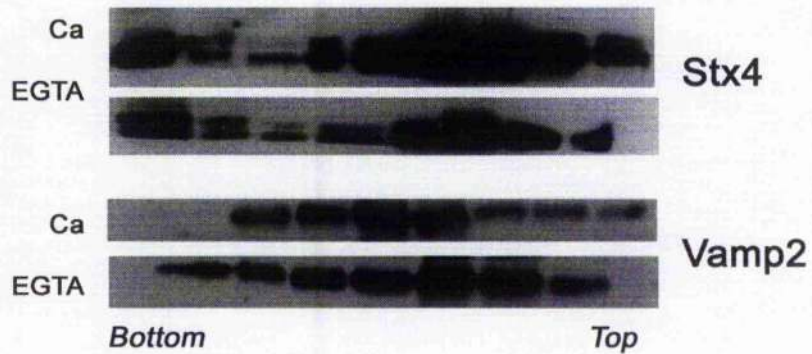


Figure 6.5

Scanned immunoblots, each lane representing an equal fraction obtained from density gradients in which the indicated v- or t-SNARE vesicles (in the presence of calcium or EGTA) have been resolved. Density-gradient fractions were resolved by SDS-PAGE (bottom-most fraction on the left, top fraction on the right) and transferred to nitrocellulose and immunolabelled with the Syntaxin4 (Stx4) or VAMP2 (Vamp2) antibody indicated at 1:1000 dilution. Results are from an individual experiment.

6.4 Discussion

The prokaryotic expression and purification of SYT7 and SYT11 proteins which lack the TM domain but possess both N- and C-terminal epitope tags has been successfully achieved. As can be seen in figure 6.1 the major species in each fraction corresponds to a protein of the expected molecular weight, and subsequent analysis (figure 6.2) clearly demonstrates appropriate antibody recognition; HIS and FLAG antibodies recognise both proteins, SYT7 and SYT11 antisera are specific for each soluble isoform. Thus the identity of the purified expressed proteins is confirmed and as such, both are suitable for use in binding assays.

Further analysis of the Coomassie-stained gel photographed in figure 6.1 reveals that other bands are visible. In particular, a band of approximately double the apparent molecular weight of each isoform is present. SYT isoforms have been demonstrated to form SDS-resistant oligomers both in the presence and absence of calcium (335), therefore this band may represent SYT7 or SYT11 dimers. The other larger proteins are likely to be bacterial contaminants, which have previously been noted to occur when SYTs are expressed in a prokaryotic system (336). The smaller molecular weight species may also be contaminants, but it is possible that these represent fragments of the expressed soluble SYT7 and SYT11 that are the result of denaturation.

In figure 6.3 Sol SYT7 is seen to bind the protein-free vesicles in a calcium-dependent manner. Based on published data this is likely to be mediated by the C2A domain (although the C2B domain was also shown to bind lipid vesicles in a calcium-dependent manner using a less-stringent vesicle-based assay such as in the current study) (337). Sol SYT11 did not bind empty phospholipid vesicles in the presence or absence of calcium, which is in agreement with previously published work (338). Sol SYT7 is seen to bind to v- and t-SNARE vesicles with an apparent greater affinity than empty vesicles alone, suggesting that there is direct binding between the vesicle-bound SNARE proteins and sol SYT7.

In figure 6.4 no binding is observed to either t- or v-SNARE vesicles with sol SYT11, indicating this isoform does not bind Syntaxin4 / SNAP23, or VAMP2. This would be expected, given the role proposed for SYT11 in the regulation of a post-endosomal or TGN GLUT4 sorting step (Chapter 5 Section 5.4). Therefore from these data, together with the data presented in Chapter 4 and Chapter 5 it is possible to conclude that SYT11 does not contribute to GSV-PM fusion in 3T3-L1 adipocytes. SYT11 may interact with an intracellular SNARE complex composed of alternative v- and t-SNARE proteins e.g.. Vti1a, Syntaxin 6, Syntaxin 10, Syntaxin 16. Such an interaction could be investigated in this way using appropriately labelled vesicles.

As can be seen in figure 6.3 Sol SYT7 binds v-SNARES and t-SNAREs in the absence of calcium. The extent of binding is increased when calcium is included in the binding buffer. SYT7 has previously been implicated in interaction with VAMP2 at the PM of Swiss 3T3 fibroblasts (339), although no direct evidence of binding was demonstrated. SYT7 has also been identified in NRK fibroblasts, where SYT7 C2A domain has been shown to bind the t-SNAREs Syntaxin4 and SNAP23, and a SNARE complex composed of Syntaxin4 / SNAP23 and VAMP7 (340). Thus, the data presented here are in agreement to previous observations, and imply that SYT7 can influence SNARE-mediated membrane fusion facilitated by the Syntaxin4 / SNAP23 / VAMP2 complex. Direct evidence of such an interaction could be investigated by means of an *in vitro* liposome fusion assay between separate Syntaxin4 / SNAP23-, and Vamp2-labelled liposomes and Sol SYT7 (as described in Tucker, Weber & Chapman 2004).

Chapter 7 Conclusions

In 2006 the global epidemic of T2DM is well underway. Much is known about the regulation of insulin action, but there remain many gaps in our knowledge. It has been proposed that 1 in 3 of the children born in the USA during the first year of this millennium will develop diabetes at some stage in their lives (341). Novel therapeutic agents designed to correct disordered insulin action in these future diabetic individuals will not be developed until the complex mechanisms regulating normal insulin action are determined.

Within the skeletal muscle, cardiac muscle or adipose cell GLUT4 is engaged in a series of sequential trafficking steps between membrane compartments, steps which are governed by SNARE-protein interactions. Upon insulin binding to its receptor at the cell surface, a cascade of protein-protein and protein-lipid interactions leads ultimately to the translocation of a GLUT4-containing specialised vesicle from an intracellular location to the plasmalemma, where the vesicle fuses by SNARE-mediated regulated exocytosis and glucose can enter the cell by flowing down its concentration gradient. The ability to stimulate glucose uptake in this way in response to insulin is significantly impaired in individuals with diabetes (204). The precise signals that regulate both GSV-PM fusion and GLUT4 intracellular trafficking remain elusive (179).

The work described in this thesis describes the investigation of members of the Synaptotagmin family of proteins in the adipocyte, and their influence on insulin-stimulated glucose uptake.

Members of the SYT family of type-1 membrane proteins have been shown to bind calcium and phospholipids, and exhibit calcium-dependent and independent SNARE protein interactions (315). SYT isoforms have been implicated in a variety of cellular processes which require membrane fusion events however most work investigating SYTs has hitherto been confined to neuronal or neuroendocrine cells.

I have demonstrated that SYTs are expressed in 3T3-L1 cells, murine skeletal muscle and human adipose tissue. In the 3T3-L1 fibroblast SYT11 is the predominant isoform, and its expression is upregulated during differentiation into a mature, insulin-sensitive adipocyte. SYT7, which is also expressed in 3T3-L1 fibroblasts (although at lower levels than SYT11) also is seen to be upregulated during differentiation.

SYT11 protein is found predominantly in the HDM fraction of the adipocyte (which corresponds to the ER and lysosomes) and a smaller amount is observed in the LDM fraction (which contains TGN markers). The location of SYT11 is not influenced by insulin stimulation. siRNA-mediated knockout of SYT11 in 3T3-L1 adipocytes results in normal basal-, and abrogated insulin-stimulated glucose uptake (which appears

to be partially overcome with increasing insulin stimulation). GLUT4 levels are reduced in GLUT4 knockout cells. SYT11 knockdown does not influence general endosomal trafficking. Finally, soluble SYT11 (devoid of the TM domain) is unable to bind phospholipid vesicles or the GSV SNAREs Syntaxin 4, SNAP23 or VAMP2.

SYT7 protein is also found mostly in the HDM fraction in 3T3-L1 adipocytes however the LDM and PM fractions also yield a lesser amount of SYT7. Like SYT11, SYT7 protein distribution is not changed following stimulation of the adipocyte with insulin. Preliminary studies suggest that siRNA-mediated depletion of SYT7 results in increased basal- and potentiated insulin-stimulated glucose uptake. The influence of SYT7 knockout on GLUT4 and endosomal traffic is yet to be determined. Lastly, the binding of SYT7 to GSV-SNARE proteins and phospholipid-containing vesicles has also been investigated, and it is possible to demonstrate calcium-dependent and independent binding of SYT7 to lipid vesicles, and to v- and t-SNARE-containing vesicles.

Together these data suggest that the SYT isoforms studied do indeed play a role in glucose uptake in the adipocyte. The potential role of each is discussed further below.

The study of SYT11 has until now been limited to examination of its individual domains, or of its function in neurons where it is thought to play a role in the regulation of neurotransmission (272). In neurons

SYT11 has been identified as a substrate for the E3 ubiquitin ligase Parkin (242), and ubiquitination of SYT11 led to its proteasomal degradation. It has been shown that ectopic expression of GLUT4 in 3T3-L1 fibroblasts results in its lysosomal degradation (342), and mistargetting of GLUT4 by depletion of Syntaxin 16) also reduced intracellular GLUT4 (324). Moreover, a recent study of insulin action in L6 cells in culture has revealed an apparent reduction in association of components of the ubiquitination-proteasome pathway components with GLUT4 upon insulin stimulation (343). Thus the reduction of GLUT4 protein seen with SYT11 knockdown suggests a potential link between SYT11 and an intracellular degradation pathway.

The SYT-family member with the most homology to SYT11 is SYT4 (228), and that together SYT4 and SYT11 comprise a unique subgroup of SYT isoforms that have lost the ability to bind phospholipid or calcium by virtue of point mutations in the C2A and C2B domains (338;344;345). That the C2A domains of both SYT4 and SYT11 have otherwise retained their sequence homology with the other SYT family members suggests that other intrinsic C2 domain functions (such as SNARE-interaction) have been retained.

It has been demonstrated that SYT4 is necessary for the maturation of Immature Secretory Granules (ISG) in PC12 cells (346). These observations are particularly interesting given the similarities that can be drawn between ISG maturation and GSV production in the

adipocyte. The ISGs of endocrine and neuroendocrine cells (which contain the peptide or catecholamine precursors) bud from the TGN and undergo a series of processing steps prior to becoming large dense core vesicles (LDCV) or Mature Secretory Granules (MSG), which subsequently fuse with the PM via a mechanism of regulated exocytosis (347).

In their studies Ahras, Otto and Tooze observed that SYT4 was present in a high density subcellular fraction that contained markers for the Golgi and ISGs. SYT4 was seen to be recruited to the ISG vesicle via protein-protein interactions, and this was independent of any intrinsic phospholipid binding properties, which is in keeping with the known binding properties of this isoform. Furthermore, the C2 domains of SYT4 were shown to bind the ISG-bound SNARE protein Syntaxin 6 in a cooperative, calcium-independent manner. Thus the closest homolog to SYT11 is present in a similar subcellular membrane compartment (albeit in a different cell type), interacts with a t-SNARE protein and is implicated in the maturation of a specialised vesicle that is fated to undergo regulated exocytosis at the plasma membrane.

The similarity with adipocyte GSVs is implicit, and it is tempting to speculate that within the adipocyte SYT11 may play a similar role in facilitation of GSV maturation. The expression, subcellular localisation, siRNA and lipid binding data presented in this thesis are supportive of

such a function, however further experimental evidence is required before such a role can be assigned to SYT11.

SYT7 has been more intensively studied than SYT11. It is seen to be expressed in most tissues, and in all higher eukaryotic organisms examined (236). Of all the C2 domains studied SYT7 C2A and C2B appear to bind phospholipids and SNAREs with a greater affinity and lower calcium dependency than any others (337;348). Once bound, the complexes formed by SYT7 with membranes and proteins disassemble slower than other SYTs (344). This is suggestive of a low-calcium requirement for the activation of SYT7.

The subcellular localisation of SYT7 has been examined in NRK fibroblasts, HEK cells, 3T3 fibroblasts and CHO cells (322;344;349) where it was observed to localise predominantly to the lysosomal compartment, and in pancreatic β -cells and PC12 neuroendocrine cells where it was seen to colocalise with lysosomes and insulin granules, and with LDCVs respectively (350;351). Where SYT7 has been observed to be associated with a vesicle, a calcium-dependent functional role has been supported (352).

In elegant Total Internal Reflection Fluorescence Microscopy (TIR-FM) studies of fibroblasts derived from SYT7-knockout mice, it was observed that in cells lacking SYT7 the fusion of lysosomal vesicles with the PM was complete, and the fusion pore intermediates commonly seen

with lysosomal exocytosis were abolished (353). In the same study SYT7 was shown to have a negative influence on the speed and extent of vesicle-PM fusion. The fusion events described remained calcium-dependent even when SYT7 was not present.

When considered together these observations are in keeping with SYT7s proposed involvement with GSV-PM fusion. The small increase in SYT7 expression seen with 3T3-L1 adipocyte differentiation may reflect the important role this isoform plays in both the fibroblast and adipocyte. A large upregulation may not be required. Secondly, the subcellular localisation data for SYT7 is in agreement with that previously described above. The increase in basal and insulin-stimulated glucose uptake seen when SYT7 is removed with siRNA may reflect the role the SYT7 protein plays in controlling the speed and extent of SNARE-mediated GSV-PM fusion. The apparent calcium requirement for GSV-PM fusion may prove to be mediated by another as yet unidentified species. As previously stated, further characterisation of the SYT7 knockout phenotype is required before any firm conclusions may be drawn.

The data presented in this thesis can be considered preliminary, as more work is required to further define the role of SYT isoforms in insulin-stimulated GLUT4 translocation in the 3T3-L1 adipocyte. Future experiments *in vitro* should include assessment of binding of the SYT7 and SYT11 isoforms to other proteins implicated in GLUT4 trafficking (e.g., Syntaxin 6, Syntaxin 16, Vti1a, GGAs and Coat proteins that

interact with clathrin). The subcellular localisation of both isoforms could be investigated by careful immunofluorescence microscopy (although the antisera available may limit this line of enquiry). Expression of epitope-tagged SYT7 and SYT11 could obviate this problem, however, as has been observed with the expression of myc-tagged GLUT4 this may result in mistargetting and degradation. The expression of the soluble isoforms of SYT7 and SYT11 in 3T3-L1 adipocytes may be expected to act in a dominant-negative manner by binding to effector molecules and preventing their interaction with endogenous protein. It would be expected that these experiments would produce a phenotype similar to that observed using antisense approaches.

Finally, despite of its existence, there has been no report of disordered carbohydrate metabolism in the SYT7 transgenic knockout mouse (223). Glucose homeostasis may not have been examined in these animals, or the myositis observed may mask an effect of SYT7 knockout. Should the *in vitro* investigations of SYT7 and SYT11 confirm an apparent role in insulin-stimulated glucose uptake, the generation of an adipose-specific knockout mouse (for either isoform) and its subsequent study would be an important step to the understanding of their influence on cellular, tissue-specific and whole organism insulin action.

Appendix 1: Oligonucleotide Sequences and PCR Products

A1.1 Published Synaptotagmin cDNA sequences

Table A1

SYT Isoform	Murine Sequence	Human Sequence
Synaptotagmin 1	NM_009306	NM_005639
Synaptotagmin 2	NM_009307	NM_177402
Synaptotagmin 3	NM_016663	NM_032298
Synaptotagmin 4	NM_009308	NM_020783
Synaptotagmin 5	NM_016908	NM_003180
Synaptotagmin 6	NM_018800	NM_205848
Synaptotagmin 7	NM_018801	NM_004200
Synaptotagmin 8	NM_018802	NM_138567
Synaptotagmin 9	NM_021889	Not Available at time of analysis
Synaptotagmin 10	NM_018803	NM_198992
Synaptotagmin 11	NM_018804	NM_152280
Synaptotagmin 12	NM_134164	NM_177963
Synaptotagmin 13	NM_030725	NM_020826
Synaptotagmin 14	NM_181546	NM_153262
Synaptotagmin 15	NM_181529	NM_181519

Table A1 Genbank accession numbers for Murine and Human SYT genes

A1.2 Reverse Transcription PCR Primer Sequences

A1.2.1 Murine Reverse Transcription PCR Primer Sequences

GLUT4	Forward	5'-GCAGCGAGTGAAGTGGAAAC-3'
	Reverse	5'-CAGGGCCAAGACATTGTT-3'
Syt 1	Forward	5'-TACTCGGAATTAGGTGGC-3'
	Reverse	5'-GTCTCTTGCCGTTCTGCA-3'
Syt 2	Forward	5'-CAGGCCAACCAGCTCACC-3'
	Reverse	5'-CGTAGCGCAAGGAGGTAC-3'
Syt 3	Forward	5'-GACTTCGACCGCTTCTCG-3'
	Reverse	5'-GAGCCACGTCGAACACCA-3'
Syt 4	Forward	5'-TGGCCTCGTCTTCACTGT-3'
	Reverse	5'-ACGTGAGGGAAGTGCTGG-3'
Syt 5	Forward	5'-CGTCATTGTCTTGAAGC-3'
	Reverse	5'-GCCAGCCCCACCGACTGC-3'
Syt 6	Forward	5'-GGACATCCAGTACGCTAC-3'
	Reverse	5'-CTATGATCTCGTTGTGGC-3'
Syt 7	Forward	5'-TGTGCCACTGGTGTGAGC-3'
	Reverse	5'-TCGGCCCAGGTTCTCTCG-3'
Syt 8	Forward	5'-ACTGGAGGCTCGGGGTCT-3'
	Reverse	5'-CACAGGCTCAGTCCGGAG-3'

Syt 9	Forward	5'-AAGCCTGCGGGAAACTGA-3'
	Reverse	5'-AAGTCGGCCAAGTCGAAG-3'
Syt 10	Forward	5'-GAGAACGAGCATCGGGAG-3'
	Reverse	5'-AAGTCTTCCGGTGCACGC-3'
Syt 11	Forward	5'- GACAAGCGGCATCGAGTG -3'
	Reverse	5'-TGTGCGACGGGCTGGTAT-3'
Syt 12	Forward	5'-TGACCAGCGGACCACTAC-3'
	Reverse	5'-CACGATCTGTTTCGTCTGG-3'
Syt 13	Forward	5'-CGACACATGCACCCCAAG-3'
	Reverse	5'-GAGGCGACTGTCACTCTG-3'
Syt 14	Forward	5'-AGCTCCTGGTAACGGTGA-3'
	Reverse	5'-CCAGTATCACCGGTAACG-3'
Syt 15	Forward	5'-TCGGTGGAGTACCAACAG-3'
	Reverse	5'-GATGATACGGTGGTGGTC-3'

A1.2.2 SYT7 RTPCR Primers

In higher eukaryotic cells SYT7 is known to have three alternatively spliced variants (236). The genomic structure of the murine SYT7 gene is shown in figure A1 below.

Figure A1

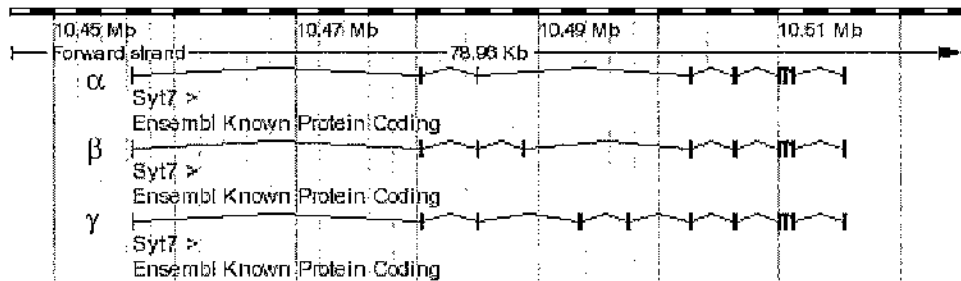


Figure A1 Schematic diagram representing the genomic structure of the murine SYT7 gene. Transcripts of SYT7 α (α), SYT7 β (β) and SYT7 γ (γ) are shown. It can be seen that SYT7 α comprises exons 1,2,3 and 7- 13, SYT7 β comprises exons 1,2,3,4 and 7- 13 and SYT7 γ comprises exons 1,2,3 and 5-13 (229).

In order to explore the expression of possible alternative isoforms of SYT7 expressed in 3T3-L1 cells RTPCR primers were designed to produce a specific product in the presence of each transcript that would be identifiable by virtue of size. The SYT7 forward primer is located in exon 2 and the SYT7 reverse primer is located in exon 8. Both of these exons are common to all three of the published SYT7 splice variants. Based upon the schematic diagram above, the expected PCR products would be 305, 437 and 647bp when these primers were used to amplify SYT7 α , SYT7 β and SYT7 γ cDNA respectively.

Table A2

Target Gene	Forward Primer Location	Reverse Primer Location	Product Size (246)
GLUT4	Exon 2	Exon 4	310
SYT1	Exon 9	Exon 11	322
SYT2	Exon 4/5	Exon 7	388
SYT3	Exon 5	Exon 7	361
SYT4*	Exon 2	Exon 2	368
SYT5	Exon 6	Exon 8	289
SYT6	Exon 3	Exon 5/6	328
SYT7 α	Exon 2	Exon 7	305
SYT7 β	Exon 2	Exon 7	437
SYT7 γ	Exon 2	Exon 8	647
SYT8	Exon 7	Exon 9	229
SYT9*	Exon 3	Exon 3	342
SYT10*	Exon 3	Exon 3	269
SYT11	Exon 2	Exon 3	305
SYT12*	Exon 4	Exon 4	369
SYT13	Exon 1	Exon 2	276
SYT14*	Exon 4	Exon 4	318
SYT15	Exon 4	Exon 5	333

Table A2: Murine RT PCR primer location and expected product sizes. * indicates non-intron-spanning primers.

A1.2.2 Human Reverse Transcription PCR Primer Sequences

Syt 1	Forward	5'-CCTGTCACCACTGTCGCGAC-3'
	Reverse	5'-GAGGGCCTGATCTTTCATCG-3'
Syt 2	Forward	5'-TGAGGAGTGGAGAGACCTGC-3'
	Reverse	5'-CAGCACGGTGACCACTACCT-3'
Syt 3	Forward	5'-CTGACACCAACGACAGGTGC-3'
	Reverse	5'-CAGCAAAGGGTGGATGGTGG-3'
Syt 4	Forward	5'-GGATGAGCAGTCGATGACCT-3'
	Reverse	5'-CTCACCCCGTCCTGAAGACT-3'
Syt 5	Forward	5'-CGACTCCAGTCGCATCAGCC-3'
	Reverse	5'-ACCAGCAGCTGGCCACTCTG-3'
Syt 6	Forward	5'-GCAGCGGCAAACACTACAGAGC-3'
	Reverse	5'-CAGGATACGCACAATCAGGG-3'
Syt 7	Forward	5'-CTGCCATCATCACCGTCAGC-3'
	Reverse	5'-TGGTGAGGGAGTTGACGAGG-3'
Syt 8	Forward	5'-GCTGGCACCACAGCTATACC-3'
	Reverse	5'-GGCTTCCAAAGTCGAACTCC-3'
Syt 10	Forward	5'-ACATCGTCACCGAGCTGTGC-3'
	Reverse	5'-CTTCTGCTGGGATGTCAGGG-3'
Syt 11	Forward	5'-GCTGCCAGTGATGGATGACC-3'

	Reverse	5'-GAGCTCCCCTCTGCTGATGC-3'
Syt 12	Forward	5'-TGAGCCTGTGGAAGCTCTGG-3'
	Reverse	5'-GTTGCTCACGGAGGAGATGG-3'
Syt 13	Forward	5'-ACGACGGAGGCTGTGACTGC-3'
	Reverse	5'-AATCAGCACCACCAGGAGGC-3'
Syt 14	Forward	5'-GGCGGGTTTCCAGATCTTGG-3'
	Reverse	5'-GTGGTGGCTGCAATTCATCC-3'
Syt 15	Forward	5'-TCAGAGCTGCTGCCTCACAC-3'
	Reverse	5'-CCTCTGGGTGATGGTCTTGC-3'

Table A3

SYT Isoform	Forward Primer Location	Reverse Primer Location	PCR Product Size (246)
SYT1	Exon 4	Exon 5/6	318
SYT2	Exon 6	Exon 9	319
SYT3	Exon 3	Exon 4	351
SYT4	Exon 2	Exon 3	322
SYT5	Exon 2	Exon 4/5	330
SYT6	Exon 2	Exon 3	277
SYT7	Exon 2	Exon 2	276
SYT8	Exon 1	Exon 4	313
SYT10	Exon 1	Exon 2	378
SYT11	Exon 2	Exon 3	337
SYT12	Exon 6	Exon 7	306
SYT13	Exon 4	Exon 5	368
SYT14	Exon 3	Exon 5	335
SYT15	Exon 1	Exon 3	360

Table A3: Expected human reverse transcription PCR primer location and expected product sizes in base pairs (246).

A1.2.3 Murine Synaptotagmin PCR product sequences

Listed below are the sequences of RT-PCR products obtained from reactions using murine brain cDNA template as described in Chapter 3. PCR products were TA-cloned into pCR-2.1 plasmids and sequenced by the University of Dundee Sequencing Service. Primer sequences are in **bold** text, PCR product underlined and plasmid sequence is in plain text. **(R)** indicates where the reverse sequencing primer was used. All sequences were analysed using Vector NTI software are found to be homologous with the published Genbank sequence (shown in brackets).

SYT1

(NM_009306 mus syt 1)

TGGACCATGCTACGGAGCTCGGATCCACTAGTAACGGCCGCCAGTGTGCTGGAATTGG
CCCTTTACTCGGAATTAGGTGGCAAGACACTGGTGATGGCTGTGTATGATTTGACCCG
TTCTCCAAGCACGACATCATTGGAGAGTTCAAAGTTCCCTATGAACACCGTGGATTTTGGC
CACGTCACAGAGGAGTGGCGCGATCTCCAGAGTGCTGAGAAAGAAGAGCAAGAGAAAC
TGGGTGACATCTGCTTCTCCCTCCGCTACGTCCCTACTGCCGGCAAGCTGACTGTTGTC
ATTCTGGAAGCCAAGAACCTGAAGAAGATGGATGTGGGTGGCTTATCTGATCCCTATGT
AAAGATTCACCTGATGCAGAACGGCAAGAGACAAGGGCGAATTCTGCAGATATCCATC
ACACTGGCGGCCGCTCGAGCATGCATCTAGAGGGCCCAATTCCGCCCTATAGTGAGTCG

SYT2

(NM_009307 mus syt 2)

ACGGCCCCTTTGGGACGAGCTCGGATCCACTAGTAACGGCCGCCAGTGTGCTGGAATT
CGCCCTTCAGGCCAACCAGCTCACCGTGGGTGTCTGCAGGCTGCGGAACTCCCAGC
CCTGGACATGGGTGGCACATCAGACCCTTATGTCAAAGTCTTCCCTCCAGACAAGA
AGAAGAAATATGAGACTAAGGTGCATCGGAAGACGCTGAACCCAGCCTTCAATGAGACA
TTCACTTTCAAGGTGCCATACCAGGAGTTAGGAGGCAAGACCCTGGTGATGGCAATCTA
TGACTTTGACCGCTTCTCTAAGCATGACATCATCGGGGAGGTGAAGGTACCCATGAACA
CAGTGGACCTTGGCCAGCCCATCGAGGAATGGAGAGACCTACAAGGCGGAGAGAAGGA
AGAGCCAGAGAAGTTGGGTGACATCTGTACCTCCTTGGGCTACGAAGGGCGAATTCTG
CAGATATCCATCACACTGGCGGCCGCTCGAGCATGCATCTAGAGGG

SYT3 (R)

(NM_016663 mus syt3)

GGCCGCCTTGGTTCCGGAGCTCGGATCCACTAGTAACGGCCGCCAGTGTGCTGGAATT
CGCCCTTGAGCCAGTCTGAACACCAGGGCCTCGTTGTACGTGGGGTTCAGTGTGTTCT
TCTTAATGGAGGTCTTCCGTTTCTTCCAGACGCGCCCTCGCTGATCAGAGAGGCCTTC
ACATAGGGGTCTGAGAAACCAGTGAGGTCCATTGCTTTGAGGTTAGAGGCCTTGATGAT
GGTCACGGTGAGGCGCCAGCCGTGGGGAGGTAGCAGAGAGAGAAGTTGAGCTCTCC
GAGATCTGCCTTTCCGAGCCACCCTCCAGGATGTCCCTCCAGAGCGGGCGGTGAGGG
GGCTGTTGAGCCAGCTCCAGCAGGTTGTCCAAAACCACCTGGCCAATGAGATCATGCC
GCGAGAAGCGGTCTGAAGTCAAGGGCGAATTCTGCAGATATCCATCACACTGGCGGCCG
CTCGAGCATGCATCTAGAGGGCCCAATTCCGCCCTATAGTGAGTCGTATTACAATCACT

SYT4

(NM_009308 mus syt 4)

AGGGGGAACCTTGAAACCGGAGGCTCGGATCCACTAGTAACGGCCGCCAGTGTGCTGG
AATTCGCCCTTTGGCCTCGTCTTCACTGTCTCTCTCTTTGCCTGGATCTGCTGTCAGAGA
AGATCAGCCAAATCCAACAAGACTCCTCCATACAAGTTTGTGCACGTGCTTAAAGGAGTT
GATATCTACCCAGAAAACCTAAGTAGCAAAAAGAAGTTTGGAGGAGATGACAAGAGTGA
AGTGAAGGGTAAAGCCGCTCTGCCAACCTTCCCTGCATCTTGACCTAGAGAAGCGAG
ACCTCAATGGCAACTTCCCAAAGCCAACCCCAAAGCTGGCAGCTCTTCTGATCTGGAA
AATGTCACCCCAAAGCTCTTTACGGAGACAGAAAAGGAGGCCAATCCCTGAGAGCTT
GAAGTCCAGCACTTCCCTCACGTAAGGGCGAATTCTGCAGATATCCATCACACTGGCGG
CCGCTCGAGCATGCATCTAGAGGGCCCAATTCCCCCTATAGTGAGTCGTATTACAATTC

SYT5

(NM_016908 mus syt 5)

GCCATCCTGGATCCGAGCTCGGATCCACTAGTAACGGCCGCCAGTGTGCTGGAATTC
GCCCTTACGGCCCGGAAGCTCACCGTCATTGTCTTGGAAAGCTAAAAACCTGAAGAAAA
TGGATGTAGGAGGACTCTCAGATCCCTATGTGAAGGTGCACCTGCTCCAGGGAGGTA
AAGGTTCCGAAGAAGAAAACCACCATTAAGAAGAACCCTGAACCCCTATTACAACGA
GGCCTTCAAGCTTGTAGGTGCCCTGTGACCAGGTGCAGAAAGTCCAGGTGGAGCTGACT
GTTCTGGATTATGACAACTGGGAAGAATGAGGCCATCGGGAGAGTGGCGGTGGGCG
CAGCAGTCGGTGGGGCTGGCTGCGGCACTGGGCTGACAAGGGCGAATTCTGCAGAT
ATCCATCACACTGGCGGCCGCTCGAGCATGCATCTAGAGGGCCCAATTCCCCCTATAGT

SYT6

(NM_018800 mus syt 6)

GCGACTGGGGGAACGGAGCCTCGGATCCACTAGTAACGGCCGCCAGTGTGCTGGAATTC
CGCCCTTGGACATCCAGTACGCTACTAGTGAAAGTGTGGACTTGGGAGAGATCATGTTCC
TCCCTCTGCTACCTGCCACAGCAGGCAGGCTCACCCCTCACAGTGATCAAGTGTGCGAAA
TCTCAAAGCAATGGACATCACAGGCTACTCAGATCCCTACGTCAAAGTATCCCTACTGTG
TGATGGACGGAGGCTGAAAAAGAAGAAAACGACCATAAAAAAGAACCCTAAACCCCG
TCTACAACGAGGCCATCATCTTTGACATCCCCCAGAAAACATGGACCAAGTGAGCCTG
CTCATCTCCGTTATGGACTATGATAGAGTTGGCCACAACGAGATCATAGAAGGGCGAAT
TCTGCAGATATCCATCACACTGGCGGCCGCTCGAGCATGCATCTAGAGGGCCCAATTCC

SYT7 α (R)

(NM_018801 mus syt 7)

ACCCGCATTTGGTTACCGGAGCTTCCGATCCACTAGTAACGGCCGCCAGTGTGCTGGA
ATTGCGCCCTTTGGCCAGGTTCTCTCGGCTGCAGCCCTCGTGGCCCTCATCCTCCTCA
GAACCTGGGGAGAGCATGAGCATCTCGCTGGTAAGGGAGTTGACGAGGTCCGAGACAG
AGGAACGGGTCTCCGTTCTGCGGTGAGACTCATCGTGTGGCGTCTGGCCGGGCACTGG
GGCTGTATTCACAGCCTTCCCTCCTGCAGGCAACTTGATGGCTTTCTTCTCACCGCGCC
CACGCCCCGAGTCTGGCGTGCCACCGTCTCCAAGGAATTCTTGTAGCGTTTGGCCAGT
TTGCGCTGACACCAGTGGCACAAAGGGCGAATTCTGCAGATATCCATCACACTGGCGG
CCGCTCGAGCATGCATCTAGAGGGCCCAATTCCCCCTATAGTGAGTCGTATTACAATTC

SYT8

(R)

(NM_018802 mus syt8)

GCCCCCTGGGGGTCCGAGCTCGGATCCACTAGTAACGGCCGCCAGTGTGCTGGAATTC
GCCCTTACAGGCTCAGTCCGGAGCTGCAGACCACGGGCCAGACAGCCAGCACCAG
GTCCACACTCTGCAGACATGTAGAGGGGATGTTTGTGAGTTTGGCATGGCACAACGTCC
CAGGCCACTCTGCCCTTCTCCAGCTCCCTACCTGGAGCTGGCTAACGGGAACCAGG
AAGACCAAGGCCTCGTTGAAGTAGGGGGTAGTCGTGCCTTTCTTGGAGGATGTTTTGCT
CTTCTCCATTTCTCTGGTTAACATAAGCTGGATCTTACGTAGGCCTCTGCACGAGT
GAGAAAGTTCAAGAAGGGAGTCCATACATGCACACGAGGGTCCAGCTCGCTGTCCAC
AAAAGTATGGCTCTCACCTGCAAGCCCCGGATTCCAGACCCCGAGCCTCCAGTAAGGGC
GAATTCTGCAGATATCCATCACACTGGCGGCCGCTCGAGCATGCATCTAGAGGGCCCAA

SYT9

(NM_021889 mus syt9)

CCGCCCGGGGCTCCCGAGCTCGGATCCACTAGTAAACGGCCGCCAGTGTGCTGGAATT
CGCCCTTAAGCCTGCGGGAACTGAACCTTCATTTAAAATATGACTGCGACTTGGAACA
GCTCATCGTGAAGATCCACAAAGCCGTCATCTGCCTGCCAAGGACTTCTCTGGGACTT
CAGATCCTTATGTCAAGATCTACTTGCTTCCTGACCGGAAAACAAAACACCAGACTAAAG
TTACACAGGAAGACCCTGAACCCTGTATTTGATGGGGTGTTTTATTTCTGTTCCTACTACA
ATGACCTTGAAGCTCGGAAGCTTCACTTCTCTGTGTATGACTTTGACAGGTTCTCTCGCC
ATGACCTGATTGGTCAGGTGGTGGTGGACCACTTCTTCGACTTGGCCGACTTAAGGGC
GAATTCTGCAGATATCCATCACACTGGCCGGCCGCTCGAGCATGCATCTAGAGGGCCCAA

SYT10

(R)

(NM_018803 mus syt10)

CGGCCCTGGTGGTACGGAGCTCGGATCCACTAGTAACGGCCGCCAGTGTGCTGGAATT
CGCCCTTAAGTCTTCCGGTGCACGCGGGTCTGAAATTTCTTCTTCTATCCGGAAGAAG
ATAGATCTTACATAAGGATCAGAAGTTCCCTGTGAAATCTTTAGCTGGGAGATCTAAAGC
TTTGATAATTTTAACTAGGAGTTCAATTTTATAATCATACTGGAGCGCAAAGTTAAGT
TTCCACAGGTCTTGACGTGGTCTTTTCTGTTGCCCTCGGAGTCAACCGATTTCTGCTTG
TAGAGTTCTGGTTTTATCCTCCCGATGCTCGTTCTCAAGGGCGAATTCTGCAGATATCCA
TCACACTGGCCGGCCGCTCGAGCATGCATCTAGAGGGCCCAATTGCCCCATAGTGAGT

SYT11

(NM_018804 mus syt11)

CGGGCCTGGTCCGAGCTCGGATCCACTAGTAACGGCCGCCAGTGTGCTGGAATTCGCC
CTTGACAAGCGGCATCGAGTGAAGACCCGAGTGCTTCGCAAGACGCTGGACCCGGTGT
TCGATGAGACCTTACCTTCTACGGCATCCCGTACAGCCAGCTGCAGGACCTGGTGCTG
CATTTCTGGTGTGCTCAGCTTTGATCGATTCTCTCGGGATGACGTCATCGGAGAGGTCAT
GGTGCCATTGGCTGGAGTGGACCCAGCACAGGCAAGGTTGAGCTGACCAGGGACATC
ATCAAGAGGAACATTCAGAAGTGCATTAGCAGAGGGGAAGTCCAGGTATCTCTGCTATA
CCAGCCCGTCCGACAAAGGGCGAATTCTGCAGATATCCATCACACTGGCCGGCCGCTCG
AGCATGCATCTAGAGGGCCCAATTGCCCCATAGTGAGTCGTATTACAATCACTGGCC

SYT12

(NM_134164 mus syt12)

GGCGCTTTGAAACGAAGCTCGGATCCACTAGTAACGGCCGCCAAGTGTGCTGGAATT
CGCCCTTTGACCAGCGGACCCTACTCGGGGACCACCCAGCCGCAAAGGCAGCCTTA
GTATAGAAGACACCTTTGAGAGCATCAGTGAGCTGGGACCCCTGGAGCTGATGGGCCG
GGAAGTGGACTTAGCCCCCTATGGTACTCTCCGAAAGTACAGTCCGGCTGACTCTCTGA
ATTCCATCTCCTCTGTGAGCAACACCTTTGGGCAGGATTTACCCTGGGCCAGGTGGAG
GTGAGCATGGACTATGATGGAGCCTCCACACCCCTCCACGTGGCAGTACTACAAGGCA
AAGACCTCCTGGAGCGGAGGAGGCCACCTTCGAGTCCCTGCTTCATGCGTGTGAGACT
GCTGCCAGACGAACAGATCGTGAAGGGCGAATTCTGCAGATATCCATCACACTGGCCG
CCGCTCGAGCATGCATCTAGAGGGCCCAATTGCCCCATAGTGAGTCGTATTACAATTC

SYT13

(NM_030725 mus syt13)

ATAGAGGGCAAGGCTACGAGCTCGGATCCACTAGTAACGGCCGCCAGTGTGCTGGAAT
TCGCCCTTCGACACATGCACCCCAAGAAGGGGTTGCTGCCCGGGACCGTGAGCCCG
ACCCGGAGAAGGCAAGGCCCGGTGTGCTTCAGGCGGCCCAACAGTTCAACATTAATAA
GTCCACGGAGCCTGTCCAGCCCCGACCTCTCCTTAAGTTCCCGGACATCTATGGTCCCC
GGCCAGCCGTGACGGCCCCAGAAGTCATCAACTACGCAGACTACACCTTGGAGACCAC
AGAGGAGTCTGCTGCACCTGCCAGCCCCAGGCCAGAGTGACAGTCCGCCAAGGGC
GAATTCTGCAGATATCCATCACACTGGCCGGCCGCTCGAGCATGCATCTAGAGGGCCCAA

SYT14

(R)

(NM_181546 mus syt14)

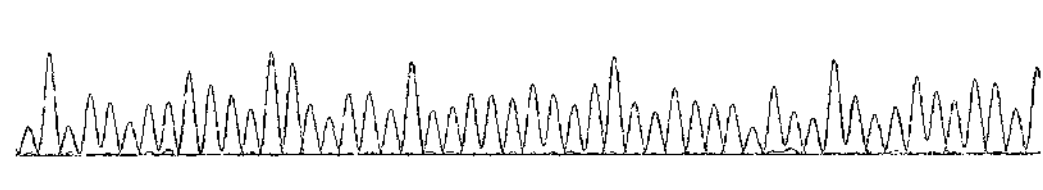
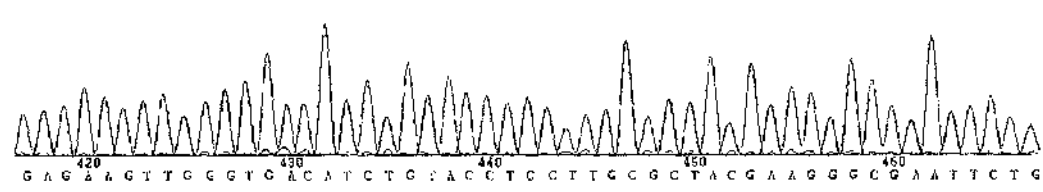
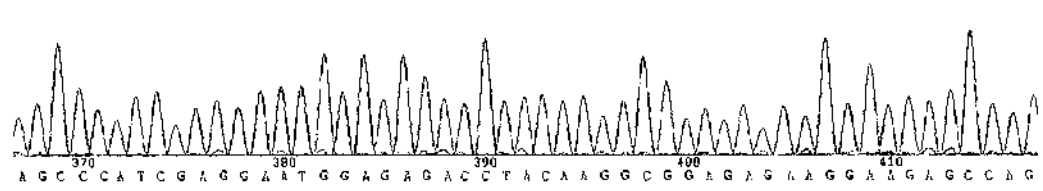
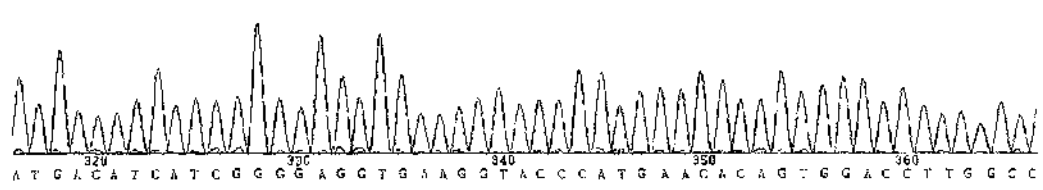
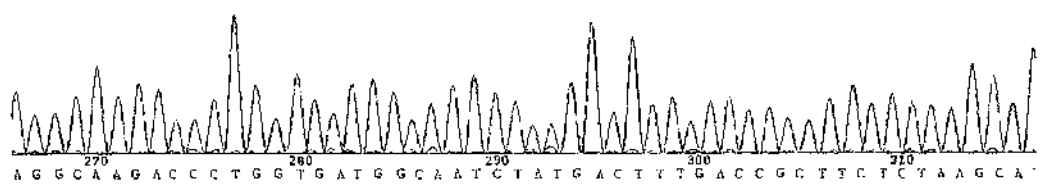
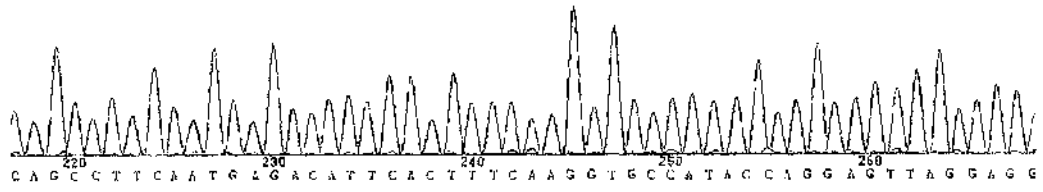
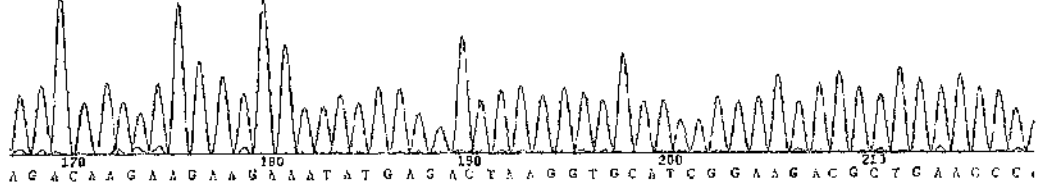
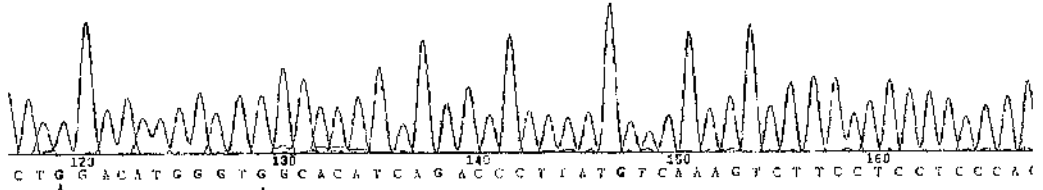
GCGAACCTTGGGTACGGAGCTCGGATCCACTAGTAACGGCCGCCAGTGTGCTGGAATT
CGCCCTTCCAGTATCACCGGTAACGACATTTTCCCTTGAAGATTCAACTTTGTTAAATAA
AAAATCTTTTCCCCACAATCTTTCTTTCTTCATGCGATGGACACCATATAGTCTAAACC
TAACTGCATAGTTTCCAATCATCTCGGATTCAACGTGGTTAAATTTGAATGTTTCTGTGAA
GACAGGGCATGGTCCTCTCTGGATGCTGGTTTGGCTCTCTGTTTTTTATAGGTAGAAG
ACAAGGTGTACCTGCCACGAGTTGCCACCTGTCCTGTTATATGTGGAAATGTCTGTGA
CAGCTGTCACCGTTACCAGGAGCTAAGGGCGAATTCTGCAGATATCCATCACACTGGC
GGCCGCTCGAGCATGCATCTAGAGGGCCCAATTCGCCCTATAGTGAGTGGTATTACAAT

A1.2.4 Murine SYT RTPCR Product Sequencing Chromatograms

Pictured below are the sequencing chromatograms corresponding to the sequences given in A1.2.3 above. Chromatograms shown begin with the first residue of each corresponding RTPCR primer.

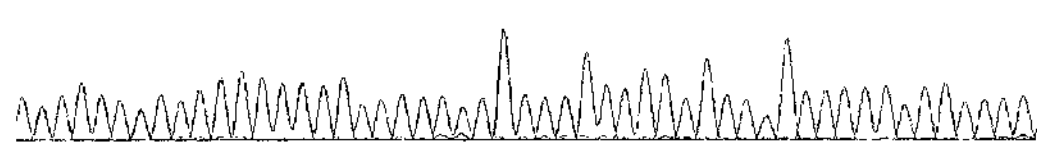
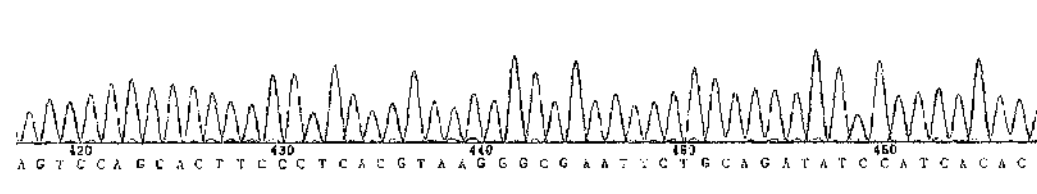
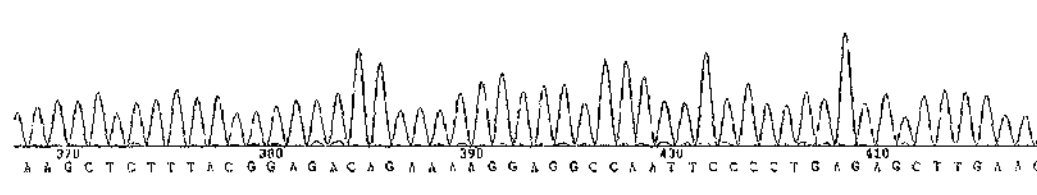
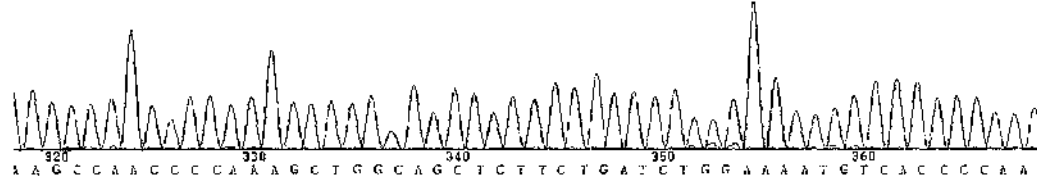
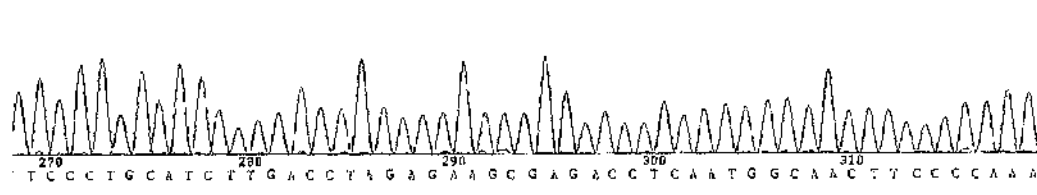
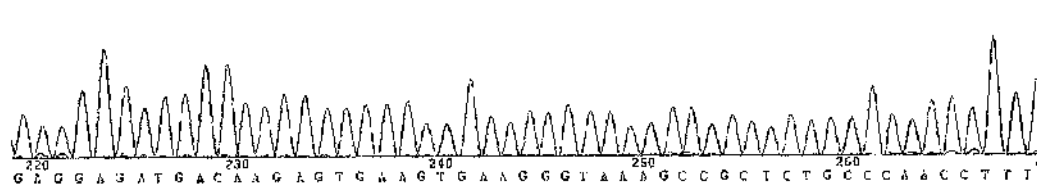
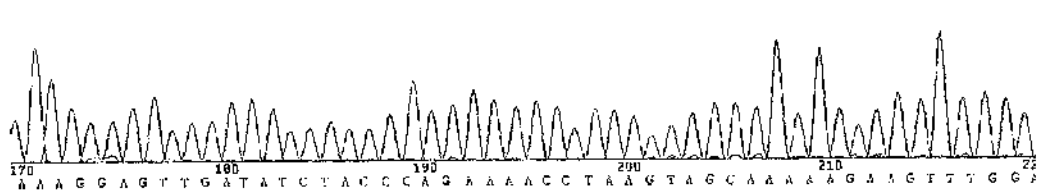
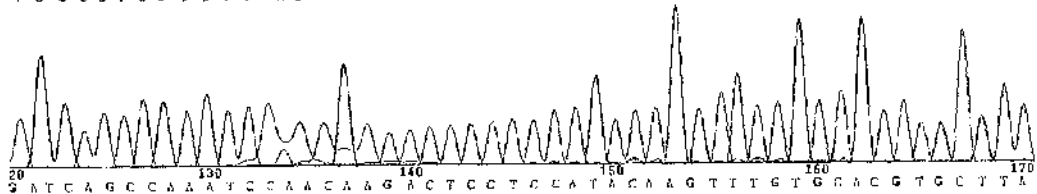
SYT2

70 80 90 100 110
CAGGCCAAACCA G C I CACCGTG GGT GTCCTGCCAGGCTGCGGAACCTCCAGCC



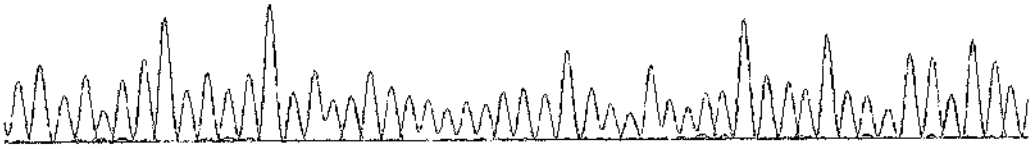
SYT4

70 T G G C C T C G T C T T C A C T G T C T C T C T T T G C C T G G A T C T G C T G T C A G A G A A 1

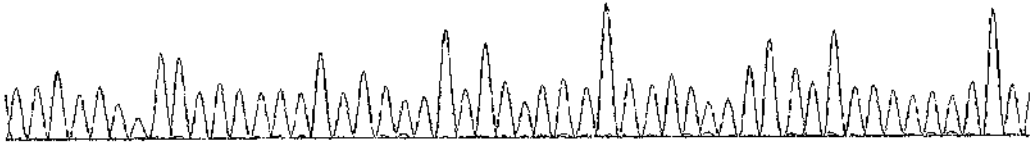


SYT5

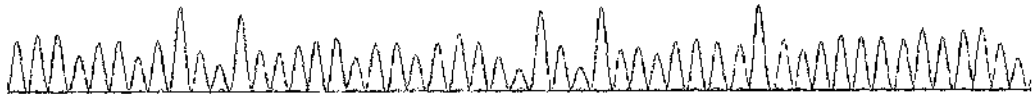
C G T C A T T G ⁹⁰ T C T T G G A A G C T ¹⁰⁰ A A A A C C T ¹¹⁰ G A A G A A A A T ¹²⁰ G G A T G T A G G A G G A C ¹³⁰



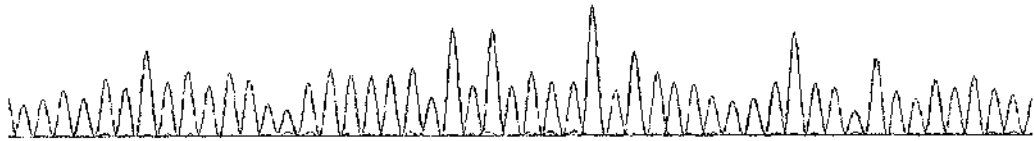
C T C T C A G A T ¹⁴⁰ C C C T A T G T G ¹⁵⁰ A A G G T C C A C C T ¹⁶⁰ G C T C C A G G G ¹⁷⁰ A G G T A A A A A G C T ¹⁸⁰



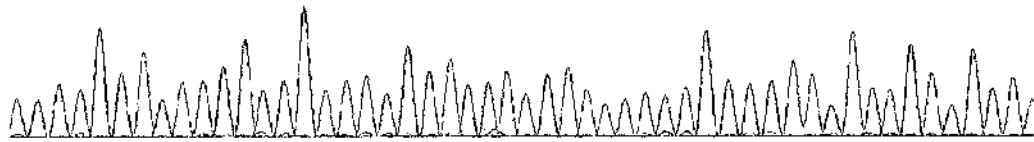
T T C C C A A G A ¹⁹⁰ A A A A C C A C C A T T A A G A A G A A C A C C C T G A ²⁰⁰ C C C C T A T T A C A ²¹⁰



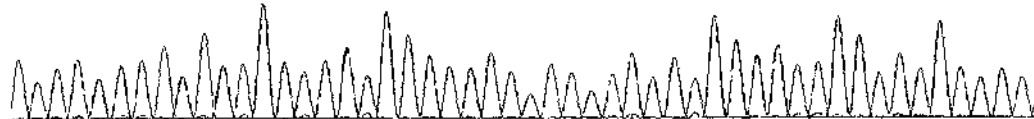
A A C G A G G C C T T C A G C T T T G A G G T G C C C T G T G A C C A G G T G C A G A A A G T C C A T ²⁴⁰



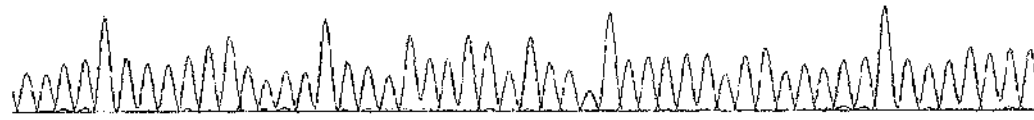
A G G T G G A G C T G A C T G T T C T G G A T T A T G B C A A A C T G G G G A A C A A T G A G G C C A ²⁹⁰



C T T E G G G A G A G T G G C G G T G G G C C C A G C A G T C G G T G G G G C T G G C C T G C G G C ³⁴⁰

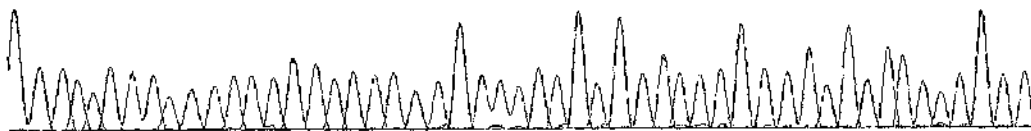


C A C T G G C C T G A C A A G G C C G A A T T C T G C A G A T A T C C A T C A C A C T G G C G G C C G ³⁹⁰

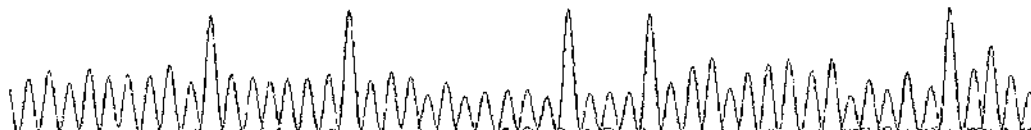


SYT6

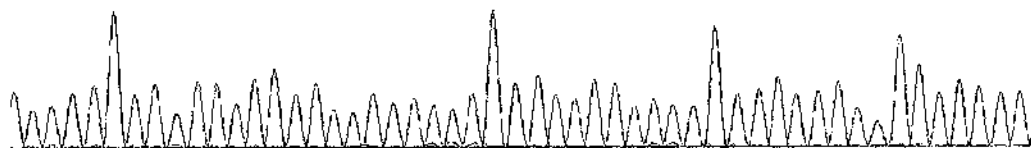
70 80 90 100 110
U G A C A T C C A G T A C G C T A C T A G T G A A A G T G Y G C A C T T G G G A G A C A T C A T C T T



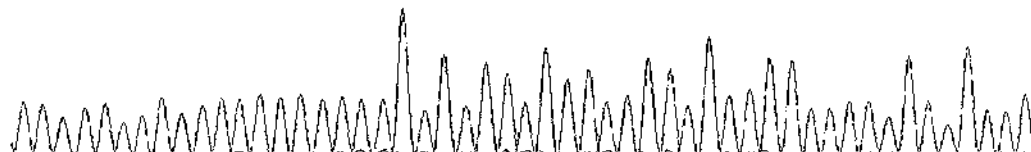
120 130 140 150 160
T C T C C C T C T G C T A C C T G C C C A C A G C A G G C A G G C T C A C C C Y C A C A G T G A T C A



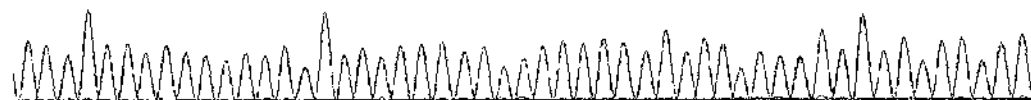
170 180 190 200 210
C A A G T G T C G A A A T C T C A A A G C A A T G G A C A T C A C A G G C T A C T C A G A T C C C Y A A



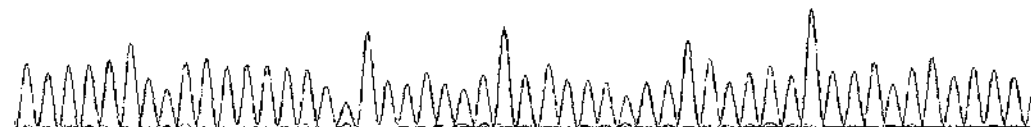
220 230 240 250 260
A C G T C A A A G T A T C C C Y A C T G T G A T C G A C G G A G G C T C A A A A A G A A G A A A A



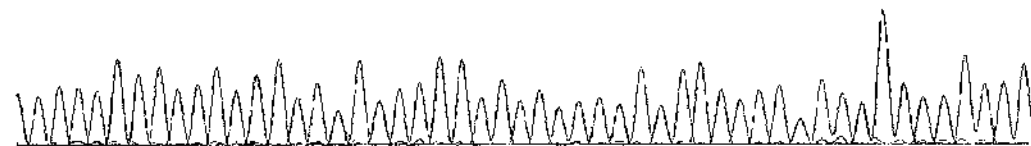
270 280 290 300 310
A U G A C C A T A A A A A A C A A C C C C T A A A C C C C G T C T A C A A C G A G G C C A T C A T C



320 330 340 350 360
C T T G A C A T C C C C C A G A A A A C A T G G A C C A A G T C A G C C T G C T C A T C T C C G T

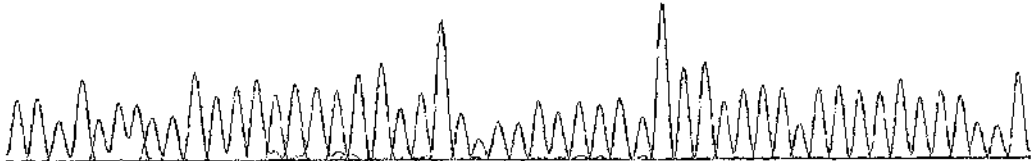


370 380 390 400 410
T T A T G G A C T A T G A T A G A G T T G G C C A C A A C C A C A T C A T A G A A C G C C G A A T T

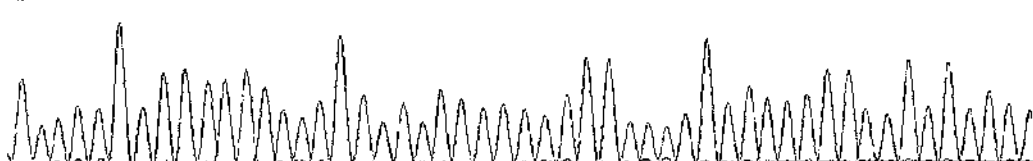


SYT7

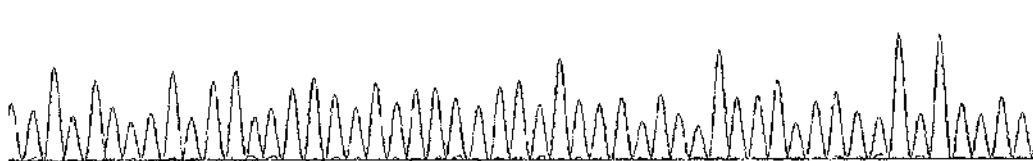
70 TCGGCCAAGGTTCTCTCGCCYGCAGCCCTCGTGGCCCTCATCCTCTCAGAA¹



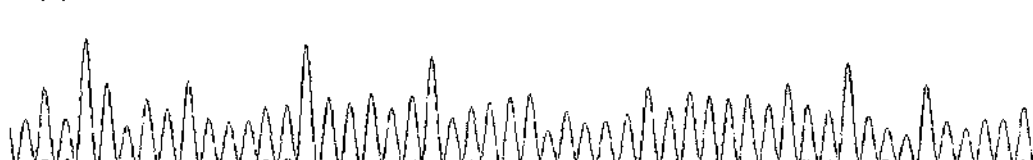
120 AACCTGGGGAGAGCATEAGCATCTCGCTGGTAAGGGAGTTGACGAGGTCCG



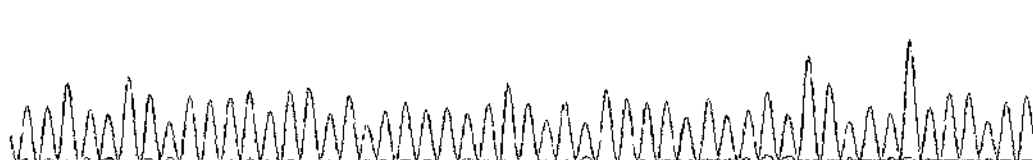
170 CGAGACAGAGSAAAGGGTCTCCCTCTCGCGGTTCAGACTCAJCCGTGTGCGGT



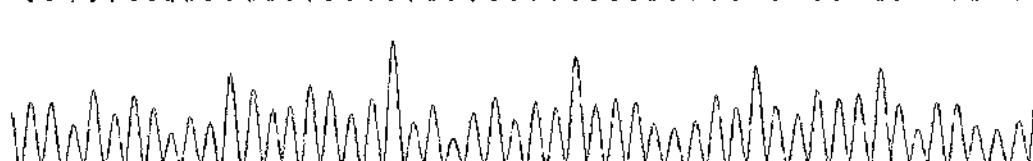
220 TCTGSCCGGGCACCTGGGGCTCTATTTCACAGCCCTTCCCTCTCTGCAGGCAACT



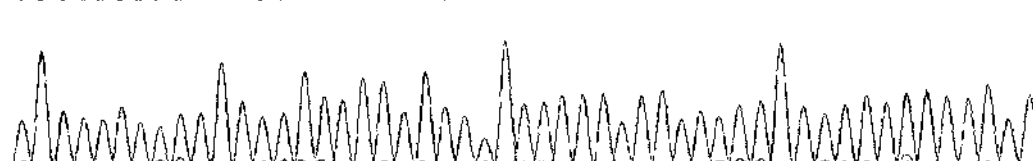
270 FTGATGGCTTTCTTCTCCCGCGCCACGCCCCGAGTCTGGCGGTGCCCAAC



320 CGTCTCCAAGGAATTCTTGTAGCGGFTTSCCCAGTTTGGGCTGACACCAGT

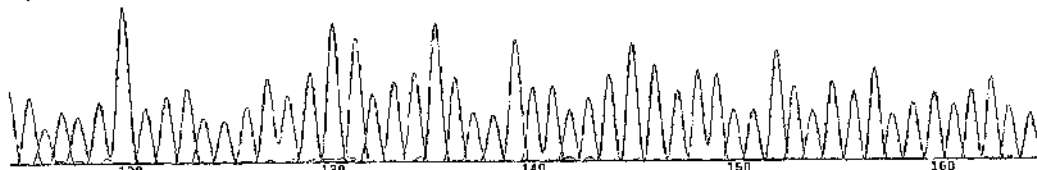


370 TGGCACAAGGGCCGAAATTTGCAGATATCCATCACACTGGCGGGCCGCTCGA

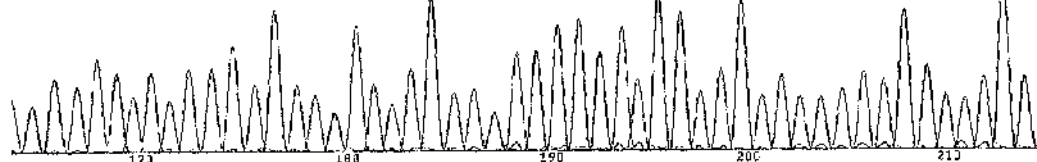


SYT8

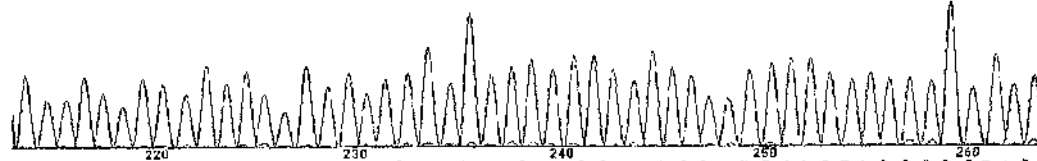
70 80 90 100 110
C A C A G G C T C A G T C C G G A G C T G C A G A C C A C G G C C C A G A C A G C C A G C C A C C A G



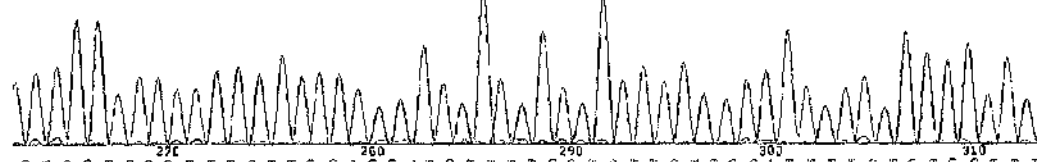
120 130 140 150 160
G G I C C A C A C T C T G C A G A C A T G T A G A G G G G A T G G T T C T C A G T T T G G C A T G G



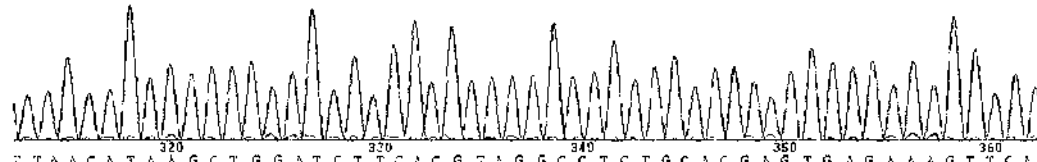
170 180 190 200 210 220 230 240 250
G C A C A A C C G T C C C A G G C C A C T C T G C C C T T C G T C C C A G C T C C C T A C C T G G A G C



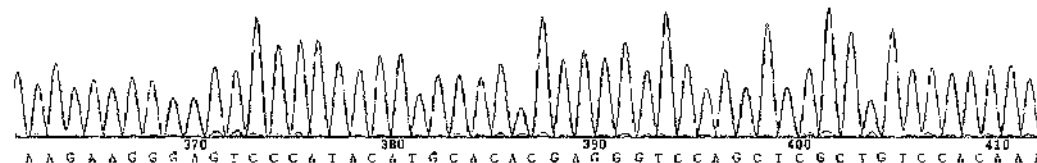
250 260 270 280 290 300 310 320 330 340
C T G G C T A A C G G A A C C A G G A A G A C A G A A G C C T C G T T G A A G T A G G G G G T A G



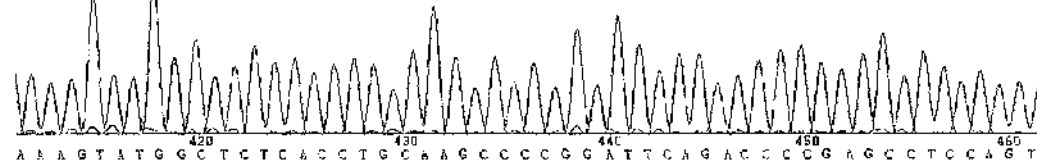
340 350 360 370 380 390 400 410 420 430
G T C G T G C C T T T T C T T G G A G G A T G T T T T G C T C T T C T T C A T T T T T C T G T G T T T



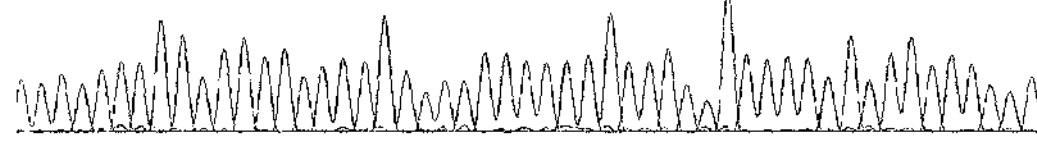
430 440 450 460 470 480 490 500 510 520
T T A A C A T A A G C T G G A T C T T C A C G G T A G G C C T C T G C A C G A G T G A G A A A G T T C A



520 530 540 550 560 570 580 590 600 610
A A G A A G G A A G T C C C A T A C A T A C A C A C G A G G G T E C A G C T C G C T G T C C A C A A A

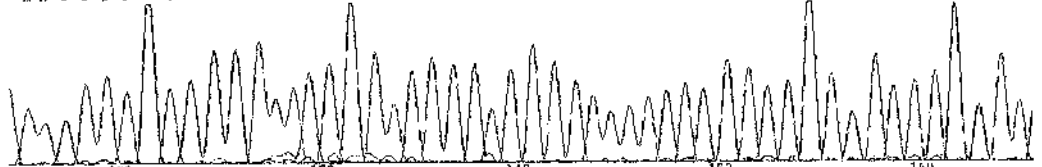


610 620 630 640 650 660 670 680 690 700
A A A G T A T G G C T C T C A C C T G C A A G C C C C G G A T T C A G A C C C G A G C C T C C A G T

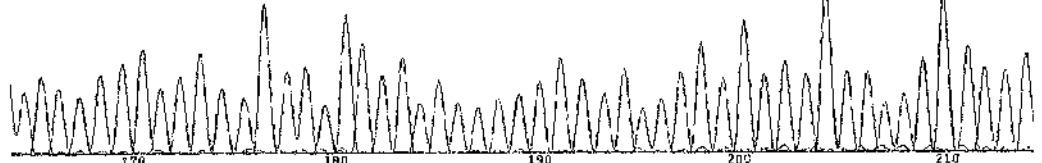


SYT9

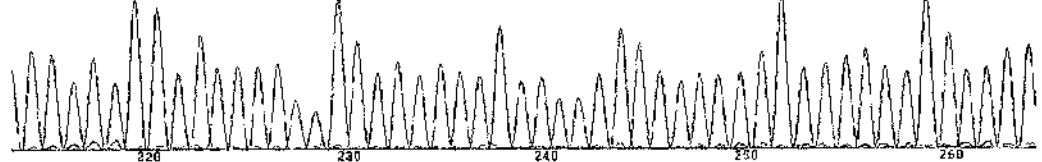
· A A G C C T ⁷⁰ G C G G G A A A C T ⁸⁰ G A A C U T C A T T T T A A A A T A T ⁹⁰ G C T G C G A C T T G G A A · ¹⁰⁰ ¹¹⁰



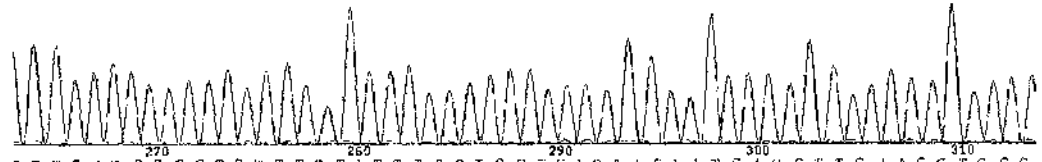
A A G C C T C A T G T G A A G A T C C A C A A A C C C G T C A A T C T G C C T G C C A A G G A C T T



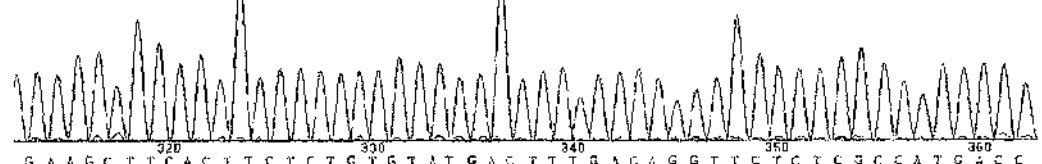
T C T C T C G G G A C T T C A G A T C C T T A T G T C A A G A T C T A C T T G C T T C C T G A C C G G



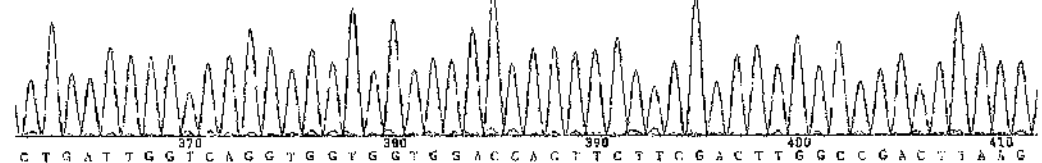
G A A A A C A A A A C A C C A G A C T A A A G T T C A C A G G A A G A C C C T G A A C C C T G T A T T



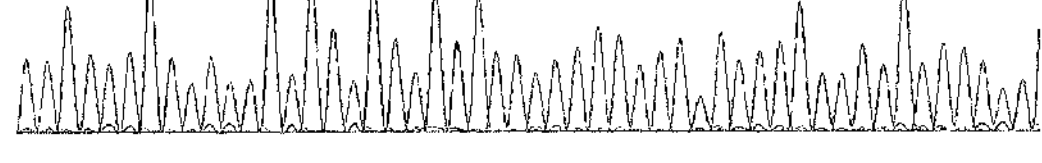
T T G A T C G G G G T G Y T T T T A T T T C C T G C T C A C T A C A A T G A C C T T G A A G C T C G G



G A A G C T T C A C T T C T C T G T A T G A C T T T G A C A G G T T C T C T C C C A T G A C C



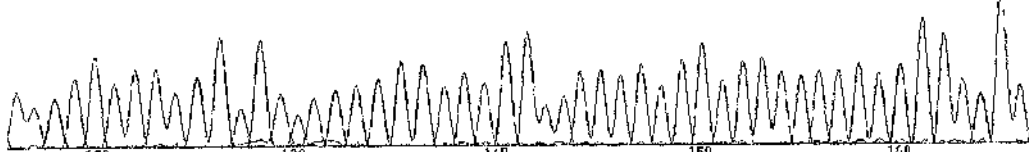
C T G A T T G G T C A G G T G G Y G G Y G S A C C A C T T C T T G G A C T T G G C C G A C T T A A G



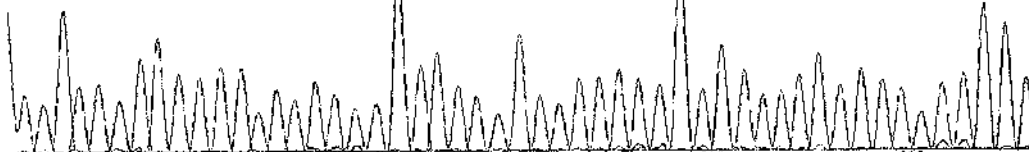
C T G A T T G G T C A G G T G G Y G G Y G S A C C A C T T C T T G G A C T T G G C C G A C T T A A G

SYT10

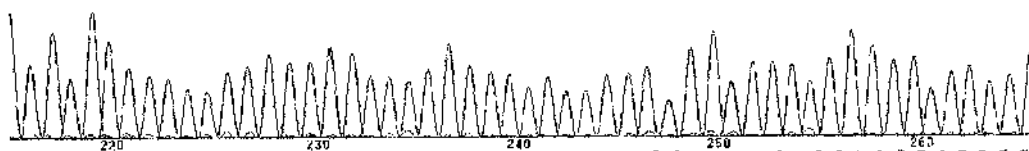
AAGTCTTCCGGTGCACGGCGGGTCTGAAATTTCTTCTTCCATATCCGGGAAGAA



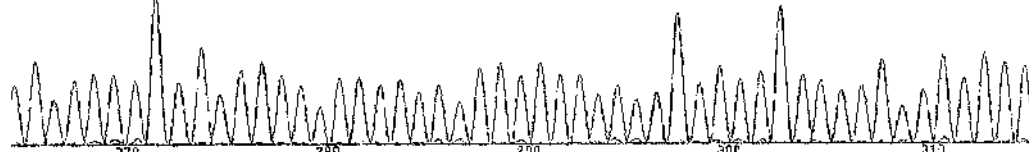
AGATAGATCTTCACATAGGATCAGAAAGTTCTGTGAARYCTFYAGCTGGG



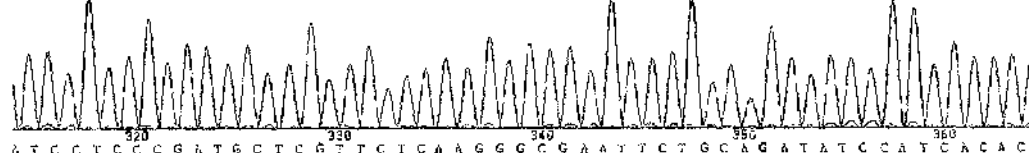
AGATCTYAAAGCITTCATAATTTTAAACAACTAGGAGTTCATTTTCATAATC



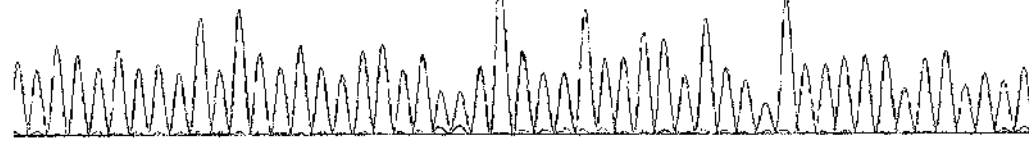
TCATATCTGGAGCSCAAAGTTAAGITTTCCACAGGTCTTTGACGGYCGTCTTTT



TCGTTCGCCCTCGGAGTCAACCGATTTCTGCTTGTGAGATTCTGGTTTAT



ATCTCTCCGATGCTCTCTTCICAAAGGCCGAAATCTGCAGATATCCATCACAC



A1.3 Taqman Realtime PCR Primer and Probe Sequences

A1.3.1 Taqman Realtime PCR Primer Sequences

β Actin	Forward	5'- TGCTCTGGCTCCTAGCACCAT -3'
	Reverse	5'-ACATCTGCTGGAAGGTGGACAGT-3'
GLUT4	Forward	5'- ACCGGATTCCATCCCACAA -3'
	Reverse	5'-CCCTTTTCCTTCCCAACCATT-3'
Syt 3	Forward	5'-GCAGATCTCGGAGAGCTCAACT-3'
	Reverse	5'-CTTTGAGGTTGCGGGCTTTGATGAT-3'
Syt 6	Forward	5'-GGACATCCAGTACGCTAC-3'
	Reverse	5'-CTATGATCTCGTTGTGGC-3'
Syt 7	Forward	5'-TGTGCCACTGGTGTGAGC-3'
	Reverse	5'-TCGGCCCAGGTTCTCTCG-3'
Syt 8	Forward	5'-AGAAATGGAAGAAGAGCAAAACATC-3'
	Reverse	5'-CCACACTCTGGAGCTGGCTAAC-3'
Syt 9	Forward	5'-CCTTATGTCAAGATCTACTTGCTTCCT-3'
	Reverse	5'-TTCCGAGCTTCAAGGTCATTGTA-3'
Syt 10	Forward	5'-AGAACGAGCATCGGGAGGATA-3'
	Reverse	5'-TCATACTGGAGCGCAAAGTTAAGT-3'
Syt 11	Forward	5'-ACAAGCGGCATCGAGTGAA-3'
	Reverse	5'-AAGGTGAAGGTCTCATCGAACAC-3'

Syt 12	Forward	5'-CAAAGGCAGCCTTAGTATACGAAGACA-3'
	Reverse	5'-CCGACTGTGACTTTTCGGAGAGTAC-3'
Syt 13	Forward	5'-TCAGGCGGCCCAACAGT-3'
	Reverse	5'-CCAAGGTGTAGTCTGCGTAGTTGAT-3'

A1.3.2 Taqman Probe Sequences

βActin	5'- TCAAGATCATTGCTCCTCCTGAGCGC-3'
GLUT4	5'-CCCTCACTACGCTCTGGGCTCTCTCC-3'
Syt 3	5'-CTGGGCGCCTCACCGTGACC-3'
Syt 7	5'-TCATGCTCTCCCCAGGTTCTGAGGA-3'
Syt 8	5'-CAAGAAAGGCACGACTACCCCCTACTTCA-3'
Syt 9	5'-CAGACTAAAGTTCACAGGAAGACCCTGAACCC-3'
Syt 10	5'-CCAGAACTCTACAAGCAGAAATCGGTTGACTC-3'
Syt 11	5'-ACCCGAGTGCTTCGCAAGACGC-3'
Syt 12	5'-CCGGGAAGTGGACTTAGCCCCCTAT-3'
Syt 13	5'-AAGTCCACGGAGCCTGTCCAGCC-3'

A1.4 SYT7 and SYT11 Immunogenic Peptides

Table A4

Peptide Name	Amino Acid Sequence	Residue Number
SYT7-1	YRDPEAASPGAPTRD	2-16
SYT7-2	GTPDSGRGRGEKKAIK	57-72
SYT11-1	KVRRDKDGPRRESGR	77- 91
SYT11-2	LLSHDKDPRGPSPAS	102- 116

Table A4 Peptides used to generate SYT7 and SYT11 antisera.

A1.5 SYT11 siRNA Sequence

5'-GCAGAGAAGAAGCACAAAGA-3'

References

- (1) Turner RC, Holman RR, Cull CA, Stratton IM, Matthews DR, Frighi V et al. Intensive blood-glucose control with sulphonylureas or insulin compared with conventional treatment and risk of complications in patients with type 2 diabetes (UKPDS 33). *Lancet* 1998; 352(9131):837-853.
- (2) Lanceraux E. *Le Diabete Maigre: Ses Symptomes, Son Evolution, Son Pronosic et son Traitement*. Union Medicale Paris 20, 205-211. 1-1-1880.
- (3) von Mering J, Minkowski O. Diabetes Mellitus Nach Pankreasextirpation. *Archives of Experimental Pathology and Pharmacology, Leipzig* 26, 371-387. 1-1-1890.
- (4) Shamoon H, Duffy H, Fleischer N, Engel S, Saenger P, Strelzyn M et al. The Effect of Intensive Treatment of Diabetes on the Development and Progression of Long-Term Complications in Insulin-Dependent Diabetes-Mellitus. *New England Journal of Medicine* 1993; 329(14):977-986.
- (5) Alberti KGMM, Zimmet PZ. Definition, diagnosis and classification of diabetes mellitus and its complications part 1: Diagnosis and classification of diabetes mellitus - Provisional report of a WHO consultation. *Diabetic Medicine* 1998; 15(7):539-553.
- (6) Dahlquist G. The aetiology of type 1 diabetes: an epidemiological perspective. *Acta Paediatrica* 1998; 87:5-10.
- (7) Eledrisi MS. Overview of the Diagnosis and Management of Diabetic Ketoacidosis. *American Journal of the Medical Sciences* 331[5], 243-251. 2006
- (8) Reaven GM. Role of Insulin Resistance in Human-Disease. *Diabetes* 1988; 37(12):1595-1607.
- (9) Medici F, Hawa M, Ianari A, Pyke DA, Leslie RDG. Concordance rate for Type II diabetes mellitus in monozygotic twins: actuarial analysis. *Diabetologia* 1999; 42(2):146-150.
- (10) Poulsen P, Kyvik KO, Vaag A, Beck-Nielsen H. Heritability of Type II (non-insulin-dependent) diabetes mellitus and abnormal glucose tolerance - a population-based twin study. *Diabetologia* 1999; 42(2):139-145.

- (11) Harris H. The Familial Distribution of Diabetes Mellitus - A Study of the Relatives of 1241 Diabetic Propositi. *Annals of Eugenics* 1950; 15(2):95-&.
- (12) Kahn CB, Soeldner JS, Gleason RE, Rojas L, CAMERINI.RA, Marble A. Clinical and Chemical Diabetes in Offspring of Diabetic Couples. *New England Journal of Medicine* 1969; 281(7):343-&.
- (13) Thomas F, Balkau B, Vauzellekervroedan F, Papoz L. Maternal Effect and Familial Aggregation in Niddm - the Codiab Study. *Diabetes* 1994; 43(1):63-67.
- (14) Neel JV. Diabetes Mellitus - A Thrifty Genotype Rendered Detrimental by Progress. *American Journal of Human Genetics* 1962; 14(4):353-&.
- (15) Dalton M, Cameron AJ, Zimmet PZ, Shaw JE, Jolley D, Dunstan DW et al. Waist circumference, waist-hip ratio and body mass index and their correlation with cardiovascular disease risk factors in Australian adults. *Journal of Internal Medicine* 2003; 254(6):555-563.
- (16) Despres JP. Is visceral obesity the cause of the metabolic syndrome? *Annals of Medicine* 2006; 38(1):52-63.
- (17) Petersen KF, Shulman GI. Etiology of insulin resistance. *American Journal of Medicine* 2006; 119(5):10S-16S.
- (18) Gallagher D, Visser M, Sepulveda D, Pierson RN, Harris T, Heymsfield SB. How useful is body mass index for comparison of body fatness across age, sex, and ethnic groups? *American Journal of Epidemiology* 1996; 143(3):228-239.
- (19) Willett WC, Manson JE, Stampfer MJ, Colditz GA, Rosner B, Speizer FE et al. Weight, Weight Change, and Coronary Heart-Disease in Women - Risk Within the Normal-Weight Range. *Jama-Journal of the American Medical Association* 1995; 273(6):461-465.
- (20) American Diabetes Association - Clinical practice recommendations 2006 - Introduction. *Diabetes Care* 2006; 29:S1-S2.
- (21) FerroLuzzi A, Garza C, Haas J, Habicht DP, Himes J, Pradilla A et al. Physical status: The use and interpretation of anthropometry - Introduction. *Physical Status: the Use and Interpretation of Anthropometry* 1995; 854:1-3.
- (22) [Anon]. Obesity: Preventing and managing the global epidemic - Introduction. *Obesity: Preventing and Managing the Global Epidemic* 2000; 894:1-253.

- (23) Lawlor DA, Chaturvedi N. Treatment and prevention of obesity - are there critical periods for intervention? *International Journal of Epidemiology* 2006; 35(1):3-9.
- (24) Lundbaek K. Diabetic Angiopathy - A Specific Vascular Disease. *Lancet* 1954; 1(FEB20):377-379.
- (25) Laing SP, Swerdlow AJ, Slater SD, Burden AC, Morris A, Waugh NR et al. Mortality from heart disease in a cohort of 23,000 patients with insulin-treated diabetes. *Diabetologia* 2003; 46(6):760-765.
- (26) Marshall SM, Flyvbjerg A. Prevention and early detection of vascular complications of diabetes. *British Medical Journal* 333, 475-480. 2-9-2006.
- (27) Ritz E, Rychlik I, Locatelli F, Halimi S. End-stage renal failure in type 2 diabetes: A medical catastrophe of worldwide dimensions. *American Journal of Kidney Diseases* 1999; 34(5):795-808.
- (28) Antonetti DA, Barber AJ, Bronson SK, Freeman WM, Gardner TW, Jefferson LS et al. Diabetic retinopathy: seeing beyond glucose-induced microvascular disease. *Diabetes* 55(9), 2401-2411. 1-9-2006.
- (29) Fong DS, Aiello LP, Ferris FL, Klein R. Diabetic retinopathy. *Diabetes Care* 2004; 27(10):2540-2553.
- (30) Vinik AI, Mehrabyan A. Diabetic neuropathies. *Medical Clinics of North America* 2004; 88(4):947-+.
- (31) Costa J, Borges M, David C, Carneiro AV. Efficacy of lipid lowering drug treatment for diabetic and non-diabetic patients: meta-analysis of randomised controlled trials. *British Medical Journal* 2006; 332(7550):1115-1118C.
- (32) Kshirsagar AV, Joy MS, Hogan SL, Falk RJ, Colindres RE. Effect of ACE inhibitors in diabetic and nondiabetic chronic renal disease: A systematic overview of randomized placebo-controlled trials. *American Journal of Kidney Diseases* 2000; 35(4):695-707.
- (33) Brenner BM, Cooper ME, de Zeeuw D, Keane WF, Mitch WE, Parving HH et al. Effects of losartan on renal and cardiovascular outcomes in patients with type 2 diabetes and nephropathy. *New England Journal of Medicine* 2001; 345(12):861-869.
- (34) Brownlee M. Biochemistry and molecular cell biology of diabetic complications. *Nature* 2001; 414(6865):813-820.

- (35) Brownlee M. The pathobiology of diabetic complications - A unifying mechanism. *Diabetes* 2005; 54(6):1615-1625.
- (36) Hammes HP, Du XL, Edelstein D, Taguchi T, Matsumura T, Ju QD et al. Benfotiamine blocks three major pathways of hyperglycemic damage and prevents experimental diabetic retinopathy. *Nature Medicine* 2003; 9(3):294-299.
- (37) Ilnytska O, Lyzogubov VV, Stevens MJ, Drel VR, Mashtalir N, Pacher P et al. Poly(ADP-ribose) polymerase inhibition alleviates experimental diabetic sensory neuropathy. *Diabetes* 2006; 55(6):1686-1694.
- (38) Salvemini D, Wang ZQ, Zweier JL, Samouilov A, Macarthur H, Misko TP et al. A nonpeptidyl mimic of superoxide dismutase with therapeutic activity in rats. *Science* 1999; 286(5438):304-306.
- (39) Perley MJ, Kipnis DM. Plasma Insulin Responses to Oral and Intravenous Glucose - Studies in Normal and Diabetic Subjects. *Journal of Clinical Investigation* 1967; 46(12):1954-&.
- (40) Eguez L, Lee A, Chavez JA, Miinea CP, Kane S, Lienhard GE et al. Full intracellular retention of GLUT4 requires AS160 Rab GTPase activating protein. *Cell Metabolism* 2005; 2(4):263-272.
- (41) Rorsman P, Eliasson L, Renstrom E, Gromada J, Barg S, Gopel S. The cell physiology of biphasic insulin secretion. *News in Physiological Sciences* 2000; 15:72-77.
- (42) Tattersall RB. Mild familial diabetes with dominant inheritance. *The Quarterly Journal of Medicine* 43(170), 339-357. 1-4-1974.
- (43) Hattersley AT, Pearson ER. Minireview: Pharmacogenetics and beyond: The interaction of therapeutic response, beta-cell physiology, and genetics in diabetes. *Endocrinology* 2006; 147(6):2657-2663.
- (44) Marchetti P, Del Prato S, Lupi R, Del Guerra S. The pancreatic beta-cell in human Type 2 diabetes. *Nutrition Metabolism and Cardiovascular Diseases* 2006; 16:S3-S6.
- (45) Zimmet PZ. Kelly West Lecture 1991 - Challenges in Diabetes Epidemiology - from West to the Rest. *Diabetes Care* 1992; 15(2):232-252.
- (46) Cleeman JI, Grundy SM, Becker D, Clark LT, Cooper RS, Denke MA et al. Executive summary of the Third Report of the National Cholesterol Education Program (NCEP) expert panel on detection, evaluation, and treatment of high blood cholesterol in

adults (Adult Treatment Panel III). *Jama-Journal of the American Medical Association* 2001; 285(19):2486-2497.

- (47) Alberti KGMM, Zimmet P, Shaw J. Metabolic syndrome - a new world-wide definition. A Consensus Statement from the International Diabetes Federation. *Diabetic Medicine* 2006; 23(5):469-480.
- (48) Reaven GM. The metabolic syndrome: is this diagnosis necessary ? *American Journal of Clinical Nutrition* 2006; 83(6):1237-1247.
- (49) Kahn R, Buse J, Ferrannini E, Stern M. The metabolic syndrome: Time for a critical appraisal - Joint statement from the American Diabetes Association and the European Association for the Study of Diabetes. *Diabetes Care* 2005; 28(9):2289-2304.
- (50) Sundstrom J, Riserus U, Byberg L, Zethelius B, Lithell H, Lind L. Clinical value of the metabolic syndrome for long term prediction of total and cardiovascular mortality: prospective, population based cohort study. *British Medical Journal* 2006; 332(7546):878-881.
- (51) Dreschfeld J. The Bradshaw Lecture of Diabetic Coma. *British Medical Journal* 2, 358-363. 1886.
- (52) Eledrisi MS, Alshanti MS, Shah MF, Brost B, Jaha N. Overview of the Diagnosis and Management of Diabetic Ketoacidosis. *American Journal of the Medical Sciences* 331[5], 243-251. 2006.
- (53) Duvillie B, Cordonnier N, Deltour L, DandoyDron F, Itier JM, Monthieux E et al. Phenotypic alterations in insulin-deficient mutant mice. *Proceedings of the National Academy of Sciences of the United States of America* 1997; 94(10):5137-5140.
- (54) Kessler A, Tomas E, Immler D, Meyer HE, Zorzano A, Eckel J. Rab11 is associated with GLUT4-containing vesicles and redistributes in response to insulin. *Diabetologia* 2000; 43(12):1518-1527.
- (55) Wood IS, Trayhurn P. Glucose transporters (GLUT and SGLT): expanded families of sugar transport proteins. *British Journal of Nutrition* 2003; 89(1):3-9.
- (56) Joost HG, Thorens B. The extended GLUT-family of sugar/polyol transport facilitators: nomenclature, sequence characteristics, and potential function of its novel members. *Molecular Membrane Biology* 2001; 18(4):247-256.

- (57) Birnbaum MJ. Identification of A Novel Gene Encoding An Insulin-Responsive Glucose Transporter Protein. *Cell* 1989; 57(2):305-315.
- (58) Leloup C, Arluison M, Kassis N, Lepetit N, Cartier N, Ferre P et al. Discrete brain areas express the insulin-responsive glucose transporter GLUT4. *Molecular Brain Research* 1996; 38(1):45-53.
- (59) Martin S, Reaves B, Banting G, Gould GW. Analysis of the Colocalization of the Insulin-Responsive Glucose-Transporter (Glut4) and the Trans-Golgi Network Marker Tgn38 Within 3T3-L1 Adipocytes. *Biochemical Journal* 1994; 300:743-749.
- (60) Choeiri C, Staines WA, Miki T, Seino S, Renaud JM, Teutenberg K et al. Cerebral glucose transporters expression and spatial learning in the K-ATP Kir6.2(-/-) knockout mice. *Behavioral Brain Research* 2006; 172(2):233-239.
- (61) Richter EA, Garetto LP, Goodman MN, Ruderman NB. Muscle Glucose-Metabolism Following Exercise in the Rat - Increased Sensitivity to Insulin. *Journal of Clinical Investigation* 1982; 69(4):785-793.
- (62) Holloszy JO. Exercise-induced increase in muscle insulin sensitivity. *Journal of Applied Physiology* 2005; 99(1):338-343.
- (63) Li DL, Randhawa VK, Patel N, Hayashi M, Klip A. Hyperosmolarity reduces GLUT4 endocytosis and increases its exocytosis from a VAMP2-independent pool in L6 muscle cells. *Journal of Biological Chemistry* 2001; 276(25):22883-22891.
- (64) Morgan HE, Randle PJ, Regen DM. Regulation of Glucose Uptake by Muscle .3. Effects of Insulin, Anoxia, Salicylate and 2-4-Dinitrophenol on Membrane Transport and Intracellular Phosphorylation of Glucose in the Isolated Rat Heart. *Biochemical Journal* 1959; 73:573-579.
- (65) Katz EB, Stenbit AE, Hatton K, Depinho R, Charron MJ. Cardiac and Adipose-Tissue Abnormalities But Not Diabetes in Mice Deficient in Glut4. *Nature* 1995; 377(6545):151-155.
- (66) Ryder JW, Kawano Y, Chibalin AV, Rincon J, Tsao TS, Stenbit AE et al. In vitro analysis of the glucose-transport system in GLUT4-null skeletal muscle. *Biochemical Journal* 1999; 342:321-328.
- (67) Kim JK, Zisman A, Fillmore JJ, Peroni OD, Kotani K, Perret P et al. Glucose toxicity and the development of diabetes in mice with muscle-specific inactivation of GLUT4. *Journal of Clinical Investigation* 2001; 108(1):153-160.

- (68) Abel ED, Peroni O, Kim JK, Kim YB, Boss O, Hadro E et al. Adipose-selective targeting of the GLUT4 gene impairs insulin action in muscle and liver. *Nature* 2001; 409(6821):729-733.
- (69) Carvalho E, Kotani K, Peroni OD, Kahn BB. Adipose-specific overexpression of GLUT4 reverses insulin resistance and diabetes in mice lacking GLUT4 selectively in muscle. *American Journal of Physiology-Endocrinology and Metabolism* 2005; 289(4):E551-E561.
- (70) Seki Y, Berggren JR, Houmard JA, Charron MJ. Glucose transporter expression in skeletal muscle of endurance-trained individuals. *Medicine and Science in Sports and Exercise* 2006; 38(6):1088-1092.
- (71) Seino S, Seino M, Bell GI. Human Insulin-Receptor Gene. *Diabetes* 1990; 39(2):129-133.
- (72) Brunetti A, Goldfine ID. Insulin-Receptor Gene-Expression and Insulin-Resistance. *Journal of Endocrinological Investigation* 1995; 18(5):398-405.
- (73) Taylor SI. Lilly Lecture - Molecular Mechanisms of Insulin Resistance - Lessons from Patients with Mutations in the Insulin-Receptor Gene. *Diabetes* 1992; 41(11):1473-1490.
- (74) Accili D, Drago J, Lee EJ, Johnson MD, Cool MH, Salvatore P et al. Early neonatal death in mice homozygous for a null allele of the insulin receptor gene. *Nature Genetics* 1996; 12(1):106-109.
- (75) Joshi RL, Lamothe B, Cordonnier N, Mesbah K, Monthieux E, Jami J et al. Targeted disruption of the insulin receptor gene in the mouse results in neonatal lethality. *Embo Journal* 1996; 15(7):1542-1547.
- (76) Michael MD, Kulkarni RN, Postic C, Previs SF, Shulman GI, Magnuson MA et al. Loss of insulin signaling in hepatocytes leads to severe insulin resistance and progressive hepatic dysfunction. *Molecular Cell* 2000; 6(1):87-97.
- (77) Bluher M, Michael MD, Peroni OD, Ueki K, Carter N, Kahn BB et al. Adipose tissue selective insulin receptor knockout protects against obesity and obesity-related glucose intolerance. *Developmental Cell* 2002; 3(1):25-38.
- (78) Bruning JC, Michael MD, Winnay JN, Hayashi T, Horsch D, Accili D et al. A muscle-specific insulin receptor knockout exhibits features of the metabolic syndrome of NIDDM without altering glucose tolerance. *Molecular Cell* 1998; 2(5):559-569.
- (79) Kumar S, O'Rahilly S. *Insulin Resistance: Insulin Action and its Disturbance in Disease*. John Wiley & Sons, 2005.

- (80) Haslam RJ, Koide HB, Hemmings BA. Pleckstrin Domain Homology. *Nature* 1993; 363(6427):309-310.
- (81) Mayer BJ, Ren RB, Clark KL, Baltimore D. A Putative Modular Domain Present in Diverse Signaling Proteins. *Cell* 1993; 73(4):629-630.
- (82) White MF, Maron R, Kahn CR. Insulin Rapidly Stimulates Tyrosine Phosphorylation of A Mr-185,000 Protein in Intact-Cells. *Nature* 1985; 318(6042):183-186.
- (83) Araki E, Lipes MA, Patti ME, Bruning JC, Haag B, Johnson RS et al. Alternative Pathway of Insulin Signaling in Mice with Targeted Disruption of the *Irs-1* Gene. *Nature* 1994; 372(6502):186-190.
- (84) Thirone ACP, Huang C, Klip A. Tissue-specific roles of IRS proteins in insulin signaling and glucose transport. *Trends in Endocrinology and Metabolism* 2006; 17(2):70-76.
- (85) Tamemoto H, Kadowaki T, Tobe K, Yagi T, Sakura H, Hayakawa T et al. Insulin-Resistance and Growth-Retardation in Mice Lacking Insulin-Receptor Substrate-1. *Nature* 1994; 372(6502):182-186.
- (86) Kadowaki T, Tamemoto H, Tobe K, Terauchi Y, Ueki K, Kaburagi Y et al. Insulin resistance and growth retardation in mice lacking insulin receptor substrate-1 and identification of insulin receptor substrate-2. *Diabetic Medicine* 1996; 13(9):S103-S108.
- (87) Sesti G, Federici M, Hribal ML, Lauro D, Sbraccia P, Lauro R. Defects of the insulin receptor substrate (IRS) system in human metabolic disorders. *Faseb Journal* 2001; 15(12):2099-2111.
- (88) Withers DJ, Gutierrez JS, Towery H, Burks DJ, Ren JM, Previs S et al. Disruption of IRS-2 causes type 2 diabetes in mice. *Nature* 1998; 391(6670):900-904.
- (89) Lavan BE, Lane WS, Lienhard GE. The 60-kDa phosphotyrosine protein in insulin-treated adipocytes is a new member of the insulin receptor substrate family. *Journal of Biological Chemistry* 1997; 272(17):11439-11443.
- (90) Fantin VR, Lavan BE, Wang Q, Jenkins NA, Gilbert DJ, Copeland NG et al. Cloning, tissue expression, and chromosomal location of the mouse insulin receptor substrate 4 gene. *Endocrinology* 1999; 140(3):1329-1337.
- (91) Fantin VR, Wang Q, Lienhard GE, Keller SR. Mice lacking insulin receptor substrate 4 exhibit mild defects in growth, reproduction, and glucose homeostasis. *American Journal of Physiology-Endocrinology and Metabolism* 2000; 278(1):E127-E133.

- (92) Liu SCH, Wang Q, Lienhard GE, Keller SR. Insulin receptor substrate 3 is not essential for growth or glucose homeostasis. *Journal of Biological Chemistry* 1999; 274(25):18093-18099.
- (93) Cantley LC. The phosphoinositide 3-kinase pathway. *Science* 2002; 296(5573):1655-1657.
- (94) Okada T, Kawano Y, Sakakibara T, Hazeki O, Ui M. Essential Role of Phosphatidylinositol 3-Kinase in Insulin-Induced Glucose-Transport and Antilipolysis in Rat Adipocytes - Studies with A Selective Inhibitor Wortmannin. *Journal of Biological Chemistry* 1994; 269(5):3568-3573.
- (95) Cheatham B, Vlahos CJ, Cheatham L, Wang L, Blenis J, Kahn CR. Phosphatidylinositol 3-Kinase Activation Is Required for Insulin Stimulation of Pp70 S6 Kinase, Dna-Synthesis, and Glucose-Transporter Translocation. *Molecular and Cellular Biology* 1994; 14(7):4902-4911.
- (96) Clarke JF, Young PW, Yonezawa K, Kasuga M, Holman GD. Inhibition of the Translocation of Glut1 and Glut4 in 3T3-L1 Cells by the Phosphatidylinositol 3-Kinase Inhibitor, Wortmannin. *Biochemical Journal* 1994; 300:631-635.
- (97) Kotani K, Carozzi AJ, Sakaue H, Hara K, Robinson LJ, Clark SF et al. Requirement for Phosphoinositide 3-Kinase in Insulin-Stimulated Glut4 Translocation in 3T3-L1 Adipocytes. *Biochemical and Biophysical Research Communications* 1995; 209(1):343-348.
- (98) Sharma PM, Egawa K, Huang Y, Martin JL, Huvar I, Boss GR et al. Inhibition of phosphatidylinositol 3-kinase activity by adenovirus-mediated gene transfer and its effect on insulin action. *Journal of Biological Chemistry* 1998; 273(29):18528-18537.
- (99) Martin SS, Haruta T, Morris AJ, Klippel A, Williams LT, Olefsky JM. Activated phosphatidylinositol 3-kinase is sufficient to mediate actin rearrangement and GLUT4 translocation in 3T3-L1 adipocytes. *Journal of Biological Chemistry* 1996; 271(30):17605-17608.
- (100) Jiang T, Sweeney G, Rudolf MT, Klip A, Traynor-Kaplan A, Tsien RY. Membrane-permeant esters of phosphatidylinositol 3,4,5-trisphosphate. *Journal of Biological Chemistry* 1998; 273(18):11017-11024.
- (101) Vinciguerra M, Foti M. PTEN and SHIP2 phosphoinositide phosphatases as negative regulators of insulin signalling. *Archives of Physiology and Biochemistry* Volume 112. 2006.

- (102) Nakashima N, Sharma PM, Imamura T, Bookstein R, Olefsky JM. The tumor suppressor PTEN negatively regulates insulin signaling in 3T3-L1 adipocytes. *Journal of Biological Chemistry* 2000; 275(17):12889-12895.
- (103) Vinciguerra M, Foti M. PTEN and SHIP2 phosphoinositide phosphatases as negative regulators of insulin signalling. *Archives of Physiology and Biochemistry* Volume 112. 2006.
- (104) Ono H, Katagiri H, Funaki M, Anai M, Inukai K, Fukushima Y et al. Regulation of phosphoinositide metabolism, Akt phosphorylation, and glucose transport by PTEN (phosphatase and tensin homolog deleted on chromosome 10) in 3T3-L1 adipocytes. *Molecular Endocrinology* 2001; 15(8):1411-1422.
- (105) Tang XQ, Powelka AM, Soriano NA, Czech MP, Guilherme A. PTEN, but not SHIP2, suppresses insulin signaling through the phosphatidylinositol 3-kinase/Akt pathway in 3T3-L1 adipocytes. *Journal of Biological Chemistry* 2005; 280(23):22523-22529.
- (106) Brazil DP, Hemmings BA. Ten years of protein kinase B signalling: a hard Akt to follow. *Trends in Biochemical Sciences* 2001; 26(11):657-664.
- (107) Brazil DP, Yang ZZ, Hemmings BA. Advances in protein kinase B signalling: AKTion on multiple fronts. *Trends in Biochemical Sciences* 2004; 29(5):233-242.
- (108) Alessi DR, James SR, Downes CP, Holmes AB, Gaffney PRJ, Reese CB et al. Characterization of a 3-phosphoinositide-dependent protein kinase which phosphorylates and activates protein kinase B alpha. *Current Biology* 1997; 7(4):261-269.
- (109) Sarbassov DD, Guertin DA, Ali SM, Sabatini DM. Phosphorylation and regulation of Akt/PKB by the rictor-mTOR complex. *Science* 2005; 307(5712):1098-1101.
- (110) Sarbassov DD, Ali SM, Sabatini DM. Growing roles for the mTOR pathway. *Current Opinion in Cell Biology* 2005; 17(6):596-603.
- (111) Ueki K, Yamamoto-Honda R, Kaburagi Y, Yamauchi T, Tobe K, Burgering BMT et al. Potential role of protein kinase B in insulin-induced glucose transport, glycogen synthesis, and protein synthesis. *Journal of Biological Chemistry* 1998; 273(9):5315-5322.
- (112) Tanti JF, Grillo S, Gremeaux T, Coffey PJ, VanObberghen E, LeMarchandBrustel Y. Potential role of protein kinase B in glucose transporter 4 translocation in adipocytes. *Endocrinology* 1997; 138(5):2005-2010.

- (113) Wang QH, Somwar R, Bilan PJ, Liu Z, Jin J, Woodgett JR et al. Protein kinase B Akt participates in GLUT4 translocation by insulin in L6 myoblasts. *Molecular and Cellular Biology* 1999; 19(6):4008-4018.
- (114) Kohn AD, Summers SA, Birnbaum MJ, Roth RA. Expression of a constitutively active Akt Ser/Thr kinase in 3T3-L1 adipocytes stimulates glucose uptake and glucose transporter 4 translocation. *Journal of Biological Chemistry* 1996; 271(49):31372-31378.
- (115) Hill MM, Clark SF, Tucker DF, Birnbaum MJ, James DE, Macaulay SL. A role for protein kinase B beta/Akt2 in insulin-stimulated GLUT4 translocation in adipocytes. *Molecular and Cellular Biology* 1999; 19(11):7771-7781.
- (116) Cho H, Mu J, Kim JK, Thorvaldsen JL, Chu QW, Crenshaw EB et al. Insulin resistance and a diabetes mellitus-like syndrome in mice lacking the protein kinase Akt2 (PKB beta). *Science* 2001; 292(5522):1728-1731.
- (117) Bae SS, Cho H, Mu J, Birnbaum MJ. Isoform-specific regulation of insulin-dependent glucose uptake by Akt/protein kinase B. *Journal of Biological Chemistry* 2003; 278(49):49530-49536.
- (118) Jiang ZY, Zhou QL, Coleman KA, Czech MP. Differential signaling by Akt1 versus Akt2 in 3T3-L1 adipocytes revealed by siRNA-mediated gene silencing. *Molecular Biology of the Cell* 2002; 13:99A.
- (119) Farese RV. Function and dysfunction of aPKC isoforms for glucose transport in insulin-sensitive and insulin-resistant states. *American Journal of Physiology-Endocrinology and Metabolism* 2002; 283(1):E1-E11.
- (120) Matsumoto M, Ogawa W, Akimoto K, Inoue H, Miyake K, Furukawa K et al. PKC lambda in liver mediates insulin-induced SREBP-1c expression and determines both hepatic lipid content and overall insulin sensitivity. *Journal of Clinical Investigation* 2003; 112(6):935-944.
- (121) Sajan MP, Rivas J, Li PF, Standaert ML, Farese RV. Repletion of atypical protein kinase C following RNA interference-mediated depletion restores insulin-stimulated glucose transport. *Journal of Biological Chemistry* 2006; 281(25):17466-17473.
- (122) Farese RV, Sajan MP, Standaert ML. Atypical protein kinase C in insulin action and insulin resistance. *Biochemical Society Transactions* 2005; 33:350-353.

- (123) Kane S, Sano H, Liu SCH, Asara JM, Lane WS, Garner CC et al. A method to identify serine kinase substrates - Akt phosphorylates a novel adipocyte protein with a Rab GTPase-activating protein (GAP) domain. *Journal of Biological Chemistry* 2002; 277(25):22115-22118.
- (124) Sano H, Kane S, Sano E, Miinea CP, Asara JM, Lane WS et al. Insulin-stimulated phosphorylation of a Rab GTPase-activating protein regulates GLUT4 translocation. *Journal of Biological Chemistry* 2003; 278(17):14599-14602.
- (125) Kramer HF, Witczak CA, Taylor EB, Fujii N, Hirshmann MF, Goodyear LJ. AS160 regulates insulin- and contraction-stimulated glucose uptake in mouse skeletal muscle. *Journal of Biological Chemistry* , epub ahead of print. 25-8-2006.
- (126) Zerial M, McBride H. Rab proteins as membrane organizers. *Nature Reviews Molecular Cell Biology* 2001; 2(2):107-117.
- (127) Huppertz C, Schurmann A, Joost HG. Abundance and Subcellular-Distribution of Gtp-Binding Proteins in 3T3-L1 Cells Before and After Differentiation to the Insulin-Sensitive Phenotype. *European Journal of Biochemistry* 1993; 215(3):611-617.
- (128) Wennerberg K, Rossman KL, Der CJ. The Ras superfamily at a glance. *Journal of Cell Science* 2005; 118(5):843-846.
- (129) Bucci C, Chiariello M. Signal transduction gRABs attention. *Cellular Signalling* 2006; 18(1):1-8.
- (130) Cormont M, Bortoluzzi MN, Gautier N, Mari M, VanObberghen E, LeMarchandBrustel Y. Potential role of Rab4 in the regulation of subcellular localization of Glut4 in adipocytes. *Molecular and Cellular Biology* 1996; 16(12):6879-6886.
- (131) Huang J, Imamura T, Olefsky JM. Insulin can regulate GLUT4 internalization by signaling to Rab5 and the motor protein dynein. *Proceedings of the National Academy of Sciences of the United States of America* 2001; 98(23):13084-13089.
- (132) Larance M, Ramm G, Stockli J, van Dam EM, Winata S, Wasinger V et al. Characterization of the role of the Rab GTPase-activating protein AS160 in insulin-regulated GLUT4 trafficking. *Journal of Biological Chemistry* 2005; 280(45):37803-37813.
- (133) Ramm G, Larance M, Guilhaus M, James DE. A role for 14-3-3 in insulin-stimulated GLUT4 translocation through its interaction with the RabGAP AS160. *Journal of Biological Chemistry* , [epub ahead of print]. 31-7-2006.

- (134) van Heusden GPH. 14-3-3 proteins: Regulators of numerous eukaryotic proteins. *Life* 2005; 57(9):623-629.
- (135) Berwick DC, Dell GC, Welsh GI, Heesom KJ, Hers I, Fletcher LM et al. Protein kinase B phosphorylation of PIKfyve regulates the trafficking of GLUT4 vesicles. *Journal of Cell Science* 2004; 117(25):5985-5993.
- (136) Odorizzi G, Babst M, Emr SD. Fab1p PtdIns(3)P 5-kinase function essential for protein sorting in the multivesicular body. *Cell* 1998; 95(6):847-858.
- (137) Sbrissa D, Ikononov OC, Shisheva A. PIKfyve, a mammalian ortholog of yeast Fab1p lipid kinase, synthesizes 5-phosphoinositides - Effect of insulin. *Journal of Biological Chemistry* 1999; 274(31):21589-21597.
- (138) Shisheva A, Sbrissa D, Ikononov O. Cloning, characterization, and expression of a novel Zn²⁺-binding FYVE finger-containing phosphoinositide kinase in insulin-sensitive cells. *Molecular and Cellular Biology* 1999; 19(1):623-634.
- (139) Shisheva A, Rusin B, Ikononov OC, DeMarco C, Sbrissa D. Localization and insulin-regulated relocation of phosphoinositide 5-kinase PIKfyve in 3T3-L1 adipocytes. *Journal of Biological Chemistry* 2001; 276(15):11859-11869.
- (140) Shisheva A. PIKfyve: the road to PtdIns 5-P and PtdIns 3,5-P-2. *Cell Biology International* 2001; 25(12):1201-1206.
- (141) Carlton JG, Cullen PJ. Coincidence detection in phosphoinositide signaling. *Trends in Cell Biology* 2005; 15(10):540-547.
- (142) Yokouchi M, Suzuki R, Masuhara M, Komiya S, Inoue A, Yoshimura A. Cloning and characterization of APS, an adaptor molecule containing PH and SH2 domains that is tyrosine phosphorylated upon B-cell receptor stimulation. *Oncogene* 1997; 15(1):7-15.
- (143) Moodie SA, Alleman-Sposeto J, Gustafson TA. Tyrosine phosphorylation of the SH2-, PH- containing adaptor protein, APS, by insulin in 3T3-L1 adipocytes. *Diabetes* 1999; 48:A332.
- (144) Ahmed Z, Smith BJ, Kotani K, Wilden P, Pillay TS. APS, an adapter protein with a PH and SH2 domain, is a substrate for the insulin receptor kinase. *Biochemical Journal* 1999; 341:665-668.
- (145) Langdon WY, Hartley JW, Klinken SP, Ruscetti SK, Morse HC. V-Cbl, An Oncogene from A Dual-Recombinant Murine Retrovirus That Induces Early B-Lineage Lymphomas. *Proceedings of the National Academy of Sciences of the United States of America* 1989; 86(4):1168-1172.

- (146) Thien CBF, Langdon WY. c-Cbl and Cbl-b ubiquitin ligases: substrate diversity and the negative regulation of signalling responses. *Biochemical Journal* 2005; 391:153-166.
- (147) Liu J, DeYoung SM, Zhang M, Doid LH, Saltiel AR. The stomatin/prohibitin/flotillin/HflK/C domain of flotillin-1 contains distinct sequences that direct plasma membrane localization and protein interactions in 3T3-L1 adipocytes. *Journal of Biological Chemistry* 2005; 280(16):16125-16134.
- (148) Watson RT, Shigematsu S, Chiang SH, Mora S, Kanzaki M, Macara IG et al. Lipid raft microdomain compartmentalization of TC10 is required for insulin signaling and GLUT4 translocation. *Journal of Cell Biology* 2001; 154(4):829-840.
- (149) Mayer BJ, Hamaguchi M, Hanafusa H. A Novel Viral Oncogene with Structural Similarity to Phospholipase-C. *Nature* 1988; 332(6161):272-275.
- (150) Ribon V, Saltiel AR. Insulin stimulates tyrosine phosphorylation of the proto-oncogene product of c-Cbl in 3T3-L1 adipocytes. *Biochemical Journal* 1997; 324:839-845.
- (151) Liu J, Kimura A, Baumann CA, Saltiel AR. APS facilitates c-Cbl tyrosine phosphorylation and GLUT4 translocation in response to insulin in 3T3-L1 adipocytes. *Molecular and Cellular Biology* 2002; 22(11):3599-3609.
- (152) Knudsen BS, Feller SM, Hanafusa H. 4 Proline-Rich Sequences of the Guanine-Nucleotide Exchange Factor C3G Bind with Unique Specificity to the First Src Homology-3 Domain of Crk. *Journal of Biological Chemistry* 1994; 269(52):32781-32787.
- (153) Chiang SH, Baumann CA, Kanzaki M, Thurmond DC, Watson RT, Neudauer CL et al. Insulin-stimulated GLUT4 translocation requires the CAP-dependent activation of TC10. *Nature* 2001; 410(6831):944-948.
- (154) Chiang SH, Hou JC, Hwang J, Pessin JE, Saltiel AR. Cloning and functional characterization of related TC10 isoforms, a subfamily of rho proteins involved in insulin-stimulated glucose transport. *Journal of Biological Chemistry* 2002; 277(15):13067-13073.
- (155) Ridley AJ. Rho GTPases and actin dynamics in membrane protrusions and vesicle trafficking. *Trends in Cell Biology* . 30-8-2006.

- (156) Kanzaki M, Pessin JE. Caveolin-associated filamentous actin (Cav-actin) defines a novel F-actin structure in adipocytes. *Journal of Biological Chemistry* 2002; 277(29):25867-25869.
- (157) Kanzaki M. Insulin receptor signals regulating GLUT4 translocation and act in dynamics. *Endocrine Journal* 2006; 53(3):267-293.
- (158) Chang L, Chiang SH, Saltiel AR. Insulin signaling and the regulation of glucose transport. *Molecular Medicine* 2004; 10(7-12):65-71.
- (159) Minami A, Iseki M, Kishi K, Wang M, Ogura M, Furukawa N et al. Increased insulin sensitivity and hypoinsulinemia in APS knockout mice. *Diabetes* 2003; 52(11):2657-2665.
- (160) Molero JC, Jensen TE, Withers PC, Couzens M, Herzog H, Thien CBF et al. c-Cb-deficient mice have reduced adiposity, higher energy expenditure, and improved peripheral insulin action. *Journal of Clinical Investigation* 2004; 114(9):1326-1333.
- (161) Mitra P, Zheng XX, Czech MP. RNAi-based analysis of CAP, Cbl, and Crkl function in the regulation of GLUT4 by insulin. *Journal of Biological Chemistry* 2004; 279(36):37431-37435.
- (162) Jebailey L, Rudich A, Huang XD, Ciano-Oliveira C, Kapus A, Klip A. Skeletal muscle cells and adipocytes differ in their reliance on TC10 and Rac for insulin-induced actin remodeling. *Molecular Endocrinology* 2004; 18(2):359-372.
- (163) Thirone ACP, Carnevalheira JBC, Hirata AE, Velloso LA, Saad MJA. Regulation of Cbl-associated protein/Cbl pathway in muscle and adipose tissues of two animal models of insulin resistance. *Endocrinology* 2004; 145(1):281-293.
- (164) Yang J, Holman GD. Comparison of Glut4 and Glut1 Subcellular Trafficking in Basal and Insulin-Stimulated 3T3-L1 Cells. *Journal of Biological Chemistry* 1993; 268(7):4600-4603.
- (165) Jhun BH, Rampal AL, Liu HZ, Lachaal M, Jung CY. Effects of Insulin on Steady-State Kinetics of Glut4 Subcellular-Distribution in Rat Adipocytes - Evidence of Constitutive Glut4 Recycling. *Journal of Biological Chemistry* 1992; 267(25):17710-17715.
- (166) Slot JW, Geuze HJ, Gigengack S, James DE, Lienhard GE. Translocation of the Glucose Transporter Glut4 in Cardiac Myocytes of the Rat. *Proceedings of the National Academy of Sciences of the United States of America* 1991; 88(17):7815-7819.

- (167) Czech MP, Buxton JM. Insulin Action on the Internalization of the Glut4 Glucose Transporter in Isolated Rat Adipocytes. *Journal of Biological Chemistry* 1993; 268(13):9187-9190.
- (168) Suzuki K, Kono T. Evidence That Insulin Causes Translocation of Glucose-Transport Activity to the Plasma-Membrane from An Intracellular Storage Site. *Proceedings of the National Academy of Sciences of the United States of America-Biological Sciences* 1980; 77(5):2542-2545.
- (169) Slot JW, Geuze HJ, Gigengack S, Lienhard GE, James DE. Immuno-Localization of the Insulin Regulatable Glucose Transporter in Brown Adipose-Tissue of the Rat. *Journal of Cell Biology* 1991; 113(1):123-135.
- (170) Holman GD, Leggio LL, Cushman SW. Insulin-Stimulated Glut4 Glucose-Transporter Recycling - A Problem in Membrane-Protein Subcellular Trafficking Through Multiple Pools. *Journal of Biological Chemistry* 1994; 269(26):17516-17524.
- (171) Martin S, Tellam J, Livingstone C, Slot JW, Gould GW, James DE. The glucose transporter (GLUT-4) and vesicle-associated membrane protein-2 (VAMP-2) are segregated from recycling endosomes in insulin-sensitive cells. *Journal of Cell Biology* 1996; 134(3):625-635.
- (172) Martin LB, Shewan A, Millar CA, Gould GW, James DE. Vesicle-associated membrane protein 2 plays a specific role in the insulin-dependent trafficking of the facilitative glucose transporter GLUT4 in 3T3-L1 adipocytes. *Journal of Biological Chemistry* 1998; 273(3):1444-1452.
- (173) Rodriguez-Boulan E, Musch A. Protein sorting in the Golgi complex: Shifting paradigms. *Biochimica et Biophysica Acta-Molecular Cell Research* 2005; 1744(3):455-464.
- (174) Shewan AM, Marsh BJ, Melvin DR, Martin S, Gould GW, James DE. The cytosolic C-terminus of the glucose transporter GLUT4 contains an acidic cluster endosomal targeting motif distal to the dileucine signal. *Biochemical Journal* 2000; 350:99-107.
- (175) Martin S, Ramm G, Lyttle CT, Meerloo T, Stoorvogel W, James DE. Biogenesis of insulin-responsive GLUT4 vesicles is independent of brefeldin A-sensitive trafficking. *Traffic* 2000; 1(8):652-660.
- (176) Rea S, James DE. Moving GLUT4: The biogenesis and trafficking of GLUT4 storage vesicles. *Diabetes* 1997; 46(11):1667-1677.

- (177) Malide D, Ramm G, Cushman SW, Slot JW. Immunoelectron microscopic evidence that GLUT4 translocation explains the stimulation of glucose transport in isolated rat white adipose cells. *Journal of Cell Science* 2000; 113(23):4203-4210.
- (178) Hashiramoto M, James DE. Characterization of insulin-responsive GLUT4 storage vesicles isolated from 3T3-L1 adipocytes. *Molecular and Cellular Biology* 2000; 20(1):416-427.
- (179) Bryant NJ, Govers R, James DE. Regulated transport of the glucose transporter glut4. *Nature Reviews Molecular Cell Biology* 2002; 3(4):267-277.
- (180) Virmani T, Han W, Liu X, Sudhof TC, Kavalali ET. Synaptotagmin 7 splice variants differentially regulate synaptic vesicle recycling. *Embo Journal* 2003; 22(20):5347-5357.
- (181) Sollner TH. Regulated exocytosis and SNARE function (Review). *Molecular Membrane Biology* 2003; 20(3):209-220.
- (182) Chieragatti E, Meldolesi J. Opinion - Regulated exocytosis: new organelles for non-secretory purposes. *Nature Reviews Molecular Cell Biology* 2005; 6(2):181-187.
- (183) McMahon HT, Missler M, Li C, Sudhof TC. Complexins: cytosolic proteins that regulate SNAP receptor function. *Cell* 1995; 83(1):111-119.
- (184) Sollner T, Whitehart SW, Brunner M, Erdjumentbromage H, Geromanos S, Tempst P et al. Snap Receptors Implicated in Vesicle Targeting and Fusion. *Nature* 1993; 362(6418):318-324.
- (185) Tucker WC, Weber T, Chapman ER. Reconstitution of Ca²⁺-regulated membrane fusion by synaptotagmin and SNAREs. *Science* 2004; 304(5669):435-438.
- (186) Shewan AM, van Dam EM, Martin S, Luen TB, Hong WJ, Bryant NJ et al. GLUT4 recycles via a trans-Golgi network (TGN) subdomain enriched in Syntaxins 6 and 16 but not TGN38: Involvement of an acidic targeting motif. *Molecular Biology of the Cell* 2003; 14(3):973-986.
- (187) Halachmi N, Lev Z. The Sec1 family: A novel family of proteins involved in synaptic transmission and general secretion. *Journal of Neurochemistry* 1996; 66(3):889-897.
- (188) Bai J, Chapman ER. The C2 domains of synaptotagmin--partners in exocytosis. *Trends Biochem Sci* 2004; 29(3):143-151.
- (189) Weber T, Zemelman BV, Mcnew JA, Westermann B, Gmachl M, Parlati F et al. SNAREpins: Minimal machinery for membrane fusion. *Cell* 1998; 92(6):759-772.

- (190) Gerst JE. SNARE regulators: matchmakers and matchbreakers. *Biochimica et Biophysica Acta-Molecular Cell Research* 2003; 1641(2-3):99-110.
- (191) Snyder DA, Kelly ML, Woodbury DJ. SNARE complex regulation by phosphorylation. *Cell Biochemistry and Biophysics* 2006; 45(1):111-123.
- (192) Brunger AT. Structure and function of SNARE and SNARE-interacting proteins. *Quarterly Reviews of Biophysics* 2005; 38(1):1-47.
- (193) Katz B, Miledi R. Timing of Calcium Action During Neuromuscular Transmission. *Journal of Physiology-London* 1967; 189(3):535-&.
- (194) Rodnick KJ, Slot JW, Studelska DR, Hanpeter DE, Robinson LJ, Geuze HJ et al. Immunocytochemical and Biochemical-Studies of Glut4 in Rat Skeletal-Muscle. *Journal of Biological Chemistry* 1992; 267(9):6278-6285.
- (195) Volchuk A, Wang QH, Ewart HS, Liu Z, He LJ, Bennett MK et al. Syntaxin 4 in 3T3-L1 adipocytes: Regulation by insulin and participation in insulin-dependent glucose transport. *Molecular Biology of the Cell* 1996; 7(7):1075-1082.
- (196) Satoh S, Nishimura H, Clark AE, Kozka IJ, Vannucci SJ, Simpson IA et al. Use of Bismannose Photolabel to Elucidate Insulin-Regulated Glut4 Subcellular Trafficking Kinetics in Rat Adipose-Cells - Evidence That Exocytosis Is A Critical Site of Hormone Action. *Journal of Biological Chemistry* 1993; 268(24):17820-17829.
- (197) Cain CC, Trimble WS, Lienhard GE. Members of the Vamp Family of Synaptic Vesicle Proteins Are Components of Glucose Transporter-Containing Vesicles from Rat Adipocytes. *Journal of Biological Chemistry* 1992; 267(17):11681-11684.
- (198) Volchuk A, Sargeant R, Sumitani S, Liu Z, He LJ, Klip A. Cellubrevin Is A Resident Protein of Insulin-Sensitive Glut4 Glucose-Transporter Vesicles in 3T3-L1 Adipocytes. *Journal of Biological Chemistry* 1995; 270(14):8233-8240.
- (199) Sumitani S, Ramlal T, Liu Z, Klip A. Expression of Syntaxin-4 in Rat Skeletal-Muscle and Rat Skeletal-Muscle Cells in Culture. *Biochemical and Biophysical Research Communications* 1995; 213(2):462-468.
- (200) St Denis JF, Cabaniols JP, Cushman SW, Roche PA. SNAP-23 participates in SNARE complex assembly in rat adipose cells. *Biochemical Journal* 1999; 338:709-715.

- (201) Olson AL, Knight JB, Pessin JE. Syntaxin 4, VAMP2, and/or VAMP3/cellubrevin are functional target membrane and vesicle SNAP receptors for insulin-stimulated GLUT4 translocation in adipocytes. *Molecular and Cellular Biology* 1997; 17(5):2425-2435.
- (202) Foran PGP, Fletcher LM, Oatey PB, Mohammed N, Dolly JO, Tavare JM. Protein kinase B stimulates the translocation of GLUT4 but not GLUT1 or transferrin receptors in 3T3-L1 adipocytes by a pathway involving SNAP-23, synaptobrevin-2, and/or cellubrevin. *Journal of Biological Chemistry* 1999; 274(40):28087-28095.
- (203) Macaulay SL, Hewish DR, Gough KH, Stoichevska V, Macpherson SF, Jagadish M et al. Functional studies in 3T3L1 cells support a role for SNARE proteins in insulin stimulation of GLUT4 translocation. *Biochemical Journal* 1997; 324:217-224.
- (204) Garvey WT, Maianu L, Zhu JH, Hancock JA, Golichowski AM. Multiple Defects in the Adipocyte Glucose-Transport System Cause Cellular Insulin-Resistance in Gestational Diabetes - Heterogeneity in the Number and A Novel Abnormality in Subcellular-Localization of Glut4 Glucose Transporters. *Diabetes* 1993; 42(12):1773-1785.
- (205) Klip A, Li G, Logan WJ. Role of Calcium-Ions in Insulin Action on Hexose-Transport in L6-Muscle Cells. *American Journal of Physiology* 1984; 247(3):E297-E304.
- (206) Klip A, Ramlal T. Cytoplasmic Ca-2+ During Differentiation of 3T3-L1 Adipocytes - Effect of Insulin and Relation to Glucose-Transport. *Journal of Biological Chemistry* 1987; 262(19):9141-9146.
- (207) Kelly KL, Deeney JT, Corkey BE. Cytosolic Free Calcium in Adipocytes - Distinct Mechanisms of Regulation and Effects on Insulin Action. *Journal of Biological Chemistry* 1989; 264(22):12754-12757.
- (208) Cheung JY, Constantine JM, Bonventre JV. Cytosolic Free Calcium-Concentration and Glucose-Transport in Isolated Cardiac Myocytes. *American Journal of Physiology* 1987; 252(2):C163-C172.
- (209) Draznin B, Sussman K, Kao M, Lewis D, Sherman N. The Existence of An Optimal Range of Cytosolic Free Calcium for Insulin-Stimulated Glucose-Transport in Rat Adipocytes. *Journal of Biological Chemistry* 1987; 262(30):14385-14388.

- (210) Khil LY, Cheon AJ, Chang TS, Moon CK. Effects of calcium on brazilin-induced glucose transport in isolated rat epididymal adipocytes. *Biochemical Pharmacology* 1997; 54(1):97-101.
- (211) Pershadsingh HA, Shade DL, Delfert DM, McDonald JM. Chelation of Intracellular Calcium Blocks Insulin Action in the Adipocyte. *Proceedings of the National Academy of Sciences of the United States of America* 1987; 84(4):1025-1029.
- (212) Whitehead JP, Molero JC, Clark S, Martin S, Meneilly G, James DE. The role of Ca²⁺ in insulin-stimulated glucose transport in 3T3-L1 cells. *Journal of Biological Chemistry* 2001; 276(30):27816-27824.
- (213) Xu JC, Koni PA, Wang PL, Li GY, Kaczmarek L, Wu YL et al. The voltage-gated potassium channel Kv1.3 regulates energy homeostasis and body weight. *Human Molecular Genetics* 2003; 12(5):551-559.
- (214) Xu JC, Wang PL, Li YY, Li GY, Kaczmarek LK, Wu YL et al. The voltage-gated potassium channel Kv1.3 regulates peripheral insulin sensitivity. *Proceedings of the National Academy of Sciences of the United States of America* 2004; 101(9):3112-3117.
- (215) Li YY, Wang PL, Xu JC, Desir GV. Voltage-gated potassium channel Kv1.3 regulates GLUT4 trafficking to the plasma membrane via a Ca²⁺-dependent mechanism. *American Journal of Physiology-Cell Physiology* 2006; 290(2):C345-C351.
- (216) Lanner JT, Katz A, Tavi P, Sandstrom ME, Zhang SJ, Wretman C et al. The role of Ca²⁺ influx for insulin-mediated glucose uptake in skeletal muscle. *Diabetes* 2006; 55(7):2077-2083.
- (217) Matthew WD, Tsavaler L, Reichardt LF. Identification of A Synaptic Vesicle-Specific Membrane-Protein with A Wide Distribution in Neuronal and Neurosecretory Tissue. *Journal of Cell Biology* 1981; 91(1):257-269.
- (218) Brose N, Petrenko AG, Sudhof TC, Jahn R. Synaptotagmin - A Calcium Sensor on the Synaptic Vesicle Surface. *Science* 1992; 256(5059):1021-1025.
- (219) Su AI, Cooke MP, Ching KA, Hakak Y, Walker JR, Wiltshire T et al. Large-scale analysis of the human and mouse transcriptomes. *Proceedings of the National Academy of Sciences of the United States of America* 2002; 99(7):4465-4470.
- (220) Baram D, Linial M, Mekori YA, Sagi-Eisenberg R. Cutting edge: Ca²⁺-dependent exocytosis in mast cells is stimulated by the

- Ca²⁺ sensor, synaptotagmin. *Journal of Immunology* 1998; 161(10):5120-5123.
- (221) Baram D, Adachi R, Medalia O, Tuvim M, Dickey BF, Mekori YA et al. Synaptotagmin II negatively regulates Ca²⁺-triggered exocytosis of lysosomes in mast cells. *Journal of Experimental Medicine* 1999; 189(10):1649-1657.
- (222) Hutt DM, Baltz JM, Ngsee JK. Synaptotagmin VI and VIII and syntaxin 2 are essential for the mouse sperm acrosome reaction. *Journal of Biological Chemistry* 2005; 280(21):20197-20203.
- (223) Chakrabarti S, Kobayashi KS, Flavell RA, Marks CB, Miyake K, Liston DR et al. Impaired membrane resealing and autoimmune myositis in synaptotagmin VII-deficient mice. *J Cell Biol* 2003; 162(4):543-549.
- (224) Perin MS, Brose N, Jahn R, Sudhof TC. Domain structure of synaptotagmin (p65). *J Biol Chem* 1991; 266(1):623-629.
- (225) Nishizuka Y. The Molecular Heterogeneity of Protein Kinase-C and Its Implications for Cellular-Regulation. *Nature* 1988; 334(6184):661-665.
- (226) Bhalla A, Tucker WC, Chapman ER. Synaptotagmin isoforms couple distinct ranges of Ca²⁺, Ba²⁺, and Sr²⁺ concentration to SNARE-mediated membrane fusion. *Mol Biol Cell* 2005; 16(10):4755-4764.
- (227) Rickman C, Craxton M, Osborne S, Davletov B. Comparative analysis of tandem C2 domains from the mammalian synaptotagmin family. *Biochem J* 2004; 378(Pt 2):681-686.
- (228) Craxton M. Synaptotagmin gene content of the sequenced genomes. *Bmc Genomics* 2004; 5.
- (229) Birney E, Andrews D, Caccamo M, Chen Y, Clarke L, Coates G et al. Ensembl 2006. *Nucleic Acids Research* 2006; 34:D556-D561.
- (230) Fukuda M, Mikoshiba K. Genomic structures of synaptotagmin II protein: comparison of exon-intron organization of the synaptotagmin gene family. *Biochem Biophys Res Commun* 2000; 270(2):528-532.
- (231) Craxton M. Genomic analysis of synaptotagmin genes. *Genomics* 2001; 77(1-2):43-49.
- (232) Craxton M, Goedert M. Alternative splicing of synaptotagmins involving transmembrane exon skipping. *Febs Letters* 1999; 460(3):417-422.

- (233) Fukuda M, Mikoshiba K. A novel alternatively spliced variant of synaptotagmin VI lacking a transmembrane domain. Implications for distinct functions of the two isoforms. *J Biol Chem* 1999; 274(44):31428-31434.
- (234) Nakhost A, Houeland G, Castellucci VF, Sossin WS. Differential regulation of transmitter release by alternatively spliced forms of synaptotagmin I. *Journal of Neuroscience* 2003; 23(15):6238-6244.
- (235) Nakhost A, Houeland G, Blandford VE, Castellucci VF, Sossin WS. Identification and characterization of a novel C2B splice variant of synaptotagmin I. *Journal of Neurochemistry* 2004; 89(2):354-363.
- (236) Fukuda M, Ogata Y, Saegusa C, Kanno E, Mikoshiba K. Alternative splicing isoforms of synaptotagmin VII in the mouse, rat and human. *Biochem J* 2002; 365(Pt 1):173-180.
- (237) Monterrat C, Boal F, Grise F, Hemar A, Lang JC. Synaptotagmin 8 is expressed both as a calcium-insensitive soluble and membrane protein in neurons, neuroendocrine and endocrine cells. *Biochimica et Biophysica Acta-Molecular Cell Research* 2006; 1763(1):73-81.
- (238) Gottfries CG, Lehmann W, Regland B. Early diagnosis of cognitive impairment in the elderly with the focus on Alzheimer's disease. *J Neural Transm* 1998; 105(8-9):773-786.
- (239) Yoo BC, Cairns N, Fountoulakis M, Lubec G. Synaptosomal proteins, beta-soluble N-ethylmaleimide-sensitive factor attachment protein (beta-SNAP), gamma-SNAP and synaptotagmin I in brain of patients with Down syndrome and Alzheimer's disease. *Dement Geriatr Cogn Disord* 2001; 12(3):219-225.
- (240) Ferguson GD, Anagnostaras SG, Silva AJ, Herschman HR. Deficits in memory and motor performance in synaptotagmin IV mutant mice. *Proc Natl Acad Sci U S A* 2000; 97(10):5598-5603.
- (241) Ferguson GD, Vician L, Herschman HR. Synaptotagmin IV: biochemistry, genetics, behavior, and possible links to human psychiatric disease. *Mol Neurobiol* 2001; 23(2-3):173-185.
- (242) Huynh DP, Scoles DR, Nguyen D, Pulst SM. The autosomal recessive juvenile Parkinson disease gene product, parkin, interacts with and ubiquitinates synaptotagmin XI. *Hum Mol Genet* 2003; 12(20):2587-2597.

- (243) Takamori M. Lambert-Eaton myasthenic syndrome as an autoimmune calcium channelopathy. *Biochem Biophys Res Commun* 2004; 322(4):1347-1351.
- (244) Ashizawa S, Brunnicardi FC, Wang XP. PDX-1 and the pancreas. *Pancreas* 2004; 28(2):109-120.
- (245) Nakajima-Nagata N, Sugai M, Sakurai T, Miyazaki J, Tabata Y, Shimizu A. Pdx-1 enables insulin secretion by regulating synaptotagmin 1 gene expression. *Biochem Biophys Res Commun* 2004; 318(3):631-635.
- (246) Yokota H, Tsujita T, Okazaki Y, Kikuya E, Oishi M. Polymorphic 33-bp repeats with promoter-like activity in synaptotagmin 11 gene. *DNA Res* 2003; 10(6):287-289.
- (247) Inoue S, Oishi M. Effects of methylation of non-CpG sequence in the promoter region on the expression of human synaptotagmin XI (syt11). *Gene* 2005; 348:123-134.
- (248) Jimenez JL, Smith GR, Contreras-Moreira B, Sgouros JG, Meunier FA, Bates PA et al. Functional recycling of C2 domains throughout evolution: a comparative study of synaptotagmin, protein kinase C and phospholipase C by sequence, structural and modelling approaches. *J Mol Biol* 2003; 333(3):621-639.
- (249) ClustalW WWW Service at the European Bioinformatics Institute. 2006.
- (250) Sutton RB, Davletov BA, Berghuis AM, Sudhof TC, Sprang SR. Structure of the first C2 domain of synaptotagmin I: a novel Ca²⁺/phospholipid-binding fold. *Cell* 1995; 80(6):929-938.
- (251) Chapman ER, Davis AF. Direct interaction of a Ca²⁺-binding loop of synaptotagmin with lipid bilayers. *J Biol Chem* 1998; 273(22):13995-14001.
- (252) Bai J, Wang P, Chapman ER. C2A activates a cryptic Ca(2+)-triggered membrane penetration activity within the C2B domain of synaptotagmin I. *Proc Natl Acad Sci U S A* 2002; 99(3):1665-1670.
- (253) Fernandez I, Arac D, Ubach J, Gerber SH, Shin O, Gao Y et al. Three-dimensional structure of the synaptotagmin 1 C2B-domain: synaptotagmin 1 as a phospholipid binding machine. *Neuron* 2001; 32(6):1057-1069.
- (254) Ubach J, Zhang X, Shao X, Sudhof TC, Rizo J. Ca²⁺ binding to synaptotagmin: how many Ca²⁺ ions bind to the tip of a C2-domain? *EMBO J* 1998; 17(14):3921-3930.

- (255) Earles CA, Bai J, Wang P, Chapman ER. The tandem C2 domains of synaptotagmin contain redundant Ca^{2+} binding sites that cooperate to engage t-SNAREs and trigger exocytosis. *J Cell Biol* 2001; 154(6):1117-1123.
- (256) Hui EF, Bai JH, Chapman ER. Ca^{2+} -triggered simultaneous membrane penetration of the tandem C2-domains of synaptotagmin I. *Biophysical Journal* 2006; 91(5):1767-1777.
- (257) Dai Z, Peng HB. Presynaptic differentiation induced in cultured neurons by local application of basic fibroblast growth factor. *J Neurosci* 1995; 15(8):5466-5475.
- (258) Micheva KD, Holz RW, Smith SJ. Regulation of presynaptic phosphatidylinositol 4,5-bisphosphate by neuronal activity. *Journal of Cell Biology* 2001; 154(2):355-368.
- (259) Eberhard DA, Cooper CL, Low MG, Holz RW. Evidence That the Inositol Phospholipids Are Necessary for Exocytosis - Loss of Inositol Phospholipids and Inhibition of Secretion in Permeabilized Cells Caused by A Bacterial Phospholipase-C and Removal of Atp. *Biochemical Journal* 1990; 268(1):15-25.
- (260) Fukuda M, Aruga J, Niinobe M, Aimoto S, Mikoshiba K. Inositol-1,3,4,5-tetrakisphosphate binding to C2B domain of IP4BP/synaptotagmin II. *J Biol Chem* 1994; 269(46):29206-29211.
- (261) Schiavo G, Gu QM, Prestwich GD, Sollner TH, Rothman JE. Calcium-dependent switching of the specificity of phosphoinositide binding to synaptotagmin. *Proc Natl Acad Sci U S A* 1996; 93(23):13327-13332.
- (262) Li LY, Shin OH, Rhee JS, Arac D, Rah JC, Rizo J et al. Phosphatidylinositol phosphates as co-activators of Ca^{2+} binding to C-2 domains of synaptotagmin 1. *Journal of Biological Chemistry* 2006; 281(23):15845-15852.
- (263) Damer CK, Creutz CE. Calcium-dependent self-association of synaptotagmin I. *J Neurochem* 1996; 67(4):1661-1668.
- (264) Chapman ER, An S, Edwardson JM, Jahn R. A novel function for the second C2 domain of synaptotagmin. Ca^{2+} -triggered dimerization. *J Biol Chem* 1996; 271(10):5844-5849.
- (265) Sugita S, Hata Y, Sudhof TC. Distinct Ca^{2+} -dependent properties of the first and second C2-domains of synaptotagmin I. *J Biol Chem* 1996; 271(3):1262-1265.
- (266) Fukuda M, Kanno E, Ogata Y, Mikoshiba K. Mechanism of the SDS-resistant synaptotagmin clustering mediated by the cysteine

- cluster at the interface between the transmembrane and spacer domains. *J Biol Chem* 2001; 276(43):40319-40325.
- (267) von Poser C, Zhang JZ, Mineo C, Ding W, Ying Y, Sudhof TC et al. Synaptotagmin regulation of coated pit assembly. *J Biol Chem* 2000; 275(40):30916-30924.
- (268) Bai J, Earles CA, Lewis JL, Chapman ER. Membrane-embedded synaptotagmin penetrates cis or trans target membranes and clusters via a novel mechanism. *J Biol Chem* 2000; 275(33):25427-25435.
- (269) Littleton JT, Bai J, Vyas B, Desai R, Baltus AE, Garment MB et al. synaptotagmin mutants reveal essential functions for the C2B domain in Ca²⁺-triggered fusion and recycling of synaptic vesicles in vivo. *J Neurosci* 2001; 21(5):1421-1433.
- (270) Mackler JM, Reist NE. Mutations in the second C-2 domain of synaptotagmin disrupt synaptic transmission at *Drosophila* neuromuscular junctions. *Journal of Comparative Neurology* 2001; 436(1):4-16.
- (271) Sudhof TC. Synaptotagmins: why so many? *J Biol Chem* 2002; 277(10):7629-7632.
- (272) Wang CT, Grishanin R, Earles CA, Chang PY, Martin TF, Chapman ER et al. Synaptotagmin modulation of fusion pore kinetics in regulated exocytosis of dense-core vesicles. *Science* 2001; 294(5544):1111-1115.
- (273) Wang CT, Lu JC, Bai J, Chang PY, Martin TF, Chapman ER et al. Different domains of synaptotagmin control the choice between kiss-and-run and full fusion. *Nature* 2003; 424(6951):943-947.
- (274) Bennett MK, Calakos N, Scheller RH. Syntaxin: a synaptic protein implicated in docking of synaptic vesicles at presynaptic active zones. *Science* 1992; 257(5067):255-259.
- (275) Yoshida A, Oho C, Omori A, Kuwahara R, Ito T, Takahashi M. Hpc-1 Is Associated with Synaptotagmin and Omega-Conotoxin Receptor. *Journal of Biological Chemistry* 1992; 267(35):24925-24928.
- (276) Chapman ER, Hanson PI, An S, Jahn R. Ca²⁺ regulates the interaction between synaptotagmin and syntaxin 1. *J Biol Chem* 1995; 270(40):23667-23671.
- (277) Shao X, Li C, Fernandez I, Zhang X, Sudhof TC, Rizo J. Synaptotagmin-syntaxin interaction: the C2 domain as a Ca²⁺-dependent electrostatic switch. *Neuron* 1997; 18(1):133-142.

- (278) Bai J, Wang CT, Richards DA, Jackson MB, Chapman ER. Fusion pore dynamics are regulated by synaptotagmin^I-SNARE interactions. *Neuron* 2004; 41(6):929-942.
- (279) Bowen ME, Wenginger K, Ernst J, Chu S, Brunger AT. Single-molecule studies of synaptotagmin and complexin binding to the SNARE complex. *Biophysical Journal* 2005; 89(1):690-702.
- (280) Perin MS. Mirror image motifs mediate the interaction of the COOH terminus of multiple synaptotagmins with the neurexins and calmodulin. *Biochemistry* 1996; 35(43):13808-13816.
- (281) Sheng ZH, Yokoyama CT, Catterall WA. Interaction of the synprint site of N-type Ca²⁺ channels with the C2B domain of synaptotagmin I. *Proc Natl Acad Sci U S A* 1997; 94(10):5405-5410.
- (282) Kim DK, Catterall WA. Ca²⁺-dependent and -independent interactions of the isoforms of the alpha1A subunit of brain Ca²⁺ channels with presynaptic SNARE proteins. *Proc Natl Acad Sci U S A* 1997; 94(26):14782-14786.
- (283) Walther K, Diril MK, Jung N, Haucke V. Functional dissection of the interactions of stonin 2 with the adaptor complex AP-2 and synaptotagmin. *Proc Natl Acad Sci U S A* 2004; 101(4):964-969.
- (284) Phillips AM, Smith M, Ramaswami M, Kelly LE. The products of the *Drosophila* stoned locus interact with synaptic vesicles via synaptotagmin. *J Neurosci* 2000; 20(22):8254-8261.
- (285) Zhang JZ, Davletov BA, Sudhof TC, Anderson RG. Synaptotagmin I is a high affinity receptor for clathrin AP-2: implications for membrane recycling. *Cell* 1994; 78(5):751-760.
- (286) Littleton JT. Mixing and matching during synaptic vesicle endocytosis. *Neuron* 2006; 51(2):149-151.
- (287) Honda A, Yamada M, Saisu H, Takahashi H, Mori KJ, Abe T. Direct, Ca²⁺-dependent interaction between tubulin and synaptotagmin I: a possible mechanism for attaching synaptic vesicles to microtubules. *J Biol Chem* 2002; 277(23):20234-20242.
- (288) Haberman Y, Grimberg E, Fukuda M, Sagi-Eisenberg R. Synaptotagmin IX, a possible linker between the perinuclear endocytic recycling compartment and the microtubules. *J Cell Sci* 2003; 116(Pt 21):4307-4318.
- (289) Popoli M. Synaptotagmin is endogenously phosphorylated by Ca²⁺/calmodulin protein kinase II in synaptic vesicles. *FEBS Lett* 1993; 317(1-2):85-88.

- (290) Davletov B, Sontag JM, Hata Y, Petrenko AG, Fykse EM, Jahn R et al. Phosphorylation of synaptotagmin I by casein kinase II. *J Biol Chem* 1993; 268(9):6816-6822.
- (291) Haghghi AP, McCabe BD, Fetter RD, Palmer JE, Hom S, Goodman CS. Retrograde control of synaptic transmission by postsynaptic CaMKII at the *Drosophila* neuromuscular junction. *Neuron* 2003; 39(2):255-267.
- (292) Hilfiker S, Pieribone VA, Nordstedt C, Greengard P, Czernik AJ. Regulation of synaptotagmin I phosphorylation by multiple protein kinases. *J Neurochem* 1999; 73(3):921-932.
- (293) Lee BH, Min X, Heise CJ, Xu BE, Chen S, Shu H et al. WNK1 phosphorylates synaptotagmin 2 and modulates its membrane binding. *Mol Cell* 2004; 15(5):741-751.
- (294) Roggero CM, Tomes CN, De Blas GA, Castillo J, Michaut MA, Fukuda M et al. Protein kinase C-mediated phosphorylation of the two polybasic regions of synaptotagmin VI regulates their function in acrosomal exocytosis. *Dev Biol* 2005; 285(2):422-435.
- (295) Applied Biosystems. User Bulletin 4303859B: Relative Quantitation Of Gene Expression: ABI PRISM 7700 Sequence. 11-12-1997.

Ref Type: Internet Communication

- (296) Hellwig B, Joost HG. Differentiation of Erythrocyte-Type (Glut1), Liver-Type (Glut2), and Adipocyte-Type (Glut4) Glucose Transporters by Binding of the Inhibitory Ligands Cytochalasin-B, Forskolin, Dipyridamole, and Isobutylmethylxanthine. *Molecular Pharmacology* 1991; 40(3):383-389.
- (297) Piper RC, Hess LJ, James DE. Differential Sorting of 2 Glucose Transporters Expressed in Insulin-Sensitive Cells. *American Journal of Physiology* 1991; 260(3):C570-C580.
- (298) Millar CA, Jess TJ, Saqib KM, Wakelam MJO, Gould GW. 3T3-L1 adipocytes express two isoforms of phospholipase D in distinct subcellular compartments. *Biochemical and Biophysical Research Communications* 1999; 254(3):734-738.
- (299) Heid CA, Stevens J, Livak KJ, Williams PM. Real time quantitative PCR. *Genome Research* 1996; 6(10):986-994.
- (300) Green H, Meuth M. Established Pre-Adipose Cell Line and Its Differentiation in Culture. *Cell* 1974; 3(2):127-133.
- (301) Deherreros AG, Birnbaum MJ. The Acquisition of Increased Insulin-Responsive Hexose-Transport in 3T3-L1 Adipocytes Correlates with Expression of A Novel Transporter Gene. *Journal of Biological Chemistry* 1989; 264(33):19994-19999.

- (302) Altschul SF, Gish W, Miller W, Myers EW, Lipman DJ. Basic Local Alignment Search Tool. *Journal of Molecular Biology* 1990; 215(3):403-410.
- (303) Fukuda M. Molecular cloning and characterization of human, rat, and mouse synaptotagmin XV. *Biochem Biophys Res Commun* 2003; 306(1):64-71.
- (304) Kanzaki M, Watson RT, Hou JCQ, Stamnes M, Saltiel AR, Pessin JE. Small GTP-binding protein TC10 differentially regulates two distinct populations of filamentous actin in 3T3L1 adipocytes. *Molecular Biology of the Cell* 2002; 13(7):2334-2346.
- (305) Lah JJ, Burry RW. Neuronotypic differentiation results in reduced levels and altered distribution of synaptophysin in PC12 cells. *J Neurochem* 1993; 60(2):503-512.
- (306) Lou XJ, Bixby JL. Patterns of presynaptic gene expression define two stages of synaptic differentiation. *Mol Cell Neurosci* 1995; 6(3):252-262.
- (307) Greenlee MH, Swanson JJ, Simon JJ, Elmquist JK, Jacobson CD, Sakaguchi DS. Postnatal development and the differential expression of presynaptic terminal-associated proteins in the developing retina of the Brazilian opossum, *Monodelphis domestica*. *Brain Res Dev Brain Res* 1996; 96(1-2):159-172.
- (308) Berton F, Iborra C, Boudier JA, Seagar MJ, Marqueze B. Developmental regulation of synaptotagmin I, II, III, and IV mRNAs in the rat CNS. *J Neurosci* 1997; 17(4):1206-1216.
- (309) Liu YY, Brent GA. Thyroid hormone-dependent gene expression in differentiated embryonic stem cells and embryonal carcinoma cells: identification of novel thyroid hormone target genes by deoxyribonucleic acid microarray analysis. *Endocrinology* 2005; 146(2):776-783.
- (310) Andrews NW. Membrane resealing: synaptotagmin VII keeps running the show. *Sci STKE* 2005; 2005(282):e19.
- (311) Sutton RB, Ernst JA, Brunger AT. Crystal structure of the cytosolic C2A-C2B domains of synaptotagmin III. Implications for Ca(+2)-independent snare complex interaction. *J Cell Biol* 1999; 147(3):589-598.
- (312) Mizushima S, Nagata S. Pef-Bos, A Powerful Mammalian Expression Vector. *Nucleic Acids Research* 1990; 18(17):5322.
- (313) Nelson JA, Reynoldskohler C, Smith BA. Negative and Positive Regulation by A Short Segment in the 5'-Flanking Region of the Human Cytomegalovirus Major Immediate-Early Gene. *Molecular and Cellular Biology* 1987; 7(11):4125-4129.

- (314) Cheng Y, Sequeira SM, Malinina L, Tereshko V, Sollner TH, Patel DJ. Crystallographic identification of Ca²⁺ and Sr²⁺ coordination sites in synaptotagmin I C2B domain. *Protein Sci* 2004; 13(10):2665-2672.
- (315) Chapman ER. Synaptotagmin: a Ca(2+) sensor that triggers exocytosis? *Nat Rev Mol Cell Biol* 2002; 3(7):498-508.
- (316) Simpson IA, Yver DR, Hissin PJ, Wardzala LJ, Karnieli E, Salans LB et al. Insulin-Stimulated Translocation of Glucose Transporters in the Isolated Rat Adipose-Cells - Characterization of Subcellular-Fractions. *Biochimica et Biophysica Acta* 1983; 763(4):393-407.
- (317) Fukuda M, Mikoshiba K. Characterization of KIAA1427 protein as an atypical synaptotagmin (Syt XIII). *Biochem J* 2001; 354(Pt 2):249-257.
- (318) Ibata K, Fukuda M, Hamada T, Kabayama H, Mikoshiba K. Synaptotagmin IV is present at the Golgi and distal parts of neurites. *J Neurochem* 2000; 74(2):518-526.
- (319) Fukuda M, Ibata K, Mikoshiba K. A unique spacer domain of synaptotagmin IV is essential for Golgi localization. *J Neurochem* 2001; 77(3):730-740.
- (320) Fukuda M, Kanno E, Ogata Y, Saegusa C, Kim T, Loh YP et al. Nerve growth factor-dependent sorting of synaptotagmin IV protein to mature dense-core vesicles that undergo calcium-dependent exocytosis in PC12 cells. *J Biol Chem* 2003; 278(5):3220-3226.
- (321) Berton F, Cornet V, Iborra C, Garrido J, Dargent B, Fukuda M et al. Synaptotagmin I and IV define distinct populations of neuronal transport vesicles. *European Journal of Neuroscience* 2000; 12(4):1294-1302.
- (322) Martinez I, Chakrabarti S, Hellevik T, Morehead J, Fowler K, Andrews NW. Synaptotagmin VII regulates Ca(2+)-dependent exocytosis of lysosomes in fibroblasts. *J Cell Biol* 2000; 148(6):1141-1149.
- (323) Perera HKI, Clarke M, Morris NJ, Hong WJ, Chamberlain LH, Gould GW. Syntaxin 6 regulates Glut4 trafficking in 3T3-L1 adipocytes. *Molecular Biology of the Cell* 2003; 14(7):2946-2958.
- (324) Proctor KM, Miller SCM, Bryant NJ, Gould GW. Syntaxin 16 controls the intracellular sequestration of GLUT4 in 3T3-L1 adipocytes. *Biochemical and Biophysical Research Communications* 2006; 347(2):433-438.

- (325) Bose A, Guilherme A, Huang SH, Hubbard AC, Lane CR, Soriano NA et al. The v-SNARE Vti1a regulates insulin-stimulated glucose transport and Acrp30 secretion in 3T3-L1 adipocytes. *Journal of Biological Chemistry* 2005; 280(44):36946-36951.
- (326) Kupriyanova TA, Kandror V, Kandror KV. Isolation and characterization of the two major intracellular Glut4 storage compartments. *Journal of Biological Chemistry* 2002; 277(11):9133-9138.
- (327) Li LV, Kandror KV. Golgi-localized, gamma-ear-containing, arf-binding protein adaptors mediate insulin-responsive trafficking of glucose transporter 4 in 3T3-L1 Adipocytes. *Molecular Endocrinology* 2005; 19(8):2145-2153.
- (328) Watson RT, Khan AH, Furukawa M, Hou JCQ, Li L, Kanzaki M et al. Entry of newly synthesized GLUT4 into the insulin-responsive storage compartment is GGA dependent. *Embo Journal* 2004; 23(10):2059-2070.
- (329) Robinson MS. Adaptable adaptors for coated vesicles. *Trends in Cell Biology* 2004; 14(4):167-174.
- (330) Grass I, Thiel S, Honing S, Haucke V. Recognition of a basic AP-2 binding motif within the C2B domain of synaptotagmin is dependent on multimerization. *Journal of Biological Chemistry* 2004; 279(52):54872-54880.
- (331) Fire A. RNA-triggered gene silencing. *Trends in Genetics* 1999; 15(9):358-363.
- (332) Zhou QL, Park JG, Jiang ZY, Holik JJ, Mitra P, Semiz S et al. Analysis of insulin signalling by RNAi-based gene silencing. *Biochemical Society Transactions* 2004; 32:817-821.
- (333) Hofacker I. Vienna Secondary mRNA Structure Prediction software. 1-1-2005.
Ref Type: Internet Communication
- (334) Vinciguerra M, Foti M. PTEN and SHIP2 phosphoinositide phosphatases as negative regulators of insulin signalling. *Archives of Physiology and Biochemistry* Volume 112. 2006.
- (335) Fukuda M, Mikoshiba K. Distinct self-oligomerization activities of synaptotagmin family. Unique calcium-dependent oligomerization properties of synaptotagmin VII. *J Biol Chem* 2000; 275(36):28180-28185.
- (336) Fukuda M. Synaptotagmins, Ca²⁺- and phospholipid-binding proteins that control Ca²⁺-regulated membrane trafficking.

Recent research developments in chemistry and physics of lipids
2003; 3:15-51.

- (337) Sugita S, Shin OH, Han W, Lao Y, Sudhof TC. Synaptotagmins form a hierarchy of exocytotic Ca²⁺ sensors with distinct Ca²⁺ affinities. *EMBO J* 2002; 21(3):270-280.
- (338) Dai H, Shin OH, Machius M, Tomchick DR, Sudhof TC, Rizo J. Structural basis for the evolutionary inactivation of Ca²⁺ binding to synaptotagmin 4. *Nat Struct Mol Biol* 2004; 11(9):844-849.
- (339) Shen SS, Tucker WC, Chapman ER, Steinhardt RA. Molecular regulation of membrane resealing in 3T3 fibroblasts. *J Biol Chem* 2005; 280(2):1652-1660.
- (340) Rao SK, Huynh C, Proux-Gillardeaux V, Galli T, Andrews NW. Identification of SNAREs involved in synaptotagmin VII-regulated lysosomal exocytosis. *J Biol Chem* 2004; 279(19):20471-20479.
- (341) Rizza R. Cure, Optimal Care and Total Commitment, the 2006 ADA Banting Award Lecture. 13-6-2006.
- (342) Shi J, Kandror KV. Sortilin is essential and sufficient for the formation of Glut4 storage vesicles in 3T3-L1 adipocytes. *Developmental Cell* 2005; 9(1):99-108.
- (343) Foster LJ, Rudich A, Talior I, Patel N, Huang XD, Furtado LM et al. Insulin-dependent interactions of proteins with GLUT4 revealed through stable isotope labeling by amino acids in cell culture (SILAC). *Journal of Proteome Research* 2006; 5(1):64-75.
- (344) Hui E, Bai J, Wang P, Sugimori M, Llinas RR, Chapman ER. Three distinct kinetic groupings of the synaptotagmin family: candidate sensors for rapid and delayed exocytosis. *Proc Natl Acad Sci U S A* 2005; 102(14):5210-5214.
- (345) von Poser C, Ichtchenko K, Shao X, Rizo J, Sudhof TC. The evolutionary pressure to inactivate. A subclass of synaptotagmins with an amino acid substitution that abolishes Ca²⁺ binding. *J Biol Chem* 1997; 272(22):14314-14319.
- (346) Ahras M, Otto GP, Tooze SA. Synaptotagmin IV is necessary for the maturation of secretory granules in PC12 cells. *Journal of Cell Biology* 2006; 173(2):241-251.
- (347) Arvan P, Castle D. Sorting and storage during secretory granule biogenesis: looking backward and looking forward. *Biochemical Journal* 1998; 332:593-610.
- (348) Li C, Ullrich B, Zhang JZ, Anderson RG, Brose N, Sudhof TC. Ca²⁺-dependent and -independent activities of neural and non-neural synaptotagmins. *Nature* 1995; 375(6532):594-599.

- (349) Caler EV, Chakrabarti S, Fowler KT, Rao S, Andrews NW. The Exocytosis-regulatory protein synaptotagmin VII mediates cell invasion by *Trypanosoma cruzi*. *J Exp Med* 2001; 193(9):1097-1104.
- (350) Gao Z, Reavey-Cantwell J, Young RA, Jegier P, Wolf BA. Synaptotagmin III/VII isoforms mediate Ca^{2+} -induced insulin secretion in pancreatic islet beta -cells. *J Biol Chem* 2000; 275(46):36079-36085.
- (351) Fukuda M, Kanno E, Satoh M, Saegusa C, Yamamoto A. Synaptotagmin VII is targeted to dense-core vesicles and regulates their Ca^{2+} -dependent exocytosis in PC12 cells. *J Biol Chem* 2004; 279(50):52677-52684.
- (352) Andrews NW, Chakrabarti S. There's more to life than neurotransmission: the regulation of exocytosis by synaptotagmin VII. *Trends Cell Biol* 2005; 15(11):626-631.
- (353) Jaiswal JK, Chakrabarti S, Andrews NW, Simon SM. Synaptotagmin VII restricts fusion pore expansion during lysosomal exocytosis. *PLoS Biol* 2004; 2(8):E233.